



**University of  
Nottingham**

UK | CHINA | MALAYSIA

**Department of Chemical and Environmental Engineering**

**Predictive models for gas-liquid two phase flows:  
Investigating dependence on liquid phase viscosity**

By

Ahad Fayyaz

Thesis submitted to the University of Nottingham  
for the degree of Doctor of Philosophy

September 2022

## Abstract

The effect of inclination angle of pipe test section and liquid viscosity of silicone oil on flow development (i.e. flow regimes and transitions) and flow characteristics are studied in this thesis. The flow characteristics that are studied include liquid holdup, structure velocity and structure frequency. Intermittent flows such as slug, cap bubbly and churn usually present a pattern in which a gas dominated structure is followed by a liquid dominated structure. For given set of superficial properties, the pattern repeats with a characteristic mean frequency.

By investigating the effect of viscosity on two-phase characteristics, the present thesis will tackle many research gaps or areas of reverification. From literature survey, it was quite evident that there is limited readily available data for medium to high viscosity therefore this present investigation will increase the breadth of medium to high viscosity datapoints in literature. Moreover, another research gap that is tackled by this thesis is the reverification of trends of various flow characteristics with viscosity. Finally, another area of improvement that is brought up by this thesis is development of general liquid holdup correlation and flow regime maps with promising results. Therefore, the present study will provide a good contribution to the research on gas-liquid two-phase flow in circular pipes. It must also be stated that effect of viscosity has been overlooked in most of the experiments in literature as they mostly used water as the liquid phase. Even though there are several campaigns (in literature) using higher liquid viscosities, the number of data points is not sufficient to make any meaningful estimate of the influence it has on the flow regimes.

An inclinable rig was used to investigate gas – liquid two – phase flow. The rig is installed with a tilting boom, allowing upward two – phase flow to be investigated at different angles from horizontal. Three different viscosities (64 cP, 91.5 cP and 236 cP) of silicone oil were investigated. The gas phase for all these runs was air. The facility at the University of Nottingham was operated at atmospheric pressure. For

each viscosity, different gas and liquid superficial velocities were experimented. The void fraction data was obtained for each set of conditions for 60 seconds using Electrical Capacitance Tomography (ECT).

The effect of inclination angle and viscosity on flow characteristics were firstly reported. The main findings can be summarised as that liquid holdup increases with liquid viscosity for a given gas and liquid superficial velocity. For a considerable change in liquid holdup, the change in viscosity must be large enough (100s of cP or so). Moreover, structure velocity also increased with liquid viscosity as well however the increase is small in comparison to that of liquid holdup. Drift flux modelling was also carried out. The range of distribution coefficient was 1.27 for 64 cP to 1.44 for 236 cP. The range of drift velocity decreases from 0.37 m/s for 64 cP to 0.32 m/s for 236 cP while Froude number ranged from 0.45 for 64 cP to 0.40 for 236 cP.

Additionally, for each inclination angle tested, a single dimensionless flow regime map was constructed, illustrating the effect of viscosity on flow regime transitions. The dimensionless number utilised was the Reynolds number. It was shown that, in comparison to utilisation of superficial velocities, Reynolds number produced much more promising results in terms of providing clear non-overlapping transition boundaries. Literature was also reviewed for horizontal and vertical orientation in order to create dimensionless flow regime maps for historical datasets.

Finally, a general liquid holdup correlation was developed using datasets from the present study and the literature. The development of model utilised a total of 2478 data points. After the development stage, further 2237 data points were tested against model presented in this study. In both scenarios, model presented in this study yielded promising results when compared to other models obtained from the literature.

## Acknowledgement

Firstly, I would like to thank University of Nottingham for providing me with the financial support throughout the course of the PhD degree.

I would also like to express my sincere appreciation to my main supervisor Dr Buddhika Hewakandamby for his support, guidance and trust in these four years of my PhD study. Moreover, I would also like to express my sincere gratitude to my second and third supervisors Dr Bagus Putra Muljadi and Dr Rajab Omar for their support and invaluable advice throughout the PhD course.

I would also like to express my deep appreciation to the technical staff of L3 lab in particular to Mel and Mick. They have been very helpful when it came to assessing the rigs and its instrumentations during the experimentation phase.

Moreover, I would also like to thank my colleagues in Multiphase Group at University of Nottingham: Nangi, Longtong, Simon and Samson for motivation, help and memories throughout the course of this degree. I would also like to thank my colleagues in the shared postgraduate room for long discussions over lunch time.

Last but not least, I would like to thank my parents, siblings and other family members abroad and in UK for their constant support.

## Table of Contents

Abstract .....	ii
Acknowledgement .....	iv
Table of Contents .....	v
List of Figures .....	x
List of Tables.....	xvii
Nomenclature .....	xx
1. Introduction .....	1
1.1. Problem statement.....	1
1.2. Objectives .....	5
1.3. Experimental reasoning.....	6
1.3.1. Experimental setup .....	6
1.3.2. Data treatment.....	6
1.3.3. Modelling .....	7
1.4. Structure of the thesis.....	7
2. Literature review .....	10
2.1. Flow pattern classifications in two-phase flow .....	12
2.1.1. Flow patterns in horizontal pipe .....	12
2.1.2. Flow pattern maps in horizontal pipe .....	17
2.1.3. Flow patterns in vertical pipe.....	21
2.1.4. Flow pattern maps in vertical pipe .....	25
2.1.5. Flow patterns in inclined pipes .....	28
2.1.6. Flow pattern maps in inclined pipes .....	30
2.2. Flow pattern transitions in two-phase flow .....	31
2.2.1. Different flow approaches in two-phase flow .....	31

2.2.2.	Flow pattern transitions for two-phase pipe systems .....	34
2.2.2.1.	Transitions in horizontal and near-horizontal pipes: .....	34
2.2.2.2.	Transitions in vertical and inclined pipes .....	41
2.3.	Experimental flow regime studies in vertical and horizontal pipelines .....	47
2.3.1.	Experimental studies on vertical inclination .....	47
2.3.2.	Experimental studies on horizontal inclination .....	50
2.4.	Liquid hold-up (or gas void fraction) models .....	51
2.5.	Conclusion .....	56
3.	Methodology.....	59
3.1.	Introduction.....	59
3.2.	Experimental arrangement .....	60
3.2.1.	Determination of the physical properties of silicone oil .....	60
3.2.2.	Description of the rig .....	65
3.3.	Gas void fraction acquisition instrumentation.....	69
3.3.1.	Electrical Capacitance Tomography: The forward and inverse problem 69	
3.3.2.	Present study ECT Configuration .....	73
3.4.	Data analysis techniques: ECT Holdup data .....	76
3.4.1.	ECT raw data .....	76
3.4.2.	Structure velocity .....	77
3.4.3.	Structure frequency .....	80
3.4.3.1.	FFT method .....	81
3.4.3.2.	Hazuku method.....	82
3.4.4.	Statistical measures: Probability density function (PDF) and standard deviation (SDEV) .....	83
3.5.	Robustness of PSD and cross-correlation results.....	85

4.	Effect of inclination angle and viscosity on two phase parameters.....	88
4.1.	Introduction.....	88
4.2.	Experimental arrangement .....	90
4.3.	Effect of inclination angle and superficial velocities on liquid holdup.....	92
4.3.1.	64 cP experimental campaign .....	92
4.3.2.	91.5 cP experimental campaign.....	100
4.3.3.	236 cP experimental campaign.....	106
4.4.	Effect of inclination angle on structure velocity .....	112
4.4.1.	64 cP experimental campaign.....	112
4.4.2.	91.5 cP experimental campaign.....	117
4.4.3.	236 cP experimental campaign.....	121
4.5.	Effect of inclination angle on structure frequency .....	126
4.5.1.	64 cP experimental campaign.....	126
4.5.2.	91.5 cP experimental campaign.....	129
4.5.3.	236 cP experimental campaign.....	132
4.6.	Verification of viscosity effect on two-phase flow parameters .....	134
4.6.1.	Impact of liquid viscosity on liquid holdup .....	134
4.6.2.	Impact of liquid viscosity on structure velocity .....	139
4.6.3.	Impact of viscosity on distribution coefficient and drift velocity .....	144
4.7.	Conclusion .....	148
5.	Investigating the effect of viscosity on flow regime maps.....	151
5.1.	Introduction.....	151
5.2.	Effect of viscosity on flow regime maps and transitions for present experimental study.....	152
5.2.1.	Methodology.....	152
5.2.2.	Observed flow pattern maps for all three experimental campaigns.....	153

5.2.3.	Comparing the results of present study to commonly used flow regime maps and experimental studies in literature .....	158
5.2.3.1.	Vertical inclination .....	158
5.2.3.2.	Horizontal inclination.....	160
5.2.3.3.	Inclined orientation .....	162
5.2.4.	Proposed flow pattern map for present study and comparisons to other experimental studies in literature .....	166
5.3.	Literature review of flow pattern experimental studies in vertical and horizontal systems.....	169
5.3.1.	Methodology including data sources utilised .....	169
5.3.2.	Investigating viscosity effect for experimental studies in literature for vertical flow patterns.....	172
5.3.3.	Investigating viscosity effect for experimental studies in literature for horizontal flow patterns .....	185
5.4.	Evaluating the performance of proposed coordinates for vertical inclination .....	197
5.5.	Conclusion .....	200
6.	Development of a general liquid holdup model.....	202
6.1.	Introduction.....	202
6.2.	Methodology .....	204
6.2.1.	Summary of experimental database utilised for model development 204	
6.2.2.	Development of the liquid holdup model.....	209
6.3.	Analysis of proposed correlation.....	213
6.3.1.	Model results for current three experimental campaigns .....	213
6.3.2.	Comparing current study with other models for experimental dataset utilised for model development .....	216

6.4. Further performance evaluation of present study model (2022) using data not utilised in model development .....	228
6.5. Conclusion .....	238
7. Conclusions and future Work .....	239
7.1. General conclusions .....	239
7.2. Future works.....	242
References.....	245

## List of Figures

Figure 2.1 – Flow regimes in gas-liquid horizontal flow .....	12
Figure 2.2 – Taitel and Dukler (1976) flow regime map for horizontal pipes.....	18
Figure 2.3 – Mandhane et al. (1974) flow regime map for air – water (see Table 2.2) .....	18
Figure 2.4 – Beggs and Brill map (1973).....	19
Figure 2.5 – Taitel and Dukler (1987) flow pattern maps investigating the effect of viscosity in a horizontal 3.8 cm diameter pipe (-- shows boundaries for 1 cP; – shows boundaries for the investigated viscosity).....	20
Figure 2.6 – Brito et al. (2013) study on effect of medium viscosity on flow patterns for pipe diameter of 50.8 mm with boundaries obtained by TUFFP (2003) model. .	20
Figure 2.7 – Flow regimes in gas-liquid vertical flow (increasing gas flow at constant liquid flow) .....	21
Figure 2.8 – Taitel et al. (1980) flow regime map for vertical two-phase system for silicone oil – air system ( $\mu = 64$ cP, $\sigma = 0.0202$ N/m, and $\rho = 922.5$ kg m <sup>-3</sup> ) .....	26
Figure 2.9 - Alruhaimani et al. (2015) flow pattern study for oil – air system for pipe diameter of 50.8 mm (Liquid viscosity = 586 cP) .....	27
Figure 2.10 – Bhaga and Weber (1981) bubble shape regime map .....	28
Figure 2.11 – Barnea et al. (1985) flow regime air – water properties for inclined systems (from horizontal) .....	30
Figure 2.12 – Weisman & Kang (1981) map at different inclinations (65°, 45°, 15°)	31
Figure 2.13 – Equilibrium stratified flow.....	35
Figure 2.14 – Flooding condition as described by Wallis (1961) .....	46
Figure 3.1 – Setup for viscosity measurements .....	62
Figure 3.2 – Schematic diagram showing the arrangement of the inclinable rig.....	65
Figure 3.3 – Relationship between absolute and normalised capacitance .....	70
Figure 3.4 – Simple square model utilised to explain the sensitivity and capacitance matrix .....	71
Figure 3.5 – Circular ECT sensor used in this study.....	74
Figure 3.6 – ECT mask configuration for inclinable rig .....	75

Figure 3.7 – A typical time series plot for vertical two-phase flow (64 cP) at a liquid and gas superficial velocity of 0.0795 and 0.125 m/s respectively. ....	77
Figure 3.8 – Time series data for plane 1 and 2 for vertical two-phase flow at a liquid and gas superficial velocity of 0.0795 and 0.125 m/s respectively. ....	78
Figure 3.9 – Cross correlation coefficient plot for vertical two-phase flow (64 cP) at a liquid and gas superficial velocity of 0.0795 and 0.125 m/s respectively. ....	80
Figure 3.10 – PSD plot for vertical two-phase flow (64 cP) at a liquid and gas superficial velocity of 0.186 and 1.836 m/s respectively.....	82
Figure 3.11 – Hazuku method for horizontal two-phase flow (64 cP) at liquid and gas superficial velocity of 0.0795 and 0.735 m/s respectively.....	83
Figure 3.12 – PDFs shown for vertical two-phase flow at a liquid viscosity and velocity of 64 cP and 0.292 m/s for different gas velocities.....	84
Figure 3.13 – Decomposing the signal in equation 3.34 into individual frequency components of 1.7, 2, 2.25 respectively.....	85
Figure 3.14 – PSD plot for the signal represented as equation 3.29.....	86
Figure 3.15 – Cross correlation applied on equations 3.30 and 3.31.....	87
Figure 4.1 – Influence of inclination angle on liquid holdup for oil viscosity of 64 cP at different liquid and gas superficial velocities.....	92
Figure 4.2 – Comparing experimental and homogeneous gas voidage for all runs at 64 cP oil.....	95
Figure 4.3 – Variation of liquid holdup for 64 cP experiments against superficial gas at five liquid velocities for each inclination angle.....	96
Figure 4.4 – Rate of change of liquid holdup against gas superficial velocity for all liquid superficial velocities at 64 cP.....	97
Figure 4.5 – Influence of inclination on holdup ratio (HR) for different liquid and gas superficial velocities at oil viscosity of 64 cP.....	99
Figure 4.6 – Influence of inclination angle on liquid holdup for different liquid and gas velocities at oil viscosity of 91.5 cP.....	101
Figure 4.7 – Comparing experimental and homogeneous gas voidage for all runs at 91.5 cP oil.....	102
Figure 4.8 – Variation of liquid holdup for 91.5 cP runs against superficial gas velocity at various liquid superficial velocities for each inclination angle.....	103

Figure 4.9 – Rate of change of liquid holdup against gas superficial velocity for all liquid superficial velocities at 91.5 cP (Vertical Inclination) .....	104
Figure 4.10 – Influence of inclination angle on holdup ratio (HR) for different liquid and gas velocities at oil viscosity of 91.5 cP.....	105
Figure 4.11 – Influence of inclination angle on liquid holdup for different liquid and gas velocities at oil viscosity of 236 cP.....	107
Figure 4.12 – Comparing experimental and homogeneous gas voidage for all runs at 236 cP oil .....	108
Figure 4.13 – Variation of liquid holdup for 236 cP runs against superficial gas velocity at various liquid superficial velocities for each inclination angle.....	109
Figure 4.14 – Rate of change of liquid holdup against gas superficial velocity for all liquid superficial velocities at 236 cP .....	110
Figure 4.15 – Influence of inclination angle on holdup ratio (HR) for different liquid and gas velocities at oil viscosity of 236 cP.....	111
Figure 4.16 – Influence of inclination angle on structure velocity for different liquid and gas velocities at oil viscosity of 64 cP.....	113
Figure 4.17 – Variation of gas velocity against mixture velocity at each inclination angle for 64 cP data .....	114
Figure 4.18 – Effect of inclination angle on $C_o$ , $U_D$ , $Fr$ and their rate of change with angle for liquid viscosity of 64 cP .....	116
Figure 4.19 – Influence of inclination angle on structure velocity for different liquid and gas velocities at oil viscosity of 91.5 cP.....	118
Figure 4.20 – Variation of gas velocity against mixture velocity at each inclination angle for 91.5 cP data .....	119
Figure 4.21 – Effect of inclination angle on $C_o$ , $U_D$ , $Fr$ and their rate of change with angle for liquid viscosity of 91.5 cP .....	121
Figure 4.22 – Influence of inclination angle on structure velocity for different liquid and gas velocities at oil viscosity of 236 cP.....	122
Figure 4.23 –Variation of gas velocity against mixture velocity at each inclination angle for 236 cP data .....	123
Figure 4.24 – Effect of inclination angle on $C_o$ , $U_D$ , $Fr$ and their rate of change with angle for liquid viscosity of 236 cP.....	125

Figure 4.25 – Influence of inclination angle on structure frequency for different liquid and gas velocities at oil viscosity of 64 cP .....	127
Figure 4.26 – Effect of Strouhal Number (based on gas superficial velocity) on Lockhart – Martinelli Parameter for all runs at silicone viscosity of 64 cP .....	128
Figure 4.27 – Influence of inclination angle on structure frequency for different liquid and gas velocities at oil viscosity of 91.5 cP .....	130
Figure 4.28 – Effect of Strouhal Number (based on gas superficial velocity) on Lockhart – Martinelli Parameter for all runs at silicone viscosity of 91.5 cP .....	131
Figure 4.29 – Influence of inclination on structure frequency for different liquid and gas velocities at oil viscosity of 236 cP .....	132
Figure 4.30 – Effect of Strouhal Number (based on gas superficial velocity) on Lockhart – Martinelli Parameter for all runs at silicone viscosity of 236 cP .....	133
Figure 4.31 – Effect of viscosity on two – phase liquid holdup at different liquid and gas velocities for various inclination angle .....	135
Figure 4.32 – Investigating the difference between liquid holdup at 64 cP and 236 cP with inclination angle for a gas superficial velocity of 1.838 m/s .....	136
Figure 4.33 – Comparison of high viscosity datasets of Gokcal (2008) and Escrig (2017) with present study’s’ high viscosity datasets in horizontal pipelines .....	138
Figure 4.34 – Comparing the effect of viscosity on liquid holdup using datasets from literature (in Table 4.9) and present study for vertical pipelines .....	139
Figure 4.35 – Effect of viscosity on two – phase structure velocity at different liquid and gas velocities for various inclination angle .....	141
Figure 4.36 – Comparing the effect of viscosity on structure velocity using datasets from literature (in Table 4.8) and present study for horizontal pipelines .....	142
Figure 4.37 – Comparing the effect of viscosity on structure velocity using datasets from literature (in Table 4.9) and present study for vertical pipelines .....	143
Figure 4.38 – Variation/range of distribution coefficient values at each viscosity tested .....	144
Figure 4.39 – Variation/range of drift velocity values at each viscosity tested .....	146
Figure 4.40 – Drift flux model for each individual viscosity and all data points .....	147

Figure 5.1 – Observed flow patterns and transitions for all three experimental campaigns investigated at five different inclination angles with gas and liquid superficial velocities on x – axis and y – axis respectively .....	155
Figure 5.2 – Observed flow patterns and transitions for all three experimental campaigns investigated at five different inclination angles with gas and liquid Reynolds Number on x – axis and y – axis respectively .....	157
Figure 5.3 – Comparing observed flow patterns and transitions for present study to observed flow patterns plotted on modified Taitel et al. (1980) based on Reynolds Number for vertical datasets .....	159
Figure 5.4 – Comparing observed flow patterns and transitions for present study to observed flow patterns plotted on Taitel and Dukler (1976) for horizontal datasets .....	160
Figure 5.5 – Comparing observed flow patterns and transitions for present study to observed flow patterns plotted on modified Mandhane et al. (1974) based on Reynolds Number for horizontal datasets .....	161
Figure 5.6 – Comparing observed flow patterns and transitions for present study to observed flow patterns plotted on modified Barnea et al. (1985) based on Reynolds Number for inclination angle of 65 degrees .....	163
Figure 5.7 – Comparing observed flow patterns and transitions for present study to observed flow patterns plotted on modified Barnea et al. (1985) based on Reynolds Number for inclination angle of 45 degrees .....	164
Figure 5.8 – Comparing observed flow patterns and transitions for present study to observed flow patterns plotted on modified Barnea et al. (1985) based on Reynolds Number for inclination angle of 15 degrees .....	165
Figure 5.9 – Proposed flow regime map for each inclination angle .....	166
Figure 5.10 – Performance of present study’s proposed flow regime map (vertical inclination) for experimental study of Alruhimani (2015) .....	168
Figure 5.11 – Performance of present study’s proposed flow regime map (horizontal inclination) for various experimental studies in literature. ....	169
Figures 5.12 (a – d) – Effect of Weber and Reynolds number in different forms on flow patterns for low viscosity datasets in vertical pipelines .....	175

Figures 5.13 (a – d) – Effect of Weber and Reynolds number in different forms on flow patterns for high / medium viscosity datasets in vertical pipelines .....	179
Figure 5.14 – Evaluating the performance of the proposed vertical flow regime map at low viscosity (Liquid Re vs Gas Re).....	181
Figure 5.15 – Evaluating the performance of the proposed vertical flow regime map at low viscosity (Liquid Re vs Gas We) .....	182
Figure 5.16 – Evaluating the performance of the proposed vertical flow regime maps at high viscosity (Liquid Re vs Gas Re and Liquid Re vs Gas We) .....	184
Figures 5.17 (a – d) – Effect of Weber and Reynolds number in different forms on flow patterns for low viscosity datasets in horizontal pipelines .....	187
Figures 5.18 (a – e) – Effect of Weber and Reynolds number in different forms on flow patterns for high viscosity datasets in horizontal pipelines .....	192
Figure 5.19 – Evaluating the performance of the proposed horizontal flow regime maps at low viscosity (Liquid Re vs Gas Re and Liquid Re vs Gas We) .....	195
Figure 5.20 – Evaluating the performance of one of the proposed horizontal flow regime map at high viscosity ( $We/Re^{0.2}$ vs $We/Re^{0.2}$ ).....	196
Figures 5.21 (a – b) – Evaluating the effect of using different coordinates on the flow regime transitions for different groups of datasets (low viscosity flow regime maps).....	198
Figures 5.22 (a – b) – Evaluating the effect of using different coordinates on the flow regime transitions for different datasets (high viscosity flow regime maps)..	199
<i>Figure 6.1 – Homogeneous gas void fraction test for Mukherjee AK (1979) dataset .....</i>	<i>206</i>
<i>Figure 6.2 – Drift flux test for Mukherjee AK (1979) dataset.....</i>	<i>207</i>
<i>Figure 6.3 – How liquid holdup varies with angle for different gas superficial velocities for a given liquid superficial velocity of 0.292 m/s at 64 cP silicone oil (Points – Experimental; Lines – Model) .....</i>	<i>213</i>
<i>Figure 6.4 – How liquid holdup varies with angle for different gas superficial velocities for a given liquid superficial velocity of 0.308 m/s at 91.5 cP silicone oil (Points – Experimental; Lines – Model) .....</i>	<i>214</i>

Figure 6.5 – How liquid holdup varies with angle for different gas superficial velocities for a given liquid superficial velocity of 0.27 m/s at 236 cP silicone oil (Points – Experimental; Lines – Model) .....	215
<i>Figure 6.6 – Overall performance of the best six models for combined dataset (all data) .....</i>	<i>226</i>
<i>Figure 6.7 – Overall performance of the best six models for combined dataset (all data except Nottingham University) .....</i>	<i>227</i>
<i>Figure 6.8 – Overall performance of the best six models for all data listed in Table 6.10.....</i>	<i>237</i>

## List of Tables

Table 2.1 – Parameters for Premoli et al. correlation (1970) .....	34
Table 2.2 – Boundaries for default Mandhane et al. (1974) map .....	40
Table 2.3 – Correlations for horizontal holdup and C for uphill and downhill flow ..	53
Table 3.1 – Physical properties of silicon oil-air mixtures at 20 °C and 1 atm for inclinable rig .....	61
Table 3.2 – Range and constant of each Ostwald viscometer .....	63
Table 3.3 – Experimental matrix for runs involving 64 cP .....	64
Table 3.4 – Experimental matrix for runs involving 91.5 cP .....	64
Table 3.5 – Experimental matrix for runs involving 236 cP .....	64
Table 4.1 – Matrix employed for three different experimental campaigns .....	91
Table 4.2 – Summary of distribution coefficient, drift velocity and Froude number at each inclination for 64 cP data .....	115
Table 4.3 – Summary of distribution coefficient, drift velocity and Froude number at each inclination for 91.5 cP data .....	120
Table 4.4 – Summary of distribution coefficient, drift velocity and Froude number at each inclination for 236 cP data .....	124
Table 4.5 – Power law coefficients for frequency data of 64 cP .....	129
Table 4.6 – Power law coefficients for frequency data of 91.5 cP .....	131
Table 4.7 – Power law coefficients for frequency data of 236 cP .....	133
Table 4.8 – Dataset from literature to further investigate the effect of viscosity on liquid holdup for horizontal pipelines .....	137
Table 4.9 – Dataset from literature to further investigate the effect of viscosity on liquid holdup for vertical pipelines .....	138
Table 4.10 –Analysing the variation of distribution coefficient with viscosity .....	145
Table 4.11 –Analysing the variation of drift velocity (DV) with viscosity .....	146
Table 4.12 – Overall viscosity effect on distribution coefficient and drift velocity.	148
Table 5.1 – Dimensionless hydraulic diameter proposed by Schlegel et al. (2012) for three experimental campaigns in this project .....	152

Table 5.2 – Testing the modified Taitel et al. (1980) model for each experimental campaign for vertical dataset .....	158
Table 5.3 – Testing the modified Barnea et al. (1985) model for each experimental campaign for inclination angles of 65, 45 and 15 degrees .....	162
Table 5.4 – Performance of proposed model for each inclination angle .....	167
Table 5.5 – Vertical experimental datasets from literature utilised for investigating the effect of viscosity on flow patterns .....	170
Table 5.6 – Horizontal experimental datasets from literature utilised for investigating the effect of viscosity on flow patterns.....	171
Table 5.7 – Percentage of each flow pattern in each flow pattern section for all four maps shown in Figures 5.12 (a – d).....	176
Table 5.8 – Percentage of each flow pattern in each flow pattern section for all four maps shown in Figures 5.13 (a – d).....	180
Table 5.9 – Additional literature datasets to test the performance of vertical flow regime maps using literature datasets of low viscosity from Table 5.5 .....	181
Table 5.10 – Evaluating the performance of both proposed vertical flow regime maps at low viscosity (Liquid Re vs Gas Re and Liquid Re vs Gas We) .....	183
Table 5.11 – Evaluating the performance of both proposed vertical flow regime maps at high viscosity (Liquid Re vs Gas Re and Liquid Re vs Gas We) .....	185
Table 5.12 – Percentage of each flow pattern in each flow pattern section for all four maps shown in Figures 5.17 (a – d).....	188
Table 5.13 – Percentage of each flow pattern in each flow pattern section for all three maps shown in Figures 5.18 (b, c and e) .....	193
Table 5.14 – Additional datasets to test the performance of horizontal flow regime maps using literature datasets of low viscosity .....	194
Table 5.15 – Evaluating the performance of both proposed horizontal flow regime maps at low viscosity (Liquid Re vs Gas Re and Liquid Re vs Gas We) .....	194
<i>Table 6.1 – Experimental datasets utilised for the development of a new liquid holdup correlation .....</i>	<i>205</i>
<i>Table 6.2 – Treatment of liquid holdup data for each individual dataset utilised in this study .....</i>	<i>208</i>

<i>Table 6.3 – List of correlations utilised for comparison to new liquid holdup correlation</i> .....	212
<i>Table 6.4 – Absolute average error (AAE), average error (AE) and standard deviation (STD) for each model – dataset combination (AK is air –kerosene, AW is air – water and AL is air – lube oil)</i> .....	218
<i>Table 6.5 – Absolute average error (AAE), average error (AE) and standard deviation (STD) for both combined dataset scenarios</i> .....	220
<i>Table 6.6 – Percentage of data within 30 % for each model – dataset combination</i> .....	222
<i>Table 6.7 – Percentage of data within 30 % for combined dataset scenarios</i> .....	223
<i>Table 6.8 – Percentage of data within 30 % for each individual set (each model – dataset combination)</i> .....	224
<i>Table 6.9 – Percentage of data within 30 % for each individual set (combined dataset scenarios)</i> .....	225
<i>Table 6.10 – Experimental dataset not utilised for the development of a new liquid holdup correlation</i> .....	229
<i>Table 6.11 – Treatment of each dataset not utilised in development of model</i> .....	231
<i>Table 6.12 – Absolute average error (AAE), average error (AE) and standard deviation (STD) for each model – dataset combination (for low liquid loading)</i> .....	232
<i>Table 6.13 – Absolute average error (AAE), average error (AE) and standard deviation (STD) for each model – dataset combination (for mixed liquid loading)</i>	233
<i>Table 6.14 – Percentage of data within 30 % for each model – dataset combination (for low liquid loading)</i> .....	234
<i>Table 6.15 – Percentage of data within 30 % for each model – dataset combination (for mixed liquid loading)</i> .....	235
<i>Table 6.16 – Overall summary of error analysis and percentage of data within 30 % for all data not utilised in model development</i> .....	236

## Nomenclature

### Abbreviations

ECT – Electrical Capacitance Tomography

PSD – Power Spectral Density

PDF – Probability Density Function

### Latin upper case (Units – only presented for non – dimensionless quantities)

A	Area, (m <sup>2</sup> )	K	Product of Froude number and square root of Re <sub>SL</sub> (-)
C <sub>0</sub>	Distribution Coefficient (-)	Ku	Kutadelaze number (-)
C <sub>1</sub> , C <sub>2</sub>	Expressions used for Kelvin – Helmholtz theory (-)	Re	Reynolds Number (-)
D	Diameter, (m)	S	Interfacial area, (m <sup>2</sup> )
E <sub>1</sub> , E <sub>2</sub>	Parameters in Premoli <i>et al.</i> (1970) correlation (-)	T	Ratio of turbulent to gravity forces acting on the gas (-)
Fr	Froude Number (-)	We	Weber Number (-)
G	Mass flux, (kg m <sup>-2</sup> s <sup>-1</sup> )	X	Lockhart-Martinelli Parameter
H <sub>L</sub>	Liquid Holdup, (% or -)	Y	Forces acting on liquid due to pressure drop and gravity (-)

### Latin lower case (Units – only presented for non – dimensionless quantities)

dp/dx	Pressure gradient (downward axis), (Pa/m)	q	Flow rate (m <sup>3</sup> /s)
g	Gravitational acceleration, (m s <sup>-2</sup> )	s	Sheltering coefficient (-)
h	Height, (m)	u	Velocity (m/s)
j	Parameter in Premoli <i>et al.</i> (1970) correlation (-)	v	Kinematic viscosity (m <sup>2</sup> s <sup>-1</sup> )
		x	Quality (-)

**Greek (Units – only presented for non – dimensionless quantities)**

$\lambda$	Liquid input content (-)	$\vartheta$	Inclination angle from horizontal (degrees)
$\mu$	Viscosity, (Pa s)		
$\sigma$	Surface Tension, (N/m)	f	Friction factor
$\rho$	Density, (kg m <sup>-3</sup> )	$\Delta$	Increment / Change
$\varepsilon$	Void fraction, (% or -)	$\tau$	Shear stress, (Pa)

**Superscript (in Equations)**

$\sim$ or *	Dimensionless variable	m	Exponent in 2.11 and 2.23
n	Exponent in 2.11 and 2.23		

**Subscript**

crit	Critical	O/D	Drift
F	Film	OV	Drift (vertical inclination)
Gi	Gas interface	OH	Drift (horizontal inclination)
GH	Gas Homogeneous	OB	Drift bubbly
GS	Gas superficial	OS $\vartheta$	Drift slug (inclination angle)
g or G	Gas	OS	Drift slug
H	Hydraulic	P	Premoli <i>et al.</i> (1970) correlation
I	Interface	R	Slip ratio
l or L	Liquid	TP	Two – phase
Li	Liquid interface	TN	Transition
LS	Liquid superficial	TR/T	Translational
M	Mixture	WG	Wall gas
WL	Wall liquid		

# 1. Introduction

## 1.1. Problem statement

In a typical oil and gas production system, hydrocarbons are brought up to the surface by drilling through the cap rock and into the reservoir. Once the drilling instrument reaches the reservoir, wells can be constructed, and hydrocarbons can be pumped up to the surface. Before the hydrocarbon mixture is transported to the marketplace, it is passed through various flowlines, risers, and other unit operations (Chaves *et al.*, 2022). Development of multiphase flow models provide an insight into the effect of physical parameters (viscosity, surface tension, density) and operational parameters (gas lift injection rates) on multiphase characteristics such as slug/flow characteristics that can be adjusted in order to maximise well production and thus net revenue. Moreover, over the last three decades, engineers have depended on simulations to model multiphase flows in a wide range of applications such as production systems and real-time optimisation of operations even though attempts to characterise such systems in a mathematical framework began six decades ago (Shippen and Bailey, 2012). There are two main challenges in the development of such mathematical models to predict two-phase systems of gas and liquid due to the complexity of the flow: limited closure relationships and numerical discontinuities.

Presently, closure relationships need to be used with caution as there are various different relationships that are invoked when conditions change. For example, the drift velocity term in the Zuber and Findlay (1965) drift model is different for bubbly, churn-turbulent and slug flow. Other models such as Lockhart and Martinelli (1949) also fail when slug flow is considered. Moreover, the complexity in flow also means that the interface between the phases is transforming continually, leading to multiple discontinuities of various length scales. The discontinuity of the dispersed phase leads to local variations in mixture properties making any model to fail. The lump parameter models capture these variations in volume average sense. Lack of studies

focussed around the impact of fluid properties on volume average quantities has to be addressed and an attempt is made in this work. Presently, the current technology (data acquisition techniques) is capable of capturing complex changes; however, the development of a general model has been difficult as there is not sufficient data covering substantial ranges of parameters such as surface tension and liquid viscosity.

Another challenge is that the prediction of complex flow behaviour (i.e. flow regime transitions as a function of inclination angle) by advanced models also induce numerical discontinuities in the overall solution for liquid holdup and pressure gradient as a function of the testing input parameters. For example, liquid holdup and pressure gradients can abruptly change (causing discontinuities in the liquid holdup and pressure gradient solutions of the CFD simulation) when there is a change in flow regime to slug flow. When these models are incorporated into larger simulations such as a reservoir with multi-segment models, these models need to be continuous, smooth and differentiable. In most cases, simpler models are used in these scenarios, adjusting the parameters to replicate the features of an advanced model. Simpler models employ techniques such as averaging, smoothing and segmentation in order to avoid introduction of additional discontinuities into the flow models. As a result, there is a significant trade-off margin between accuracy and simplicity. For example, the Lockhart – Martinelli (L – M) model is used for pressure drop modelling (Lockhart and Martinelli, 1949). The model is simple however it is based on separated flow model which ultimately results in low accuracy for flow classifications such as bubbly and slug flow. In addition, distribution coefficient and drift velocity usually take up a constant value in many drift flux models (Toshiba from Coddington and Macian, 2002). However, lack of physical reality in determination of distribution coefficient and drift velocity does make the use of such drift flux models lose some accuracy.

Regardless of process application, the distribution of gas and liquid simultaneously flowing in pipes is fundamentally important to design engineers as it allows optimisation of pipeline and downstream processes in order to attain an economical

and reliable design for the application in question. The distribution of liquid and gas in gas – liquid two – phase flow in a pipe at specific liquid and gas superficial velocities is better known as flow regime or pattern. The flow regimes are not only dependent upon superficial velocities, but also on the physical parameters of the fluid as well as the pipe geometry. Most flow regime maps are plotted on liquid superficial velocity versus gas superficial velocity, disregarding the influence of the physical properties (i.e. viscosity, density, surface tension) on flow regime. In other words, it means an air – water flow regime map for fixed geometry will most likely introduce some discrepancies in determination of flow regimes of a mineral oil – air system.

Slug flow is a dominant flow pattern in gas – liquid two – phase flow as it occurs at all inclination angles for given set of superficial conditions. The key characteristic of slug flow is its intrinsic unsteadiness. The length of the slugs can acquire values greater than 10 D and have significant momentum (Griffith and Wallis, 1961). Therefore, slug suppressing techniques are used in industrial application in order to restrict any damage to process equipment. These large lengths of slugs generate dynamic fluid forces which introduces structural equipment vibration, resulting in component failures due to fatigue or resonance (Mohammed *et al.*, 2019). In addition to their behaviour, researchers such as Schlegel *et al.* (2012) have quantified a limit on diameter of the pipe for existence of slug flow. According to them, hydraulic diameter less than 40 will sustain slug flow in pipelines due to Rayleigh instability. For variables investigated in this study, hydraulic diameter was around 45 and slug flow was observed, as shown in Chapter 2. Zhu (2019) also utilised the Schlegel *et al.* (2012) criterion to evaluate the hydraulic diameter for their system. Their system had a hydraulic diameter of around 40. Their study focussed on the effect of inclination angle on existence of Taylor bubbles in large diameter pipes. For vertical pipe systems, they did not observe slug flow as well. Instead, they labelled their flow patterns as churn-slug and churn-annular. The emphasis must be placed here that both these works are heavily based on air – water systems and the effect of higher viscosity was completely disregarded.

In case of heavy oil reserves, the transportation of viscous and denser fluids is a demanding problem which requires significant understanding of flow characteristics. Heavy oil are characterised by their high density, high viscosity and high-heavy fraction components. By range proposed by Guo *et al.* (2016), heavy oils have an API range between 10 and 22 (densities between 934 to 1000 kg m<sup>-3</sup>) while it has an oil viscosity of greater than 100 cP. The physical parameters of interest in these industries such as nuclear, petroleum and water are liquid viscosity and gas density while the flow characteristics of interest usually involve liquid holdup (or void fraction), structure velocity and structure frequency. Prediction of these characteristics with minimum discrepancy is imperative for operation of transport systems. However, limited studies on these flow characteristics in relation to effect of liquid viscosity (and gas density) must always be taken into consideration because most correlations for flow characteristics are based on low to medium viscosity systems.

A complete study on the effect of viscosity over a wide range of inclination angles on flow regimes and characteristics has been an area of limited attention within multiphase flow research. Nevertheless, researchers have usually focussed on one inclination or another. For example, Gokcal (2008) only focussed on horizontal for investigating high viscosity effects on flow regimes and characteristics while Alruhaimani (2015) did the same but for vertical inclination. Thus, lack of data on different medium to high viscosities and inclination angles are still an area of limited attention which this research venture attempts to tackle.

Revolving around the framework explained in this sub – section, the aim of the research venture is to investigate the effect of viscosity (particularly medium to high viscosity) on flow regimes and flow characteristics such as liquid holdup, structure velocity and frequency at different inclination angles. Authors have proposed range of values for high and medium viscosity oils. For example, Brito *et al.* (2013) characterised medium viscosity oils having a range of values between 10 cP and 180 cP. In comparison, Pereyra *et al.* (2012) classified that low viscosity oils have a value less than 7 cP while high viscosity oils were classified as having values between 140

cP and 700 cP. The present study utilises three different oils with a distinct dynamic viscosity each – 64 cP, 91.5 cP and 236 cP. According to both studies, 64 cP and 91.5 cP will be considered medium while 236 cP is considered high viscosity.

## 1.2. Objectives

Keeping the aim of the project in mind, key objectives of this project are listed below:

1. To generate different flow regimes at various gas and liquid superficial velocities at different inclination angles for three distinct dynamic viscosities.
2. To acquire liquid holdup time series data of generated flow regimes using ECT
3. To develop and utilise various data processing methods (i.e. cross correlation) in order to study the flow characteristics from ECT data.
4. To identify gaps in viscosity dataset for experimental two – phase flow studies focussed on flow patterns and characteristics. (Discussed more in Chapter 2)
5. To investigate the effect of inclination angle and viscosity on flow characteristics which (in this case) comprise of liquid holdup, structure velocity and structure frequency.
6. To verify trends proposed by previous authors for the effect of viscosity on flow characteristics such as liquid holdup and structure velocity.
7. To generate a new dimensionless flow regime map at each inclination angle for each viscosity
8. To generate an overall flow regime map (covering all viscosities) for each inclination angle.
9. To produce and compare dimensionless flow regime maps for vertical and horizontal orientation developed from historical data to dimensionless flow pattern maps developed using experimental dataset from present study.
10. To develop a generalised liquid holdup model through utilisation of a large databank acquired from literature and in-house

### 1.3. Experimental reasoning

In this section, reasons for experimental setup, data treatment methods and modelling will be briefly explained.

#### 1.3.1. Experimental setup

As mentioned earlier, three different viscosities of silicone oil are utilised in this project. Besides the non – conductive nature of silicone oil needed for ECT, silicone oil can provide similar viscosities to heavy oil which is an area of great interest within the oil and gas industry. The gas phase in this project is air. Utilisation of air is not only safer and easier to handle but it also allows comparison between different datasets in literature as most research investigations are based on air. The rig system (inclinable rig) is explained in detail in Chapter 3. The inclinable rig can be rotated in steps of five degrees from horizontal. Overall, these factors not only allow the effect of viscosity on flow characteristics to be investigated but also the effect of inclination angle can be tackled as well. The diameter of the pipe is 67 mm which is intermediate as described by Escrig (2017).

The instrumentation technique in this research venture is ECT which is a non – intrusive technique providing various useful attributes about the flow distribution in question. The attributes extracted from ECT data involves average liquid holdup, time series traces, PDF, PSD, structure frequency and structure velocity.

#### 1.3.2. Data treatment

The data acquired from ECT was treated using in-house MATLAB codes as the software-based codes were not open source. Using in-house codes allowed not only a better understanding of instrumentation techniques, but it also enables to understand any limitation of the technique as well. Chapter 3 explains treatment of ECT data in detail.

### 1.3.3. Modelling

Chapters 5 and 6 involve modelling of general correlations (liquid holdup / flow regime) with some / limited physical phenomena. The basis for this revolves around evaluation of general model to explain and predict experimental observations.

### 1.4. Structure of the thesis

The complete thesis is divided into seven chapters. The summary of each chapter is as follows:

#### **Chapter 1. Introduction**

In this chapter, contents of the thesis are summarised. It also justifies the motive behind this research project. It describes the problems faced within two – phase flows involving high viscosity oil. In addition, it also explains how these problems can affect the robustness of the two – phase system. Finally, it briefly explains methodology utilised for this research project.

#### **Chapter 2. Literature review**

This chapter describes the related literature survey. Firstly, different flow regimes at horizontal, inclined and vertical inclinations are defined. From this, different transition mechanisms from one flow regime to another were explained in detail. Experimental studies for vertical and horizontal pipelines were also collated and explained in this chapter. Finally, liquid holdup correlations were explained and compared to various other authors.

#### **Chapter 3. Methodology**

In this chapter, inclinable rig along with the instrumentation technique (i.e. ECT) are explained in detail. Each component of the inclinable rig is analysed for its function.

Moreover, treatment of the ECT data was also detailed and critically evaluated. Overall, key parameters that were extracted from ECT data and its treatment involve mean liquid holdup, structure velocity, structure frequency, PDF, and PSD.

#### **Chapter 4. Effect of inclination angle and viscosity on two phase parameters**

In this chapter (Sections 4.3-4.5), the effect of inclination angle on two phase parameters is presented for each investigated viscosity. For each viscosity, the results are presented for three different flow characteristics: liquid holdup, structure frequency and structure velocity.

In this chapter (Section 4.6), the effect of viscosity on two phase parameters is also presented. The results are presented here for each investigated inclination angle, emphasising the effect of viscosity on flow characteristics.

#### **Chapter 5. Investigating the effect of viscosity on flow regime maps**

Flow regimes observed for all viscosities are mapped into a dimensionless flow regime map for each inclination angle. Using the observed flow regimes, transition boundaries capturing the effect of viscosity are proposed for each inclination angle. Thereafter, experimental studies for horizontal and vertical pipelines were utilised in order to create dimensionless flow regime maps for historical data. Finally, effectiveness of the proposed flow regime maps was critically evaluated.

#### **Chapter 6. Development of a new general liquid holdup model**

Literature survey was undertaken in order to collect datasets covering a wide range of physical parameters and diameters for liquid holdup. A general liquid holdup correlation was developed using various datasets and its performance was compared against existing models.

## **Chapter 7. Conclusion and future work**

In this chapter, key findings and issues for each chapter were pointed out. In addition, possibilities for future work were also suggested in this chapter.

## 2. Literature review

Flow pattern classification through utilisation of flow regime maps has been an area of devoted attention by numerous investigators. For most of the work on vertical upflow, flow regime maps have been based on superficial velocities (Sterling, 1968; Wallis, 1969 and Zhang *et al.*, 1997). In comparison, other authors utilise corrected superficial velocities in order to ensure that the given flow regime map can be translated to other set of properties (Weisman and Kang, 1981). The problem with utilising superficial velocities as coordinates for flow regime maps is the lack of physical reality which some authors have attempted to incorporate into their flow regime maps (Hewitt and Roberts, 1969). Nevertheless, some authors have attempted to propose more complex dimensionless numbers such as Abdelsalam *et al.* (2016) study in which their proposed slippage number was correlated to mixture Froude number. Even though it produced promising results in segregating different flow regimes, it does not include some physical properties such as viscosity and surface tension which have an impact on flow regime characterisation. Moreover, Amani *et al.* (2020) investigated the effect of surfactant concentration on flow regime maps for air – water systems. They utilised a liquid Weber number against gas Weber number for their coordinates. In contrast, Da Hlaing *et al.* (2007) utilised liquid Reynolds number against gas Reynolds number as their coordinates for characterisation of different flow regimes. Comparing both of these studies, it can be demonstrated that Amani *et al.* (2020) coordinates do not include viscosity in their coordinates while Da Hlaing *et al.* (2007) does not include surface tension in their coordinates. In addition, most flow regime studies are usually limited to air – water or low viscosity with limited studies on high viscosity oils in recent decades (Alruhaimani, 2015).

Similar limitations persist for horizontal and inclined systems. For horizontal orientation, one of the most commonly used map is Mandhane *et al.* (1974) which utilises liquid versus gas superficial velocity. Their study provides a correction factor which allows their map to be translated for different physical parameters. In contrast,

Taitel and Dukler (1976) utilised a set of five dimensionless numbers by utilising two  $y$  – axes and one  $x$  – axis. Amaya-Gómez *et al.* (2019) also investigated liquid Reynolds number against gas Reynolds number for pipes of all inclinations. Furthermore, promising progress on horizontal flow regime map has been demonstrated by work carried out by Osundare *et al.* (2022). Their study utilised mixture Froude number versus ratio of gas superficial to liquid superficial velocity. Therefore, as discussed in Introduction, effect of physical properties especially viscosity on flow regime transitions will be experimentally investigated in this research investigation with an aim of creating a dimensionless flow regime map based on physical reality which is a lacking factor in many existing flow regime maps.

In addition, prediction of liquid holdup through utilisation of various correlations is also an area of great interest within numerous two – phase applications. While authors have published numerous correlations, each correlation will have its limitation in terms of evaluating liquid holdup. Some limitations are listed here: poor prediction of low liquid holdup values, limited correlations for viscous datasets in comparison to low viscosity systems and lack of experimental data for high and medium viscosities. Due to these limitations, effect of viscosity and inclination angle on two – phase characteristics (structure velocity, frequency and liquid holdup) will also be experimentally investigated.

Hence, Chapter 2 will discuss the literature survey undertaken for this project and will consist of the following topics:

1. Flow pattern classifications are discussed for horizontal, vertical and inclined systems in Section 2.1.
2. Transition mechanisms are compared for all possible flow regimes in Section 2.2.
3. Flow regime experimental studies for vertical and horizontal pipelines are discussed in Section 2.3.
4. Liquid holdup correlations are discussed in Section 2.4.

## 2.1. Flow pattern classifications in two-phase flow

The deformable interface in gas – liquid two – phase flow can take various shapes and forms. Even though the shape of interface is usually difficult to determine as it is in a continual rapid dynamic movement, publications in two – phase flow literature prove that the distribution of liquid and gas phases show similarities across pipe geometries, assisting us in classification of the flow into flow regimes or patterns depending on how the phases are distributed.

Over the last few decades, investigators have differed in how they have classified different flow patterns for pipes of all inclinations, but most authors agree on the following flow regimes mentioned in the following sub-sections.

### 2.1.1. Flow patterns in horizontal pipe

For two-phase flow in horizontal pipes, most researchers agree on six different types of flow regimes which exist due to the different distribution of the liquid and gas phase (Hewitt and Hall-Taylor, 1970). Figure 2.1 shows how the distribution of gas and liquid varies depending on those flow regimes in horizontal pipes.

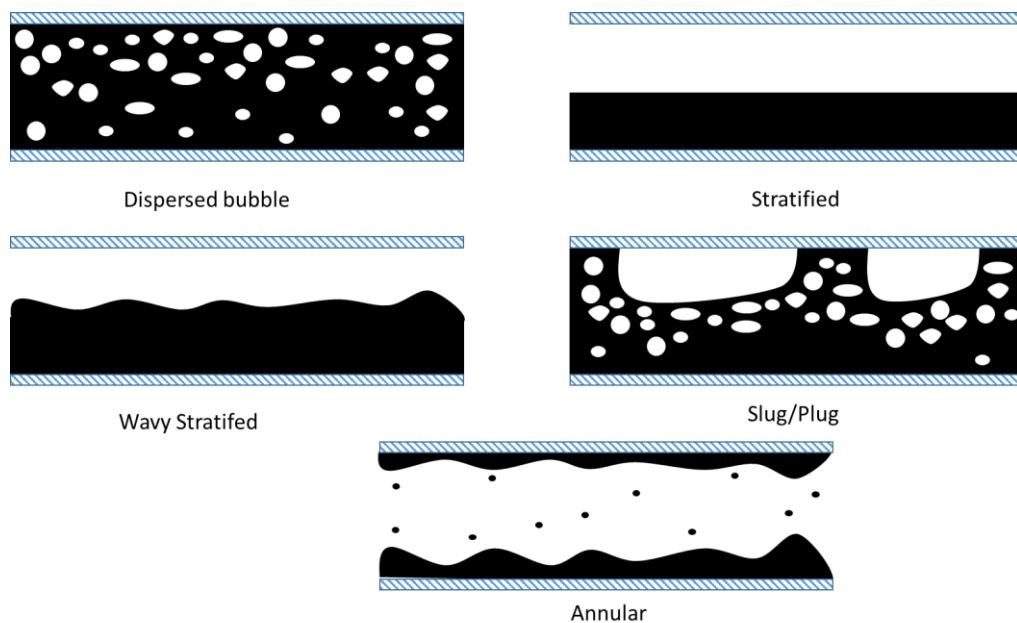


Figure 2.1 – Flow regimes in gas-liquid horizontal flow

## **Bubbly flow**

Bubbly flow occurs as a result of turbulent forces which would disperse the bubbles. This usually occurs at high liquid and low gas superficial velocities. If the liquid superficial velocity is not sufficiently high, gas bubbles would accumulate at the top of the pipe and coalesce to form slug or plug flow.

Experimental studies have shown that the void fraction, interfacial area concentration and bubble frequency as a function of  $r/R$  (Radial Position) reach a local maximum near the upper pipe wall. Moreover, the profiles flatten with rising void fraction. For air – water studies, the peak void fraction and peak interfacial area concentration can reach up to 0.65 and  $1000 \text{ m}^2/\text{m}^3$  respectively (Andreussi *et al.*, 1999; Kocamustafaogullari and Wang, 1991). Kong and Kim (2017) also reported similar values for peak void fraction and interfacial area concentration of 0.6 and  $1000 \text{ m}^2/\text{m}^3$  respectively. Increments in gas flow (or decrease in liquid flow) increases the local void fraction, interfacial area concentration and bubble frequency (Kocamustafaogullari *et al.*, 1994).

Bubble size distribution is also another important feature of bubbly flow in horizontal pipes. The bubble size tends to reduce near the pipe walls as reported in study by Kocamustafaogullari and Wang (1991) for pipe diameter of 50.3 mm. Similar studies on bubble size distribution for different pipe diameters have also been carried out (Sanders *et al.*, 2008; Razzaque *et al.*, 2003). In comparison to vertical bubbly flow, there is no double size peaking as reported by various authors (Michiyoshi & Serizawa, 1986; Matsui, 1984; Liu, 1989).

The axial bubble interface velocity as a function of radial position demonstrated an almost uniform distribution except near the upper pipe wall where there is a rapid decrease in velocity. The interface velocity was found to increase with gas flow (Kocamustafaogullari and Huang., 1994).

Another interesting feature of bubbly flow is its axial liquid mean velocity profile as a function of radial position. The profile has a uniform distribution at all points except near the upper wall where reduction in velocity is observed (Bottin *et al.*, 2014). In addition to that, liquid velocity distribution forms a fully developed turbulent pipe flow in the lower section of the pipe (Iskandrani and Kojasoy, 2001).

### **Stratified flow**

In stratified flow, liquid flows in the lower part of the pipe while the gas flows above it which usually occurs at a low gas and liquid superficial velocity. The interface between gas and liquid phases is smooth, as shown in Figure 2.1. Moreover, interface usually takes a concave shape when the liquid superficial velocity is low (Rea, 1998). Taitel and Dukler (1976) utilised smooth stratified flow with constant liquid layer height as a basis for flow pattern transitions in horizontal flow (details in Section 2.2). They regarded that stratified to wavy, wavy to slug and wavy to annular transitions were dependent upon wave growth on a smooth stratified liquid layer. In wavy stratified flow, interface between gas and liquid phase is wavy because waves grow on a smooth stratified liquid layer initiated due to energy transfer from the faster moving gas stream. This flow regime occurs at similar liquid superficial velocities but slightly higher gas superficial velocities in comparison to smooth stratified flow.

Even though most authors divide stratified flow regime into two different flow patterns (smooth stratified and wavy stratified), various experimental studies have classified stratified flow into different sub-regimes (Wijayanta *et al.*, 2022; Chen *et al.*, 1997; Lin and Hanratty, 1986; Hudaya *et al.*, 2019). Therefore, according to their definitions, stratified flow can be classified into six sub-regimes which are as follows:

- Smooth stratified flow (Wijayanta *et al.*, 2022; Hudaya *et al.*, 2019).
- Two-dimensional wave flow: Flat interface and no curvature at the interface.
- Three-dimensional wave flow: Liquid phase tends to climb the pipe wall due to wave spreading effect. There exists a slight concave down curvature at the gas – liquid interface.

- Roll wave flow: Some parts of liquid phase rise up the wall of the pipe. In contrast to 3D wave, there exists a significant curvature at the gas – liquid interface.
- Entrained droplet flow: Here, liquid droplets are escaped from the liquid stratified surface. Therefore, entrainment and deposition phenomena occur. With a high enough gas velocity, annular flow pattern can occur (Chen *et al.*, 1997).
- Pseudo-slug flow: Liquid slug touches the pipe only momentarily with no occurrence of any blockage. (Lin and Hanratty, 1986; Hudaya *et al.*, 2019).

### **Slug flow**

Observations of various authors have demonstrated that waves usually grow on an initial stratified smooth layer if the liquid flow is increased. For low gas flow rates, wave fills up the pipe and plug or slug flow occurs. Slug or plug flow is characterised by a sequence of liquid slugs followed by longer gas bubbles flowing at top of the pipe with a liquid film beneath it. The liquid slug region travels at much higher velocities in comparison to the velocity of the film beneath the gas bubble in front of the liquid slug. The liquid is ejected from the back of the slug which initially has a high velocity but soon decelerates to a similar velocity to the film velocity.

Depending on the gas superficial velocity, liquid slug region can contain small bubbles. However, for low superficial gas velocity i.e. plug flow, liquid slug region has very insignificant amount of gas bubbles. The existence of small bubbles in the liquid slugs is due to three main factors: fragmentation of the bubble tail, their entrainment out of the bubble wake, and their drift relative to the mean flow (Fabre and Line, 1992).

Another key characteristic of slug flow is variation of slug frequency with mixture superficial velocity. Slug frequency reaches a minimum at a certain mixture velocity and this observation has been demonstrated by various authors for various phase

superficial velocity and pipe diameter (McNulty, 1987; Baker *et al.*, 2003; Heywood and Richardson, 1979).

On the opposite spectrum at very high gas superficial velocities, term frothy surges is utilised to describe the flow pattern where slug region is very aerated (Coney, 1974). When these surges do not reach the top of the pipe, the term semi – slug flow is utilised to describe the flow distribution. It is more correct to call this regime wavy stratified flow (Sakaguchi *et al.*, 1979). An important quantity of interest is measurement of void fraction within the liquid slug region which will vary axially and cross – sectionally. Other important parameters of interest include structure velocity, structure frequency, slug region length, bubble region length and liquid height of the film.

### **Annular flow**

In contrast to slug flow, for higher gas velocities, insufficient liquid is present to fill the pipe thus wave is swept around the pipe to form annular flow (Lin and Hanratty, 1987; Butterworth, 1967; Taitel and Dukler, 1976). Therefore, annular flow can be described as follows: liquid phase partially flowing as a film swept around the pipe and partially as entrained drops carried by the gas core. There is steady interchange of liquid between the film and drops within the gas core. Due to perpendicular nature of the tube axis in horizontal flow, film is thicker at the bottom in comparison to the top of the pipe. It must be pointed out that the liquid film is not smooth but rather is covered with ripples known as disturbance waves.

Difference in film thickness round the periphery is illustrated by Butterworth and Pulling (1973). One interesting parameter which illustrates the approaching transition to annular flow from stratified flow is fraction of wall wetted (for annular, it must be one). It has been illustrated that lower gas velocity is required for fully wetted wall at higher liquid superficial velocities compared to lower liquid superficial velocities (Fukano *et al.*, 1983). Furthermore, it has been observed that entrained fraction is small but significant for stratified flow in comparison to annular flow where

the entrained fraction is much more significant (Meng *et al.*, 2001). The behaviour of different fluid system also makes a difference. For example, it has been demonstrated that entrained fraction was of greater magnitude for air – oil system in comparison to air – water system (Badie, 2000). The difference in terms of physical parameters lies within viscosity and surface tension values however it can't be definitely determined which parameter caused the difference.

Mist flow (or spray flow) is usually classified as an extreme form of annular flow where nearly all of the liquid is transferred from the liquid film as liquid drops into the gas core. Usually, this is result of higher gas superficial velocities compared to typical annular flow.

#### 2.1.2. Flow pattern maps in horizontal pipe

Taitel and Dukler (1976) proposed, as shown in Figure 2.2, that transition boundaries in horizontal pipe can be constructed by utilising five dimensionless numbers:  $X$ ,  $Y$ ,  $Fr$ ,  $T$  and  $K$ . Step by step methodology is provided by Taitel and Dukler (1976) on which dimensionless numbers will be used for a given set of flow conditions.

Solid brown line represents  $T$  while other dimensionless numbers can be determined self – explanatorily. Annular dispersed liquid flow represents all forms of annular flow with various degrees of liquid entrainment while intermittent flow represents plug and slug flow.

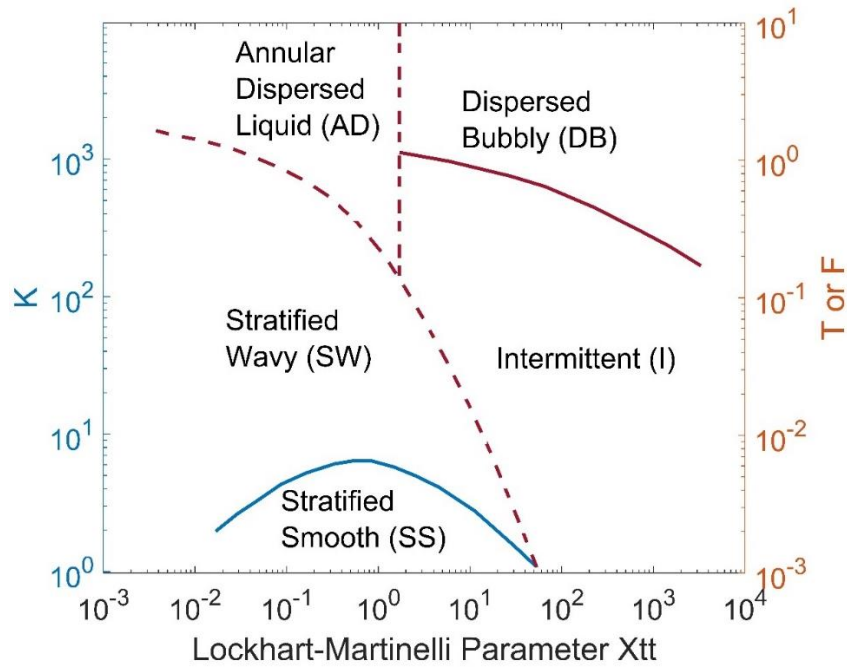


Figure 2.2 – Taitel and Dukler (1976) flow regime map for horizontal pipes

One other popular flow regime map for horizontal pipe systems is Mandhane *et al.* (1974) who considered a large number of data points (5935 data points). Contrasting Taitel and Dukler (1976), it is not a dimensionless flow regime map. Figure 2.3 shows this map for air – water system (see Table 2.2). The transition boundaries used for this map are given in Section 2.2.2.

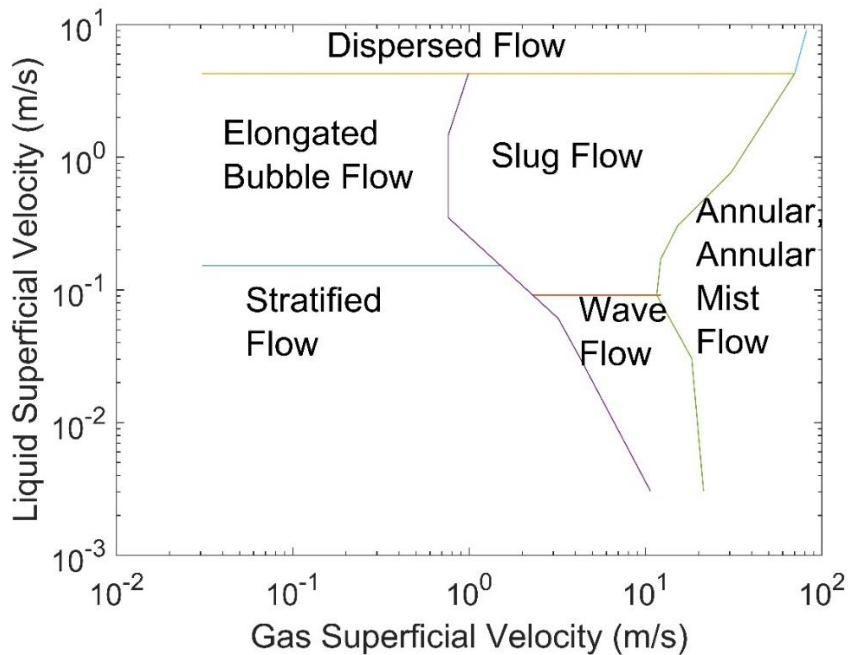


Figure 2.3 – Mandhane *et al.* (1974) flow regime map for air – water (see Table 2.2)

Beggs and Brill (1973) also proposed a flow regime map (Figure 2.4) for horizontal pipes using different coordinates: Froude number  $Fr$  and (liquid) input content  $\lambda$  input which is better known as liquid volume fraction  $q_L/(q_L+q_G)$ .

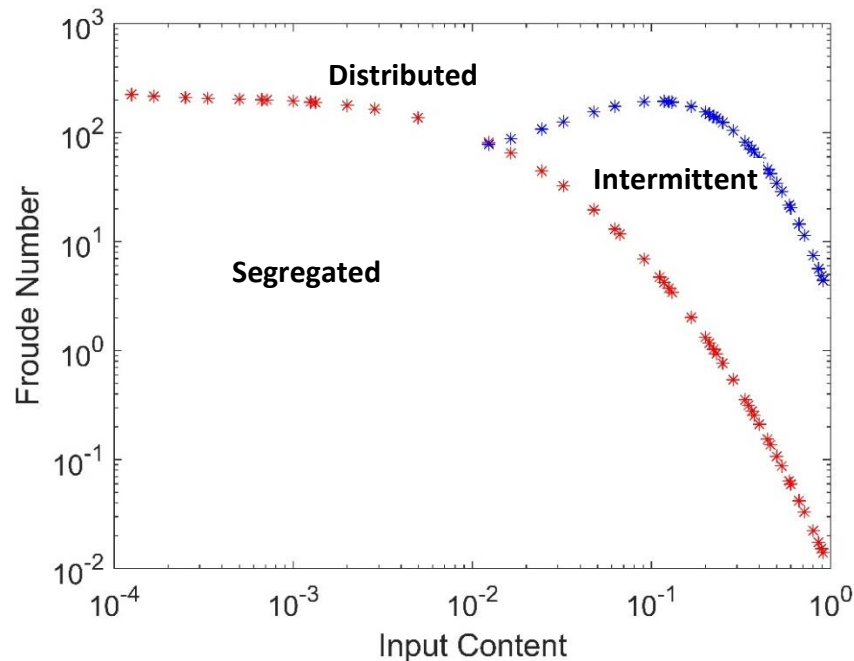


Figure 2.4 – Beggs and Brill map (1973)

In contrast to Taitel and Dukler (1976) and Mandhane *et al.* (1974), there are three flow regimes in this flow regime map: segregated (annular, wavy stratified, stratified), intermittent (plug, slug) and distributed (bubble, mist).

Taitel and Dukler (1987) investigated the effect of viscosity on flow regime transitions, as shown in Figure 2.5. The transition boundary for stratified to intermittent flow is moving down when the liquid viscosity is increased from 90 cP to 165 cP, diminishing the stratified region and increasing the intermittent region. In comparison to low viscosity systems such as air-water, their investigation also showed that the pipe length has a substantial effect on stratified to nonstratified transition for viscous systems.

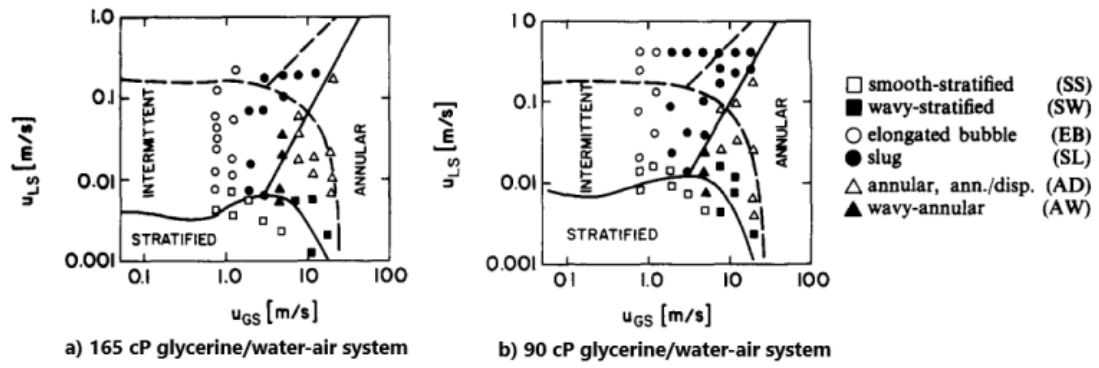


Figure 2.5 – Taitel and Dukler (1987) flow pattern maps investigating the effect of viscosity in a horizontal 3.8 cm diameter pipe (-- shows boundaries for 1 cP; – shows boundaries for the investigated viscosity)

Brito *et al.* (2013) investigated the effect of medium viscosity on flow patterns in a 50.8 mm horizontal pipe, as shown in Figure 2.6. According to Brito *et al.* (2013), smooth stratified region diminishes with viscosity which is in agreement with Taitel and Dukler (1987) map represented in Figure 2.5. TUFFP – University of Tulsa Fluid Flow Project (2003) model was used to obtain the transition boundaries.

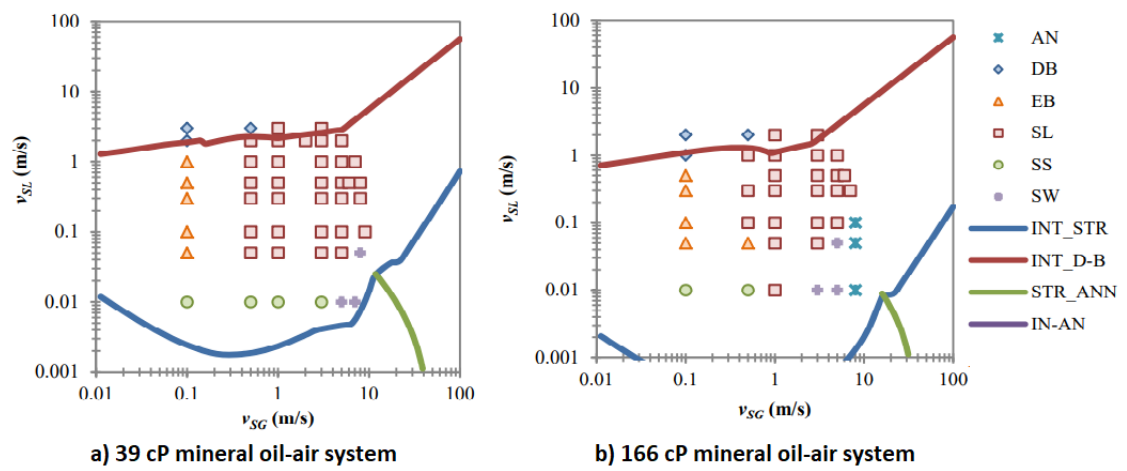
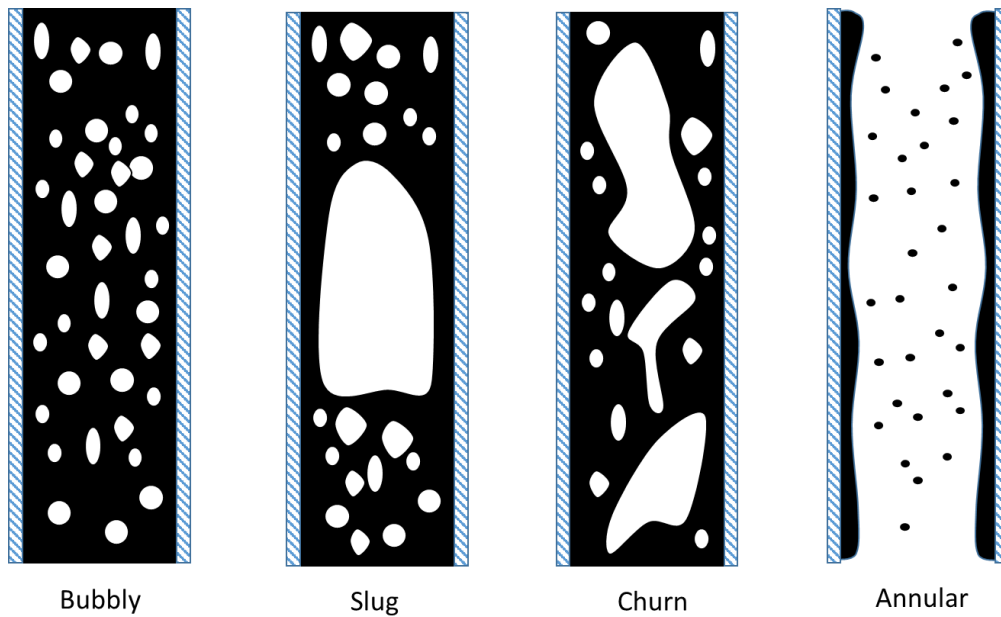


Figure 2.6 – Brito *et al.* (2013) study on effect of medium viscosity on flow patterns for pipe diameter of 50.8 mm with boundaries obtained by TUFFP (2003) model.

### 2.1.3. Flow patterns in vertical pipe

Similarly, many different flow regimes have been used in flow pattern maps for vertical pipes however four main flow classifications can be used to describe flow in vertical pipe systems (Hewitt and Hall-Taylor, 1970). Figure 2.7 shows how the distribution of gas and liquid varies with flow regimes in vertical pipes.



*Figure 2.7 – Flow regimes in gas-liquid vertical flow (increasing gas flow at constant liquid flow)*

#### **Bubbly flow**

In bubbly flow, liquid phase is the continuous medium in which gas phase is dispersed as bubbles. These bubbles are usually of non – uniform size and travel with a complex motion within the liquid phase (with some bubbles undergoing coalescence and other bubbles breaking up). Moreover, this complex motion and behaviour has driven various researchers to classify bubbly flow into sub – regimes / patterns. For example, wall – peaking and core – peaking flows are one pair of sub – regimes (Serizawa and Kataoka, 1988). They based these sub – regimes on the congregation location of the bubbles: near the pipe walls and at the centre of the pipe. Bubble distribution is significantly impacted by the size of bubbles present in the flow. Liu

and Bankoff (1993) found out that larger bubbles (usually greater than 6 mm) stay away from the wall while small bubbles (usually less than 5 mm) gather at the wall.

Not only that, but it was also reported by Shawkat *et al.* (2008) that pipe size has an effect on transition from core to wall peaking bubbly flow. They demonstrated that pipes with a diameter of 50 mm showed a smooth evolution from wall to core peak for increasing void fraction for different liquid flow conditions. In comparison, for pipe diameter of 200 mm, the transition from wall to core peak was not smooth. Moreover, Mendez-Diaz *et al.* (2012) determined critical Weber and Reynolds number criterion for transitions between wall and core peaking bubbly flow. It was found that Reynolds and Weber number of less than 1500 and 8 respectively will result in a wall peak distribution.

Bhaga and Weber (1981) presented a bubble shape regime map. The map and the numbers utilised within the map are discussed in more detail in next section. They defined eight different bubble shape regimes which are as follows: spherical, oblate ellipsoidal, oblate ellipsoidal (disk), oblate ellipsoidal cap, spherical cap (closed wake), spherical cap (open wake), skirted (smooth) and skirted (wavy). Liu *et al.* (2015) investigated the bubble shape in water and high viscosity glycerol aqueous solution. They found that the bubble shape in water is dominated by inertial force and surface tension whereas viscosity plays a bigger role in bubble shape for glycerol aqueous solution. Zhen *et al.* (2019) investigated bubble shape and rise velocity in viscous liquids for high temperatures and pressures. They found out that bubble rise velocity decreases with increasing pressure and decreasing temperature.

Another pair of sub – regimes of bubbly flow is discrete bubbly and dispersed bubbly. For lower liquid superficial velocities, gas bubbles are usually suspended as discrete substances (example would be cap bubbles or ellipsoidal shaped bubbles) in a liquid continuum (low turbulence). In contrast, dispersed bubbly flow occurs at higher liquid velocities due to high turbulence within the liquid phase. The two factors that usually determine bubble size and concentration are collisions between bubbles and bubble break up due to turbulence in the liquid phase (Taitel *et al.*, 1980).

## Slug flow

Slug flow is characterised by a sequence of large bullet shaped bubbles known as Taylor bubbles and a liquid slug region containing gas bubbles. Taylor bubble is surrounded by a thin liquid film flowing downwards. At the end of the Taylor bubble, gas is entrained to create more gas bubbles. These gas bubbles are either carried down into liquid slug or back into the tail of the next Taylor bubble. Moreover, the structure of the liquid slug is quite complex (Mori *et al.*, 1999). Three distinct regions were identified for liquid slug:

1. Swelling region (front zone) is located at the end of the Taylor bubble. This is the area from which the gas is being entrained from and returned into Taylor bubble.
2. Wake zone follows the swelling region. In this region, vortex is observed as reported by various researchers (van Hout *et al.*, 2002)
3. Low void fraction zone constitutes remaining of the liquid slug region

For both upward and downward vertical two-phase flow, it was shown that the Taylor bubble travelling in a vertical pipe is symmetrical in shape. However, when pipe is inclined, the Taylor bubble tends to migrate towards the wall of the pipe (Azzopardi, 2006, p. 71-80; Bouyahiaoui, 2020). Moreover, length of liquid slug and Taylor bubbles have been investigated by various authors. Lengths of liquid slug and Taylor bubbles increase with gas superficial velocity (Azzopardi *et al.*, 2015; Pioli *et al.*, 2012).

Another interesting characteristic of interest for slug flow is the slug holdup for which various authors have investigated the effect of viscosity on this parameter with a focus on developing correlations for its prediction (Nuland, 1999; Kora *et al.*, 2011; Wang *et al.*, 2014; Al-Safran *et al.*, 2015; and Al-Ruhaimani *et al.*, 2017). Al-Safran *et al.* (2015) demonstrated that inertial and viscous forces determine the processes of bubble entrainment, loss and fragmentation in the slug front. These processes governed by inertial and viscous forces determine the slug liquid holdup. Al-

Ruhaimani *et al.* (2017) evaluated the effect of oil viscosity (127–586 cP) on slug liquid holdup for vertical pipes and demonstrated that mixture velocity has a considerable impact on the slug liquid holdup for varying liquid viscosities.

### **Churn flow**

At higher gas superficial velocities, Taylor bubble in slug flow will break down into an unstable pattern which can be defined by the oscillatory motion (or churning motion) of the liquid in the tube. Other terms describing this flow regime is breaking up of slug flow (froth flow) and semi – annular flow. Transition from slug to churn is further discussed in Section 2.2.

The liquid slugs that usually bridge the pipe will become shorter and frothier. The increase in gas superficial velocity also causes the slug to be blown through by the gas phase. The liquid slug region repeatedly breaks, fall backwards and merges with the oncoming slug. In other words, continuity of the liquid slug is repeatedly destroyed (Shoham, 2006, p. 151-154; Taitel *et al.*, 1980). The falling film (in the case of slug flow) is no longer observed because majority of the liquid in this flow regime is either transported in the form of large interfacial waves better known as huge waves and liquid droplets. The shape of the Taylor bubble is also distorted and is much narrower in comparison to one in slug flow (Taitel *et al.*, 1980). The velocity of these huge waves is lower than the liquid slugs and is dependent upon the axial extent of the wave (Sekoguchi and Mori, 1997).

One other characteristic of churn flow is its distinct frictional pressure gradient at lower superficial velocities. Pressure gradient relationship with gas superficial velocity is positive and then negative. This is an important distinction as this contrasts with the pressure gradients for slug and annular flow. For slug flow, it is negative while it is positive for annular flow (Sawai *et al.*, 2004).

## Annular flow

In annular flow, liquid phase partly flows as a film on the pipe walls with small ripples called disturbance waves while remaining of the liquid phase is carried as liquid drops by the high velocity gas core. There is a continuous exchange between the liquid film and liquid drops within the gas core. The processes that occur during these exchanges are better known as entrainment of liquid into the gas core and redeposition of liquid drops back into the film (Whalley *et al.*, 1974). Disturbance waves travel slower than the huge waves in churn flow. Towards the transition from churn to annular flow, huge waves and disturbance waves can co – exist with one another (Sekoguchi and Mori, 1997).

Wang *et al.* (2020) investigated the droplet size observed in annular flow. For increasing viscosity, the PDF of droplet size in annular flow migrates towards larger sizes and a broader range of sizes is seen. Moreover, surface tension has also been investigated by various authors (Ueda, 1979; Jepson *et al.*, 1990). The main findings on effect of surface tension is that size of droplets decreases when surface tension decreases. Simmons and Hanratty (2001) showed that vertical and horizontal annular flows have similar particle size distribution if the gas velocity is high enough.

At even higher gas superficial velocities, all the liquid can be travelling as liquid droplets. In this case, the flow can be described as mist flow. Moreover, at higher liquid superficial velocities, wisps of liquid are observed rather than liquid droplets within the gas core.

### 2.1.4. Flow pattern maps in vertical pipe

One of the most commonly used maps for vertical systems is Taitel *et al.* (1980). Their work was mainly focussed on air – water systems for pipe diameters of 25 and 51 mm. Transition Equations 2.30, 2.42, 2.44, 2.47 and 2.56 were utilised for determination of boundary lines for Taitel *et al.* (1980) map.

In this research study, three different viscosities were explored in order to investigate the effect of liquid viscosity on flow regime transitions. Taitel *et al.* (1980) flow regime map is represented for silicone oil – air system with lowest viscosity ( $\mu = 64$  cP,  $\sigma = 0.0202$  N/m, and  $\rho = 922.5$  kg m<sup>-3</sup>) in Figure 2.8. The entry length to diameter ratio used is 16 for pipe diameter of 0.067 m.

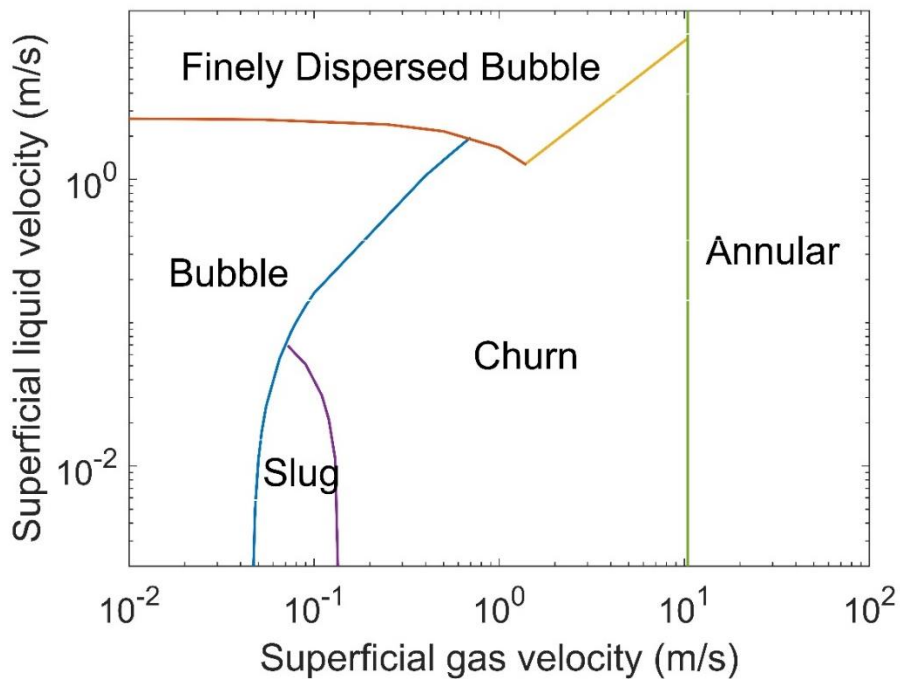


Figure 2.8 – Taitel *et al.* (1980) flow regime map for vertical two-phase system for silicone oil – air system ( $\mu = 64$  cP,  $\sigma = 0.0202$  N/m, and  $\rho = 922.5$  kg m<sup>-3</sup>)

In Figure 2.9, flow pattern map in Alruhaimani *et al.* (2017) study for liquid viscosity of 586 cP is presented. The pipe diameter was 50.8 mm. They carried out this investigation for three other viscosities (127, 213 and 401 cP). They demonstrated that a decrease in viscosity shifts the intermittent – annular transition to occur at high superficial gas velocity, resulting in a larger intermittent region. However, no noticeable effect was noticed for bubble – slug or slug – churn transitions.

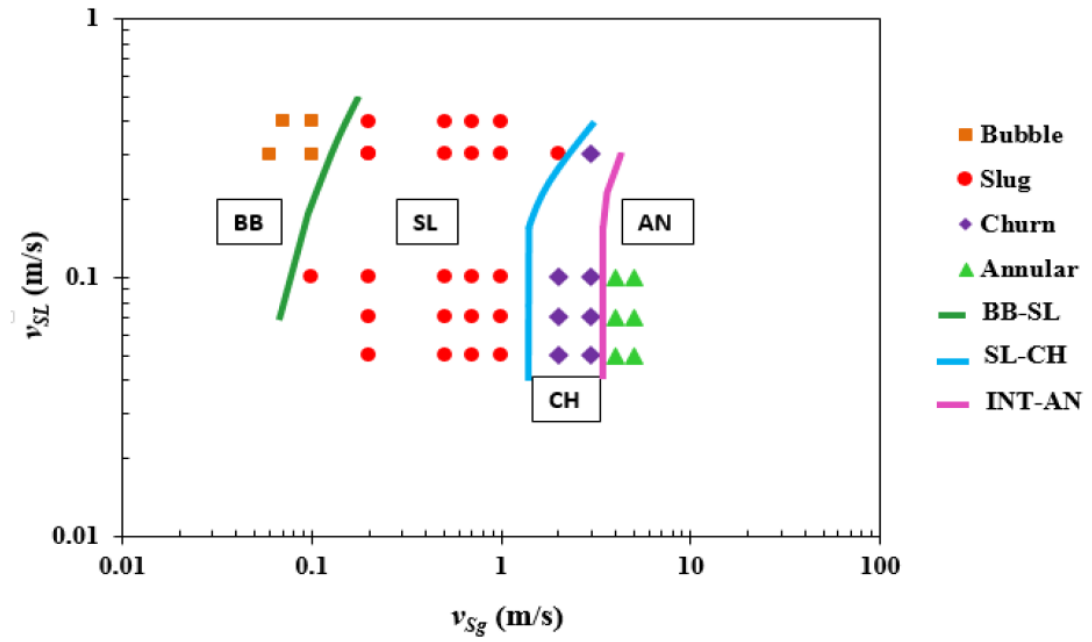


Figure 2.9 - Alruhimani et al. (2017) flow pattern study for oil – air system for pipe diameter of 50.8 mm (Liquid viscosity = 586 cP)

Bhaga and Weber (1981) map is shown in Figure 2.10. The dimensionless numbers used to characterise bubble shape are Reynolds ( $Re$ ), Eotvos ( $Eo$ ) and Morton ( $Mo$ ) number (given by Equations 2.1 -2.3). The characteristic bubble length is presented by  $d_e$  which is calculated by  $\left(\frac{6V}{\pi}\right)^{\frac{1}{3}}$ .

$$Re = \frac{\rho u d_e}{\mu} \tag{2.1}$$

$$Eo = \frac{g d_e^2 \rho}{\sigma} \tag{2.2}$$

$$Mo = \frac{g \mu^4}{\rho \sigma^3} \tag{2.3}$$

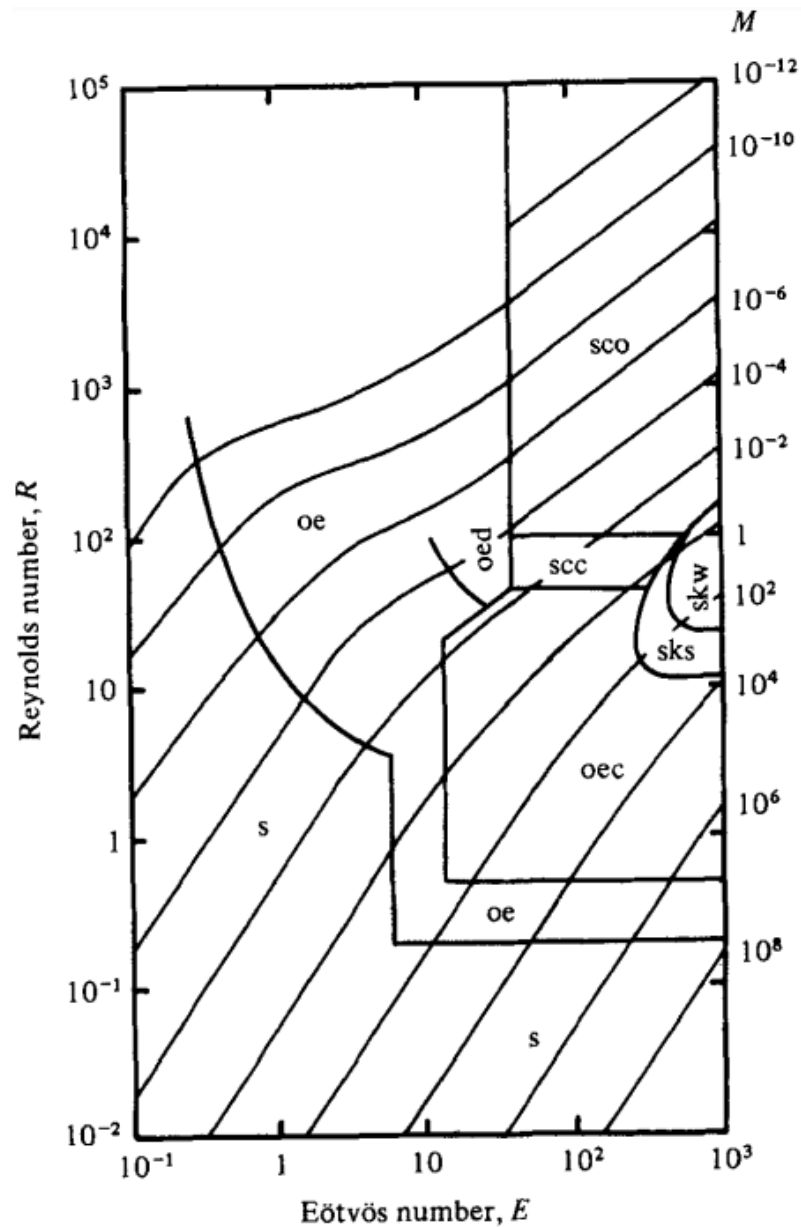


Figure 2.10 – Bhaga and Weber (1981) bubble shape regime map

### 2.1.5. Flow patterns in inclined pipes

Transitions from one regime to another in inclined systems are usually based on definitions of flow regimes in horizontal or vertical pipelines. Therefore, in this section, observations in literature will be discussed since the features of each regime has already been discussed. Most authors have classified flow patterns into four types for inclined pipes: stratified, intermittent, annular, and bubbly (Barnea *et al.*, 1985; Vieira *et al.*, 2018).

Barnea *et al.* (1985) investigated air – water systems for pipe diameters of 25 and 51 mm. Major effect on flow regime transition was observed for small changes in inclination from horizontal by Barnea *et al.* (1985). They showed that smooth stratified flow does not exist for pipe inclination of greater than 0.25 degrees while wavy stratified flow was not observed above 20 degrees for liquid superficial velocities of greater 0.001 m/s. Vieira *et al.* (2018) investigated air – oil systems for pipe diameter of 60 mm. Similarly to Barnea *et al.* (1985), their study did not observe stratified flow above 20 degrees. In contrast, Syikilili *et al.* (2022) showed that stratified wavy flow was observed for inclination angles of 5 – 25 degrees.

Dispersed bubbly was observed for inclination angles of 70° and 90° in the study by Syikilili *et al.* (2022) whereas cap bubble was observed for all inclinations. Vieira *et al.* (2018) could not observe dispersed bubbly flow for their study due to limitations of liquid flow rate. They observed cap bubble for inclinations angles greater than 30 degrees.

Vieira *et al.* (2018) study demonstrated that elongated bubble region diminishes with inclination angle and disappear at inclination angles greater than 30 degrees with cap bubbles occurring at inclination angles greater than 30. The observation is in sync with Barnea *et al.* (1985) as they also observed that elongated bubble region disappears at angles greater than 30 degrees and dispersed bubble flow occurs at angles greater than 30 degrees. In contrast, elongated bubble flow in the study of Syikilili *et al.* (2022) occurs for inclination angles between 0 and 60 degrees. Slug flow was observed at all inclinations for all these studies.

Barnea *et al.* (1985) also demonstrated that small changes in inclination from vertical has little impact on the flow regime, Churn flow was not evident in their study for inclination angles of less than 70 degrees. Similarly, Vieira *et al.* (2018) only observed churn flow for inclination angles of between 70 and 78 degrees.

Vierira *et al.* (2018) demonstrated that annular flow was observed for all inclinations that they tested. They also observed that the gas velocity required to achieve annular flow decreased with increasing inclination angle.

### 2.1.6. Flow pattern maps in inclined pipes

Similarly, some efforts have been made for flow pattern maps in inclined pipes however few researchers have extended the mechanisms used in vertical or horizontal flow regime maps to inclined pipes. One such example is Barnea *et al.* (1985) who extended flow regime transitions from Taitel *et al.* (1980) to inclined systems. For air – water properties, Barnea *et al.* (1985) flow regime maps are plotted in Figure 2.11 for three different inclination angles.

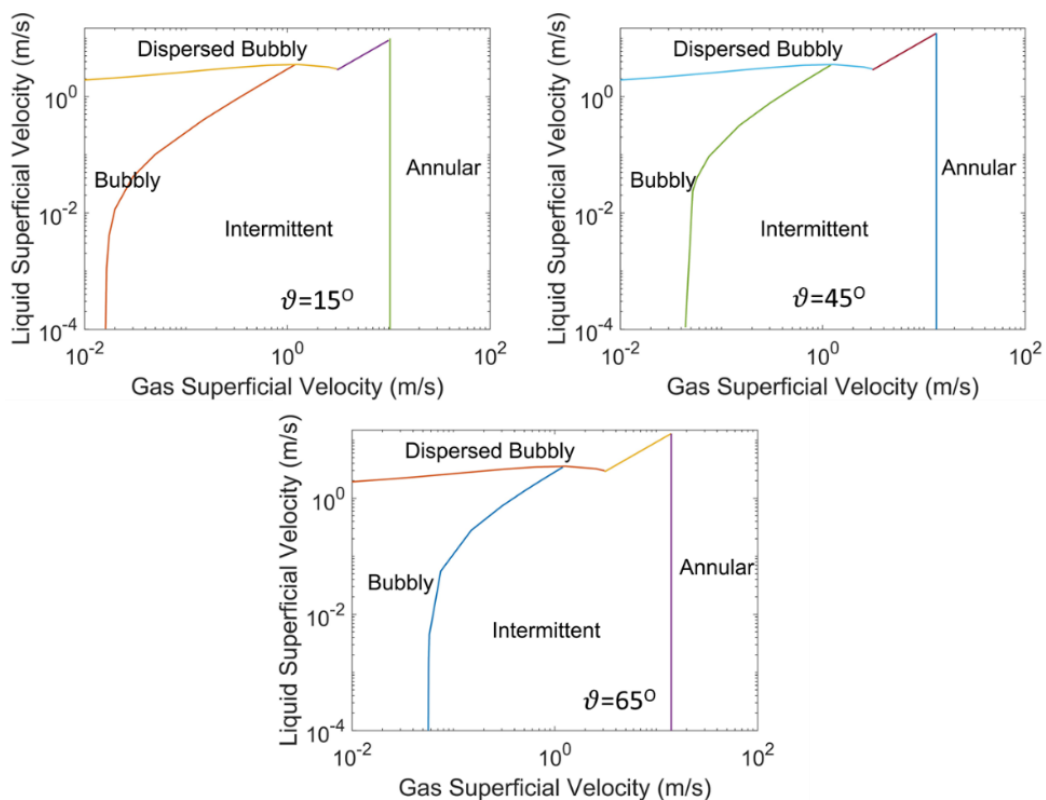


Figure 2.11 – Barnea *et al.* (1985) flow regime air – water properties for inclined systems (from horizontal)

Other commonly used flow regime map includes Weisman and Kang (1981), as shown in Figure 2.12. The transition boundaries are discussed in Section 2.2.2.

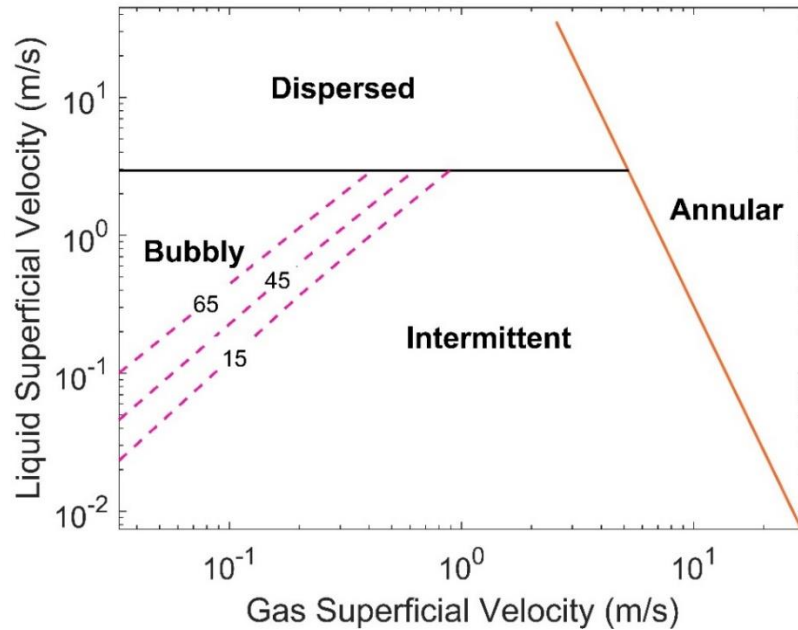


Figure 2.12 – Weisman & Kang (1981) map at different inclinations (65°, 45°, 15°)

## 2.2. Flow pattern transitions in two-phase flow

Most of the work on flow pattern transitions has been empirical which has serious implications because utilising such a flow pattern map on different conditions will lead to considerable amount of error. In this section, various transition models based on physical (some) and empirical concepts will be laid out.

### 2.2.1. Different flow approaches in two-phase flow

Depending on the flow regime and pipe orientation, the approach to determine the flow regime will be different which introduces various parameters and limitations such as phase distribution, velocity profile and nature of flow which must be taken into consideration for accurate prediction. There are three main types of flow approaches utilised in order to determine the void fraction within a pipe system:

1. In homogeneous flow theory, the phases are uniformly mixed and moving at a mixture velocity. Moreover, there is no slip (difference between gas velocity and liquid velocity) between the phases. The main basis for this model is the thermodynamic attainment between the phases. Therefore, this model is no longer applicable when there is a contraction or expansion in pipe because this leads to a change in pressure which in turn leads to flashing of the components in the liquid phase. Due to this, thermodynamic assumption is not maintained anymore. The homogeneous model requires correction for two parameters which are the non-uniform velocity and slip between the two phases.
2. In separated flow theory, each phase has its own unique velocity which means that a slip ratio  $U_R$  exists where  $u_G$  is greater than  $u_L$ . The slip ratio  $U_R$  is one if the flow is homogeneous. Otherwise, various correlations are used in order to evaluate this slip ratio for two-phase flow.
3. Zuber and Findlay (1965) presented the drift flux model in which they introduced a new parameter known as the drift velocity. The drift velocity is known as the velocity of the gas or liquid phase in relation to the mixture. The drift flux model is applicable for flow regimes where liquid phase is continuous.

Before the theories are explained, an expression concerning void fraction in terms of quality and density of the two phases is derived in Equation 2.4 upon taking ratio of liquid mass velocity to gas mass velocity.

$$\frac{G_{TP}x_G}{G_{TP}(1-x_G)} = \frac{u_{GS}\rho_G}{u_{LS}\rho_L} \quad (2.4)$$

The actual velocities for gas and liquid phases can be given in terms of (superficial) gas and liquid velocities respectively by Equations 2.5 and 2.6.

$$u_G = \frac{u_{GS}}{\varepsilon} \quad (2.5)$$

$$u_L = \frac{u_{LS}}{1 - \varepsilon} \quad (2.6)$$

Therefore, an expression for void fraction is obtained as shown in Equation 2.7.

$$\varepsilon = \frac{1}{1 + \frac{u_G (1 - x_G) \rho_G}{u_L x_G \rho_L}} \quad (2.7)$$

Usually, empirical multipliers are used for homogeneous void fraction in order to correct for slip velocity. For example, Armand (1946) proposed that this multiplier can take a value of 0.833 with other authors proposing similar values (Zuber and Findlay, 1965). Otherwise, various correlations are used in order to evaluate this slip ratio ( $U_R$ ) for two-phase flow. One of the simplest correlations was an algebraic correlation (Equation 2.8) by Chisholm (1973). He proposed that slip ratio  $U_R$  relied upon the density of both phases and gas quality.

$$U_R = \left[ 1 - x_G \left( 1 - \frac{\rho_L}{\rho_G} \right) \right]^{\frac{1}{2}} \quad (2.8)$$

Premoli *et al.* (1970) based their correlation based on an analysis of a large data bank of two-phase flow. They proposed an equation for slip ratio  $U_R$  taking the form of Equation 2.9 with a limiting criteria that  $(1+jE_2)^{-1}$  is greater than  $E_2$ . Otherwise, slip ratio  $U_R$  is set to one (homogeneous case). Table 2.1 shows the how each parameter in Equation 2.9 can be calculated.

$$U_R = 1 + E_1 \left( \frac{j}{1 + E_2 j} - jE_2 \right)^{0.5} \quad (2.9)$$

Table 2.1 – Parameters for Premoli et al. correlation (1970)

Parameter	Method of calculation
<b>j</b>	$\frac{\varepsilon_{GH}}{1 - \varepsilon_{GH}}$
<b>E<sub>1</sub></b>	$1.578Re_P^{-0.19} \left(\frac{\rho_L}{\rho_G}\right)^{0.22}$
<b>E<sub>2</sub></b>	$0.0273We_P Re_P^{-0.51} \left(\frac{\rho_L}{\rho_G}\right)^{-0.08}$
<b>Re<sub>P</sub></b>	$\frac{G_L + G_G}{\mu_L} D$
<b>We<sub>P</sub></b>	$\frac{(G_L + G_G)^2 D}{\sigma \rho_L}$

Earlier works on drift flux models only considered one (relative velocity) or the other effect (distribution coefficient) into account for prediction of volumetric distribution. Zuber and Findlay (1965) analysed the effects of flow-concentration distribution and relative velocity of the two phases on the prediction of volumetric distribution across the pipe cross section. Equation 2.10 shows these effects into a single relation.

$$\frac{u_{GS}}{\varepsilon} = C_O(u_{GS} + u_{LS}) + u_O \quad (2.10)$$

### 2.2.2. Flow pattern transitions for two-phase pipe systems

In this section, firstly, the transitions in horizontal and near-horizontal pipes are explained, followed by the transitions in vertical and inclined pipe systems.

#### 2.2.2.1. Transitions in horizontal and near-horizontal pipes:

Taitel *et al.* (1976) developed a model for predicting flow pattern transitions in horizontal and near-horizontal pipes based on equilibrium stratified flow which is shown in Figure 2.13.

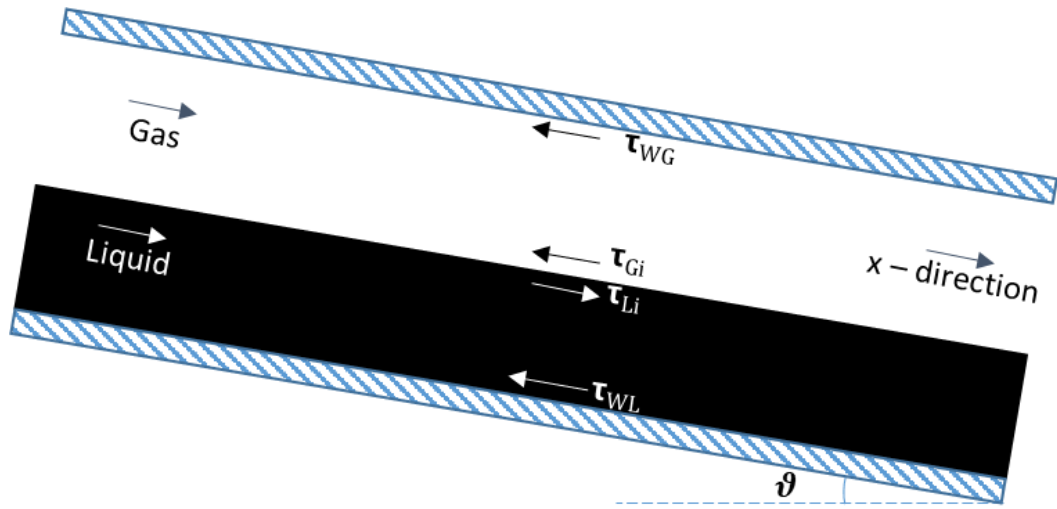


Figure 2.13 – Equilibrium stratified flow

The momentum balance for liquid and gas phase are given by Equations 2.11 and 2.12 respectively. The sign convention used in Equations 2.11 and 2.12 are shown in Figure 2.13 for the interfacial shear stress.

$$-A_L \left( \frac{dp}{dx} \right)_L - \tau_{WL} S_L + \tau_i S_i + \rho_L A_L g \sin(\vartheta) = 0 \quad (2.11)$$

$$-A_G \left( \frac{dp}{dx} \right)_G - \tau_{WG} S_G - \tau_i S_i + \rho_G A_G g \sin(\vartheta) = 0 \quad (2.12)$$

The pressure drops in both phases  $\left( \frac{dp}{dx} \right)_L$  and  $\left( \frac{dp}{dx} \right)_G$  are equated, yielding Equation 2.13. Conventional equations for shear stress and Blasius form friction factors were utilised here.

$$\frac{\tau_{WG} S_G}{A_G} - \frac{\tau_{WL} S_L}{A_L} + \tau_i S_i \left( \frac{1}{A_L} + \frac{1}{A_G} \right) + (\rho_L - \rho_G) g \sin(\vartheta) = 0 \quad (2.13)$$

A dimensional analysis on Equation 2.13 was carried out, resulting in Equation 2.14. The Lockhart-Martinelli parameter X is ratio of pressure drop for liquid flow only to pressure drop for gas flow only (Equation 2.14a) while Y (Equation 2.14b) represent ratio of forces acting on the liquid due to pressure drop and gravity. All the

dimensionless variables depend on  $\widetilde{h}_L$  ( $h_L/D$ ). Therefore, by fixing  $Y$ ,  $X$  can be obtained from  $\widetilde{h}_L$  for all flow conditions, pipe inclination and pipe diameter.

$$X^2 \left[ (\widetilde{u}_L \widetilde{D}_L)^{-n} \widetilde{u}_L^2 \frac{\widetilde{S}_L}{\widetilde{A}_L} \right] - \left[ (\widetilde{u}_G \widetilde{D}_G)^{-m} \widetilde{u}_G^2 \left( \frac{\widetilde{S}_G}{\widetilde{A}_G} + \frac{\widetilde{S}_I}{\widetilde{A}_L} + \frac{\widetilde{S}_I}{\widetilde{A}_G} \right) \right] - 4Y = 0 \quad (2.14)$$

$$X^2 = \frac{\frac{4C_L}{D} \left( \frac{u_{LS}D}{v_L} \right)^{-n} \frac{\rho_L u_{LS}^2}{2}}{\frac{4C_G}{D} \left( \frac{u_{GS}D}{v_G} \right)^{-m} \frac{\rho_G u_{GS}^2}{2}} \quad (2.14a)$$

$$Y = \frac{(\rho_L - \rho_G)g \sin \vartheta}{\frac{4C_G}{D} \left( \frac{u_{GS}D}{v_G} \right)^{-m} \frac{\rho_G u_{GS}^2}{2}} \quad (2.14b)$$

### **Transitions from stratified flow to slug or annular flow**

The transition from stratified flow to slug or annular flow is the result of Helmholtz instability due to the decrease in pressure over a large wave when the gas accelerates over the wave crest (Taitel *et al.*, 1978). Therefore, the transition will only take place when the magnitude of upward Bernoulli force exceeds that of the downward gravity force. Bernoulli's principle is quite important in fluid dynamics and states that total pressure (sum of static and dynamic pressure) at any location along a streamline is constant (Milne-Thomson, 1960). The upward Bernoulli forces are result of decreased pressure over the wave crest when the gas accelerates over the wave crest. At lower gas flows, the growing wave blocks the passage of the gas which leads to the formation of liquid bridge, forming slug flow. When the liquid level is low, the liquid is swept around the pipe's circumference, leading to annular flow.

Using the Kelvin-Helmholtz theory (Milne-Thomson, 1960), the criteria for wave growth for a horizontal pipe is given by Equation 2.15.  $C_1$  is dependent upon the size or amplitude of the waves, as shown in Equation 2.16. The quantity  $h_G'$  is gas height above a disturbed liquid wave peak ( $h_L'$ ).

$$u_G > C_1 \left( \frac{g(\rho_L - \rho_G)h_G}{\rho_G} \right)^{0.5} \quad (2.15)$$

$$C_1 = \left[ \frac{2}{\frac{h_G}{h_G'} \left( \frac{h_G}{h_G'} + 1 \right)} \right]^{0.5} \quad (2.16)$$

For near-horizontal pipe systems with round geometry, Equation 2.17 is utilised where  $C_2$  is equal to  $1 - \widetilde{h}_L$ .

$$u_G > C_2 \left( \frac{g(\rho_L - \rho_G) \cos(\vartheta) A_G}{\rho_G dA_L/dh_L} \right)^{0.5} \quad (2.17)$$

The criteria above in dimensionless terms is given by Equation 2.18 where  $Fr^*$  is the modified Froude number as given in Equation 2.19. Therefore, the transition from stratified to slug or annular can be determined using X and Fr for a fixed Y.

$$Fr^{*2} \left[ \frac{1}{C_2^2} \frac{\widetilde{u}_G^2}{\widetilde{A}_G} \frac{d\widetilde{A}_L}{d\widetilde{h}_L} \right] \geq 1 \quad (2.18)$$

$$Fr^* = \sqrt{\frac{\rho_G}{\rho_L - \rho_G} \frac{u_{GS}}{\sqrt{Dg \cos(\vartheta)}}} \quad (2.19)$$

### **Transitions from smooth stratified flow to wavy stratified**

The transition from smooth stratified flow to wavy stratified flow occurs when the gas velocity is enough for waves to grow without exceeding the criteria required for annular or slug flow transition from stratified flow, as shown in Equation 2.20. This criterion can be given by Equation 2.21 where K is the product of Froude number and square root of Reynolds number based on liquid superficial velocity. Therefore, this transition is determined by X and K for a fixed Y. For sheltering coefficient, Jeffrey

(1925, 1926) recommended a value of 0.3 however Benjamin (1959) proposed a much smaller value of 0.01 to 0.03 for wavy and smooth interfaces.

$$u_G \geq \left[ \frac{4v_L(\rho_L - \rho_G)g\cos(\vartheta)}{s\rho_G u_L} \right]^{0.5} \quad (2.20)$$

$$K \geq \frac{2}{\sqrt{\bar{u}_L}\sqrt{\bar{u}_G}\sqrt{s}} \quad (2.21)$$

### **Transitions from intermittent to dispersed flow**

The transition from intermittent to dispersed bubble flow is dependent upon the turbulent fluctuations due to the liquid phase. The transition will only occur when these fluctuations ( $F_T \gg F_B$ ) overcome the buoyant forces tending to keep the gas at the top. The force of buoyancy per unit length ( $F_B$ ) is given by Equation 2.22.

$$F_B = g(\rho_L - \rho_G)A_G\cos(\vartheta) \quad (2.22)$$

The force due to turbulence  $F_T$  depends on liquid density, interfacial area and radial velocity fluctuation  $\bar{u}'$  (Levich, 1962) and is given by Equation 2.23.

$$F_T = \frac{\rho_L \bar{u}'^2 S_i}{2} \quad (2.23)$$

The radial velocity fluctuation  $\bar{u}'$  is proportional to the liquid friction factor  $f_L$  and liquid velocity squared, as shown in Equation 2.24.

$$\bar{u}'^2 = u_L^2 \left( \frac{f_L}{2} \right) \quad (2.24)$$

Hence, the transition to dispersed bubble flow occurs when  $F_T$  (force due to turbulence) is greater than  $F_B$  (force due to buoyancy) as shown in Equation 2.25. For this flow regime transition, the dimensionless form utilised is shown in Equation 2.26

where T is the ratio of turbulent to gravity forces acting on the gas. The transition is dependent upon X and T for a fixed Y.

$$u_L \geq \left[ \frac{4A_G}{S_i} \frac{g \cos(\vartheta)}{f_L} \left( 1 - \frac{\rho_G}{\rho_L} \right) \right]^{0.5} \quad (2.25)$$

$$T^2 \geq \left[ \frac{8\bar{A}_G}{\bar{S}_i \bar{u}_L^2 (\bar{u}_L \bar{D}_L)^{-n}} \right] \quad (2.26)$$

From these transition conditions, it can be induced that the transitions involving viscous systems such as silicon oil – air will lead to certain changes in their flow regime map:

1. The transition from stratified smooth to wavy stratified flow will occur at a lower gas velocity for a constant liquid velocity. Similarly, stratified smooth to annular flow also shifts to lower gas velocity.
2. Larger diameter will also shift towards higher gas velocities.

Mandhane *et al.* (1974) proposed transition boundaries based on collation of various air-water systems into their map, enabling their use for other systems through the utilisation of two correction factors for gas and liquid superficial velocities. These correction factors are given by Equations 2.27 and 2.28. Table 2.2 shows the boundaries for Mandhane *et al.* (1974) default map. Units are not SI here, as proposed in methodology section and Nomenclature. The units are presented in ft/s. For conversion to SI units (m/s), each value in Table 2.2 can be multiplied by 0.3048.

Table 2.2 – Boundaries for default Mandhane et al. (1974) map

Transition	$u_{SG}$ (ft/s)	$u_{SL}$ (ft/s)
Stratified to elongated bubble	0.10	0.50
	5.00	0.50
Wave to slug	7.50	0.30
	40.00	0.30
Elongated bubble and slug to dispersed bubble	0.10	14.00
	230.00	14.00
	35.00	0.01
Stratified and elongated bubble to wave and slug	14.00	0.10
	10.50	0.20
	2.50	1.15
	2.50	4.80
	3.25	14.00
Wave and slug to annular mist	70.00	0.01
	60.00	0.10
	38.00	0.30
	40.00	0.56
	50.00	1.00
	100.00	2.50
Dispersed bubble to annular – mist	230.00	14.00
	269.00	30.00

$$\text{Corrected X Coordinate} = \left(\frac{\rho_G}{0.0808}\right)^{0.2} \left(\frac{\rho_L}{62.4} \frac{72.4}{\sigma}\right)^{0.25} \left(\frac{\mu_G}{0.0818}\right) \quad (2.27)$$

$$\text{Corrected Y Coordinate} = \left(\frac{\mu_L}{1.0}\right)^{0.2} \left(\frac{\rho_L}{62.4} \frac{72.4}{\sigma}\right) \quad (2.28)$$

**Transitions from bubbly flow to slug flow**

Taitel *et al.* (1980) proposed a model for flow pattern transitions in vertical (steady) gas-liquid flow. The basis behind the dispersed bubbly flow to slug flow transition is an agglomeration process. Typical bubble void fraction for this transition ranges from 0.25 to 0.30 (Griffith and Synder, 1964). Some researchers utilised the maximum packing void fraction of 0.52 in order to determine a bubble void fraction of 0.30 for this (Radovicich and Moissis, 1962). Equation 2.29 shows the equation used for bubbly flow to slug transition by Taitel *et al.* (1980). They used a transition void fraction of 0.25.

$$\frac{u_{GS}}{\varepsilon} = \frac{u_{LS}}{1 - \varepsilon} + u_o \quad (2.29)$$

Therefore, using transition void fraction ( $\varepsilon_{TN}$ ) of 0.25, Equation 2.30 can be obtained for bubble-slug flow transition for two-phase flow in vertical pipes. Griffith and Wallis (1961) used a transition void fraction of 0.18 and Taylor bubble rise velocity (of gas bubbles) of 0.24 basing it solely on air-water systems.

$$u_{LS} = 3u_{GS} - 1.15 \left[ \frac{g(\rho_L - \rho_G)\sigma}{\rho_L^2} \right]^{0.25} \quad (2.30)$$

Mishima and Ishii (1984) used a different value for translational void fraction of 0.3 in comparison to 0.25 used by Taitel *et al.* (1980). They proposed Equation 2.31 for transitions from bubbly to slug flow.

$$u_{LS} = \left( \frac{3.33}{C_o} - 1 \right) u_{GS} - \frac{0.76}{C_o} \left[ \frac{g(\rho_L - \rho_G)\sigma}{\rho_L^2} \right]^{0.25} \quad (2.31)$$

Not only that, but they also related distribution coefficient to gas and liquid densities for bubbly flow to slug transition in round tubes (see Equation 2.32).

$$C_o = 1.2 - 0.2 \sqrt{\frac{\rho_G}{\rho_L}} \quad (2.32)$$

In addition to that, distribution coefficient has been correlated to inclination angle by Bendikson (1984). Furthermore, many researchers have linked  $C_o$  to Reynolds number (Frechou, 1986). Equation 2.33 shows the equation proposed by Bendikson for  $C_o$ .

$$C_o(\vartheta) = C_o(0^0) + [C_o(90^0) - C_o(0^0)] \sin^2 \vartheta \quad (2.33)$$

Not only that, Bendikson (1984) also expressed the drift velocity in terms of horizontal and vertical drift velocities (see Section 2.4), shown in Equation 2.34.

$$u_o = u_{oV} \cos \vartheta + u_{oH} \sin \vartheta \quad (2.34)$$

Barnea *et al.* (1985) incorporated the effect of inclination for bubbly to slug flow by utilising the model by Taitel *et al.* (1980). Equation 2.35 is proposed by Barnea *et al.* (1985) which is similar to Equation 2.30 except the sine term is not incorporated in Equation 2.30.

$$u_{LS} = 3u_{GS} - 1.15 \left[ \frac{g(\rho_L - \rho_G)\sigma}{\rho_L^2} \right]^{0.25} \sin(\vartheta) \quad (2.35)$$

The lift force  $F_L$  ensures that bubbles are kept dispersed while the normal component of buoyancy enhances the transition to slug or plug flow (Barnea *et al.* 1985). Hence, for an inclined pipe to exhibit dispersed bubbly flow at low liquid rates, the condition can be given by Equation 2.36.

$$F_B \cos(\vartheta) < F_L \quad (2.36)$$

The buoyancy ( $F_B$ ) and lift force ( $F_L$ ) are given by Equations 2.37 and 2.38 respectively.  $C_L$  represents the lift coefficient while  $A_N$  is the projected area of the bubble.

$$F_B = \frac{1}{6} D^3 (\rho_L - \rho_G) g \quad (2.37)$$

$$F_L = \frac{C_L A_N \rho_L [u_o \sin(\vartheta)]^2}{2} \quad (2.38)$$

In comparison, Hasan and Kabir (1988) proposed the transition criteria for bubbly to slug regime as Equation 2.39 for inclination from vertical. Their data showed that the rise velocity of the bubbles is not significantly affected by inclination angle.

$$u_{GS} = [0.43u_{LS} - 0.357u_o] \cos(\vartheta) \quad (2.39)$$

Rough slug flow upper limit was determined by earlier researchers for air-water systems. The limit was determined to be 100 mm (Cheng *et al.*, 1998). Schlegel *et al.* (2012) concluded that slug flow does not exist for larger pipes due to Rayleigh-Taylor instability. It must be emphasised Schlegel *et al.* (2012) work is heavily based on air – water systems. They suggested that the slug flow does not exist in pipes with nondimensional diameter greater than 40 (see Equation 2.40). The diameter is nondimensionalised using capillary length scale  $\sqrt{\sigma / g\Delta\rho}$ . Therefore, for slug flow to exist, Equation 2.40 is true according to Schlegel *et al.* (2012).

$$D_H^* = \frac{D_H}{\sqrt{\frac{\sigma}{g\Delta\rho}}} \leq 40 \quad (2.40)$$

However, at higher liquid velocities even for  $\varepsilon > 0.25$ , the turbulent forces break larger bubbles into smaller bubbles especially when the fluctuations lead to formation of bubbles of critical size, as shown in Equation 2.41 (Brodkey, 1967). At this critical size, the coalescence is suppressed, and a dispersed bubble flow persists for  $\varepsilon > 0.25$ .

$$d_{crit} = \left[ \frac{0.4\sigma}{(\rho_L - \rho_G)g} \right] \quad (2.41)$$

Therefore, turbulent-based dispersion at high liquid rates for vertical pipes can be correlated via Equation 2.42 as proposed by Taitel *et al.* (1980).

$$u_{LS} + u_{GS} = 4 \left\{ \frac{D^{0.429}}{v^{0.072}} \left( \frac{\sigma}{\rho_L} \right)^{0.089} \left[ \frac{g(\rho_L - \rho_G)}{\rho_L} \right]^{0.446} \right\} \quad (2.42)$$

Barnea *et al.* (1985) modified Equation 2.42 for the turbulent-based dispersion at high liquid rates to take into account for coalescence, as shown in Equation 2.43.

$$\left[ \frac{\sigma}{(\rho_L - \rho_G)g} \right]^{0.5} \left[ \frac{\rho_L}{\sigma} \right]^{0.6} \left[ \frac{v_L^{0.2}}{D^{1.2}} \right]^{0.4} (u_{LS} + u_{GS})^{1.12} = 1.49 + 8.52 \left[ \frac{u_{GS}}{u_{LS} + u_{GS}} \right]^{0.5} \quad (2.43)$$

Beyond  $\varepsilon=0.52$ , bubble flow cannot exist regardless of the turbulent energy available hence Equation 2.44 can be used for this transition line.

$$\varepsilon = \frac{u_{GS}}{u_{GS} + u_{LS}} = 0.52, \quad 0.48u_{GS} = u_{LS} \quad (2.44)$$

In comparison, Weisman and Kang (1981) also suggested a criterion which is given in Equation 2.45 for transition to dispersed flow. It is independent upon inclination angle. The parameter  $g_c$  is a conversion parameter for gravitational acceleration.

$$\left[ \frac{\left( \frac{dp}{dx} \right)_{SL}}{(\rho_L - \rho_G)g} g_c \right]^{0.5} \left[ \frac{g_c \sigma}{(\rho_L - \rho_G)gD^2} \right]^{0.25} = 9.7 \quad (2.45)$$

In Weisman and Kang (1981) map, intermittent-bubble transition for inclination from vertical is given by Equation 2.46.

$$\frac{u_{GS}}{\sqrt{gD}} = \frac{0.45(u_{GS} + u_{LS})}{\sqrt{gD}} (1 - 0.65 \cos(\vartheta)) \quad (2.46)$$

### Transitions from slug flow to churn flow.

The transition from slug flow to churn flow has been tackled through the use of many different physical concepts (Taitel *et al.*, 1980; Wallis, 1961; Mishima and Ishii, 1984). Taitel *et al.* (1980) based this transition on the oscillatory motion of the liquid slug (entrance effect) and can be evaluated by using Equation 2.47 where  $l_E/D$  is entry length to diameter ratio required to establish stable slug flow.

$$\frac{l_E}{D} = 40.6 \left( \frac{u_M}{\sqrt{gD}} + 0.22 \right) \quad (2.47)$$

In comparison, Mishima and Ishii (1984) used wake effect mechanism to predict the transition from slug to churn flow (see Equation 2.48). They considered that the transition will occur when the average void fraction over the whole section is greater than the slug-bubble section. Just prior to this transition, the tail of preceding Taylor bubble starts to contact with the nose of the following bubble. Due to this, the liquid slugs become unstable due to the wake effect, causing destruction and creation of liquid slugs.

$$\varepsilon = \frac{u_{GS}}{C_O u_M + \frac{0.35(\rho_L - \rho_G)gD}{\rho_L}} \quad (2.48)$$

Another mechanism used by researchers for slug to churn transition is the flooding mechanism, as shown in Figure 2.14. It comprises the transition of downward film flow to upward film flow in case of churn flow (Wallis, 1961). McQuillan and Whalley (1985) correlated the flooding point with dimensionless liquid and gas velocity, as stated by Equations 2.49 and 2.50.

$$u_{L^*} = u_L \rho_L^{0.5} (gD(\rho_L - \rho_G))^{-0.5} \quad (2.49)$$

$$u_{G^*} = u_G \rho_G^{0.5} (gD(\rho_L - \rho_G))^{-0.5} \quad (2.50)$$

The dimensionless velocities can then be linked to a constant C, as shown in Equation 2.51.

$$u_L^{0.5} + u_G^{0.5} = C \quad (2.51)$$

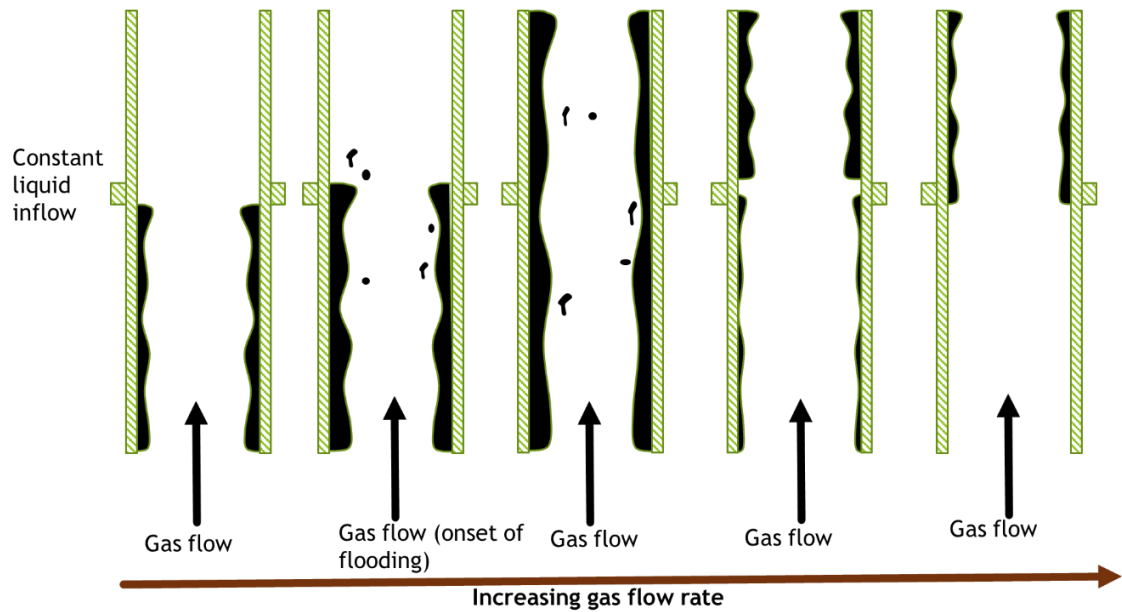


Figure 2.14 – Flooding condition as described by Wallis (1961)

Hasan and Kabir (1988) proposed that slug to churn transition take the form of Equations 2.52 and 2.53.

$$\rho_G u_{GS}^2 = 0.0067(\rho_L u_{LS}^2)^{1.7} \text{ for } \rho_L u_{LS}^2 < 50 \quad (2.52)$$

$$\rho_G u_{GS}^2 = 17.1 \log_{10} \rho_L u_{LS}^2 - 23.2 \text{ for } \rho_L u_{LS}^2 < 3300 \quad (2.53)$$

### Transitions from churn flow to annular flow

Annular flow cannot exist unless the gas velocity is sufficient enough to ensure that the entrained liquid droplets can be carried upwards with gas therefore this transition can be related by drag and gravity forces acting on such drops, as shown in Equation 2.54.

$$u_G = \frac{2}{\sqrt{3}} \left[ \frac{g(\rho_L - \rho_G)d_I}{\rho_G C_D} \right]^{0.5} \quad (2.54)$$

The maximum stable diameter of the drop ( $d_I$ ) is dependent upon the impact force of the gas and surface tension effects holding the gas together and is given by Equation 2.55 (Hinze, 1955). The selected values of  $k$  (critical weber number) and  $C_D$  (drag coefficient) were 30 and 0.44 respectively. Hence, using these values, the following transition line equation (Equation 2.56) was produced.

$$d_I = \frac{k\sigma}{\rho_G u_G^2} \quad (2.55)$$

$$\frac{u_{GS} \rho_G^{0.5}}{[\sigma g(\rho_L - \rho_G)]^{0.25}} = 3.1 \quad (2.56)$$

Moreover, for annular flow in inclination from horizontal, Equation 2.56 was modified by Barnea *et al.* (1985) in order to incorporate the effect of inclination by multiplying 3.1 by  $[\sin(\vartheta)]^{0.25}$ .

Also, the transition to annular flow in Weisman and Kang (1981) map for all inclination angles is given by Equation 2.57.

$$Fr_G(Ku_G) = 25 \left( \frac{u_{GS}}{u_{LS}} \right)^{\frac{5}{8}} \quad (2.57)$$

## 2.3. Experimental flow regime studies in vertical and horizontal pipelines

### 2.3.1. Experimental studies on vertical inclination

In this section, experimental studies on flow regime in vertical pipelines will be explored. Most of the work is focussed on low viscosity (usually air – water). One key objective of this study is to construct flow regime maps through utilising historical datasets for vertical and horizontal orientations. Since the focus of the thesis is on

effect of medium to high viscosities on flow regime classifications, a complete review on flow regime studies will be carried out for viscosities of all magnitudes. Therefore, the selection of data was based on accessibility of data available in literature.

Spedding *et al.* (1998) utilised visual/video techniques and pressure loss fluctuation characteristics to study flow patterns in a 26 mm diameter vertical pipe. They presented two new transitional relations for predicting slug to churn and churn to annular boundaries. Similarly, Taitel *et al.* (1980) experimentally investigated flow patterns in 25 mm and 51 mm pipes for air – water systems. They also theoretically developed flow pattern transitions as discussed in Section 2.2, showing good agreement between the two. Moreover, Govier and Short (1958) investigated effect of four different diameters (16 mm to 63.5 mm) on flow regimes for an air – water systems. They classified their flow regimes into the following groups: slug, froth, ripple and film. Barnea *et al.* (1983, 1985) investigated flow patterns in pipes of varying diameters (12.3, 25, 51 mm) for air – water systems. Some other experimental studies on flow patterns for air – water systems include Ansari and Azadi (2016), Mi *et al.* (2001), Kaji *et al.* (2009) and Shanmugam (1994).

Moreover, Rozenblitz *et al.* (2006) studied the effect of surface tension on flow patterns in a vertical pipe with a diameter of 25 mm. They compared flow regimes in air – water and air – water system with surfactant. They observed changes in the tendency to coalescence between air bubbles however the transition boundaries did not greatly vary. Moreover, they classed their flow regimes into four different classes: slug, churn, bubbly and annular.

Rosa *et al.* (2010) utilised the visual observations along with void fraction traces and its associated PDF to study flow patterns for an air – water system in a 26 mm diameter vertical pipe. Differently to Rozenblitz *et al.* (2006), they classified the flow regimes into six different classes: bubbly, spherical cap, slug, unstable slug, semi-annular and annular. Furthermore, Lucas *et al.* (2005) extensively investigated air – water bubbly and slug flow regime in a vertical pipe with a diameter of 51.2 mm.

Similarly, Julia *et al.* (2008) also utilised a similar diameter size of 50.8 mm in order to study flow regimes in vertical pipelines for an air – water system.

Other than surface tension, other authors have focussed on effect of viscosity on flow patterns in vertical pipes as well. Some medium viscosity works include Szalinski *et al.* (2010) and Furukawa and Fukano (2001). Szalinski *et al.* (2010) compared the flow patterns in a silicone oil (5 cP) – air and water – air systems for a pipe diameter of 67 mm. The air – water system experienced more coalescence than air – silicone oil (5 cP) system, resulting in larger bubbles in air – water system. The churn – annular transition occurs at a low gas velocity for silicone oil compared to water. Moreover, Furukawa and Fukano (2001) also investigated the effect of three viscosities (1, 6 and 17 cP) on flow patterns for a pipe diameter of 19.2 mm. They observed that bubbly to slug flow transition occurs at a lower gas velocity with increasing liquid viscosity while the churn to annular flow regime occurs at higher gas velocity with increasing liquid viscosity.

There seems to be a lack of literature data in medium / high viscosity regime (i.e. 16 cP to 127 cP). Nevertheless, authors such as Alruhaimani (2015) and Akhiyarov *et al.* (2010) both studied high viscosity systems. Alruhaimani (2015) studied the effect of four liquid viscosities (127, 213, 401 and 586 cP) on flow regimes in pipe diameter of 50.8 mm. They classified the flow regimes into four different classes: bubbly, slug, churn and annular. They found that a decrease in liquid viscosity causes the intermittent-annular transition to occur at a higher gas superficial velocity, resulting a larger intermittent region. Moreover, they also observed that viscosity had no effect on bubble-slug and slug-churn transitions. They also observed that bubbly flow only occurred at high liquid superficial velocities (greater than 0.3 m/s) and low gas superficial velocities. In comparison, Akhiyarov *et al.* (2010) only studied slug flow in a mineral oil – natural gas system for a pipe diameter of 52.5 mm.

### 2.3.2. Experimental studies on horizontal inclination

The availability of data for horizontal pipes for any scenario is limited. Weisman *et al.* (1979) studied different two-phase systems and diameters to study the effect on flow patterns and transitions. They utilised visual observations along with pressure drop fluctuations to identify flow regimes. In comparison, Barnea *et al.* (1985) studied the effect of diameter (25, 51 mm) in an air – water system on flow patterns. Moreover, Govier and Omer (1962) also investigated air – water system in order to study flow pattern classifications for a pipe diameter of 26 mm. They used the following classifications: stratified, wavy, plug, slug and bubbly.

Morshed *et al.* (2020) also investigated the effect of Newtonian and Non-Newtonian liquids on flow pattern classifications for a pipe diameter of 73.66 mm. Similarly, Lamari (2001) also investigated air – water systems for a pipe diameter of 25.4 mm in order to study flow regime classifications. Moreover, Xia and Chai (2012) also investigated the effect of inclination angle from horizontal on flow regime classifications for a pipe diameter of 150 mm.

Limited studies by authors have been carried out on high viscosities. For example, Gokcal *et al.* (2006) utilised a high viscosity oil with air in order to study the effect of viscosity on flow patterns for a pipe diameter of 50.8 mm. The viscosities in their study were 587 cP, 378 cP, 257 cP and 181 cP. The flow regimes observed using high speed video camera were stratified wavy, elongated bubble, slug, annular, slug – dispersed and slug – annular. They observed that the shape of the elongated bubble change with an increase in liquid viscosity while frequency of elongated bubble also increased. Similarly, Taitel and Dukler (1987) also investigated the effect of viscosity (90 cP and 165 cP) on flow patterns in a 38 mm pipe. However, they utilised water – glycerine solutions instead of high viscous oil to achieve a desired viscosity. They reported that pipe length effects significantly influence the transition from stratified flow to nonstratified for high viscosity oils compared to low viscosity oil.

Brito *et al.* (2013) investigated effect of medium to high viscosity oils for a pipe diameter of 50.8 mm. The viscosities investigated in their study were 39, 60, 108 and 166 cP. While most of their dataset corresponded to slug flow, other flow regime investigated were stratified smooth, stratified wavy, elongated bubble, dispersed bubble and annular. They demonstrated that stratified smooth region diminishes with an increase in liquid viscosity. Whereas, they observed that transition from intermittent flow to dispersed bubble flow occurs at higher superficial gas velocities for low viscosity systems than high viscosity system.

#### 2.4. Liquid hold-up (or gas void fraction) models

The liquid holdup or gas void fraction correlations are usually classified into four different types. Firstly, slip ratio correlations calculates gas void fraction (hence liquid holdup) based on the slippage between both phases. Secondly,  $K\varepsilon_H$  correlations evaluates gas void fraction by assigning a multiplier to the homogeneous gas void fraction. The third type of gas void fraction correlations is the drift flux model which takes into account the non-uniformity of the flow through relating the gas velocity ( $u_{GS}/\varepsilon$ ) to the distribution coefficient  $C_0$ , mixture velocity  $u_M$  and drift velocity  $u_0$ . Finally, general correlations are usually empirical correlations in nature with some or limited physical principles.

#### **Vertical Inclination**

For slug flow in vertical pipes, vertical drift velocity ( $u_{OS}$  or  $u_{OV}$ ) takes the form given by equation 2.58 (Davies and Taylor, 1950). The constant 0.328 matches closely to experimental measurements of 0.35 (Bendikson, 1984).

$$u_{OV} = u_{OS} = 0.35 \left( 1 - \frac{\rho_G}{\rho_L} \right) \sqrt{gD} \quad (2.58)$$

The vertical slug liquid holdup correlation proposed by Griffith and Wallis (1961) is given in Equation 2.59 where  $u_T/u_m$  can be derived from the drift flux equation (see Equation 2.60).

$$1 - \varepsilon = 1 - \frac{1 - \lambda}{\frac{u_{TR}}{u_M}} \quad (2.59)$$

$$\frac{u_{TR}}{u_M} = C_0 + \frac{u_{OS}}{u_M} \quad (2.60)$$

### **Horizontal Inclination**

For horizontal pipe systems, Benjamin (1968) found that horizontal drift velocity can be given by Equation 2.61.

$$u_{OH} = 0.54 \left( 1 - \frac{\rho_G}{\rho_L} \right) \sqrt{gD} \quad (2.61)$$

Beggs and Brill (1973) proposed that liquid holdup can be evaluated by using the horizontal holdup as a correction factor as shown in Equation 2.62. Table 2.3 shows the correlations put forward by Beggs and Brill (1973) for coefficient C and horizontal holdup. The parameter  $N_{LV}$  is the liquid velocity number (see equation 2.72).

$$H_L(\vartheta) = H_L(0) \left\{ 1 + C \left[ \sin(1.8\vartheta) - \frac{1}{3} \sin^3(1.8\vartheta) \right] \right\} \quad (2.62)$$

Table 2.3 – Correlations for horizontal holdup and C for uphill and downhill flow

Flow Pattern (Horizontal)	$H_L(0)$ – Holdup in horizontal pipe	C+ (uphill)	C- (downhill)
Segregated	$\frac{0.98\lambda^{0.4846}}{Fr^{0.0868}}$	$(1 - \lambda) \ln \left[ \frac{0.011N_{LV}^{3.539}}{\lambda^{3.768}Fr^{1.614}} \right]$	
Intermittent	$\frac{0.845\lambda^{0.5351}}{Fr^{0.0173}}$	$(1 - \lambda) \ln \left[ \frac{2.96\lambda^{0.305}Fr^{0.0978}}{N_{LV}^{0.4473}} \right]$	$(1 - \lambda) \ln \left[ \frac{4.7N_{LV}^{0.1244}}{\lambda^{0.3692}Fr^{0.5056}} \right]$
Distributed	$\frac{1.065\lambda^{0.5824}}{Fr^{0.0609}}$	0	

### Inclined Inclination

For bubbly flow, the void fraction for inclined pipes can be evaluated by using Hasan and Kabir (1988) proposition – Equation 2.63. The range of angle used here were up to 32 ° from vertical.

$$\varepsilon = \frac{u_{GS}}{C_O u_M + u_{OB}} \quad (2.63)$$

The rise velocity for large bubbles in bubbly flow is given by Equation 2.64. It is dependent upon the densities of the two phases as well as the interfacial surface tension. It must be stressed that Eotvos numbers of less than one must be avoided as the effect of viscosity become prominent at those numbers (Harmathy, 1960).

$$u_{OB} = 1.53 \left[ \frac{g(\rho_L - \rho_G)\sigma}{\rho_L^2} \right]^{0.25} \quad (2.64)$$

Hasan and Kabir (1988) also presented an equation for slug flow void fraction of the same form as Equation 2.63, but the drift velocity is dependent upon pipe inclination as shown in Equation 2.65.

$$u_{OS\vartheta} = u_{OS}\sqrt{\cos(\vartheta)} (1 + \sin(\vartheta))^n \quad (2.65)$$

Bonnecaze *et al.* (1971) presented the liquid holdup in slug flow for inclined pipelines in the form of Equation 2.66.

$$1 - \varepsilon = 1 - \frac{1 - \lambda}{\left[ 1.2 + \frac{0.35 \left( 1 - \frac{\rho_G}{\rho_L} \right) \sqrt{gD}}{u_M} \right]} = 1 - \frac{1 - \lambda}{\left[ 1.2 + 0.35 \left( 1 - \frac{\rho_G}{\rho_L} \right) \sqrt{Fr} \right]} \quad (2.66)$$

Also, the liquid film holdup for vertical pipes can be given by Equation 2.67.

$$u_M = (\varepsilon_F)u_T + (1 - \varepsilon_F)u_F \quad (2.67)$$

Moreover, Woldesemayat and Ghajar (2007) also proposed a void fraction correlation (independent upon flow regimes) which is given by Equation 2.68.  $P_a/P_s$  denotes the ratio of atmospheric pressure to system pressure.

$$\varepsilon = \frac{u_{SG}}{u_{SG} \left( 1 + \left( \frac{u_{SL}}{u_{SG}} \right) \left( \frac{\rho_G}{\rho_L} \right)^{0.1} \right) + 2.9 \left[ \frac{gD\sigma(1 + \cos\vartheta)(\rho_L - \rho_G)}{\rho_L^2} \right]^{0.25} (1.22 + 1.22 \sin\vartheta)^{\frac{P_a}{P_s}}} \quad (2.68)$$

Mukherjee and Brill (1983) proposed a general type of correlation for uphill liquid holdup (Equation 2.69) where they fitted six constants ( $C_1$  to  $C_6$ ).

$$H_L = \exp (C_1 + C_2 \sin \vartheta + C_3 \sin^2 \vartheta + C_4 N_L^2) \frac{N_{GV}^{C_5}}{N_{LV}^{C_6}} \quad (2.69)$$

In Equation 2.69,  $N_L$ ,  $N_{GV}$  and  $N_{LV}$  are the liquid viscosity number, gas velocity number and liquid viscosity number (see Equations 2.70 – 2.72).

$$N_L = \mu \left( \frac{g}{\rho_L \sigma^3} \right)^{0.25} \quad (2.70)$$

$$N_{GV} = u_{SG} \left( \frac{\rho_L}{g\sigma} \right)^{0.25} \quad (2.71)$$

$$N_{LV} = u_{SL} \left( \frac{\rho_L}{g\sigma} \right)^{0.25} \quad (2.72)$$

For all the drift flux models, Equation 2.10 can be used to calculate the void fraction. In Zuber and Findlay (1965) correlation, distribution coefficient is fixed at 1.2 while drift velocity is calculated using Equation 2.64. Similarly, Toshiba from Coddington and Macian (2002) fixed distribution coefficient and drift velocity at 1.08 and 0.45 respectively for his drift – flux correlation – see Equation 2.73.

$$u_G = 1.08u_M + 0.45 \quad (2.73)$$

However, Jowitt *et al.* (1984) from Leung (2005) related  $C_o$  to gas and liquid densities rather than proposing a constant value. The equation proposed by them for distribution coefficient is given by Equation 2.74 while Equation 2.75 shows the drift velocity for this correlation.

$$C_o = 1 + 0.796 \exp \left( -0.061 \sqrt{\frac{\rho_G}{\rho_L}} \right) \quad (2.74)$$

$$u_o = 0.034 \left( \sqrt{\frac{\rho_G}{\rho_L}} - 1 \right) \quad (2.75)$$

Choi *et al.* (2012) also proposed a drift flux model where the distribution coefficient is given by 2.76 while the drift velocity is given by Equation 2.77. The parameters A and B in Equation 2.77 are 0.0246 and 1.606 respectively.

$$C_o = \frac{2}{1 + \left(\frac{Re}{1000}\right)^2} + \frac{1.2 - 0.2 \sqrt{\frac{\rho_G}{\rho_L}} (1 - \exp(-18\varepsilon))}{1 + \left(\frac{1000}{Re}\right)^2} \quad (2.76)$$

$$u_o = A \cos\vartheta + B \left(\frac{g\sigma\Delta\rho}{\rho_L^2}\right)^{0.25} \sin\vartheta \quad (2.77)$$

In contrast, Armand – Massina from Leung (2005) correlation is a  $K_{\varepsilon H}$  correlation which is given by equation 2.78.

$$\varepsilon = [0.833 + 0.167x] \varepsilon_{GH} \quad (2.78)$$

In addition to review of liquid holdup models, open literature survey for experimental studies for liquid holdup is included in Chapter 6.

## 2.5. Conclusion

In this chapter, literature survey on two – phase flow was undertaken with focus on the following topics: flow regime classifications (and maps), flow regime transitions and experimental flow regime/pattern studies in literature and existing liquid holdup models in literature.

In vertical pipelines, there are four main types of flow regimes: bubbly, slug, churn, and annular. As discussed, the most commonly used flow regime map is Taitel *et al.* (1980) which is a semi – empirical flow regime map. Other commonly utilised flow regime maps are Mishima and Ishii (1984) and Hewitt and Roberts (1969). Whereas, in horizontal pipelines, there are six main types of flow regimes: stratified, wavy, slug, plug, annular and bubbly (Hewitt and Hall-Taylor, 1970). It was determined that the

most commonly used flow regime maps for horizontal pipelines are Taitel and Dukler (1976) and Mandhane *et al.* (1974). Taitel and Dukler (1976) is a dimensionless flow regime map utilising five different dimensionless numbers as discussed in Section 2.1 while Mandhane *et al.* (1974) utilised superficial coordinates and considered a large amount of data points. Furthermore, it considers slug and plug (or elongated bubble) flow separately unlike Taitel and Dukler (1976). Mechanisms for flow regime transitions from one flow regime to another in inclined, vertical and horizontal orientation were further discussed in Section 2.2.

As discussed earlier, numerous experimental studies on flow pattern classification exists in vertical and horizontal pipelines for low viscosity. For vertical pipe systems, various experimental have been published for air – water flow systems (Spedding *et al.*, 1998; Taitel *et al.*, 1980; Govier and Short, 1958; Barnea *et al.*, 1983 and Barnea *et al.*, 1985). Effect of surface tension have also been investigated by various authors (Rozenblitz *et al.*, 2006). Even though studies have been limited on medium to high viscosity, some notable works include Szalinski *et al.* (2010), Furukawa and Fukano (2001), Alruhimani (2015) and Akhiyarov *et al.* (2010). From the literature survey, the lacking factor seems to be datasets or studies on medium to medium – high viscosities (i.e 16 cP to 127 cP). Similarly for horizontal pipelines, low viscosity datasets are numerous in literature (Weisman *et al.*, 1979; Barnea *et al.*, 1985; Govier and Omer, 1962 and Lamari, 2001). Notable studies for high viscosity systems include Gokcal *et al.* (2006), Taitel and Dukler (1987) and Brito *et al.* (2013). Even though a decent number of high viscosity studies exist for horizontal systems, lack of (or limited) coverage of each flow regime in a given experimental study is a limiting factor.

Different types of liquid holdup or gas void fraction correlations were also discussed in Section 2.4 and are as follows:

1. Slip ratio correlations calculates liquid holdup based on slippage that exists between gas and liquid phase. An example of such correlation is Premoli *et al.* (1970).

2.  $K_{\epsilon_H}$  correlations applies a multiplier to the homogenous gas void fraction. Armand – Massina correlation is an example of this correlation (See equation 2.78).
3. Drift flux models are based on relating gas velocity ( $u_{GS}/\epsilon$ ) to distribution coefficient, mixture velocity and drift velocity. Jowitt *et al.* (1984) is an example of drift flux model.
4. General correlations are usually empirical or semi – empirical models. In Section 2.4, Mukherjee and Brill (1983) was presented as an example (See Equations 2.69 – 2.72).

## 3. Methodology

### 3.1. Introduction

The test section of the inclinable rig consists of an acrylic pipe with an inner diameter and length of 67 mm and 6 m respectively. The rig utilised was already assembled and has been used by various researchers at University of Nottingham (Abdulkadir, 2011; Hernandez-Perez, 2008; Escrig, 2017). The transparent nature of the pipe is advantageous to the aims and objectives of this project discussed in Chapter 1 as it allows flow distribution of the phases (i.e. flow patterns or regimes) to be observed. Furthermore, ECT (Electrical Capacitance Tomography) utilised in this study has two sensors located at 4.4 and 4.489 m from the mixer entry. ECT data can be utilised/treated in order to evaluate various flow characteristics: Probability Density Function, Power Spectral Density, time series, liquid holdup, structure velocity and structure frequency. The details of the twin – plane ECT are discussed in Section 3.3 with analysis techniques discussed in Sections 3.4 and 3.5.

The rig is installed with a tilting boom, allowing upward two – phase flow to be investigated at different angles from horizontal. Other features of the rig are further discussed in Section 3.2.2. Fluids utilised in this study are silicone oil and air. Using silicone oil is also advantageous to the aims and objectives of this study because different viscosity grades of silicone oil can be mixed in order to achieve the desired viscosity without greatly impacting other physical parameters of the oil. Using air is also advantageous as it allows comparison of the present study to datasets in literature in this field as majority of the work is done with air in literature. More details on fluid properties are discussed in Section 3.2.1. Therefore, the rig can be used to study the effect of viscosity on various multiphase characteristics at different angles.

In this chapter, the features of the rig alongside the instrumentation embedded within the rig system will be described in detail. Furthermore, the data analysis techniques will also be discussed.

## 3.2. Experimental arrangement

### 3.2.1. Determination of the physical properties of silicone oil

Fluids used in this study are silicone oil and air. The main objective of the project involves investigating the effect of viscosity on two – phase flow parameters and flow regime characteristics (transitions between flow regimes). Three different silicone oil mixtures of different viscosity each were prepared and thus investigated. Silicone oil with a desired viscosity was achieved by mixing a low viscosity silicone oil with a high viscosity silicone oil in order to achieve that particular dynamic viscosity.

Silicone oil is thermally stable at both cold and hot extreme temperatures however the viscosity of silicone oil will vary greatly at these extremes. Moreover, it is also resistant to fire and electrical hazards, making it extremely safe as well. Finally, it has no odour, toxicity and chemical transference to other components (Sandberg and Sundqvist, 1982).

If any silicon oil vapours are observed, the rig must be shut down in a safe manner as mentioned in the process risk assessment. It is advised at all times to have the extractor fans on during the operation of the rig. Having said that, if silicon oil vapours are somehow inhaled, it is advised to introduce yourself to fresh air. If any symptoms still persist, medical attention should be sought.

The physical properties of the three silicone oil mixtures at 20 °C and 1 atm are shown in Table 3.1.

Table 3.1 – Physical properties of silicon oil-air mixtures at 20 °C and 1 atm for inclinable rig

Fluid		Viscosity (cP)	Density (kg/m <sup>3</sup> )	Surface tension (N/m)	Relative permittivity
Silicone oil mixtures	Mix 1	64	922.5	0.0202	2.7
	Mix 2	91.5	922.5		
	Mix3	236	931.7		
Air		0.0185	1.225		1

The density of silicone oil  $\rho_S$  was experimentally obtained using a gravity bottle with a volume ( $V_B$ ) of 50.628 cm<sup>3</sup>. The empty bottle ( $m_B$ ) was first weighed. After that, the density bottle is filled with silicon oil a little above the mark to ensure that the capillary in the stopper is filled up as well when the stopper is placed back. It must also be ensured that excess oil is wiped off after placing the stopper back. Finally, the bottle with silicone oil content and stopper is kept in a water bath of 20 °C until the content equilibrates to 20 °C. The mass of content and bottle ( $m_{S+B}$ ) are weighed, allowing the calculation of silicon oil density using Equation 3.1.

$$\rho_S = \frac{m_{S+B} - m_B}{V_B} \quad (3.1)$$

The dynamic viscosity of the liquid is described as the ratio between applied shear stress and rate of shear of a liquid. The kinematic viscosity is described as the resistance to flow of a fluid under gravity. The kinematic viscosity  $\nu$  is the ratio of the liquid's dynamic viscosity to its density thus the dynamic viscosity can be determined by multiplying kinematic viscosity with the density of the liquid which was determined through the utilisation of gravity bottle. The importance of evaluating viscosity is fundamentally significant for the situations involving the following scenarios: optimum storage, handling, and operational conditions (our case – oil and gas industry).

For kinematic viscosity measurements, Ostwald viscometers (two D and one E U-tube) were utilised. The use of D or E U-type viscometer is dependent on their kinematic viscosity measurement range (see Table 3.2). Figure 3.1 shows the setup for viscosity measurements. The level on the right side in the charged viscometer is brought up 7 mm above marking A. After that, time taken  $t$  for liquid interface to move from A to B is measured. Each silicone oil mixture was repeated at least three times. For cleaning the viscometer after each run, acetone was used initially however it does not dissolve all of the silicon oil. It must be stressed that it is extremely flammable. Therefore, other solvents were trialled, and it was found that hexane completely dissolves silicon oil therefore it was used to wash away the silicon oil with final rinsing carried out by using water. Fume cupboard was used due to the hazardous nature of hexane oil. After that, dry air was used to completely dry the viscometer.

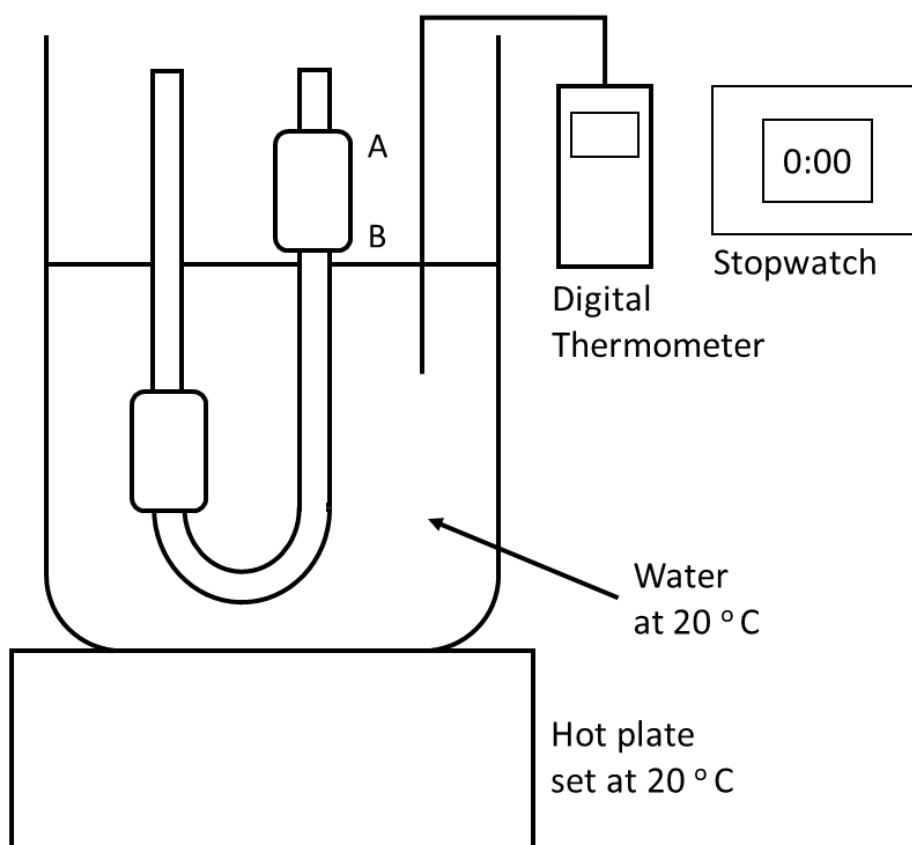


Figure 3.1 – Setup for viscosity measurements

The calibrated viscometers of glass capillary type should be used to determine kinematic viscosity of the fluid within the limits of the precision applicable for that particular viscometer type. The test method (viscometer) is dependent on the behaviour of the sample and is therefore intended for Newtonian fluids. Based on past experience from research projects at University of Nottingham, viscosity dealt in this project can be classed as Newtonian. Moreover, for any particular viscometer, the time of flow of a fixed volume of fluid is directly proportional to the kinematic viscosity of the liquid as shown in Equation 3.2 where C is the constant of proportionality which, in this case, is the calibration constant of the viscometer shown in Table 3.2. The calibration constant is dependent on gravitational acceleration at the site of calibration.

$$v = \Delta t \cdot C \quad (3.2)$$

*Table 3.2 – Range and constant of each Ostwald viscometer*

<b>Ostwald viscometer type</b>	<b>Proportionality constant (mm<sup>2</sup>/s/s)</b>	<b>Maximum kinematic viscosity (mm<sup>2</sup>/s)</b>	<b>Minimum kinematic viscosity (mm<sup>2</sup>/s)</b>
D (one)	0.08587	17.2	85.9
D (two)	0.09212	18.4	92.1
E	0.3376	67.5	337.6

The experimental matrix for each viscosity investigated is presented by Tables 3.3 – 3.5. In Table 3.3, the matrix for experiments involving 64 cP is shown. A total of 600 points were investigated for 64 cP experiments. The matrix for each campaign was selected such that all flow regimes that can be observed in this rig were covered. Moreover, for the purpose of developing the liquid holdup correlation, it was decided to select maximum possible number of gas superficial velocities, liquid superficial velocities and inclination angles.

*Table 3.3 – Experimental matrix for runs involving 64 cP*

<b>u<sub>SL</sub></b> <b>(m/s)</b>	0.080, 0.133, 0.186, 0.239, 0.292
<b>u<sub>SG</sub></b> <b>(m/s)</b>	0.032, 0.064, 0.125, 0.250, 0.375, 0.500, 0.735, 1.103, 1.471, 1.838, 2.329, 2.819
<b>ϑ</b> <b>(degrees)</b>	0, 5, 15, 25, 35, 45, 55, 65, 75, 90

In Table 3.4, the matrix for runs involving 91.5 cP is shown. A total of 220 points were investigated for 91.5 cP experiments.

*Table 3.4 – Experimental matrix for runs involving 91.5 cP*

<b>u<sub>SL</sub></b> <b>(m/s)</b>	0.084, 0.196, 0.308, 0.392
<b>u<sub>SG</sub></b> <b>(m/s)</b>	0.032, 0.064, 0.125, 0.250, 0.375, 0.500, 0.735, 1.103, 1.471, 1.838
<b>ϑ</b> <b>(degrees)</b>	0, 15, 45, 65, 90

The matrix for runs involving 236 cP is shown in Table 3.5. A total of 165 points were investigated for 236 cP experiments.

*Table 3.5 – Experimental matrix for runs involving 236 cP*

<b>u<sub>SL</sub></b> <b>(m/s)</b>	0.070, 0.170, 0.270
<b>u<sub>SG</sub></b> <b>(m/s)</b>	0.032, 0.064, 0.125, 0.250, 0.375, 0.500, 0.735, 1.103, 1.471, 1.838
<b>ϑ</b> <b>(degrees)</b>	0, 15, 45, 65, 90

After 64 cP experiments were carried out, filters were cleaned and re – inserted back into system. This allowed higher liquid superficial velocities to be achieved for 91.5 cP experiments. Moreover, high gas superficial velocities (2.329, 2.819) were not utilised for 91.5 and 236 cP because it caused unstable oscillations on the rig platform. When the rig was filled with 236 cP, highest liquid superficial velocity that was achievable was similar to the highest superficial velocity achieved by 64 cP. The reduction of liquid superficial velocity for 236 cP experiments is most likely linked to viscous losses for the pump.

### 3.2.2. Description of the rig

Figure 3.2 shows an overview of the inclinable rig which will be used in this study. It consists of a cyclone, mixer, two liquid flowmeters, three air flowmeters, a cooling system, silicone oil tank, centrifugal pump and a 67 mm diameter acrylic pipe with a length of 6 m.

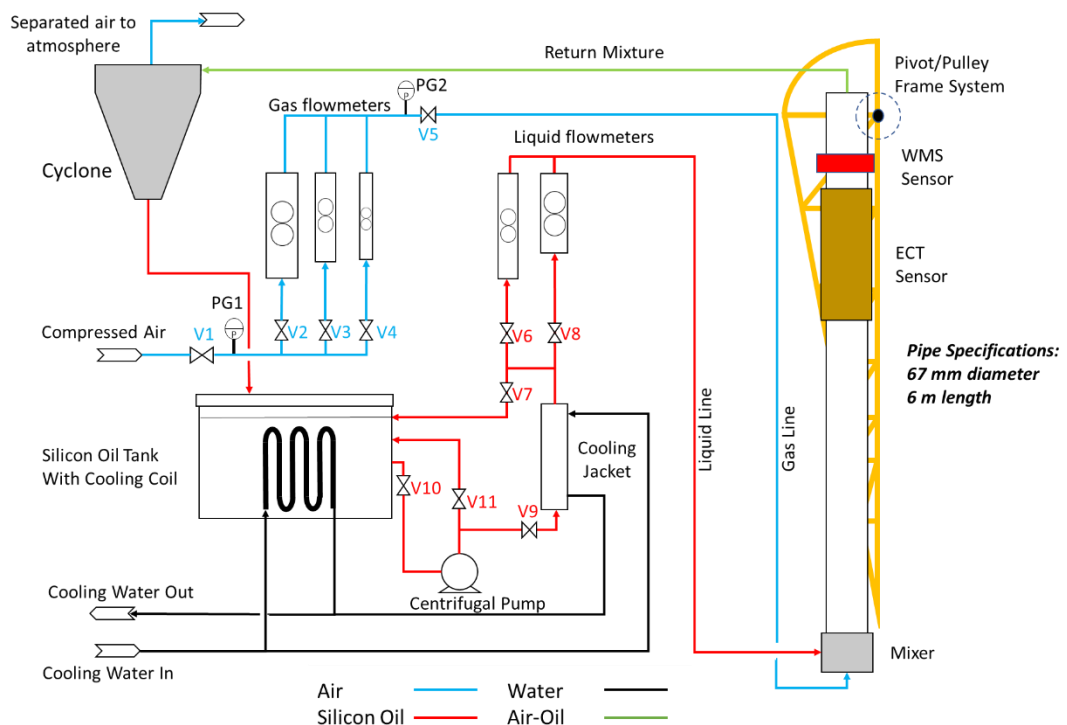


Figure 3.2 – Schematic diagram showing the arrangement of the inclinable rig

Individual components of the inclinable rig are explained in further detail through the list shown below:

- **Mixer and flowmeters:** As shown in Figure 3.2, there is a mixing region at the beginning which guarantees gas and liquid are well-mixed at the entrance of the pipe. A 38 mm ID PVC pipe with 96 3 mm diameter holes was used as the gas injector. Top end of this pipe is sealed. A concentric arrangement was used. There are two liquid and three air flow meters. The use of a certain flowmeter for each fluid depends on what flowrate is required because one flowmeter for each fluid is for high rates while the other ones are for low rates. The overall experimental range for liquid velocity is from 0.070 to 0.392 m/s while the overall experimental range for gas velocity is from 0.032 to 2.819 m/s. The rig becomes unstable above these ranges due to turbulence of the flow within the pipe system so surpassing these flow rates is not advised. Variable area volumetric flowmeters were used to measure the liquid flow rates. For this study, volumetric flowmeter for high flow was only utilised. This flowmeter had an uncertainty of 2 l/min. All flow patterns can be observed in this pipe except annular and stratified flow due to the reason given above. Due to this, flow regime classification and transition work is limited and does not include all possible regimes for each inclination angle.
- **Air supply:** The air is fed into the mixing chamber from compressed air system at a high pressure of 6 barg. The air coming from the system (6 barg) is reduced to a pressure of 1.5 barg by V1, as represented by pressure gauge one (PG1). There is another pressure gauge (PG2) after the gas flowmeters which must be noted for each data point in order to normalise the gas flowrates to atmospheric conditions. The pressure after the gas flowmeters can be controlled by either opening or closing valve 5. The typical range utilised for this gauge varied between 10 and 12 psig. The correction equation is represented as Equation 3.6.
- **Silicon oil supply:** The silicon oil is stored in the liquid tank of volume 600 L and is pumped into the mixing region through a centrifugal pump.

- **Cooling systems:** There are two points where the excess heat produced due to centrifugal pumping of the flow is removed. Firstly, there is a cooling coil in the silicon oil tank which removes excess heat produced from pump. Moreover, there is a cooling jacket as well just before the silicon oil is pumped into the mixer region.
- **Data acquisition:** After the mixing region, the flow flows through the pipe and passes both Electrical Capacitance Tomography (ECT) and Wire Mesh Sensor (WMS) which are explained in more detail in Sections 3.3 - 3.5 where their principle, features and uncertainties are explained in more detail.
- **Cyclone:** After the void fraction instrumentation, the flow then passes through a cyclone system which ensures that air is released to the atmosphere while the liquid silicon oil sinks to the bottom due to gravity and centrifugal forces. From previous works on this rig, it was observed that mist cloud was formed for churn flow which were mitigated through the use of a filter which hinder the release of mist to the surroundings above.

As mentioned earlier, there are two liquid flowmeters however only the high liquid flowmeter was utilised. The high liquid flowmeter must be calibrated as, at different viscosities, the actual flowrate or velocity will differ from that on the flowmeter. The idea is to measure the time it takes a liquid interface to move up the pipe for a known distance and correlate this to the flowmeter value. The Electrical Capacitance Tomography (ECT) was used in order to measure this time through a data analysis technique known as cross-correlation because it has two planes. Hence, the ECT will allow the evaluation of the time it takes for a liquid interface to move from plane 1 to plane 2. The distance between the two planes is known at 0.089 m therefore an actual representation of the velocity can be evaluated by dividing the distance by time. Cross-correlation is discussed in more detail in Sections 3.4.2 and 3.5. This must be repeated for a series of liquid flow rates (three to four) at each viscosity. Equations 3.3 – 3.5 shows the calibration equations for 64, 91.5 and 236 cP oils respectively. Constants have a unit of  $\text{m s}^{-1} \text{L}^{-1} \text{min}$ . The corresponding  $R^2$  for each fit is also included after each equation. The linear fit is quite good as it ranges between 0.98 and 0.998

which is close to 1. Escrig (2017) used the same method to obtain his calibration curve as well.

$$u_{LS (64 \text{ cP})} = 0.0053 * \text{Flowmeter Reading} \quad (3.3) \quad R^2 = 0.98$$

$$u_{LS (91.5 \text{ cP})} = 0.0056 * \text{Flowmeter Reading} \quad (3.4) \quad R^2 = 0.998$$

$$u_{LS (236 \text{ cP})} = 0.0049 * \text{Flowmeter Reading} \quad (3.5) \quad R^2 = 0.9941$$

The gas flow rate must be corrected as the gauge pressure (PG2) and calibrated flowmeter pressure are different so Equation 3.6 can be used to correct for this.  $Q_G'$  and  $Q_G$  are meter gas flowmeter reading and corrected gas flowmeter reading respectively.

$$Q_G = Q_G' \sqrt{\frac{p_R}{p_O}} \quad (3.6)$$

As mentioned earlier, in order to study multiphase characteristics in any pipe system, it is important that void fraction can be obtained through a series of instrumentation. For liquid holdup or void fraction, many instrumentation devices are available: Electrical Capacitance Tomography (ECT), Electrical Resistance Tomography (ERT) and Wire-Mesh Sensors (WMS). However, the accuracy and form of data produced is different for all techniques. For the rig presented for this study, two instrumentation techniques were available: dual plane ECT and single plane WMS. The reason for selecting ECT boiled down to the fact that this study focussed on flow characteristics such structure velocity which can be calculated using ECT as it has two planes. Moreover, mean phase distribution obtained from ECT and WMS are in good agreement for most datasets except at low void fractions where largest deviations are observed. The WMS (Wire Mesh Sensor) values were 4% below that of ECT for high liquid superficial velocity and low void fraction. (Azzopardi *et al.*, 2010). Another reason for not utilising WMS is the slow draining time of the oil. Wires in WMS get

coated with the oil. The film thickness increases with the viscosity. Slow drainage time affects the measurement as it leads to a lower void fraction measurement.

### 3.3. Gas void fraction acquisition instrumentation

#### 3.3.1. Electrical Capacitance Tomography: The forward and inverse problem

Electrical Capacitance Tomography (ECT) is an instrumentation technique that allows the determination of permittivity distribution for a mixture of two di-electric materials by measuring the capacitances between combination of electrode-pairs placed around sensor's perimeter. The number of electrodes (E) used in this study is 8 which also determines the number of independent electrode-pair capacitance measurements (M) (see Equation 3.7). Therefore, the total number of measurements in this study are 28. The image produced by ECT is inscribed onto a 32x32 square pixels which means that 1024 elements are computed from using the 28 measurements. Due to the limited measurements that are available, the idea is to find the best approximated solution to the problem (Xie *et al.*, 1992, Huang *et al.*, 1989).

$$M = \frac{E(E - 1)}{2} \quad (3.7)$$

The normalised capacitance of air is taken to be zero while for silicon oil it is set at one. The relationship between absolute (C) and normalised capacitance  $C_n$  is shown in Equation 3.8.  $C_H$  represents the capacitance for the higher permittivity material only while  $C_L$  represents the capacitance for the lower permittivity material.

$$C_n = \frac{C - C_L}{C_H - C_L} \quad (3.8)$$

Similarly, the normalised permittivity measured between any pair of electrodes are set in a similar fashion i.e. zero when the pipe is empty and one when it is filled with

silicone oil. The relationship between absolute ( $K$ ) and normalised permittivity  $K_n$  is shown in Equation 3.9. In Equation 3.9,  $K_H$  represents the permittivity for the higher permittivity material only while  $K_L$  represents the permittivity for the lower permittivity material (Isaksen, 1996).

$$K_n = \frac{K - K_L}{K_H - K_L} \quad (3.9)$$

The relationships in Equations 3.8 and 3.9 are shown in Figure 3.3. These correlations are shown to be linear for both parameters.

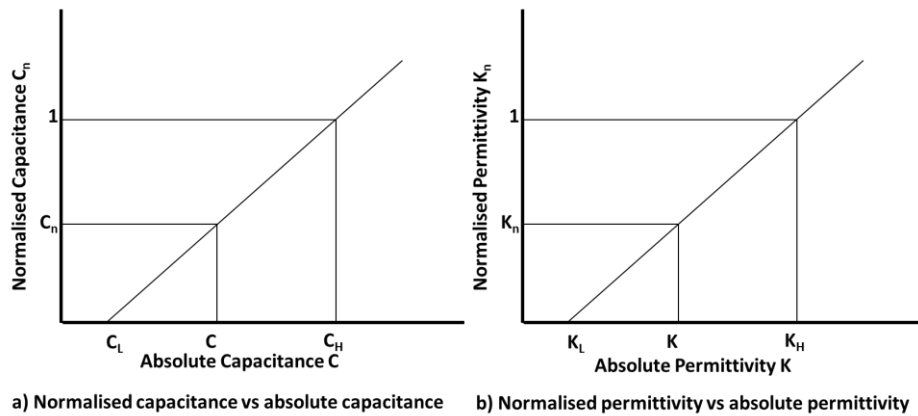
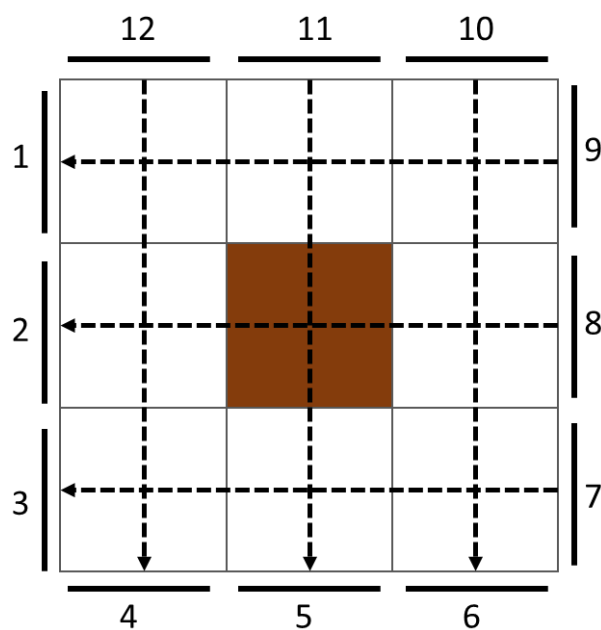


Figure 3.3 – Relationship between absolute and normalised capacitance

The sensitivity matrix used in ECT will be explained using a simple square sensor model shown in Figure 3.4 (Yang and Byars, 1999). Ignoring any electrode coupling, there are six total electrode-pairs for this model which are 1 – 9, 2 – 8, 3 – 7, 12 – 4, 11 – 5 and 10 – 6. The field lines are shown to be straight for simplification. In reality, this is not the case. For each pixel, there is a different sensitivity matrix for each electrode-pair, comprising a total of six different sensitivity matrices. For instance, the middle pixel is filled with the higher permittivity, so the affected electrode-pairs that will contain this pixel are 11 – 5 and 2 – 8. Equation 3.10 shows a typical format of a sensitivity matrix.

$$\begin{pmatrix} S_A & S_B & S_C \\ S_D & S_E & S_F \\ S_G & S_H & S_I \end{pmatrix} \quad (3.10)$$

So, for the suggested example in Figure 3.4, the sensitivity matrix for electrode pair 11 – 5 will be such that  $S_B$ ,  $S_E$  and  $S_H$  will have a value of one with remaining elements taking a value of zero. Similarly, the sensitivity matrix for electrode pair 2 – 8 can be represented such that  $S_D$ ,  $S_E$  and  $S_F$  will be equal to one with remaining elements in the matrix taking a value of zero. For other four electrode-pairs, all the elements in the matrix will be zero. The process can be repeated for each individual pixel in order to generate a sensitivity matrix at each electrode-pair to study the variation of capacitance between electrode-pairs.



*Figure 3.4 – Simple square model utilised to explain the sensitivity and capacitance matrix*

The capacitance between any two opposing electrodes will only be affected if the pixel intercepts the electric field lines between these electrodes. In order to calculate capacitance for each electrode pair, the elemental normalised capacitance for each pixel is also determined by again filling each pixel with the higher permittivity material. In total, there will be nine total normalised capacitance measurements for the example in Figure 3.4.

Superposition Theorem is then applied in order to determine the capacitance between any electrode pair as shown in Equation 3.11. The  $m$  subscript is the

electrode-pair the capacitance calculation is relevant to. The parameters  $S_A, S_B$  etc. represents the sensitivity coefficient for a given pixel at  $m_{th}$  electrode pair while  $K_A, K_B$  etc. represent the values of normalised permittivity in a given pixel.  $P_m$  is a constant which ensures that the capacitance values remain valid.

$$C_m = P_m(S_A K_A + S_B K_B + \dots \dots S_I K_I) \quad (3.11)$$

Equation 3.11 can be written in the form of a matrix, concisely summarising all the concepts explained through the use of the simple square model. Equation 3.12 shows this summarised relationship where  $C$  is an  $M$  (measurements)  $\times$   $1$  matrix containing the normalised electrode pair capacitances  $C_m$ .  $K$  represents the normalised pixel permittivity as a  $N \times 1$  matrix while  $S$  is an  $M \times N$  which contains the set of sensitivity matrices for each electrode pair. Equation 3.12 is also defined as the forward problem for ECT.

$$C = S.K \quad (3.12)$$

However, the parameter that is the interest in an experiment utilising ECT is the permittivity distribution from the capacitance distribution between electrode-pairs surrounding the sensor, introducing an inverse problem. In order to accomplish this solution, a method known as Linear Back-Projection (LBP) is used (Isaken, 1996). The permittivity of an individual pixel  $K_n$  can be calculated by using Equation 3.13 through utilising capacitance measurements from Equation 3.12.  $S_{nm}$  represents the sensitivity coefficients at pixel  $n$  and  $m_{th}$  electrode-pair while  $Q_n$  are sets of normalising constants for pixel  $n$ .

$$K_n = \sum Q_n S_{nm} C_m \quad (3.13)$$

So, for the example in Figure 3.4, the normalised permittivity for middle pixel can be given by Equation 3.14.

$$K_E = Q_E(S_{E(9-1)}C_{9-1} + S_{E(7-3)}C_{7-3} + S_{E(8-2)}C_{8-2} + S_{E(12-4)}C_{12-4} + S_{E(11-5)}C_{11-5} + S_{E(10-6)}C_{10-6}) \quad (3.14)$$

Again, Equation 3.14 can be summarised in the form of a matrix as shown in Equation 3.15 where  $K$  is an  $N \times 1$  matrix consisting the normalised permittivity at each pixel  $N$ . Moreover,  $S_T$  is the transpose of the normalised sensitivity map. As mentioned before,  $C$  represents the  $M \times 1$  matrix comprising the normalised capacitances at each electrode-pair.

$$K = S_T C \quad (3.15)$$

The LBP algorithm (default ECT reconstruction algorithm of ECT software) has some characteristics which are crucial for analysis of the void fraction data. They are as follows:

- Generally, the LBP algorithm will always underestimate areas of low permittivity.
- It also overestimates areas of low permittivity which also means that some pixels that should have a zero value will have a finite value assigned to them.
- The mean permittivity of all the pixels evaluated by the LBP solution will be extremely close to that of the sensor containing test material. Therefore, this model is useful in determining an average void fraction.
- The image produced by LBP will be slightly approximated and deviated from the true image as the method spreads the true image over the whole area of the sensor.

### 3.3.2. Present study ECT Configuration

The ECT used for this study is a circular sensor (Figure 3.5) unlike the simple square model shown in Figure 3.4. The ECT is a pre-existing system and has been utilised by various researchers (Escrig, 2017) at University of Nottingham. The normalised

permittivity values of each pixel shown in Figure 3.5 are related to the volume ratio of the material with a higher permittivity at that pixel location (liquid holdup or gas voidage). As shown in Figure 3.5, the number of total pixels used to estimate the cross section of the sensor is only 812 compared to the total number of pixels (1024) in a 32 x 32 grid.

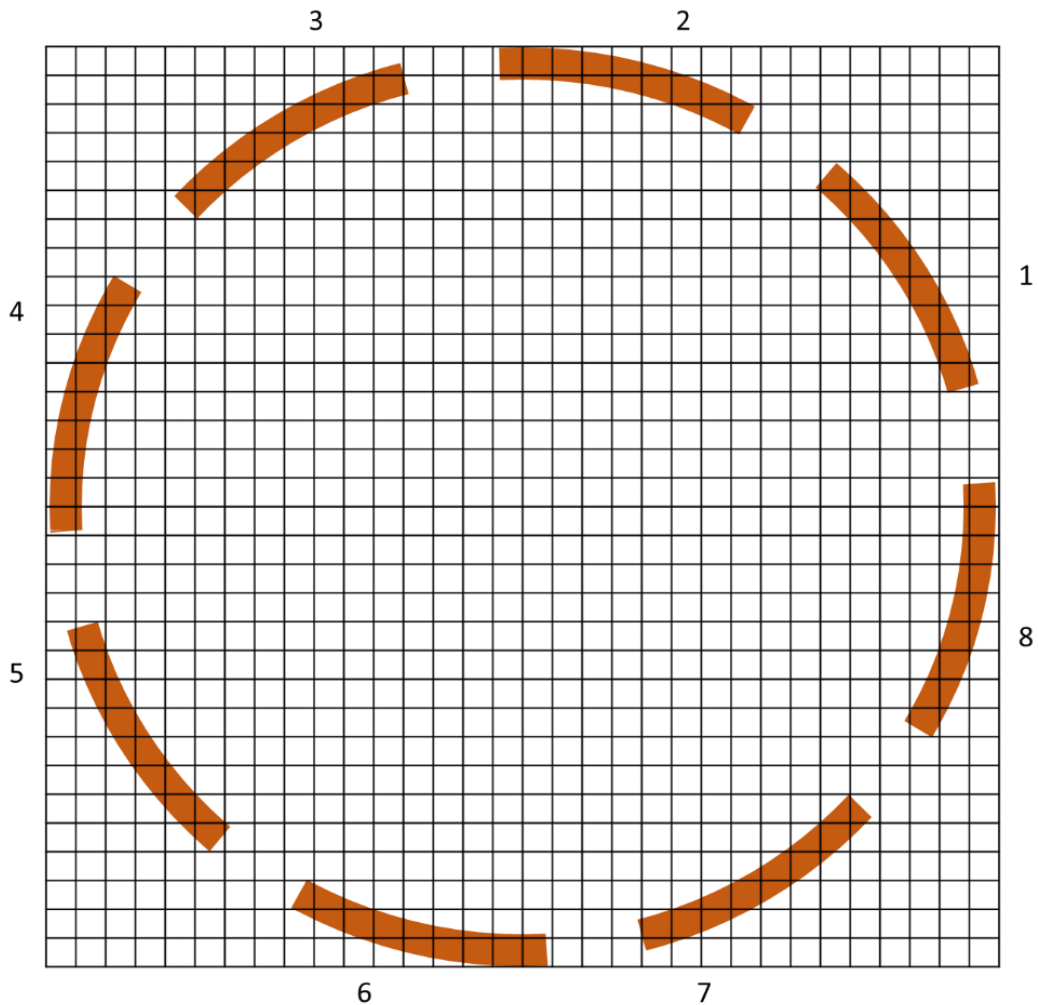


*Figure 3.5 – Circular ECT sensor used in this study*

In this project, the dual-plane ECT will be utilised which means there are two measurement planes. Each measurement plane is protected by guard electrodes from each side and has 8 measurement electrodes with an axial length of 35 mm each. The mask utilised for the ECT in this project is shown in Figure 3.6. The calibration of the probes should be carried out by acquiring readings with gas only

flow and liquid only flow before any acquisition of project data (Azzopardi *et al.*, 2010).

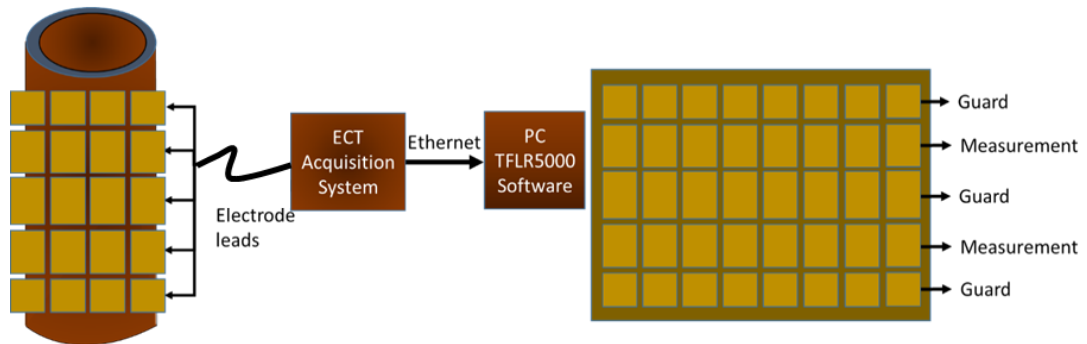


Figure 3.6 – ECT mask configuration for inclinable rig

There are two main ways through which the permittivity and void fraction can be related using a capacitance-based model: series and parallel (Yang and Byars, 1999). The capacitance is proportional to permittivity and is inversely proportional to volume ratio.

The void fraction in the parallel configuration is evaluated such that the air and silicon oil are parallel to the electric field. When capacitors are connected in parallel, the capacitances are added up. Equation 3.16 shows the relationship between effective permittivity and void fraction for parallel configuration while Equation 3.17 shows an expression derived from Equation 3.16 for void fraction.

$$K_E = \varepsilon_L K_H + \varepsilon_G K_L \quad (3.16)$$

$$\varepsilon_G = \frac{K_E - K_H}{K_L - K_H} \quad (3.17)$$

The void fraction in the series configuration is evaluated such that both phases are in series. In this case, the capacitor is mathematically evaluating by adding the reciprocals. Equation 3.18 shows the relationship between effective permittivity and void fraction for series configuration while Equation 3.19 shows an expression derived from Equation 3.18 for void fraction.

$$\frac{1}{K_E} = \frac{\varepsilon_G}{K_L} + \frac{\varepsilon_L}{K_H} \quad (3.18)$$

$$\varepsilon_G = \frac{K_H - K_E}{K_H - K_L} \cdot \left(\frac{K_L}{K_E}\right) \quad (3.19)$$

Another similar technique to ECT is Electrical resistivity tomography (ERT) in terms of acquisition and data collection however it does not use dielectric properties of the phases. Rather, it is based on conductance differences of the two phases. As mentioned earlier, the liquid investigated in this project is silicon oil which is non-conductive unlike water therefore ERT is inapplicable for the fluid system in question.

### 3.4. Data analysis techniques: ECT Holdup data

#### 3.4.1. ECT raw data

For ECT data acquisition, the commercial TFLR5000 software was used which saves the data file as a bcp file. Through this software, the file is converted into two avr format files which can be read in MATLAB – one for each plane. The ECT data was first recorded at 1000 Hz for 60 s and was repeated at 4000 Hz for 60 s. Therefore, number of points  $n$  will depend on the frequency. The structure data such as void fraction and structure velocity using software frequencies of 1000 Hz and 4000 Hz for same conditions were compared. It yielded that void fraction did not change by much however, for high liquid and gas superficial velocities, structure velocity differed. In order to ensure accurate acquisition of structure velocity, 4000 Hz was utilised for those points. There are many important two-phase characteristics that can be extracted from the ECT data and are as follows: time series data, probability density function (PDF), structural frequency, and structure velocity. As mentioned in Section 3.2, ECT data is recorded as liquid holdup however for time series analysis it can be converted to gas void fraction if required. Figure 3.7 shows a typical gas void fraction time series plot for vertical two-phase flow (64 cP) at a liquid and gas superficial velocity of 0.0795 and 0.125 m/s respectively.

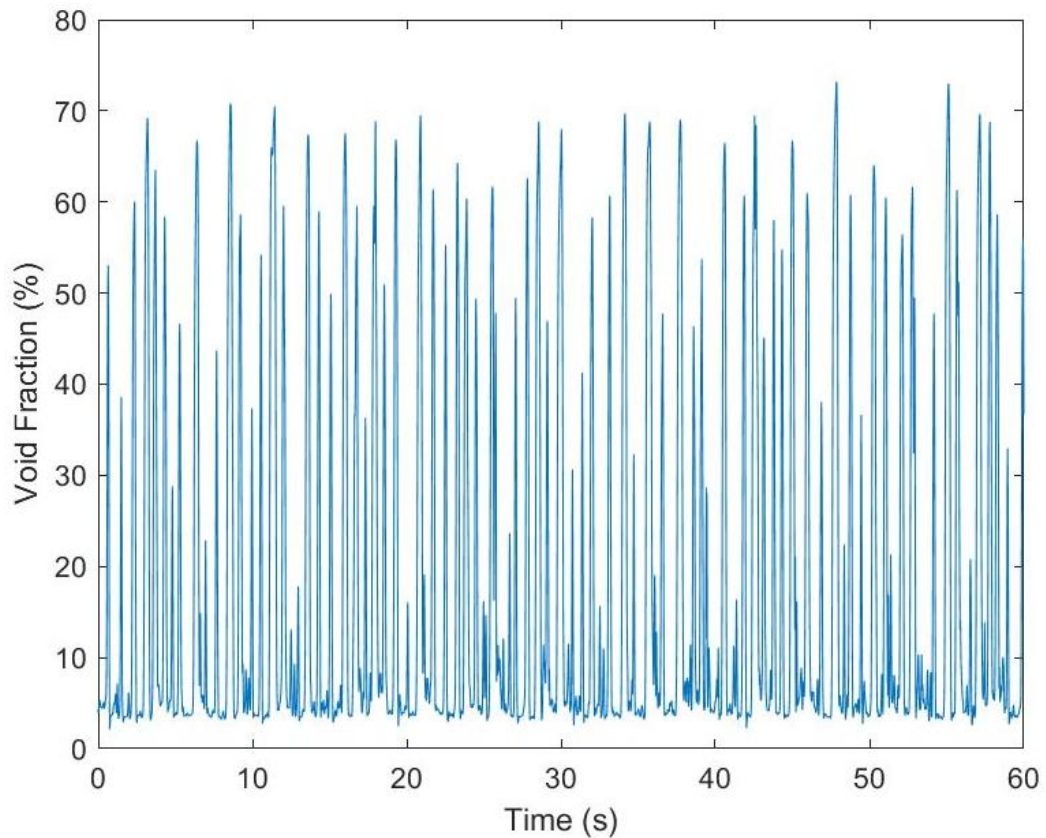


Figure 3.7 – A typical time series plot for vertical two-phase flow (64 cP) at a liquid and gas superficial velocity of 0.0795 and 0.125 m/s respectively.

Therefore, the mean liquid holdup  $\mu_\varepsilon$  can be evaluated by Equation 3.20.

$$\mu_\varepsilon = 0.5 * \left( \frac{\sum_{i=1}^n \varepsilon_{iPlane1}}{n} + \frac{\sum_{i=1}^n \varepsilon_{iPlane2}}{n} \right) \quad (3.20)$$

Since a twin – plane ECT is being used, measurement planes are separated by a small distance of 0.089 (discussed in next subsection). Difference between liquid holdup (or gas void fraction) for both phases is small therefore it was decided to average values for both planes.

#### 3.4.2. Structure velocity

Because the ECT has two planes, cross correlation can be used to determine the velocity of the intermittent structures. The distances from the mixer to the first and

second plane are 4.4 and 4.489 m respectively. The distance difference of 0.089 m between the planes allows the capturing of the time lag of intermittent structures flowing in the pipe system from plane 1 to plane 2, as shown in Figure 3.8. Also, it can be utilised to calibrate for liquid velocities in the similar fashion.

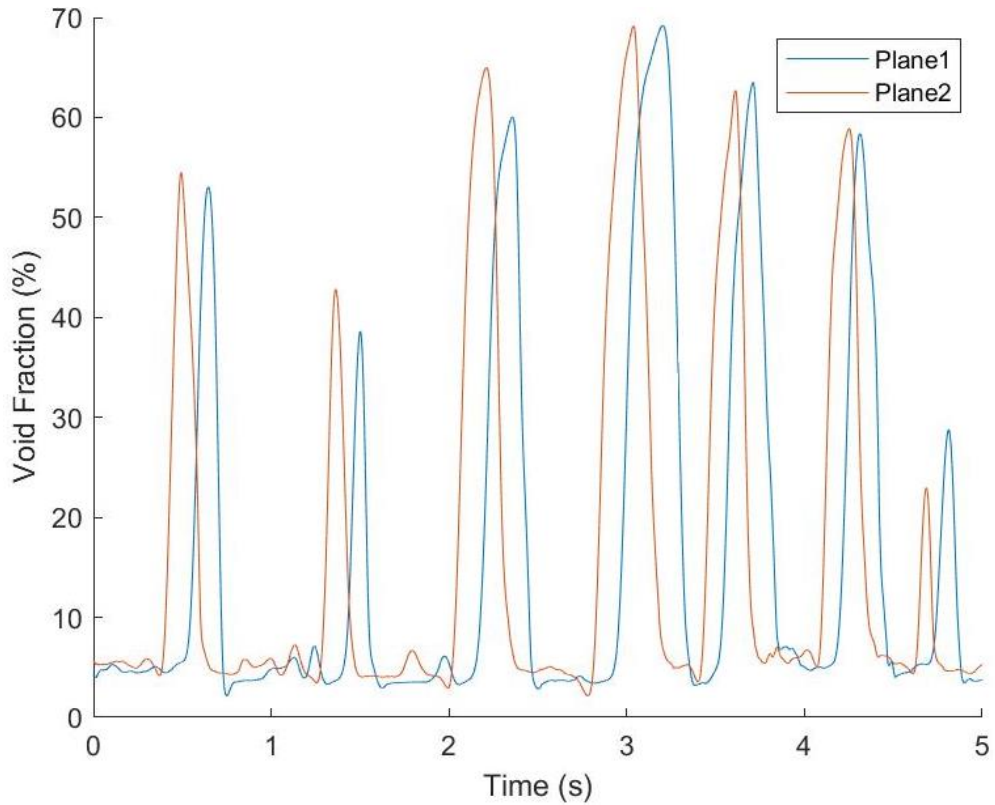


Figure 3.8 – Time series data for plane 1 and 2 for vertical two-phase flow at a liquid and gas superficial velocity of 0.0795 and 0.125 m/s respectively.

The cross co-variance of two data sets (plane 1 and 2) can be computed through the expected value operator using Equation 3.21.

$$C_{12} = E\{[x_1(t) - \mu_1] \cdot [x_2(t + \tau) - \mu_2]\} = \lim_{T \rightarrow \infty} \frac{1}{T} \int_0^T [x_1(t) - \mu_1][x_2(t + \tau) - \mu_2] dt \quad (3.21)$$

The cross co-variance can be related to the cross-correlation function  $R_{12}$  and is shown in Equation 3.22.

$$C_{12} = [R_{12}(\tau) - \mu_1\mu_2] \quad (3.22)$$

Finally, these definitions can be related to the correlation coefficient function  $p_{12}$ , defined by Equation 3.23 (Bendat and Piersol, 2010).

$$p_{12} = \frac{R_{12}(\tau)}{\sigma_1 \sigma_2} \quad (3.23)$$

From Equation 3.23, the time lag at which  $p_{12}$  is maximum can be evaluated which allows the determination of the structure velocity. The way this is done is by overlapping the signals until the both signals coincides over each other. Knowing the distance between the planes, the structure velocity can be evaluated using Equation 3.24.

$$U_s = \frac{0.089}{\tau_{p_{MAX}}} \quad (3.24)$$

Figure 3.9 shows how the cross-correlation coefficient varies with lag for vertical two-phase flow (64 cP) at a liquid and gas superficial velocity of 0.0795 and 0.125 m/s respectively. Lag on x-axis in Figure 3.9 shows the number of points rather than time lag. The number of points was converted to time lag by the multiplying the frequency of the dataset and number of points from zero axis at which the cross-correlation coefficient is a maximum.

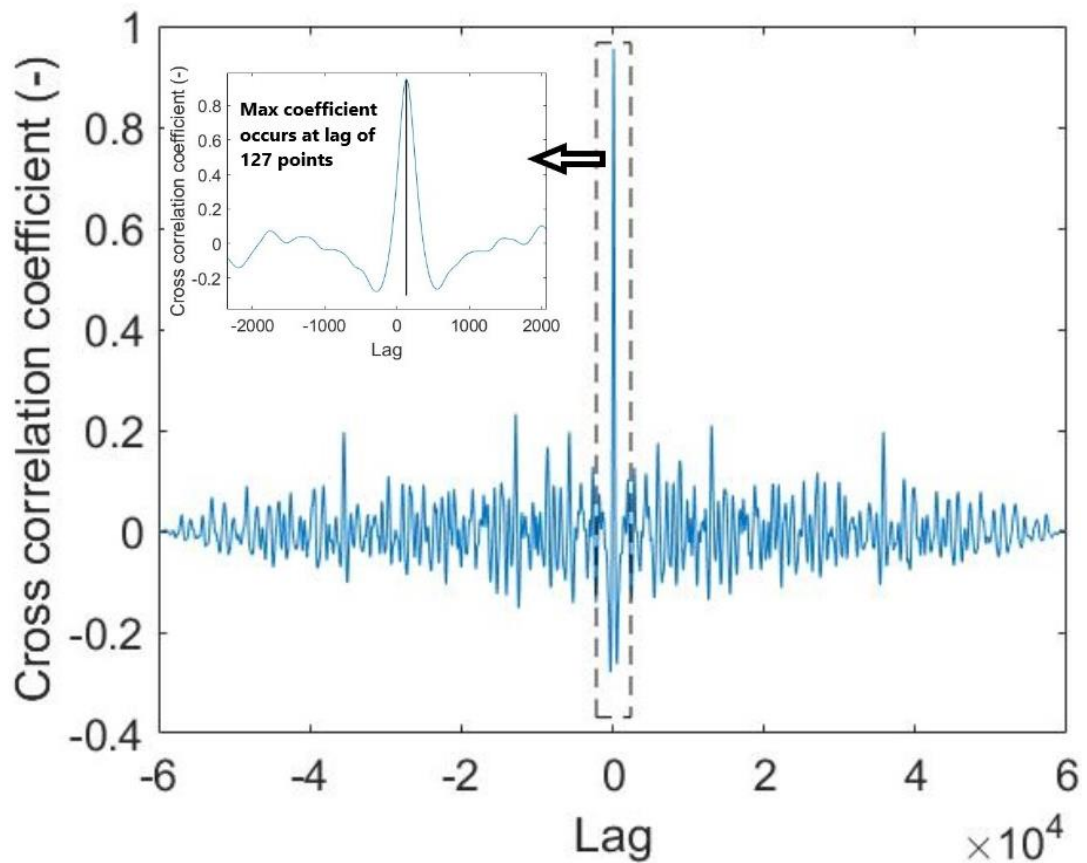


Figure 3.9 – Cross correlation coefficient plot for vertical two-phase flow (64 cP) at a liquid and gas superficial velocity of 0.0795 and 0.125 m/s respectively.

### 3.4.3. Structure frequency

Another important characteristic of the two-phase flow that can be captured through the ECT data is the structure frequency of intermittent structures (present in all flow regimes for this study) flowing in the pipe. In this study, flow regimes observed are discrete (ellipsoidal/cap) bubbly, slug and churn. They present a repeating pattern where a gas dominated structure is followed by a liquid dominated structure, resulting in a characteristic mean frequency. The structure frequency is defined as the total number of slugs / cap bubbles that pass through a certain cross section per second. There are two main methods through which this information can be obtained and are as follows:

- 1) Power spectral density function by performing an autocorrelation technique known as FFT

- 2) Utilising the Hazuku method from Hazuku *et al.* (2008) – Counting peaks through using a MATLAB code (self – written)

#### 3.4.3.1. FFT method

The finite Fourier transform of the void fraction time series is given by Equation 3.25. In simpler terms, this function decomposes the void fraction time series into its constituent frequencies.

$$FFT = \int_0^T x(t)e^{-2\pi ift} dt \quad (3.25)$$

After performing the finite Fourier transform, the power spectral density (PSD) function can be evaluated using Equation 3.26. The power of the decomposed constituents can be related to their frequency through the PSD function. The PSD evaluation is repeated for plane 2 so the average dominant frequency  $f_D$  is evaluated through Equation 3.27 by averaging the frequency with maximum power at each plane.

$$PSD (Plane 1) = \int_0^T R_{11}(\tau)e^{-2\pi if\tau} d\tau \quad (3.26)$$

$$f_D = \frac{1}{2}(f_{PSD_{MAXP1}} + f_{PSD_{MAXP2}}) \quad (3.27)$$

A typical PSD plot for vertical two – phase flow (64 cP) at a liquid and gas superficial velocity of 0.186 and 1.836 m/s respectively is shown in Figure 3.10.

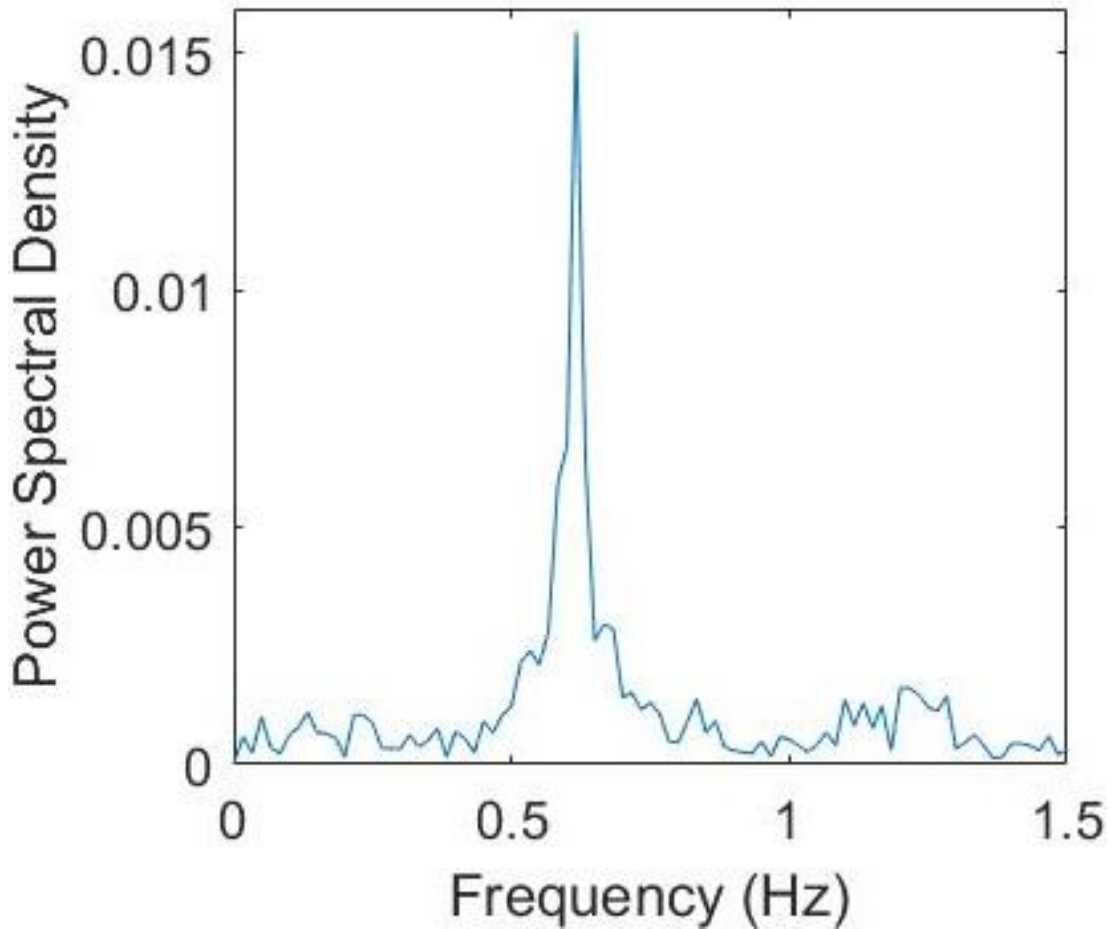


Figure 3.10 – PSD plot for vertical two-phase flow (64 cP) at a liquid and gas superficial velocity of 0.186 and 1.836 m/s respectively.

#### 3.4.3.2. Hazuku method

Another method that can be used to determine structure frequency is the Hazuku method from Hazuku *et al.* (2008) which works on the basis of applying two thresholds. The first threshold is the mean of the time series data while the second threshold is the mean of the data points above the mean. A slug in this method is considered as one when the trough passes below the lower threshold and the peak crosses the upper threshold. Figure 3.11 shows how the Hazuku method is implemented for horizontal two-phase flow (64 cP) at liquid and gas superficial velocity of 0.0795 and 0.735 m/s respectively. The red line is the upper threshold while the yellow line is the lower threshold.

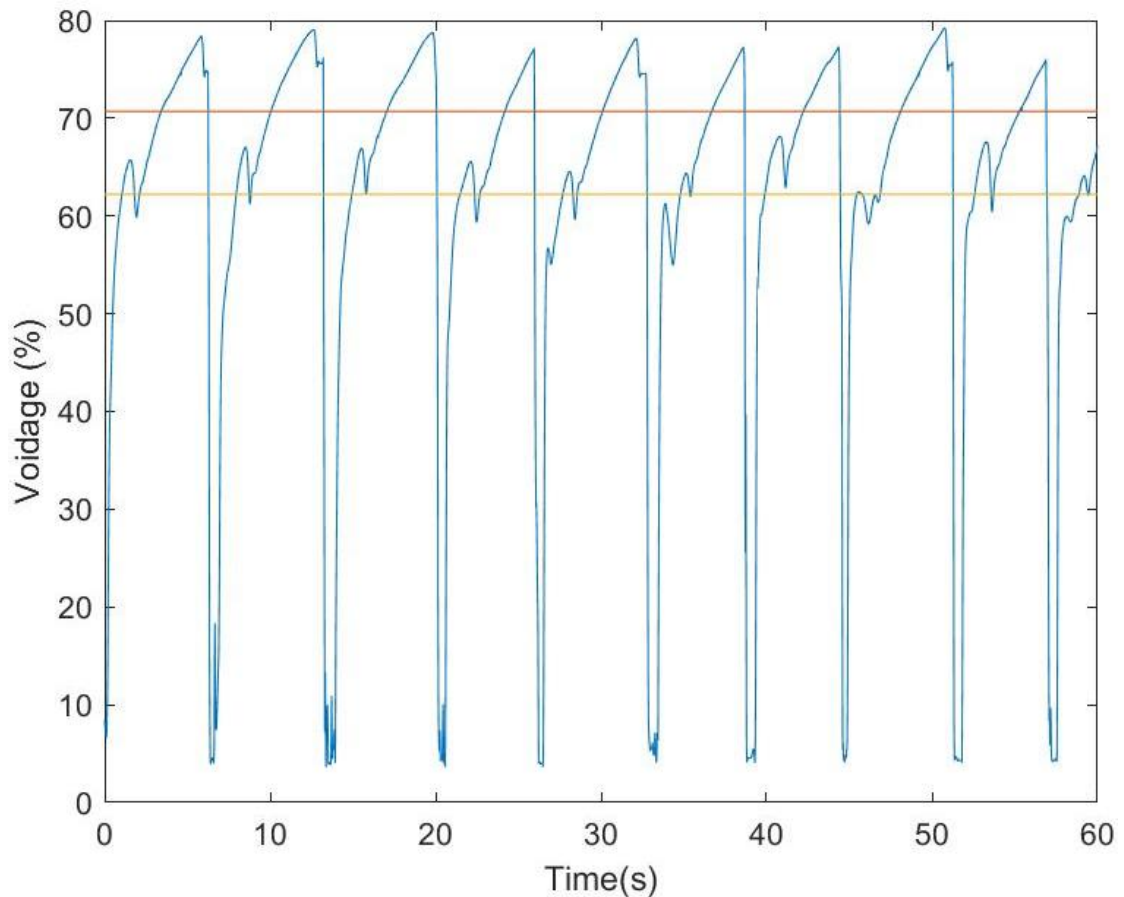


Figure 3.11 – Hazuku method for horizontal two-phase flow (64 cP) at liquid and gas superficial velocity of 0.0795 and 0.735 m/s respectively

#### 3.4.4. Statistical measures: Probability density function (PDF) and standard deviation (SDEV)

There are two major statistical measures that were carried out in order to further analyse the void fraction obtained from ECT: Probability Density Function (PDF) and standard deviation (SDEV). The main principle of the PDF is to determine the frequency at which each void fraction value in the time series data occur at. There are usually two main conditions which a PDF should satisfy:

- 1)  $\int_{-\infty}^{\infty} f(t)dt = 1.$
- 2)  $f(t) \geq 0$  for all void fraction values

The area under the PDF must be equal to one as stated by condition one. These PDF curves are extremely useful in identifying flow regimes through using the Costigan and Whalley (1997) criteria. Figure 3.12 shows the implementation of this criteria on defining flow regimes for vertical two-phase flow at a liquid viscosity and velocity of 64 cP and 0.292 m/s respectively for different gas velocities. It can be seen that bubbly flow has one major peak at low void fraction which is its characteristics. Unlike at lower viscosities, the bubbly flow consists of a single bubble taking a shaped of an ellipsoid rather than multiple smaller bubbles. For slug flow, it has two major peaks. The peak at lower void fraction is represented as the liquid slug region while the peak at higher void fraction represents the Taylor Bubble region. For churn flow, it is characterised by a single peak at high void fraction with a low PDF of lower void fraction values.

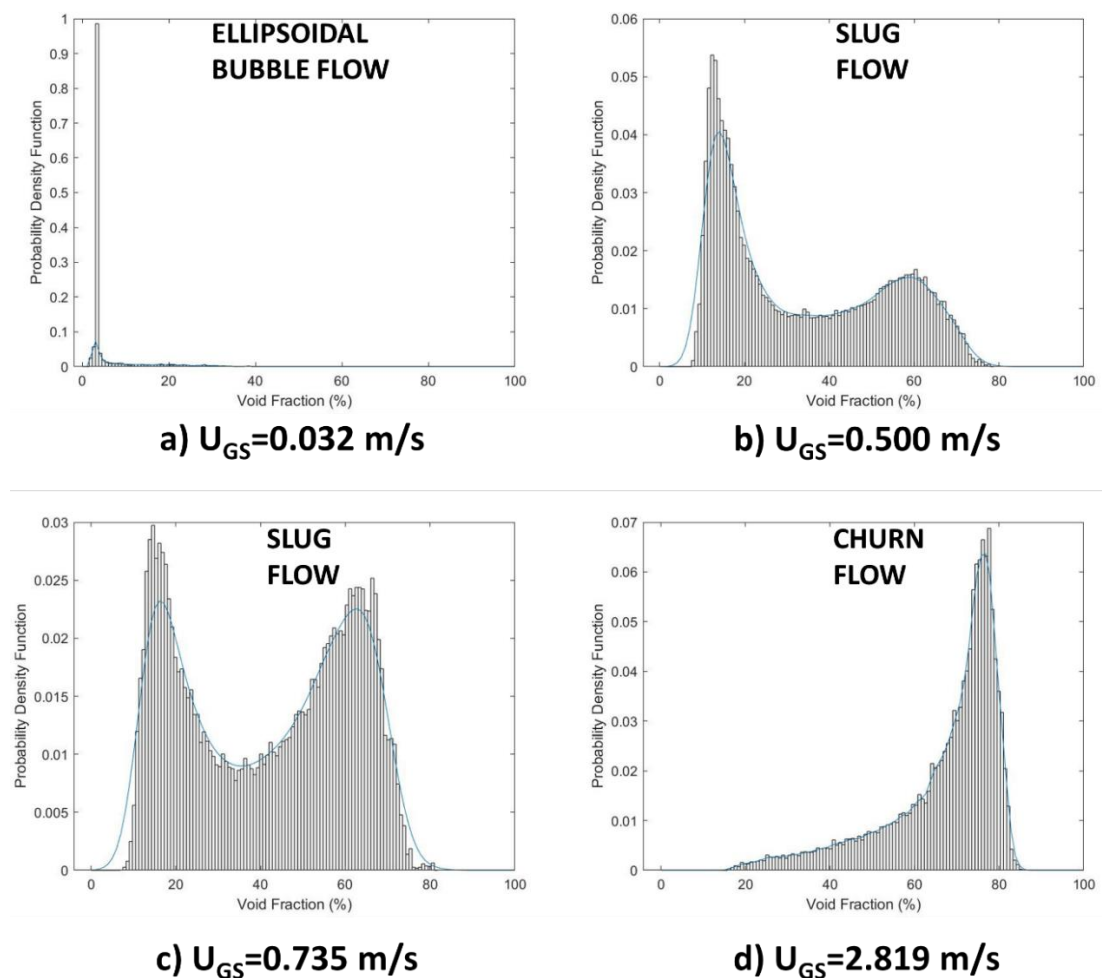


Figure 3.12 – PDFs shown for vertical two-phase flow at a liquid viscosity and velocity of 64 cP and 0.292 m/s for different gas velocities

One other statistical measure that was used to analyse the spread of the data was standard deviation. Equation 3.28 shows how standard deviation was calculated.

$$\sigma = \sqrt{\frac{1}{N} \sum_t^N (\varepsilon - \bar{\varepsilon})^2} \quad (3.28)$$

### 3.5. Robustness of PSD and cross-correlation results

A total of three tests were carried out to ensure the generated code in MATLAB is reliable and robust. Firstly, a test was created in order to assess the reliability of the PSD code that was generated in MATLAB. Three sine curves are added together to form Equation 3.29. Figure 3.13 shows the decomposition of this signal into three signals of differing frequency each. The frequencies of these signal are shown in bold in equation 3.29.

$$y = \sin(2 * \mathbf{2} * \pi * x) + \sin(2 * \mathbf{2.25} * \pi * x) + \sin(2 * \mathbf{1.7} * \pi * x) \quad (3.29)$$

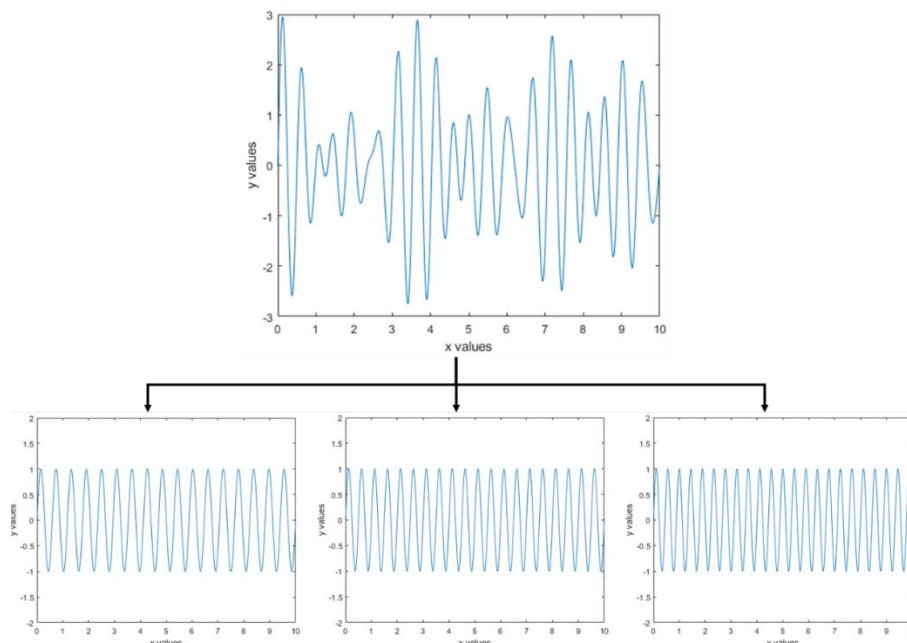


Figure 3.13 – Decomposing the signal in equation 3.34 into individual frequency components of 1.7, 2, 2.25 respectively

The power spectral density or PSD was performed on the complex signal represented in Equation 3.29 and the PSD plot for this signal is shown in Figure 3.14. As shown, there are three different frequencies in the signal. Moreover, it is worth noting that, the rest of the frequencies are plotted with a zero power.

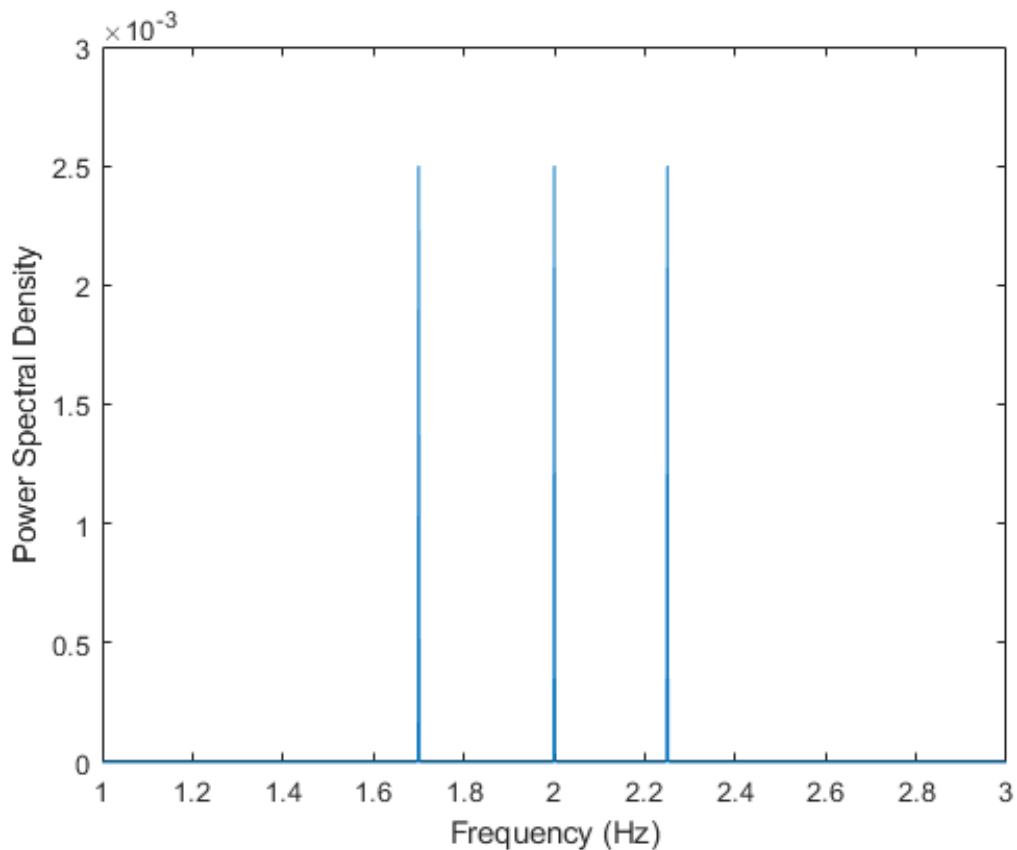


Figure 3.14 – PSD plot for the signal represented as equation 3.29

The second test was performed for the Hazuku method. The reason for using a second method for frequency identification is because PSD, at times, results in multiple dominant frequencies. In that case, the need for Hazuku method is inevitable. Hazuku method is utilised because identification of a flow regime is dependent upon our definition of what really is a structure. In PSD, result includes all structures including bubbles and cap bubbles instead of large structures.

Hazuku method was manually applied first and then was implemented in MATLAB. It was ensured that the MATLAB code which used the findpeak function did not miss any peak. For this reason, the manual counting using Hazuku method was compared

to MATLAB Hazuku method for a large number of data points. The results matched 100 %.

The third test (see Figure 3.15) was performed on the xcorr function in MATLAB utilised for cross-correlation coefficient. In order to test this code, sin and cos equations (Equations 3.30 and 3.31) were used because they have a known lag of 0.25 between them.

$$y = \sin(2\pi t) \quad (3.30)$$

$$y = \cos(2\pi t) \quad (3.31)$$

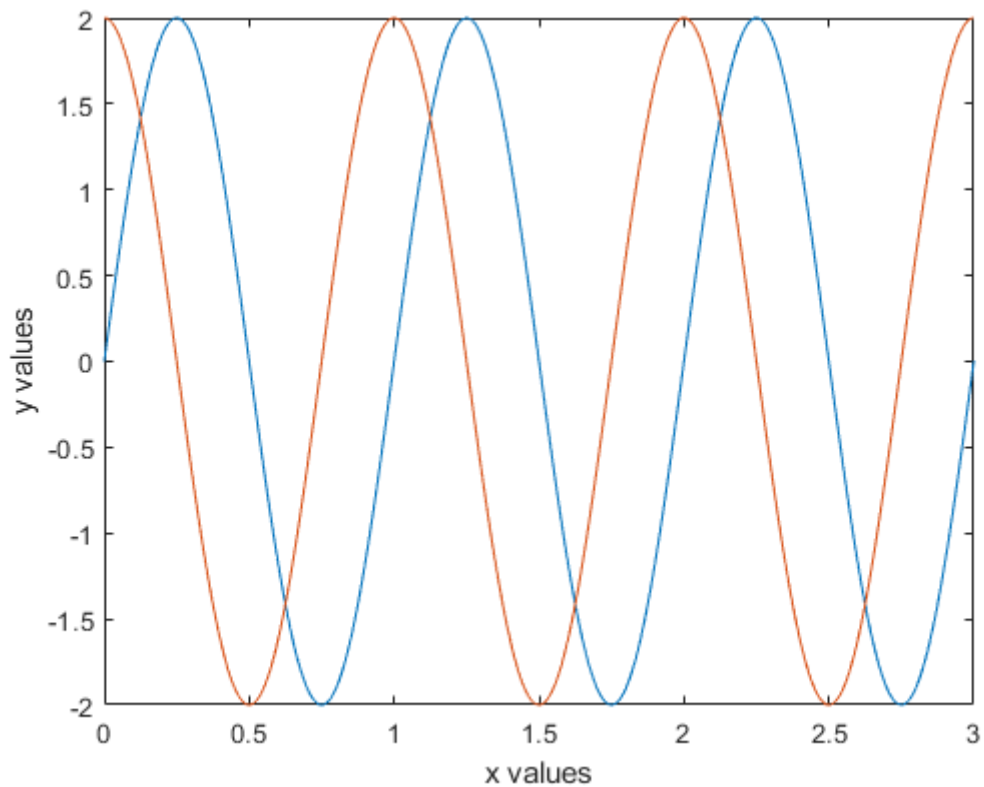


*Figure 3.15 – Cross correlation applied on equations 3.30 and 3.31*

Applying the ideas explained in Section 3.4.2, the code returned a value 0.250 (to 3 dp) which is exactly the same as the known lag of 0.25. Above 3 decimal places, the timelag was recorded as 0.2495 which is still 99.8 % accurate to the known lag of 0.25.

## 4. Effect of inclination angle and viscosity on two phase parameters

### 4.1. Introduction

The inclination angle has a profound effect on two – phase parameters such as liquid holdup, structure velocity and structure frequency. As the inclination angle is increased from horizontal to vertical inclination, the influence of the buoyancy force on the gas bubbles induces them to accumulate in the upper section of the pipe. Thus, the varying relative motion of both phases at different inclinations for same operational conditions produces different two – phase distribution in the pipe. As a result, different intermittent characteristics (i.e. frequency, velocity and holdup) are observed with increasing inclination at similar operational conditions. For example, frequency of intermittent flow (i.e. cap, slug, and churn) may vary drastically when analysing vertical and horizontal inclination. In a horizontal pipe, the size of the whole slug unit (Taylor bubble plus liquid slug) is generally much larger than it would be in a vertical pipe for same operational conditions.

Moreover, there have been various experimental studies investigating the effect of inclination angle on various flow characteristics (i.e. slug frequency, structure velocity and liquid holdup) however these studies are often limited in terms of parameters investigated. For example, works of Mukherjee (1979) and Beggs (1972) investigated variation of liquid holdup with inclination angle, utilising a wide range of operational conditions. Mukherjee (1979) focused on air – kerosene system for a pipe diameter of 38.1 mm while Beggs (1972) focused on air – water system for pipe diameters of 25.4 and 38.1 mm. These systems involve low liquid viscosity (not more than 1 or 2 cP) which means that viscosity effect was overlooked. In general, most of the works in two – phase flow is focussed on air – water systems. The continuous depletion of light conventional oils has increased the attractiveness of research into high viscosity oils. Gokcal (2008) investigated the effect of various viscosities (and other operational conditions) on slug frequency, slug velocity and liquid holdup but

this work is limited to horizontal inclination. Nevertheless, other works such as Stanislav *et al.* (1986) was carried out for slightly inclined pipe (maximum 9 degrees) using a liquid viscosity of 7 mPa.s.

Furthermore, knowledge of inclination angle on slugging within pipelines is also fundamental to operation of an oil and gas (or any multiphase flow application) platform and constitutes as one of the main challenging flow-assurance problems in oil and gas fields. In a typical oil and gas system, pipelines can be vertical, horizontal or inclined depending on its geographical topology.

At certain operational conditions, serious vibrations can be observed on rigs/platforms as a result of (severe) slugging. Usually, large Taylor bubbles can form when the gas is expanding due to the decreasing pressure when a two – phase mixture is flowing up in a riser. Investigating this bracket of operational conditions where unstable flows occur is central in preventing such instabilities when crafting and operating such large systems. Hence, an in-depth investigation of these slug characteristics with inclination angle at different liquid viscosities would assist design engineers to produce an economical, safe and robust operational arrangements.

The effect of fluid properties such as viscosity on two – phase flow parameters is essential for designing of transportation and production systems such as that in oil and gas industry. The conventional oil resources are depleting at an alarming rate due to increasing world energy demand, making high viscosity oils an important source of future energy fuels. High percentage of heavy oil (~70 %) remaining in the world's reserves also attracts vast amount of interest in researching high viscosity oils (Elshawaf, 2018). Most of the detailed investigations in two – phase flow have revolved around horizontal or vertical air – water or air – glycerin (in water) systems. Nevertheless, some research studies have investigated effect of viscosity on slug flow characteristics such as that of Gokcal (2008) however it is focussed on horizontal inclination only.

Moreover, investigating the effect of a specific fluid property solely such as viscosity in an experimental investigation can be quite difficult because other physical properties of the fluid can also alter (i.e. water and glycerin – water systems). For example, adding glycerin in water alters the viscosity of the fluid however it also impacts the density of the fluid by some margin. Therefore, a detailed analysis of viscosity into two – phase flow parameters is essential by ensuring that all other physical properties such as surface tension and liquid density are not altered by a significant factor. Furthermore, the surface tension of water – air systems is around 72 dynes/cm while crude oil and gas industry usually has a surface tension around 30 dynes/cm. Hence, differences in surface tension for both air – water and air – oil systems will have significant differences in the distribution of liquid and gas in flowing pipelines. For example, Nadler and Mewes (1995) showed that increases in surface tension will lead to an increase in liquid holdup.

The influence of inclination angle on two – phase characteristics at three different oil viscosities (64, 91.5 and 236 cP) will be presented in this chapter. Dual plane ECT (Electrical Capacitance Tomography) will be used for measurement of the two – phase characteristics. The two – phase characteristics investigated in this study are as follows: liquid holdup, structure velocity and structure frequency. The translational velocity of the intermittent structures will be obtained by cross – correlating the time series data of both planes. The structure frequency was obtained using PSD (Power Spectral Density) and Hazuku Method. The analytical techniques for evaluation of these parameters were explained in Chapter 3.

#### 4.2. Experimental arrangement

The inclinable two – phase flow apparatus was used. The setup of the inclinable rig was explained in Chapter 3. The pipeline in the rig has an inner diameter of 67 mm and can be inclined in steps of 5 degrees from horizontal to vertical position. The fluids utilised for these experiments are silicone oil of various viscosities and air which are also discussed in Chapter 3. Three different silicone oil viscosities were

investigated for a number of gas and liquid superficial velocities, and inclination angles. Table 4.1 enlists the matrix employed for each experimental campaign.

*Table 4.1 – Matrix employed for three different experimental campaigns*

$\mu_L$ (cP)	$u_{SL}$ (m/s)	$u_{SG}$ (m/s)	$\vartheta$ (degrees)	Points
64	0.080, 0.133, 0.186, 0.239, 0.292	0.032, 0.064, 0.125, 0.250, 0.375, 0.500, 0.735, 1.103, 1.471, 1.838, 2.329, 2.819	0, 5, 15, 25, 35, 45, 55, 65, 75, 90	600
91.5	0.084, 0.196, 0.308, 0.392	0.032, 0.064, 0.125, 0.188, 0.250, 0.375, 0.500, 0.735, 1.103, 1.471, 1.838	0, 15, 45, 65, 90	220
236	0.070, 0.170, 0.270	0.032, 0.064, 0.125, 0.188, 0.250, 0.375, 0.500, 0.735, 1.103, 1.471, 1.838	0, 15, 45, 65, 90	165

Experiments were carried out to collect 985 data points. The ECT was used to collect data at 1000 Hz for most of the datasets. For higher gas superficial velocities, it was increased to 4000 Hz for cross correlation of dual plane signals. The reason for this is to ensure capturing of fast moving intermittent structures at these higher gas superficial velocities.

Sections 4.3 to 4.5 will focus on the impact of inclination angle on flow characteristics. In addition, effect of viscosity is investigated in Section 4.6. For Section 4.6, 315 points were selected from overall 985 points (highlighted in red). Therefore, only a fraction of data is presented for viscosity analysis. Lowest and highest viscosity were selected in order to investigate the maximum effect possible of viscosity on flow parameters.

### 4.3. Effect of inclination angle and superficial velocities on liquid holdup

#### 4.3.1. 64 cP experimental campaign

Liquid holdup was measured using dual plane ECT sensor. Figure 4.1 shows variation of liquid holdup with inclination angle for all runs at a liquid viscosity of 64 cP. There are five sub graphs in total, each referring to a specific liquid superficial velocity. Each sub-graph has twelve lines, each representing a superficial gas velocity.

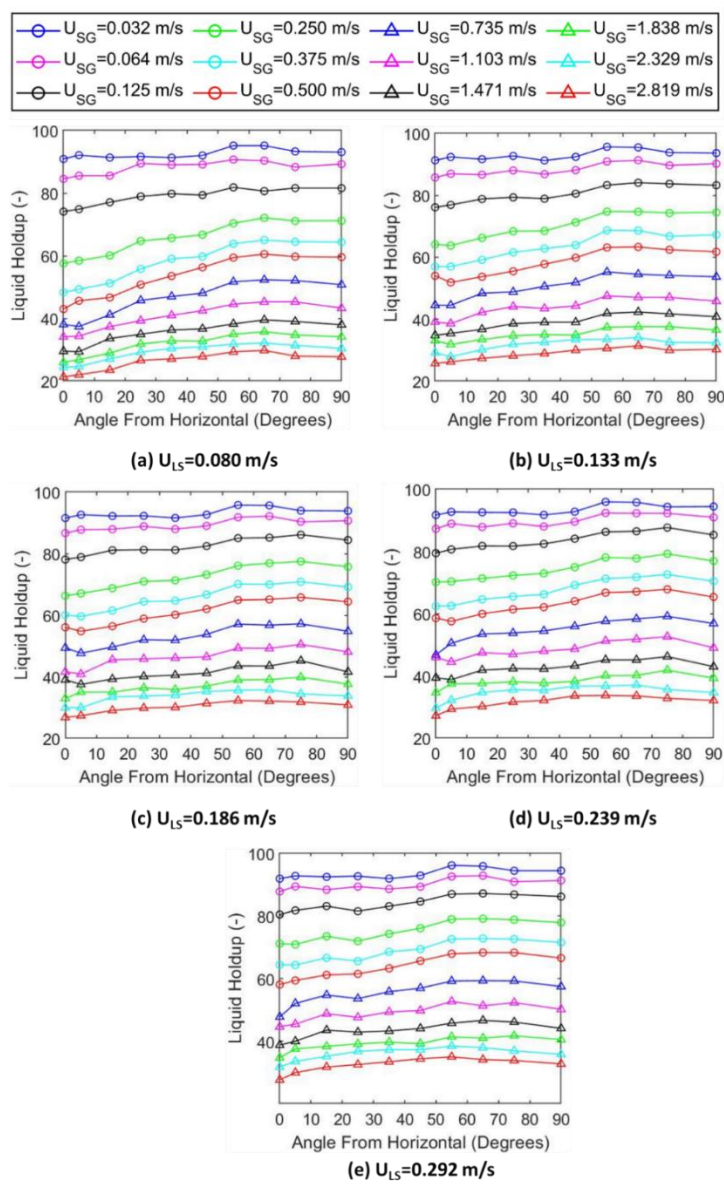


Figure 4.1 – Influence of inclination angle on liquid holdup for oil viscosity of 64 cP at different liquid and gas superficial velocities

At a specific liquid superficial velocity, liquid holdup decreases with an increase in gas superficial velocity. The range of liquid holdup values for 64 cP runs varied from 21 % to 96 % (0.21 – 0.96). Through analysing the shape of each line, it was evaluated and proposed that a second or third – order polynomial function is a good fit with an excellent  $R^2$ . The complete analysis of this and proposed liquid holdup correlation are further discussed in Chapter 6.

One interesting aspect of Figure 4.1 is the analysis of the point at which the liquid holdup reaches a maximum. In total, there are 60 lines of which 43.3 % of the lines reach a maximum at an inclination angle of 65 degrees while 56.7 % of the lines (equally distributed over both angles at 28.3 % each) reach a maximum at an inclination angle of 75 or 55 degrees. For each individual line, absolute percentage difference between liquid holdup at horizontal inclination and maximum liquid holdup is greater than the absolute percentage difference between liquid holdup at vertical inclination and maximum liquid holdup. For example, for liquid and gas superficial velocity of 0.186 m/s and 1.103 m/s respectively, the percentage increase in liquid holdup from horizontal inclination to the inclination with the maximum liquid holdup at 75 degrees was 21.4 %. In comparison, the percentage decrease from the maximum at 75 degrees to the vertical inclination was only 4.7 %. The ratio of the percentage increase, in this case, to the percentage decrease is almost 5 times (actual value is 4.5). Moreover, the range of percentage increases in liquid holdup from horizontal inclination up to inclination with the maximum liquid holdup when comparing all runs was 4.6 – 40.8 % while range of percentage decreases in liquid holdup from the inclination with the maximum liquid holdup to vertical inclination varied between 0.3 and 8.0 %. For all runs, the range of ratio of the percentage increase to the percentage decrease varies between 2.0 and 49.1, showing that the percentage rise is always greater than the percentage decrease. From this analysis, it can also be understood that the liquid holdup at vertical inclination never reaches the same value as the liquid holdup at horizontal inclination.

The percentage increases in liquid holdup from horizontal inclination to the inclination with the maximum liquid holdup are smaller in magnitude for lower gas

superficial velocities compared to higher gas superficial velocities. However, when comparing liquid superficial velocities, the difference is not significant except for lowest liquid superficial velocity. The same is true for percentage decreases in liquid holdup from the inclination with maximum liquid holdup to the vertical inclination. More on superficial velocities is discussed in Figure 4.3.

The trend of liquid holdup against inclination angle for a given gas and liquid superficial velocity is analogous to that of Beggs and Brill (1973). As the angle of the pipe is increased from horizontal, gravitational force acting on the liquid induces a reduction in liquid velocity. The result is an increase in slippage and thus liquid holdup. However, this only happens until a specific inclination angle. The maximum in the case of 64 cP experiments occurs at an inclination angle of 55 – 75 degrees. The experimental maximum closely matches with experimental work carried out by Beggs and Brill (1973) who found it to be approximately 50°. Similarly, results from proposed liquid holdup correlation by Mukherjee (1979) is consistent with maximum of 50 degrees proposed by Beggs and Brill (1973). After the maximum, an increase in inclination angle ultimately bridges the entire pipe which, in turn, reduces holdup due to reduced slippage between phases.

Moreover, Beggs and Brill (1973) showed that holdup is approximately unchanging between inclination angles of +20 and +90 degrees. In the case of 64 cP work, the liquid holdup does not change much for inclination angles greater than 55 degrees. The reduction in the rate of change of liquid holdup near vertical inclinations is one of the main reasons why vertical liquid holdup correlations perform reasonably well for near vertical inclinations (Beggs and Brill, 1973).

Figure 4.2 shows how experimental gas void fraction (complement of liquid holdup) compares with the homogeneous gas void fraction (or gas voidage) for 64 cP oil at each inclination angle. Homogenous void fraction evaluates the void fraction of a two – phase system assuming that the gas and liquid travel at the same velocity (i.e. slip ratio is 1). However, due to buoyancy force acting on the gas phase, the slip ratio is always greater than unity. As a result, experimental void fraction is always less than

the homogeneous void fraction. It can be seen that no experimental point lies above the red  $x = y$  line. It can be observed that the points plotted in Figure 4.2 resemble a plot of experimental void fraction against gas superficial velocity. The dispersion of points is due to the utilisation of five different liquid superficial velocities for this experimental campaign.

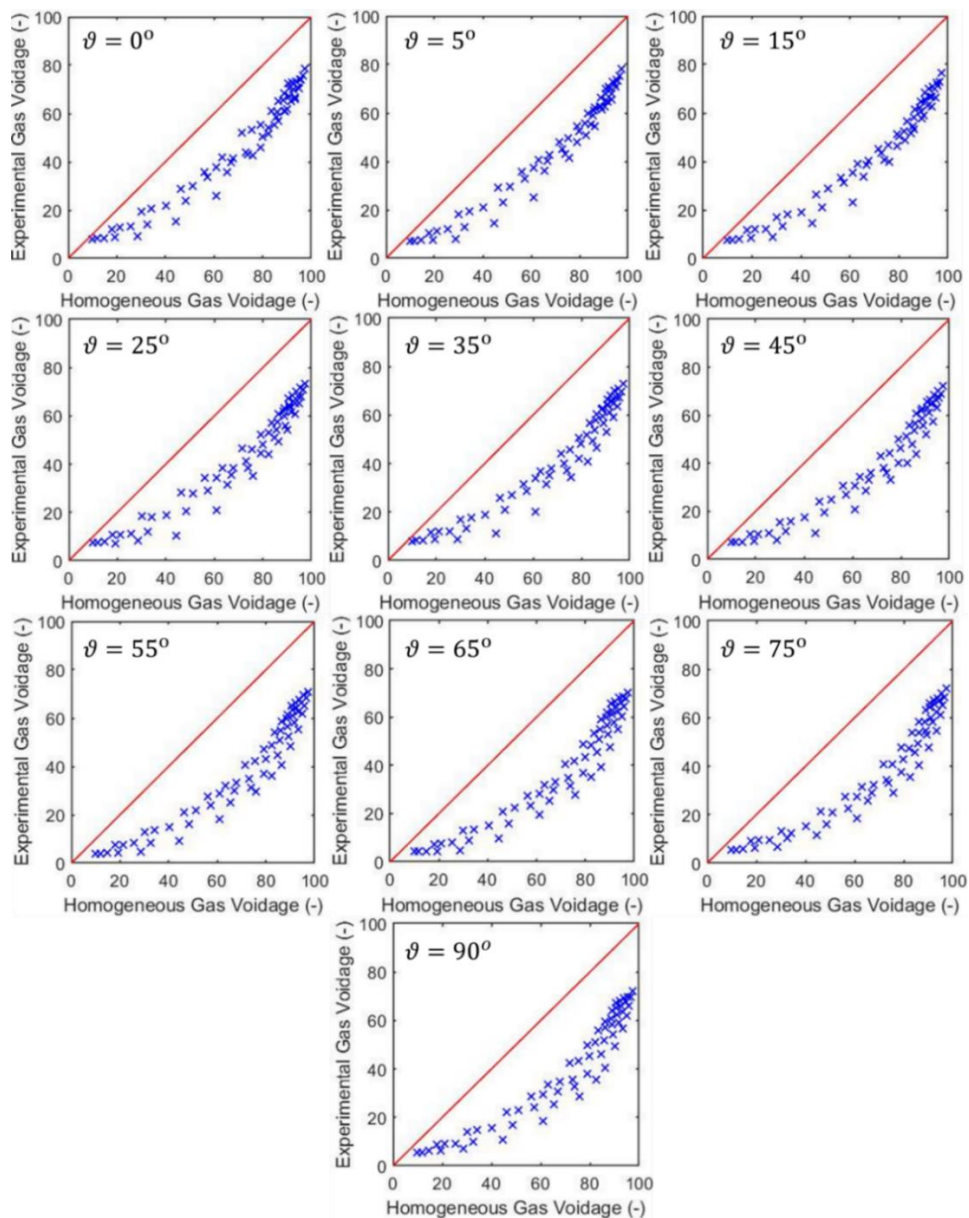


Figure 4.2 – Comparing experimental and homogeneous gas voidage for all runs at 64 cP oil

Figure 4.3 shows how liquid holdup varies with superficial gas velocity at five different liquid superficial velocities for 64 cP experiments. There are ten sub-graphs, each referring to a specific inclination angle. As discussed earlier, the liquid holdup decreases with gas superficial velocity while it increases with liquid superficial velocity. The changes in liquid holdup are more sensitive at lower gas superficial velocities compared to higher gas superficial velocities. At higher gas superficial velocities, changes in liquid holdup slows down.

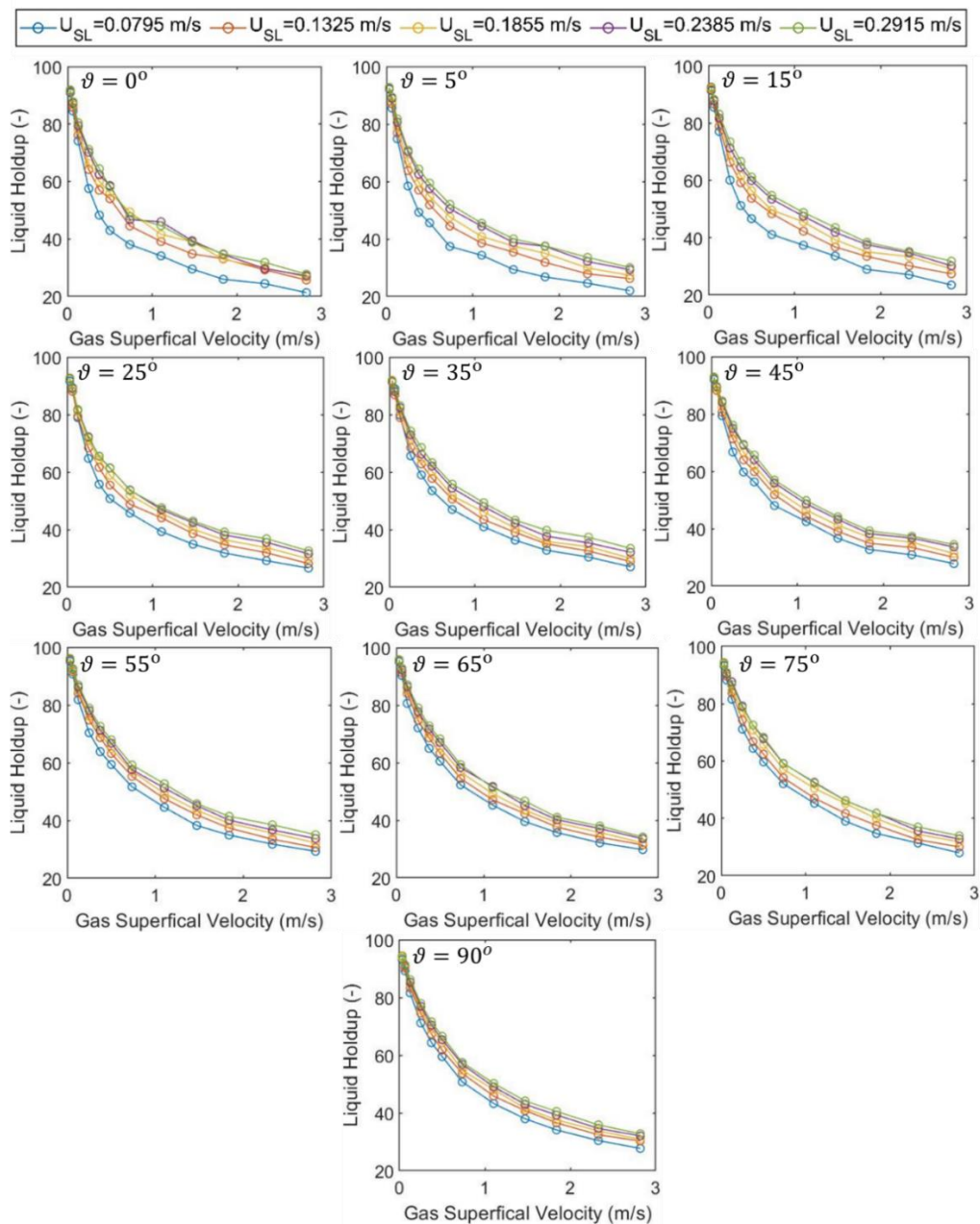


Figure 4.3 – Variation of liquid holdup for 64 cP experiments against superficial gas at five liquid velocities for each inclination angle

The analysis of Figure 4.3 demonstrates that the rate at which liquid holdup decreases slows down as the gas superficial velocity is increased at a fixed liquid superficial velocity. The analysis can be further supplemented by plotting the rate of change of liquid holdup against gas superficial velocity, as shown in Figure 4.4 for vertical inclination. Rate of change of liquid holdup (in Figure 4.4) was calculated by dividing the difference between liquid holdup values for two consecutive gas superficial velocities at a given liquid superficial velocity by the difference between those two consecutive gas superficial velocities. The calculated value is then plotted against the highest superficial gas velocity. For liquid superficial velocity of 0.0795 m/s at vertical inclination, rate of change of liquid holdup decreases from 87 to 38 (difference of 49 occurring over a much smaller span of gas superficial velocities) as superficial gas velocity is increased from 0.125 m/s to 0.500 m/s. However, it decreases from 38 to 6 (difference of 32 occurring over a much large span of gas superficial velocities) when gas superficial velocity is increased from 0.500 m/s to 2.819 m/s.

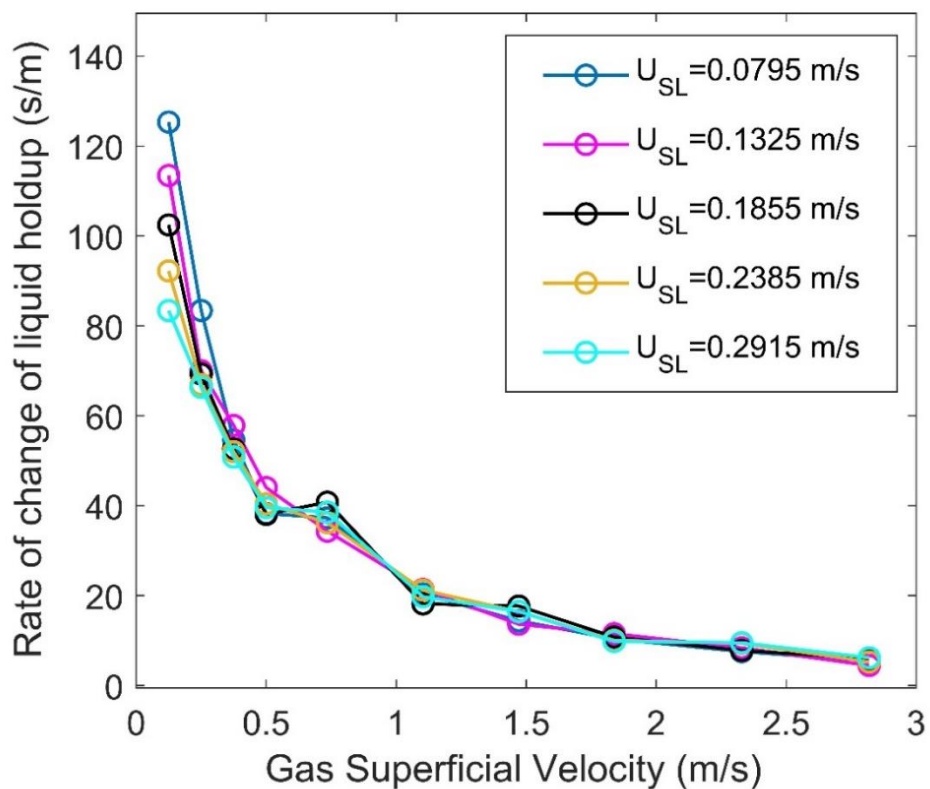


Figure 4.4 – Rate of change of liquid holdup against gas superficial velocity for all liquid superficial velocities at 64 cP

Since rate of change is calculated, it is expected that the rate will decrease with gas superficial velocity; however, due to tighter decreases in liquid holdup between some gas superficial velocities, small increases in rate (at 0.735 m/s) are observed. Nevertheless, overall trend is a decrease in rate with gas superficial velocity.

Similarly, it was considered to investigate rate of change of liquid holdup with liquid superficial velocity. However, due to small magnitude of liquid superficial velocities investigated as well as the limited number of liquid superficial velocities investigated, the analysis is limited only to gas superficial velocities for rate of change of liquid holdup.

The liquid holdup can also be presented by holdup ratio. Holdup ratio is the ratio of the following quantities:

- 1) Experimental liquid holdup using ECT to its complement.
- 2) Homogeneous liquid holdup to homogeneous gas holdup (or void fraction).

Mathematically, this parameter can be evaluated or defined using Equation 4.1.

$$\text{Holdup or slip ratio} = \frac{\frac{1 - \varepsilon_g}{\varepsilon_g}}{\frac{1 - \varepsilon_{gH}}{\varepsilon_{gH}}} = \frac{u_g}{u_l} \quad [4.1]$$

Using this parameter normalises the liquid holdup by using the input homogeneous liquid and gas fractions.

For each individual angle, the holdup ratio was plotted against gas superficial velocity at five different liquid superficial velocities for 64 cP experiments, as shown in Figure 4.5. The quantity holdup ratio (HR) was utilised by Govier and co-workers (1975). The ratio can vary from unity to values of 100 depending on whether the flow is (pseudo)homogeneous or not. Values near unity would also imply that the slip velocity is close to zero as would be expected in homogeneous flow. The lowest

holdup ratio for 64 cP runs was 1.24 while the maximum holdup ratio was 15.04. It can be noted in these graphs that there are many peaks and troughs for each inclination. Govier and co-workers (1975) related these peaks and troughs to flow pattern transitions in vertical and horizontal pipelines. However, the maximum and minimum are not so clear in the case of 64 cP experiments except for lowest liquid superficial velocity. Nevertheless, holdup ratio still provides a way of normalising liquid holdup (or gas phase fraction). The use of holdup ratio is essential and useful in enabling the comparison of different datasets with different physical properties.

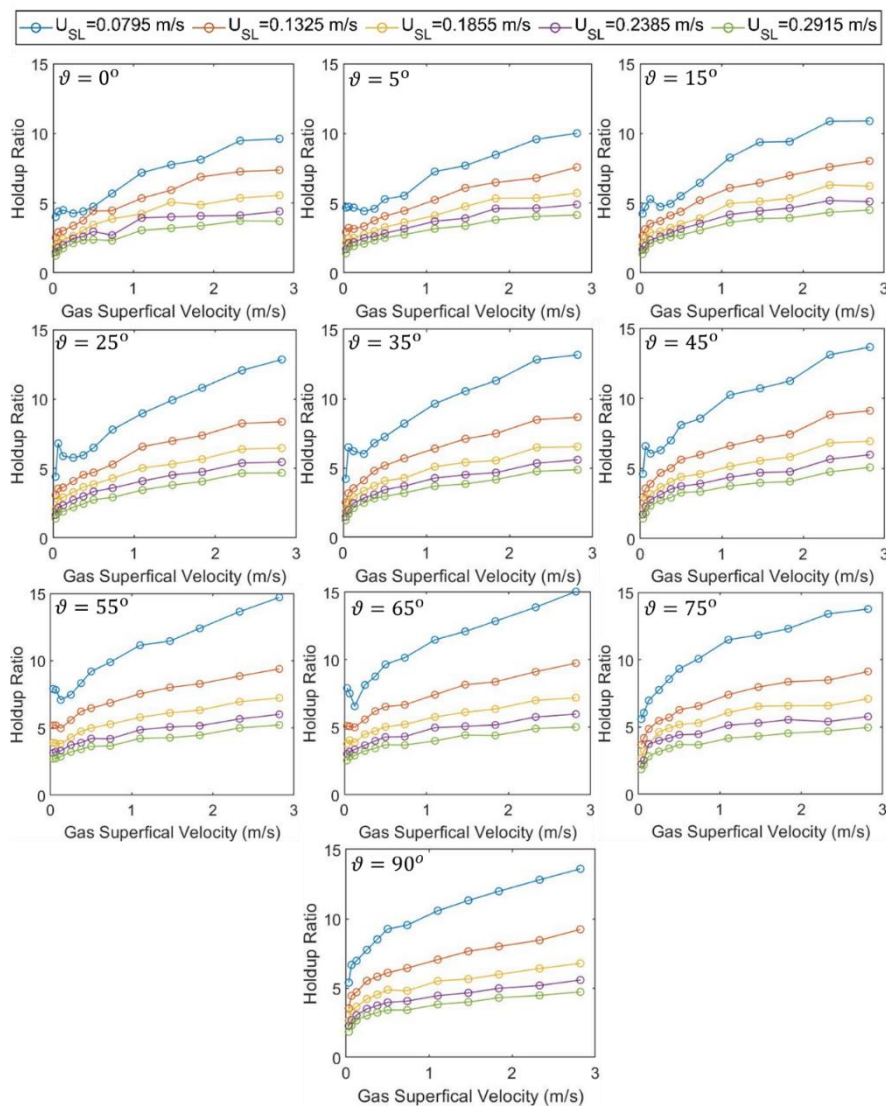


Figure 4.5 – Influence of inclination on holdup ratio (HR) for different liquid and gas superficial velocities at oil viscosity of 64 cP

#### 4.3.2. 91.5 cP experimental campaign

The second experimental campaign involved investigating a liquid viscosity of 91.5 cP. The influence of inclination angle on liquid holdup for all runs at a liquid viscosity of 91.5 cP is shown in Figure 4.6. There are four sub graphs in total, each referring to a specific liquid superficial velocity. Each sub-graph has eleven lines, each representing a superficial gas velocity. The range of liquid holdup values for 91.5 cP runs varied from 29 % to 95 % (0.29 – 0.95).

Again, it is of great importance to analyse the inclination angle at which the liquid holdup reaches a maximum. In total, there are 44 cases which all except one (45 degrees) reach a maximum at 65 degrees. However, it must be emphasised that a wider range of inclination angles (10 angles) were investigated for 64 cP experiments compared to only five inclination angles for 91.5 cP experiments. Therefore, exact determination or a tight range (like in the case of 64 cP experiments) cannot be determined. For 64 cP, maximum liquid holdup occurred at angles of 55 to 75 degrees however most cases (43.3 %) recorded a maximum liquid holdup at 65 degrees. This matches with the mode angle of 65 degrees (97.7 % of all cases recorded) at which maximum liquid holdup occurs for 91.5 cP experimental campaign.

For all runs, the range of percentage increases in liquid holdup from horizontal inclination up to inclination with the maximum liquid holdup was 2.5 – 27.3 % while range of percentage decreases in liquid holdup from the inclination with the maximum liquid holdup to vertical inclination varied between 0.5 and 6.2 %. For all runs, the range of ratio of the percentage increase to the percentage decrease varies between 1.2 and 29.8.

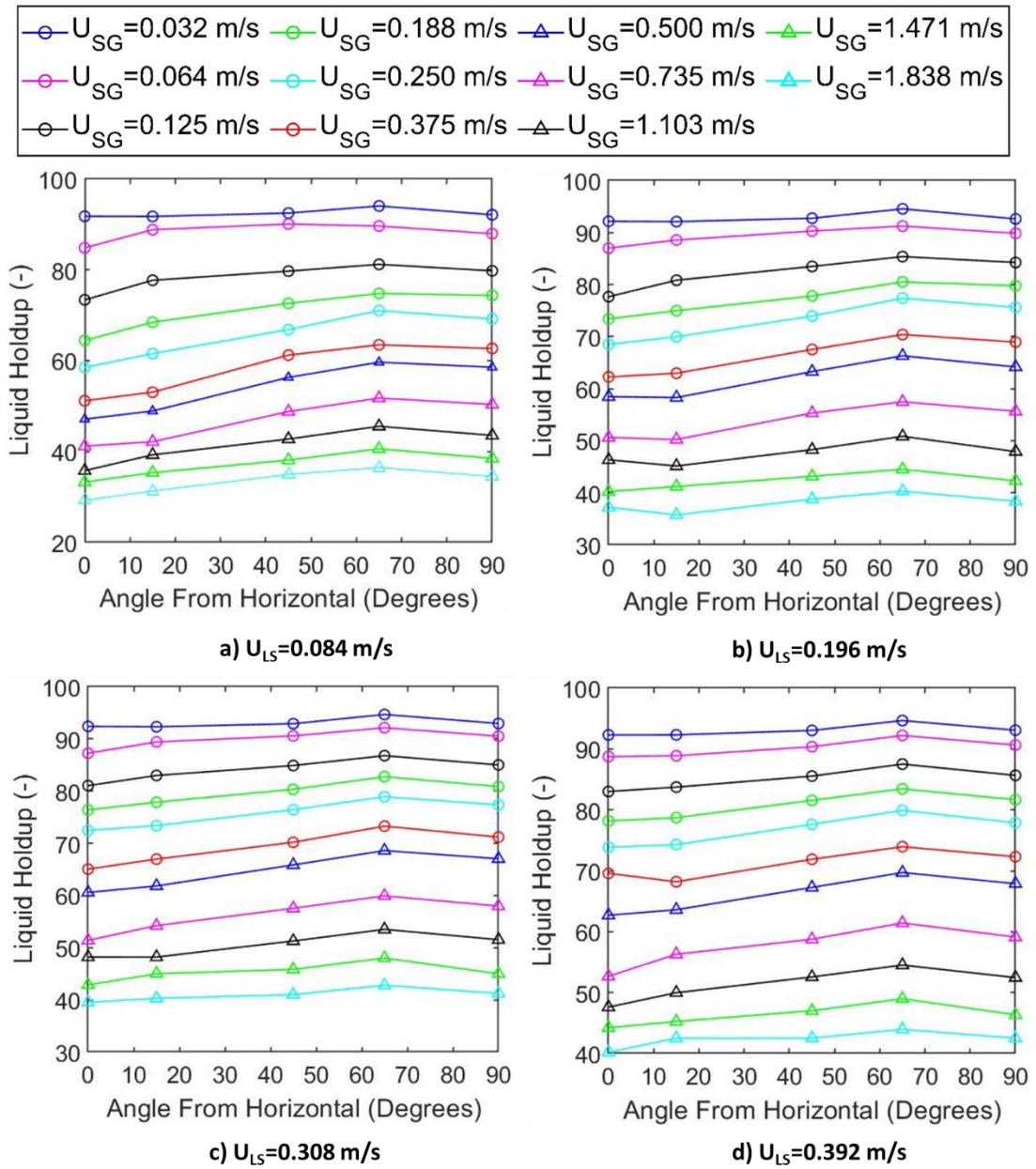


Figure 4.6 – Influence of inclination angle on liquid holdup for different liquid and gas velocities at oil viscosity of 91.5 cP

Figure 4.7 shows how experimental gas voidage (complement of liquid holdup) compares with the homogeneous gas void fraction for 91.5 cp oil at each inclination angle. With exception of 2 points, all experimental points lie below the red  $x - y$  line. However, the difference between those points and red line is extremely small. The main reason for this discrepancy is believed to be caused by the measurement (ECT) technique error. As observed in Figure 4.2, points plotted resemble a plot of experimental void fraction against gas superficial velocity while dispersion of the data is due to the fact that four different liquid superficial velocities were investigated.

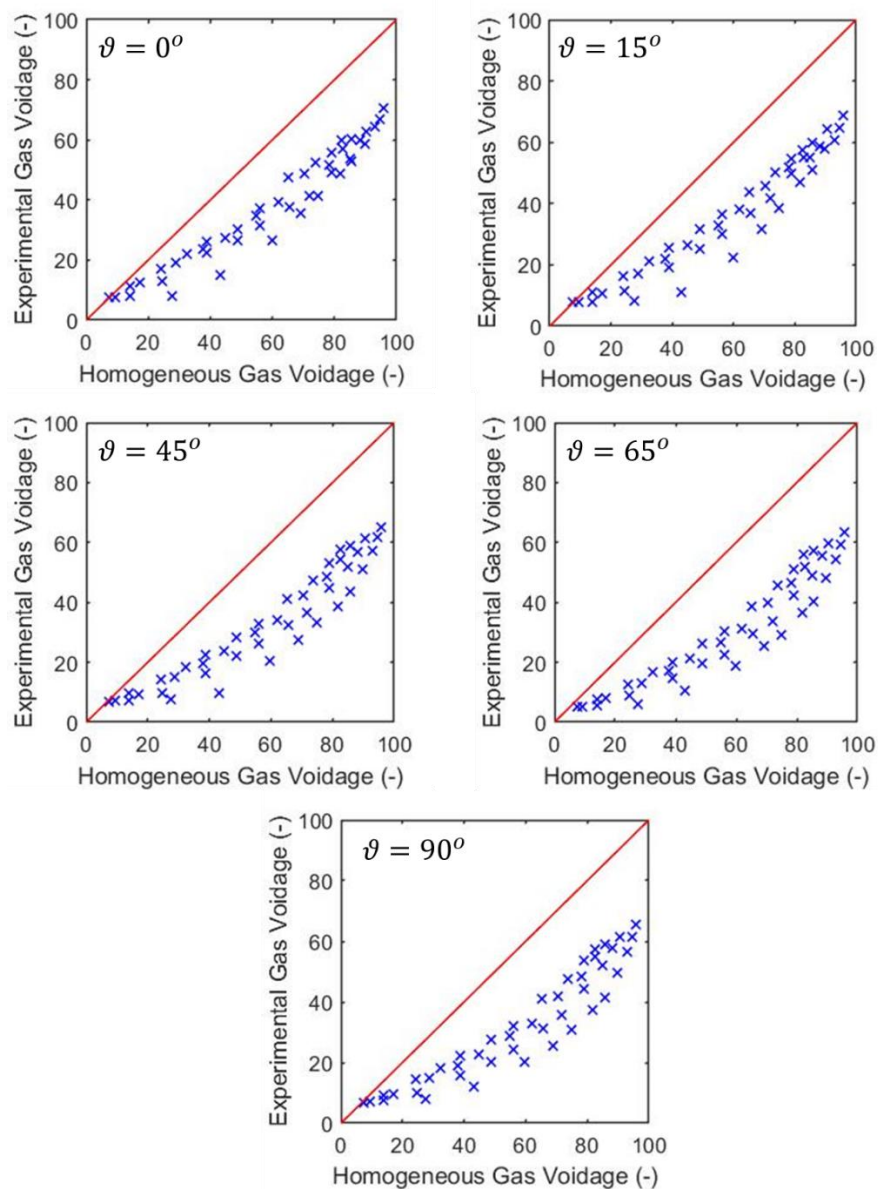


Figure 4.7 – Comparing experimental and homogeneous gas voidage for all runs at 91.5 cP oil

Figure 4.8 shows how liquid holdup for 91.5 cP runs varies with gas and liquid superficial velocities for each inclination angle. Again, it can be observed that changes in liquid holdup are sensitive at low gas superficial velocities compared to changes at high superficial velocity.

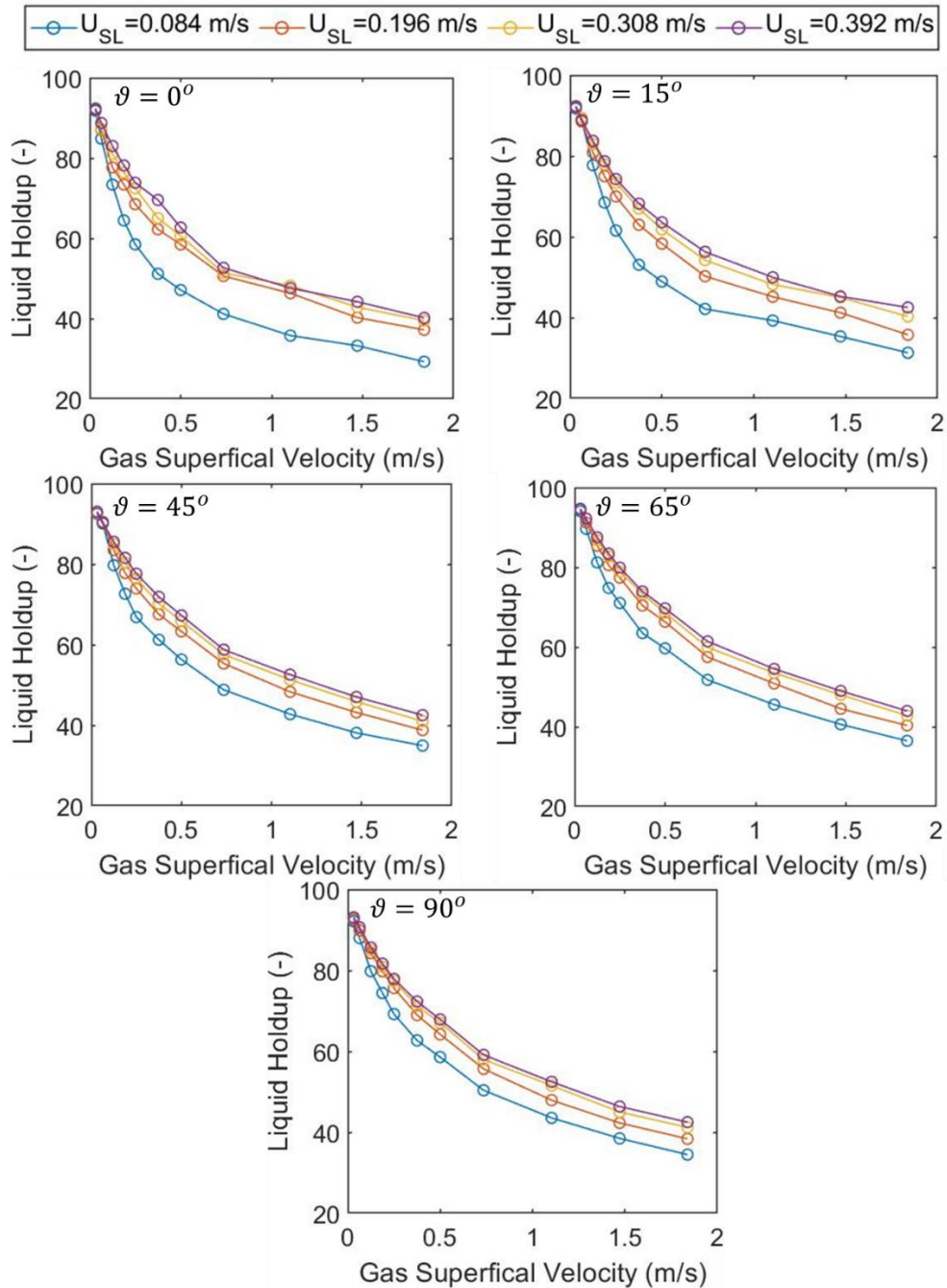


Figure 4.8 – Variation of liquid holdup for 91.5 cP runs against superficial gas velocity at various liquid superficial velocities for each inclination angle

Similarly to 64 cP, rate of change of liquid holdup was plotted against gas superficial velocities at all liquid superficial velocities for vertical inclination at liquid viscosity of 91.5 cP, as shown in Figure 4.9. As discussed for 64 cP, it can be observed that the rate of change of liquid holdup is much steeper at low gas superficial velocities while it slows down for higher gas superficial velocities. As discussed in Figure 4.4, small increases in rate are observed between some gas superficial velocities however overall trend is decreasing rate with gas superficial velocity. The reason as mentioned for 64 cP is due to small decrease in liquid holdup between some gas superficial velocity.

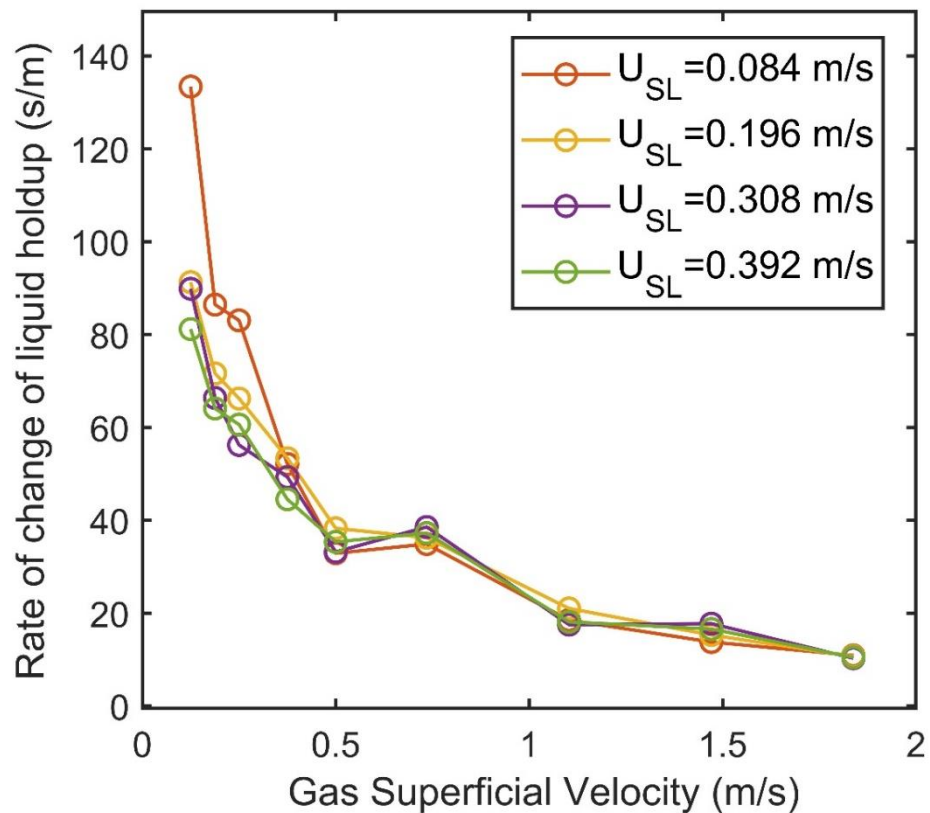


Figure 4.9 – Rate of change of liquid holdup against gas superficial velocity for all liquid superficial velocities at 91.5 cP (Vertical Inclination)

For each individual angle, the holdup ratio was plotted against gas superficial velocity at five different liquid superficial velocities for 91.5 cP experiments, as shown in Figure 4.10. The range of holdup ratio for 91.5 cP runs was from 0.97 to 12.56. It can be noted in these graphs that there are many peaks and troughs for each inclination.

Again, the maximum and minimum are not so clear in the case of 91.5 cP experiments except for lowest liquid superficial velocity therefore flow regime transitions cannot be determined using this method.

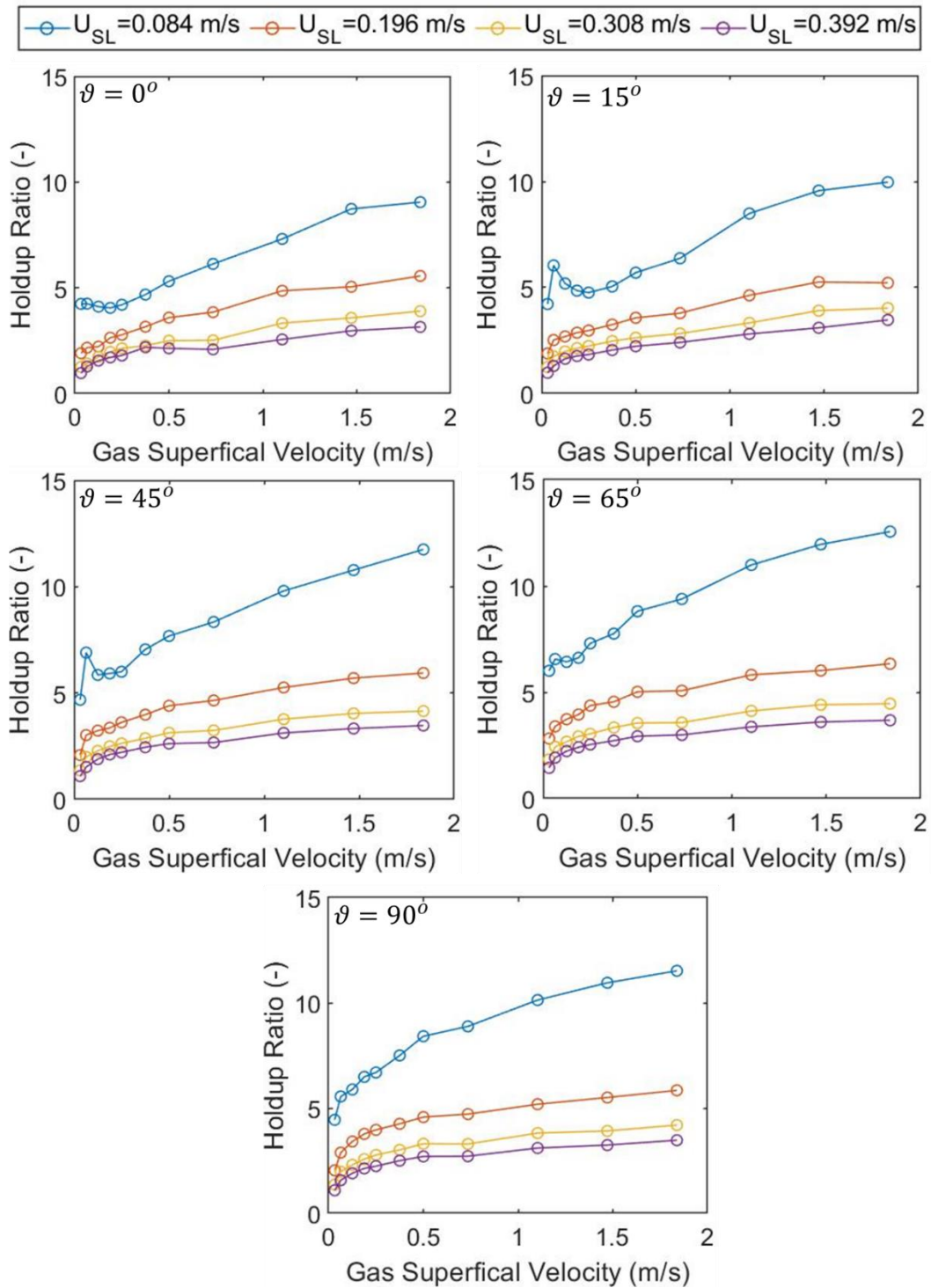


Figure 4.10 – Influence of inclination angle on holdup ratio (HR) for different liquid and gas velocities at oil viscosity of 91.5 cP

#### 4.3.3. 236 cP experimental campaign

The third experimental campaign involved investigating a liquid viscosity of 236 cP. The influence of inclination angle on liquid holdup for all runs at a liquid viscosity of 236 cP is shown in Figure 4.11. There are three sub graphs in total, each referring to a specific liquid superficial velocity. Each sub-graph has eleven lines, each representing a superficial gas velocity. The range of liquid holdup values for 236 cP runs varied from 34 % to 96 % (0.34 – 0.96). One interesting observation regarding the liquid holdup range is that the minimum liquid holdup increases with viscosity while the maximum almost stays constant at around 95 – 96 %.

Similar to 64 cP and 91.5 cP experimental campaign, the angle at which maximum liquid holdup occurs was also analysed for 236 cP. Overall, there are 33 lines of which 60.6 % of the lines reach a maximum at 65 or 45 degrees. For 64 cP experiments, none of the maximums occurred at 45 degrees while only one case had a maximum at 45 degrees for 91.5 cP. In comparison, there are many cases for 236 cP which exhibits a maximum at 45 degrees. The main reason for this discrepancy could be due to the fact that 64 cP runs involved investigating a wide range of inclination angles compared to 91.5 cP and 236 cP runs.

Moreover, the range of percentage increases in liquid holdup from horizontal inclination up to inclination with the maximum liquid holdup when comparing all runs was 4.7 – 32.7 % while range of percentage decreases in liquid holdup from the inclination with the maximum liquid holdup to vertical inclination varied between ~0 and 2.61 %.

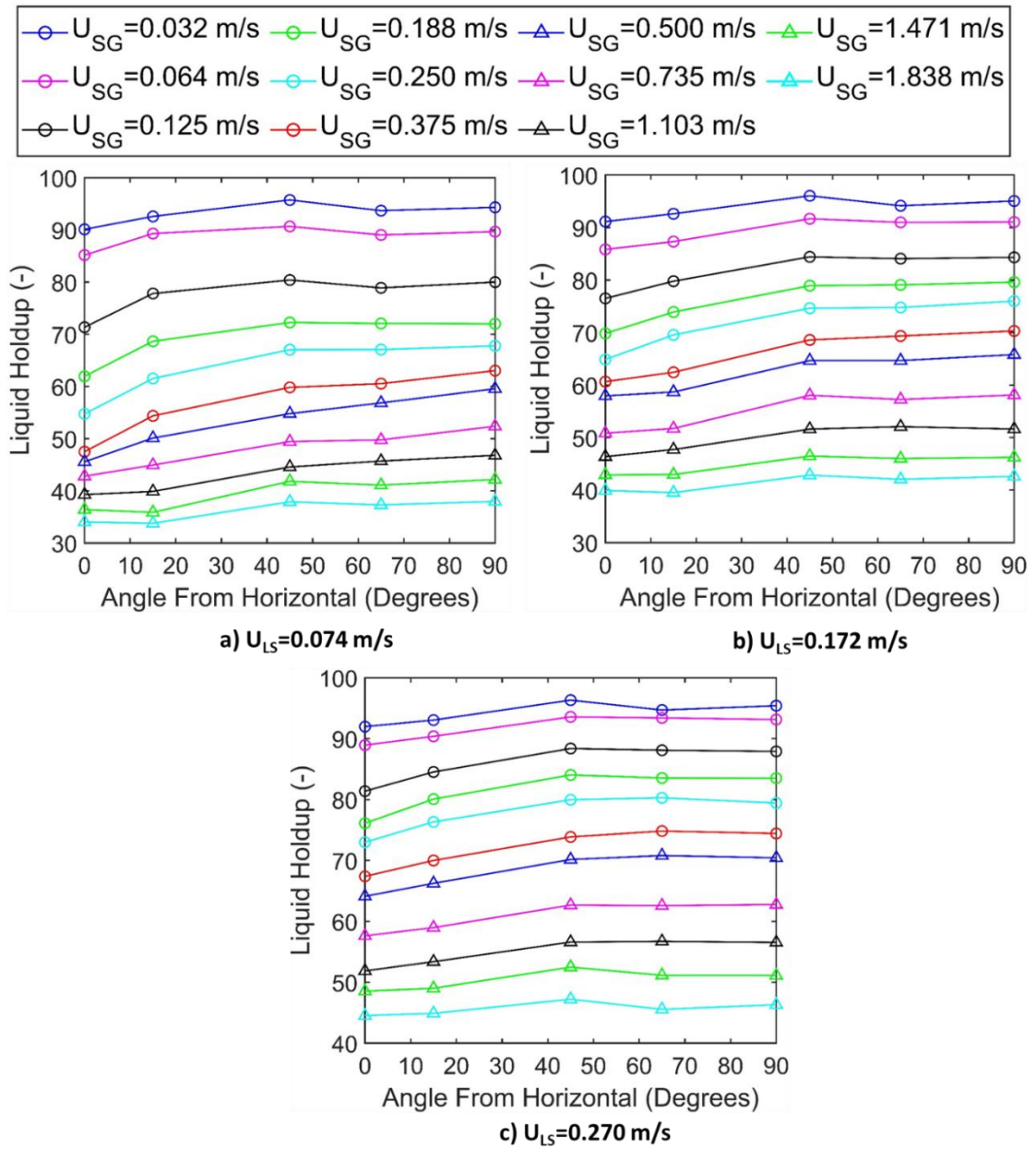


Figure 4.11 – Influence of inclination angle on liquid holdup for different liquid and gas velocities at oil viscosity of 236 cP

Figure 4.12 shows how experimental gas voidage (complement of liquid holdup) compares with the homogeneous gas void fraction for 236 cP oil at each inclination angle. All experimental points lie below the red  $x - y$  line. As mentioned for Figures 4.2 and 4.7, Figure 4.12 resembles a plot of experimental void fraction against gas superficial velocity while the dispersion of points is due to different liquid superficial velocities that are being investigated.

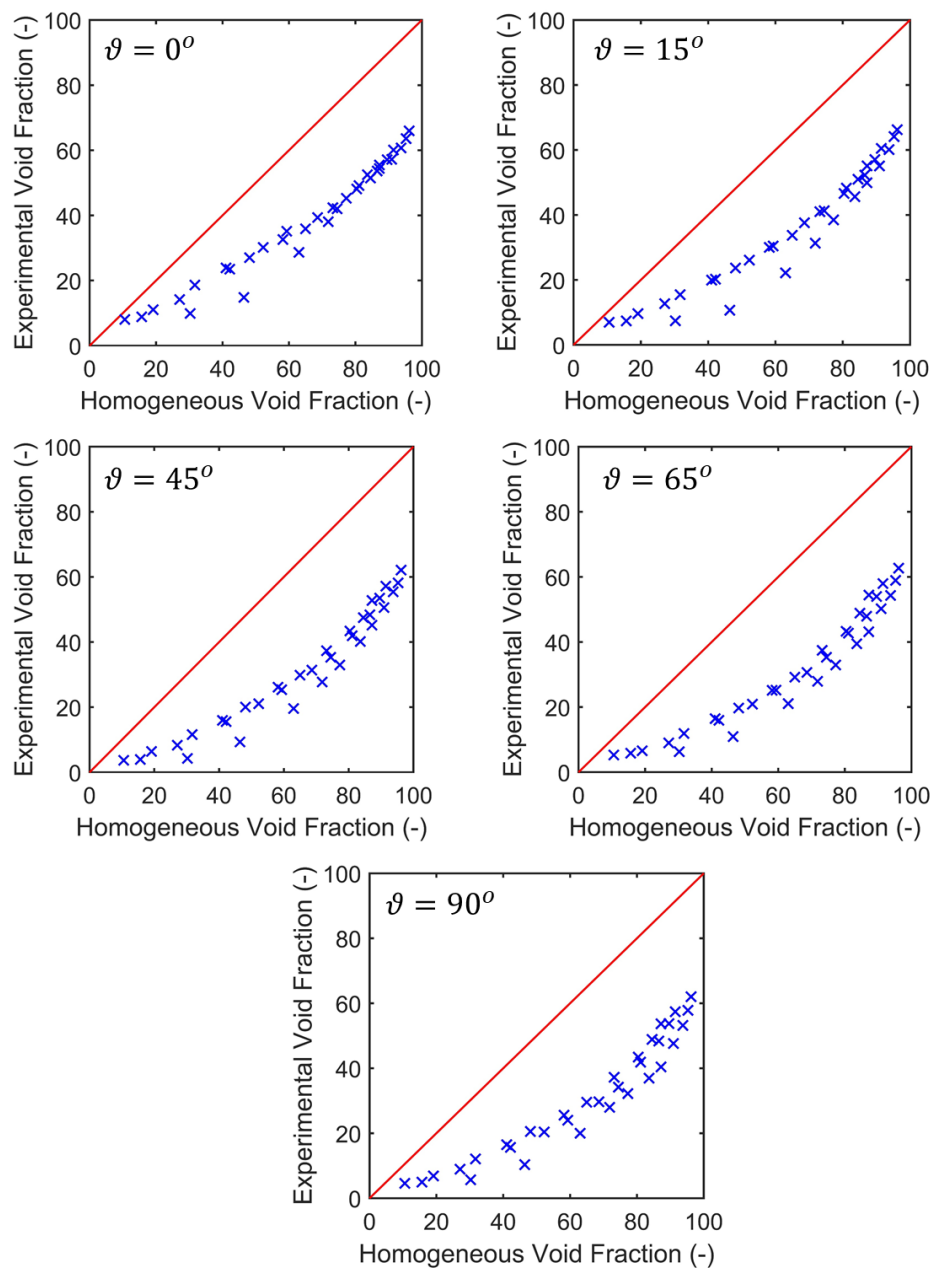


Figure 4.12 – Comparing experimental and homogeneous gas voidage for all runs at 236 cP oil

Figure 4.13 shows how liquid holdup for 236 cP runs varies with gas and liquid superficial velocities for each inclination angle. The response of liquid holdup to changes in gas superficial velocity is more enhanced for lower gas superficial velocities compared to higher superficial velocities.

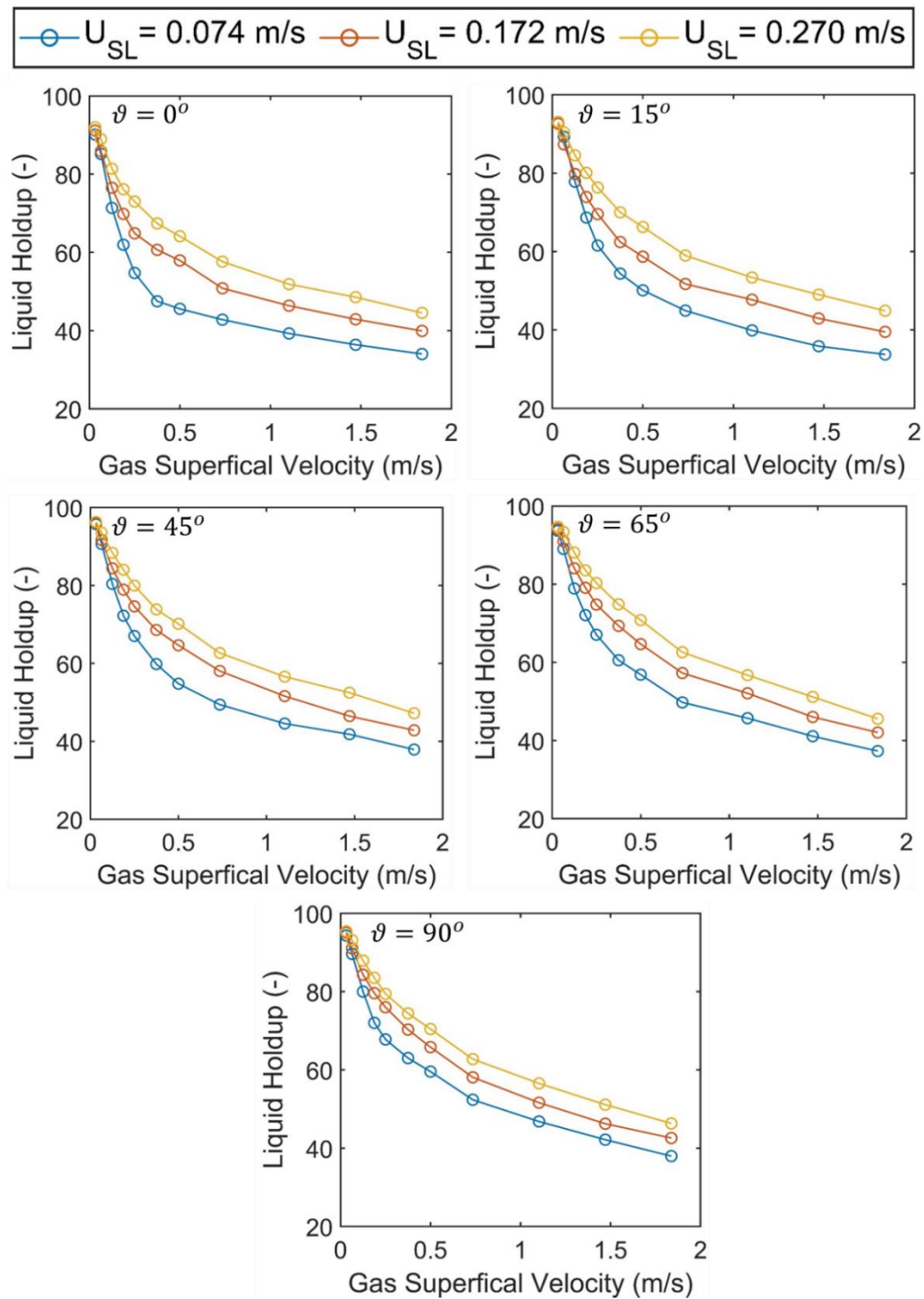


Figure 4.13 – Variation of liquid holdup for 236 cP runs against superficial gas velocity at various liquid superficial velocities for each inclination angle

Figure 4.14 shows rate of change of liquid holdup with gas superficial velocity. Similar trends to 64 cP and 91.5 cP runs are observed. The rate of change of liquid holdup is very sensitive at low superficial gas velocities compared to high superficial gas velocities. As discussed in Figures 4.4 and 4.9, small increases in rate are observed between some gas superficial velocities however overall trend is decreasing rate with gas superficial velocity. The reason as mentioned for 64 cP and 91.5 cP is due to small decrease in liquid holdup between some gas superficial velocities.

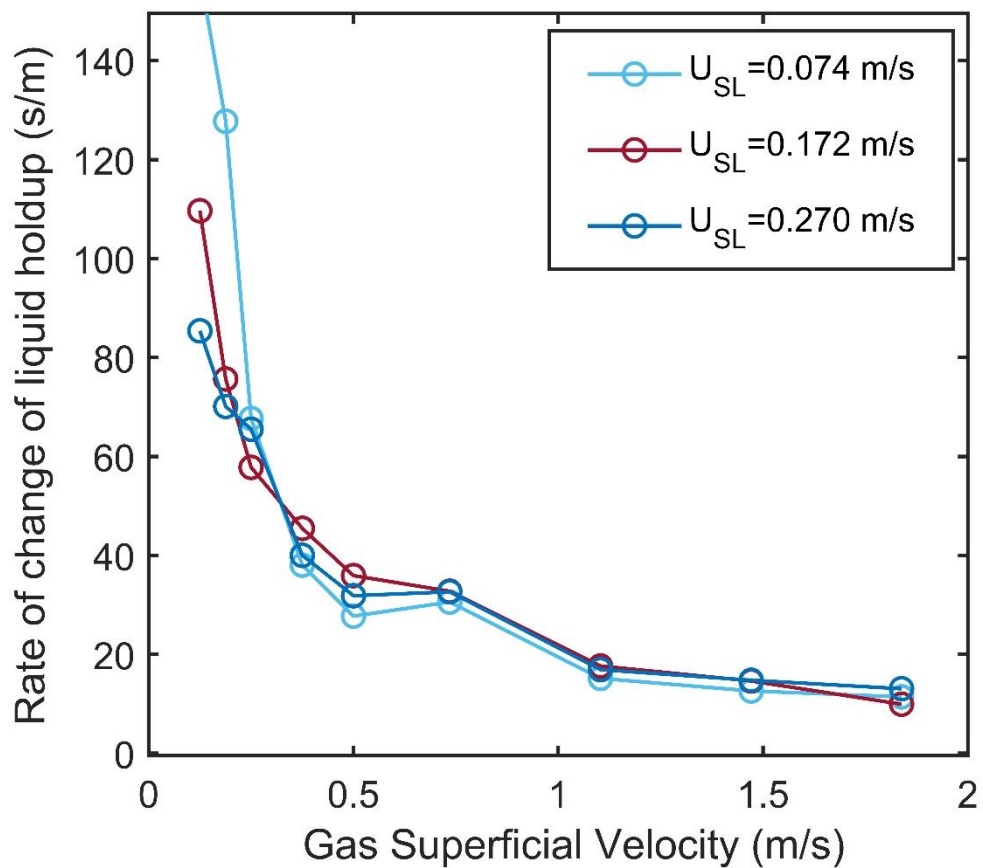


Figure 4.14 – Rate of change of liquid holdup against gas superficial velocity for all liquid superficial velocities at 236 cP

For each individual angle, the holdup ratio was plotted against gas superficial velocity at five different liquid superficial velocities for 236 cP experiments, as shown in Figure 4.15. The lowest holdup ratio for 236 cP runs was 1.35 while the maximum holdup ratio was 15.32. Similar to 64 cP and 91.5 cP experiments, maximum and minimum

at all liquid superficial velocities could not be clearly defined to study flow regime transitions.

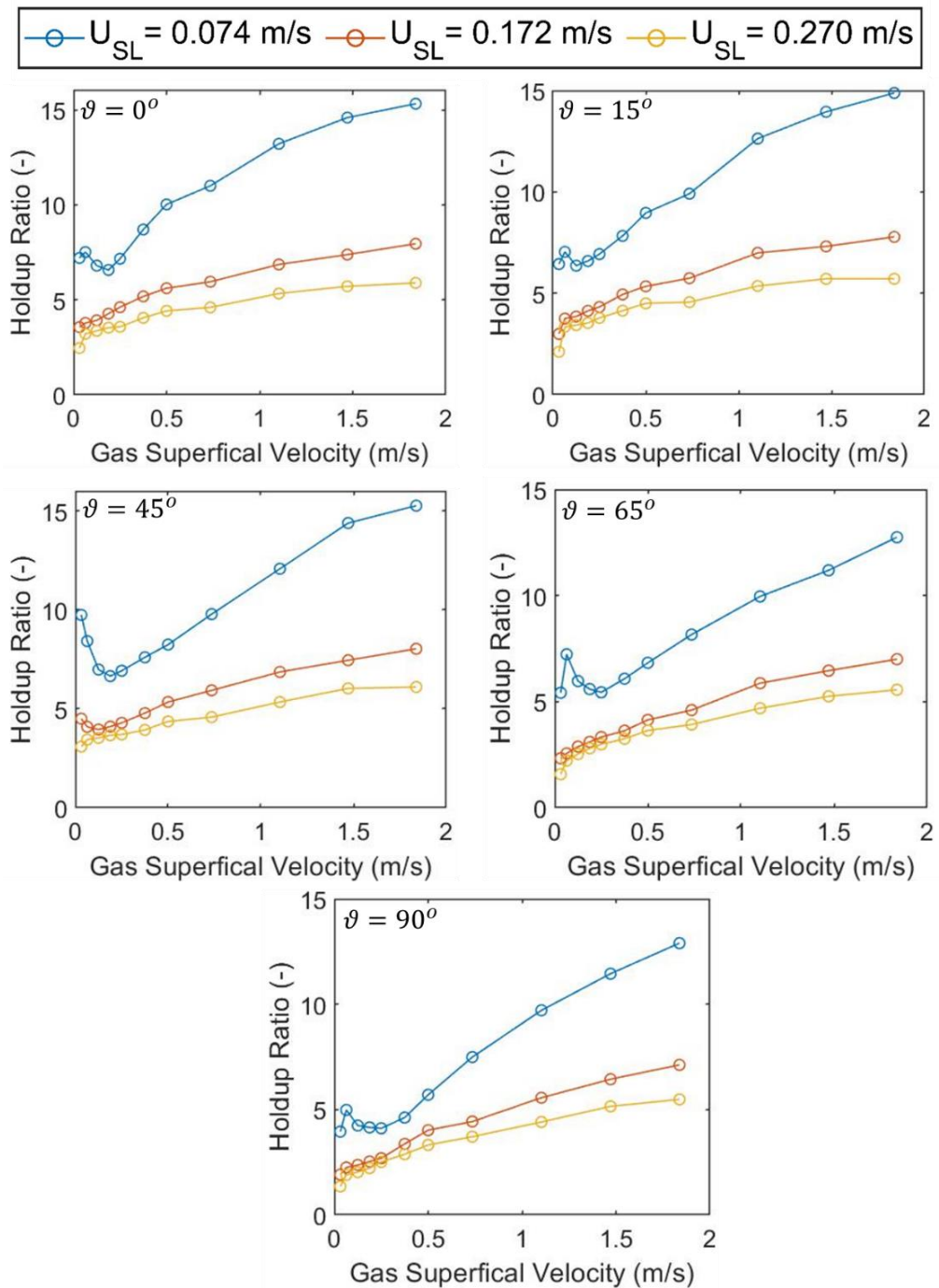


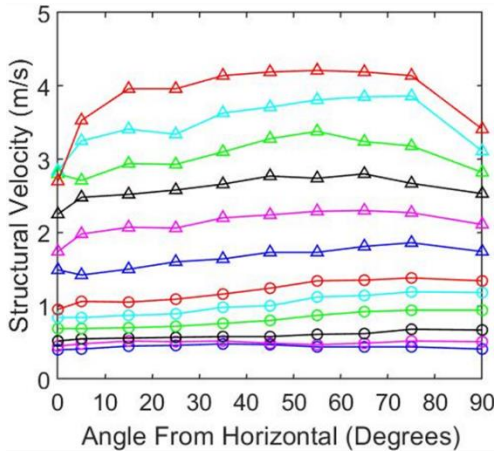
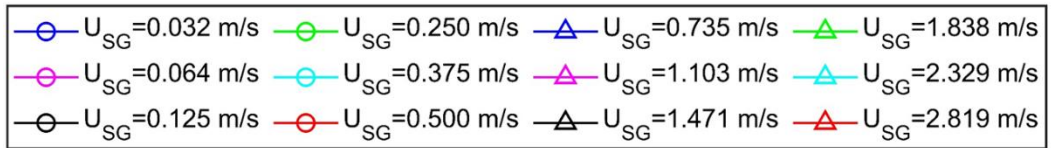
Figure 4.15 – Influence of inclination angle on holdup ratio (HR) for different liquid and gas velocities at oil viscosity of 236 cP

## 4.4. Effect of inclination angle on structure velocity

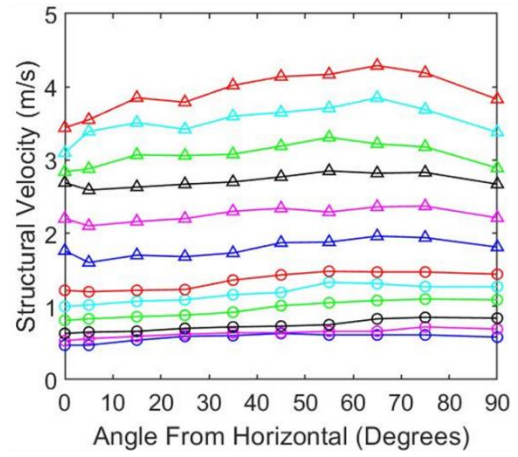
### 4.4.1. 64 cP experimental campaign

Structure velocity was obtained by cross-correlating the dual plane signals of the ECT. Figure 4.16 shows the variation of structure velocity against inclination angle for all runs at liquid viscosity of 64 cP. There are five sub graphs in total. Each sub graph refers to a specific liquid superficial velocity. Each sub-graph has twelve lines in total where each line is represented by a superficial gas velocity. The typical trend should resemble a second order polynomial however error in measurements by ECT at high gas and liquid superficial velocities can impact on the accuracy of structure velocity. Another source of error is the rapid and high fluctuations in rotameter readings at high gas superficial velocities.

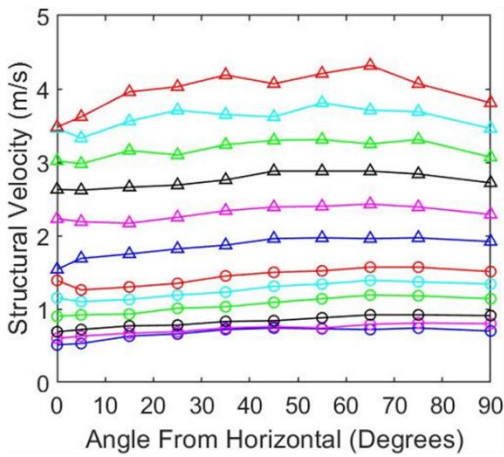
At increasing liquid superficial velocities for given gas superficial velocities (or vice versa), the structure velocity also increases, an agreement of Nicklin's equation (Nicklin, 1962). Each line plotted in Figure 4.16 first increases with increasing inclination angle, reaching a maximum. After that, increases in inclination angle decreases the structure velocity. There are sixty individual lines in total of that 55 of them have a maximum at inclination angles between 55 – 75 degrees which is in close agreement to that reported value of 50 degrees by Zukoski (1966). The maximum structure velocity can be explained by considering the two opposing forces acting on the system: buoyancy and friction. Balancing of these two forces produces a maximum somewhere between 55 and 75 degrees.



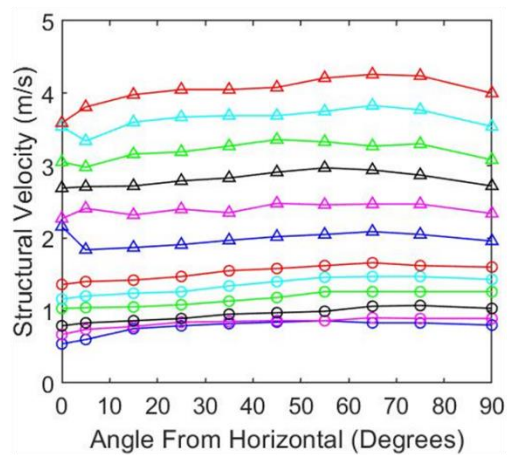
**a)  $U_{LS}=0.080$  m/s**



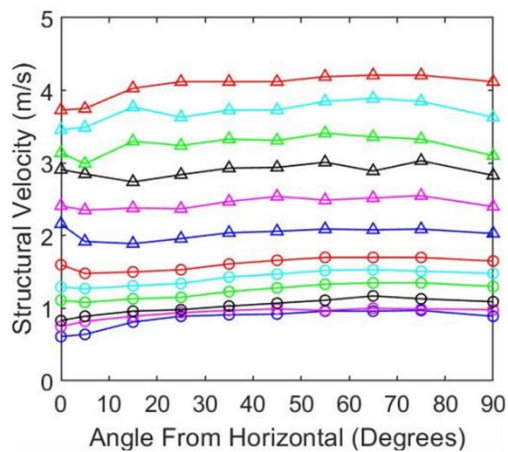
**b)  $U_{LS}=0.133$  m/s**



**c)  $U_{LS}=0.186$  m/s**



**d)  $U_{LS}=0.239$  m/s**



**e)  $U_{LS}=0.292$  m/s**

Figure 4.16 – Influence of inclination angle on structure velocity for different liquid and gas velocities at oil viscosity of 64 cP

Figure 4.17 shows how the gas velocity (gas superficial velocity divided by gas void fraction) varies with mixture superficial velocity at each inclination angle for 64 cP data.

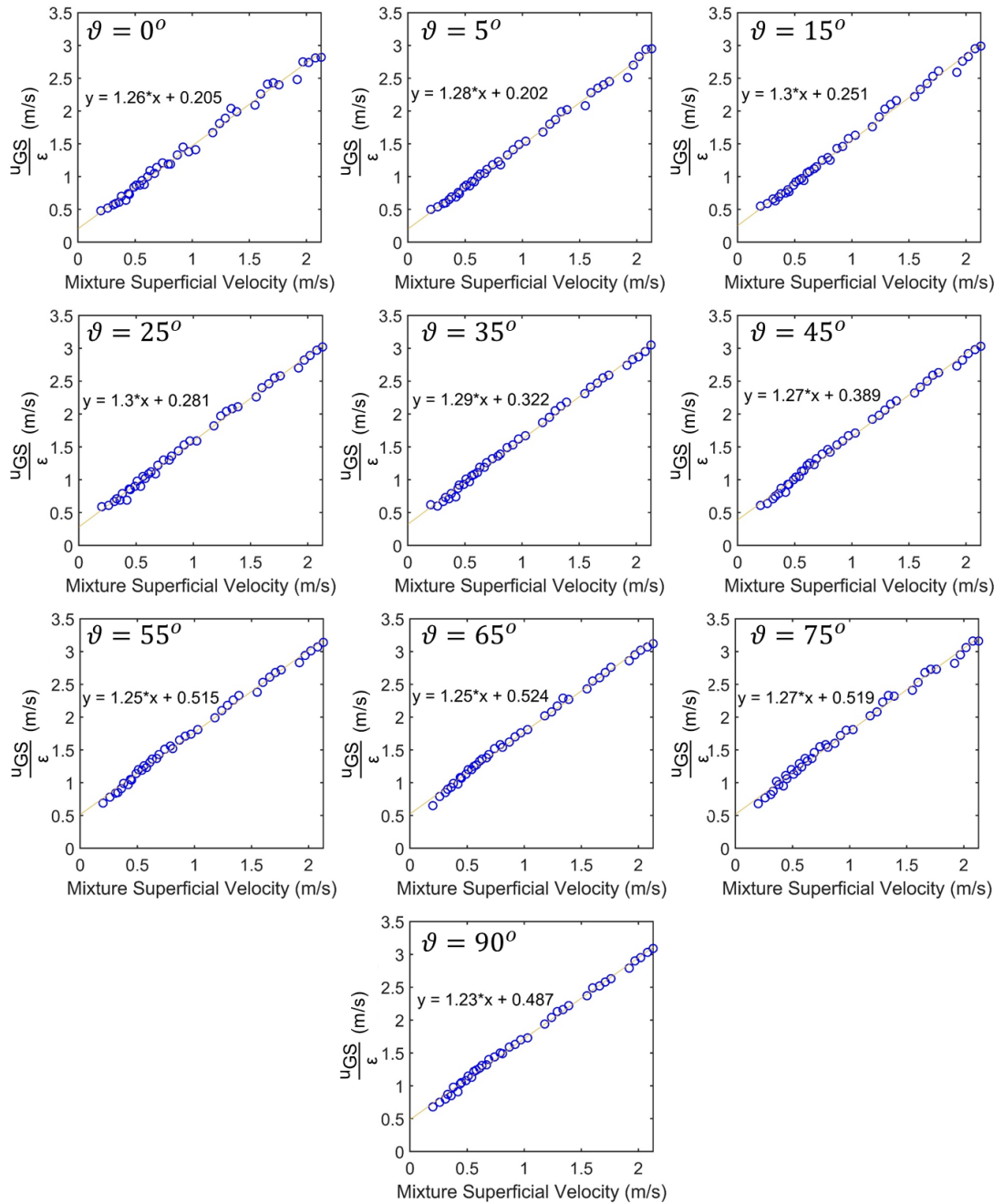


Figure 4.17 – Variation of gas velocity against mixture velocity at each inclination angle for 64 cP data

The two lowest superficial gas velocities (0.032, 0.064) and two highest gas superficial velocities (2.329, 2.819) were not used for this analysis. From this plot, the distribution coefficient and drift velocity can be determined. The gradient corresponds to the distribution coefficient while the y – intercept corresponds to the drift velocity.

Table 4.2 summarises the distribution coefficient, drift velocity and Froude Number at each inclination angle for 64 cP data. Froude number was evaluated using Equation 2.58. The distribution coefficient ranges between 1.23 and 1.30 while the drift velocity varies between 0.202 and 0.524. Drift velocity reaches a maximum at an inclination angle of 65 degrees. The distribution coefficient variation with angle is not significant (only 0.07 over the whole range of inclination angles). The overall range for Froude number varies between 0.249 and 0.646. The  $R^2$  for each line was also evaluated and it can be seen that the linear fit of each line is appropriate as  $R^2$  is close to 1. For the whole dataset, it varies between 0.993 and 0.997.

*Table 4.2 – Summary of distribution coefficient, drift velocity and Froude number at each inclination for 64 cP data*

Angle	$C_o$	$V_d$	$Fr = V_d/(Dg)^{0.5}$	$R^2$
0	1.26	0.205	0.253	0.993
5	1.28	0.202	0.249	0.997
15	1.30	0.251	0.310	0.995
25	1.30	0.281	0.347	0.996
35	1.29	0.322	0.397	0.997
45	1.27	0.389	0.480	0.996
55	1.25	0.515	0.635	0.996
65	1.25	0.524	0.646	0.996
75	1.27	0.519	0.640	0.994
90	1.23	0.487	0.601	0.997

Graphical representation of each parameter from drift flux model in Table 4.2 with inclination angle is represented by Figure 4.18. Moreover, their rate of change with angle was also evaluated for each property. It can be observed that rate of change with angle is much higher for drift velocity and Froude number compared to distribution coefficient. Maximum recorded rate of change with angle for distribution coefficient was 0.004 while maximum recorded rate of change with angle for drift velocity and Froude number was 0.013 m/s and 0.016 respectively. The trends of drift velocity, distribution coefficient and Froude number were discussed through Table 4.2.

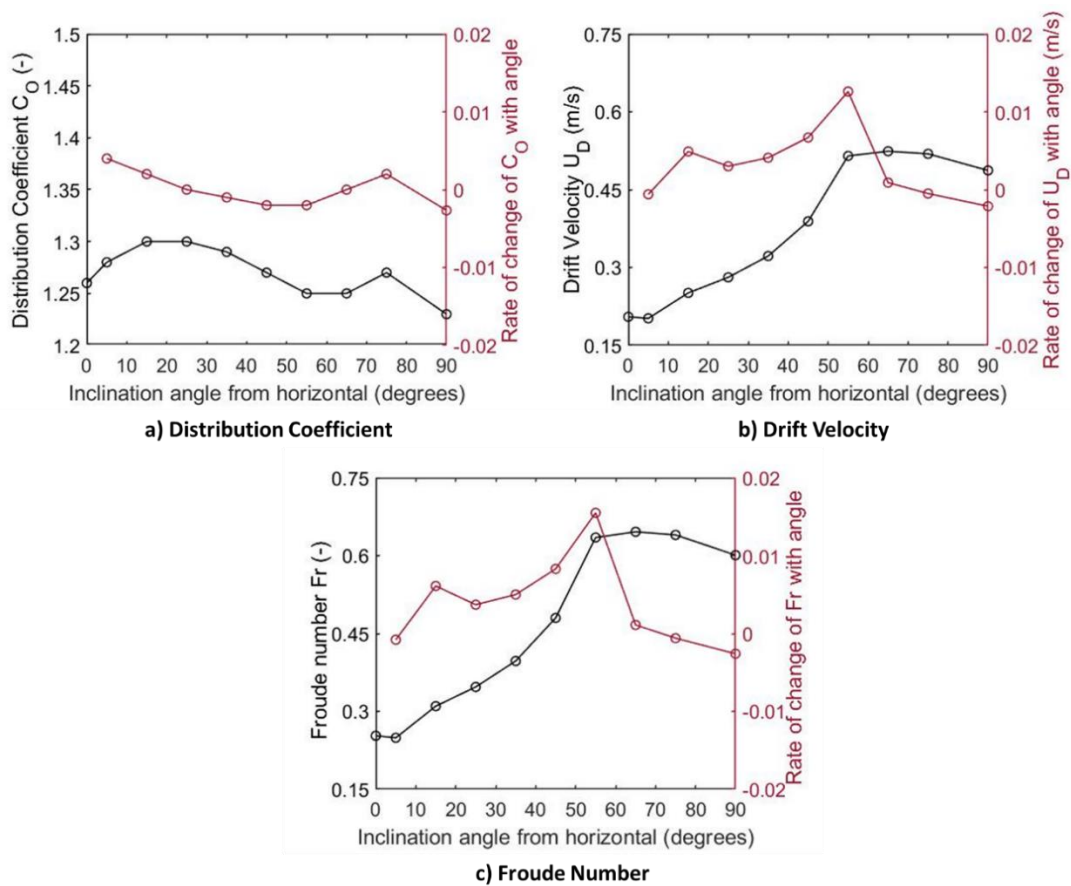


Figure 4.18 – Effect of inclination angle on  $C_O$ ,  $U_D$ ,  $Fr$  and their rate of change with angle for liquid viscosity of 64 cP

Rate of change of  $C_o$  with angle first decreases with inclination angle (up to 55 degrees). Then, rate of change of  $C_o$  increases up until inclination angle of 75 degrees with the rate decreasing again when inclination angle is increased from 75 to 90 degrees.

In comparison, rate of change of drift velocity with angle increases up until 15 degrees, then it decreases slightly for increase in inclination angle from 15 degrees to 25 degrees. After 25 degrees, rate of change of drift velocity with angle increases with inclination angle until it reaches a peak at 55 degrees. Finally, rate of change of drift velocity with angle decreases significantly as inclination increases from 55 to 65 degrees after which rate decreases very slowly. Similar trend is observed for Froude Number.

#### 4.4.2. 91.5 cP experimental campaign

The variation in structure velocity with inclination angle for all runs at liquid viscosity of 91.5 cP are presented in Figure 4.19. Four liquid superficial velocities (each represented by a sub graph with eleven lines representing a gas superficial velocity each) were investigated. Comparing reported maximum of 50 degrees by Zukoski (1966), most cases (38 / 44) for 91.5 cP seem to peak around 65 or 45 degrees. The agreement between the two is close.

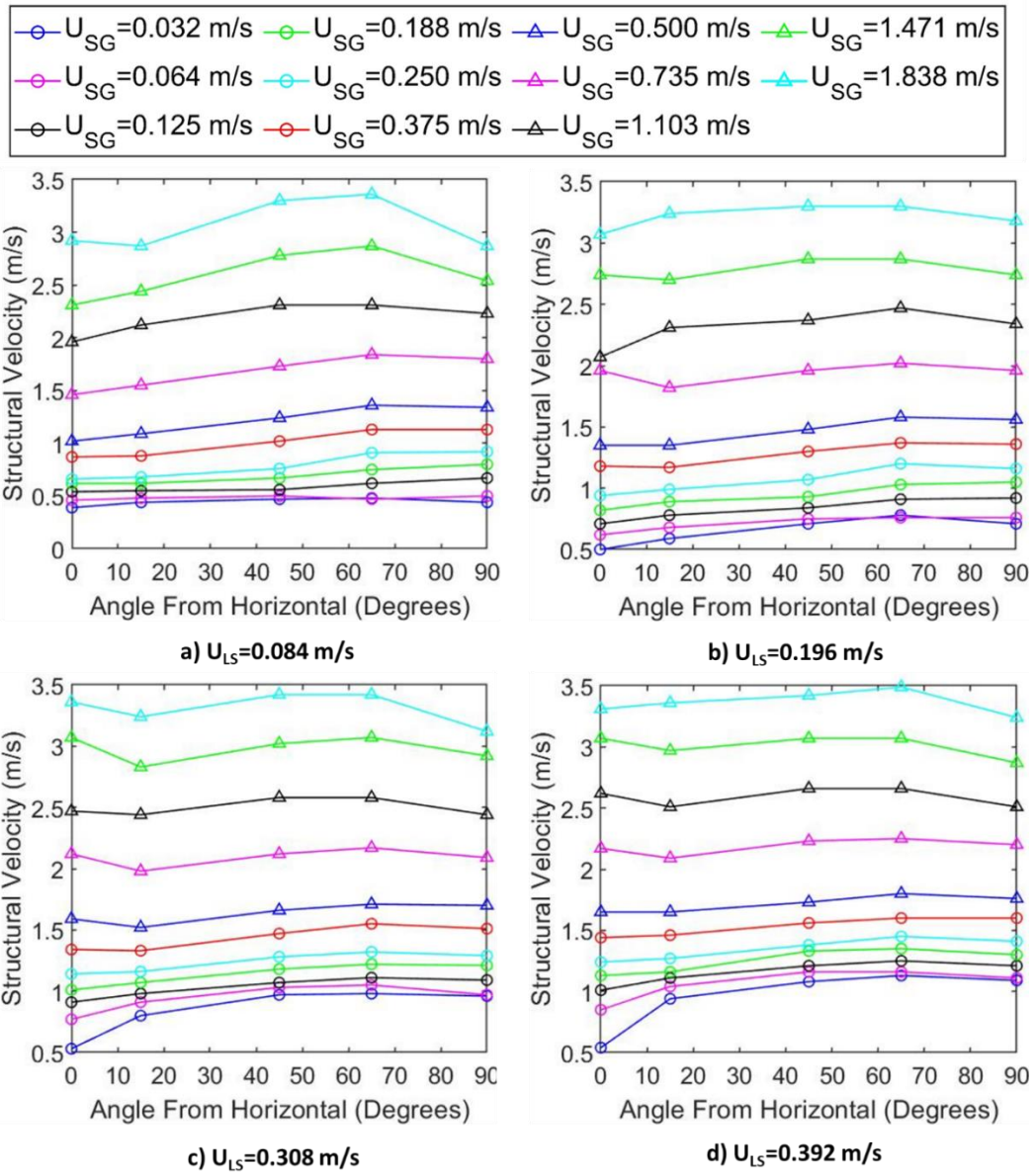


Figure 4.19 – Influence of inclination angle on structure velocity for different liquid and gas velocities at oil viscosity of 91.5 cP

Figure 4.20 shows how the gas velocity (gas superficial velocity divided by gas void fraction) varies with mixture superficial velocity at each inclination angle for 91.5 cP data.

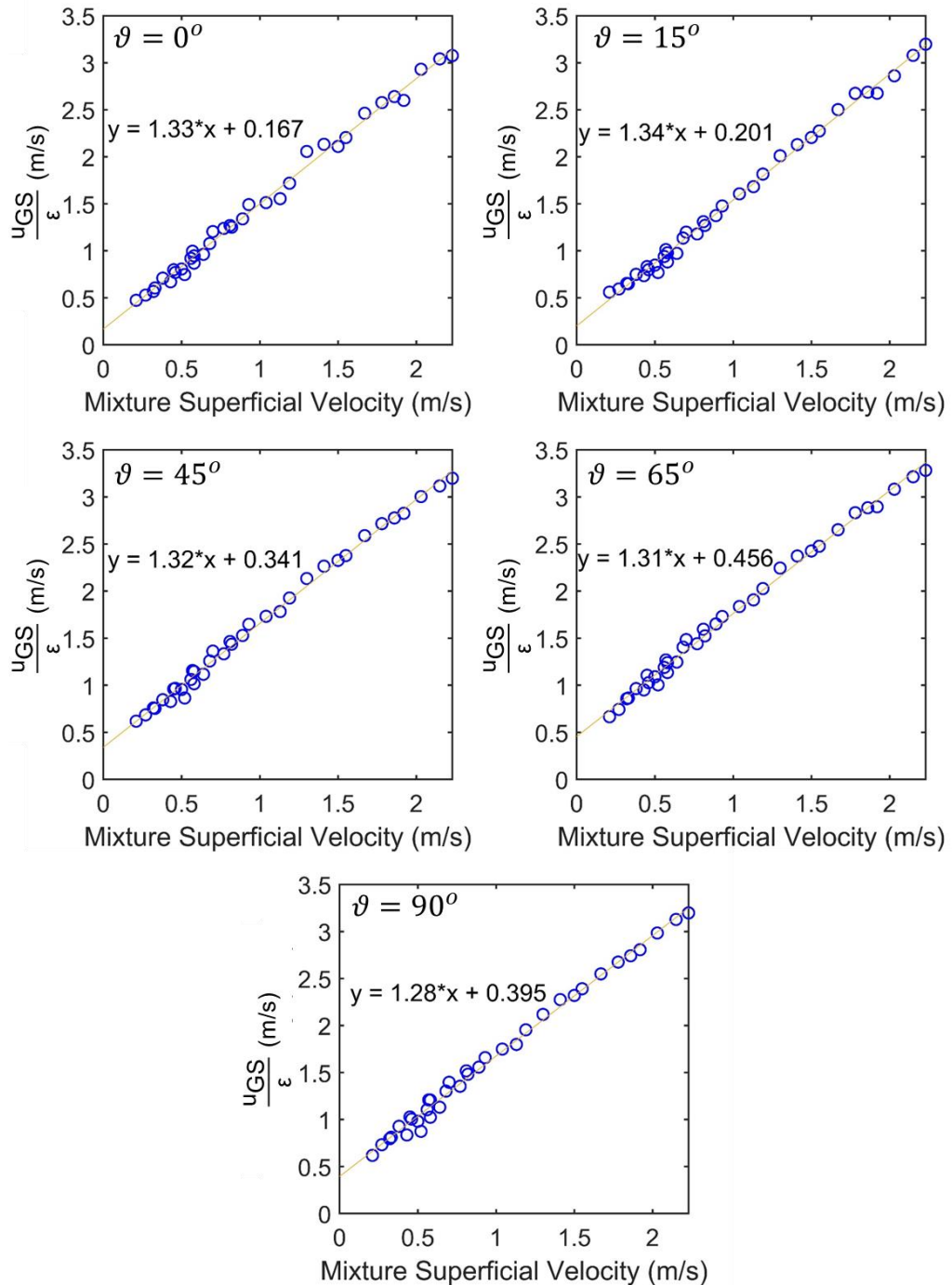


Figure 4.20 – Variation of gas velocity against mixture velocity at each inclination angle for 91.5 cP data

For analysis, similar process to 64 cP was followed in order to determine the distribution coefficients and drift velocities.

Table 4.3 summarises the distribution coefficient, drift velocity and Froude Number at each inclination angle for 91.5 cP data. Again, range of distribution coefficient is small (varies by 0.06) while the drift velocity varies between 0.167 and 0.456. In comparison to 64 cP, drift velocity reaches a maximum at same inclination angle of 65 degrees. Comparing 64 cP and 91.5 datasets, distribution coefficient are higher for 91.5 cP while drift velocity and Froude numbers are lower for 91.5 cP.

*Table 4.3 – Summary of distribution coefficient, drift velocity and Froude number at each inclination for 91.5 cP data*

Angle	$C_o$	$V_d$	Fr	$R^2$
0	1.33	0.167	0.206	0.994
15	1.34	0.201	0.248	0.996
45	1.32	0.341	0.421	0.995
65	1.31	0.456	0.562	0.995
90	1.28	0.395	0.487	0.993

Figure 4.21 shows variation of distribution coefficient, drift velocity and Froude number along with their rate of change with inclination angle for 91.5 cP experiments. Similar to 64 cP, drift velocity and Froude number experienced higher rate of change compared to distribution coefficient which, in case of 91.5 cP, stays at almost zero. The rate of change of  $C_o$  with angle is almost constant with inclination angle while the rate of change of drift velocity and Froude number with angle increases with inclination angle up to 65 degrees after which rate of change of drift velocity and Froude number decreases.

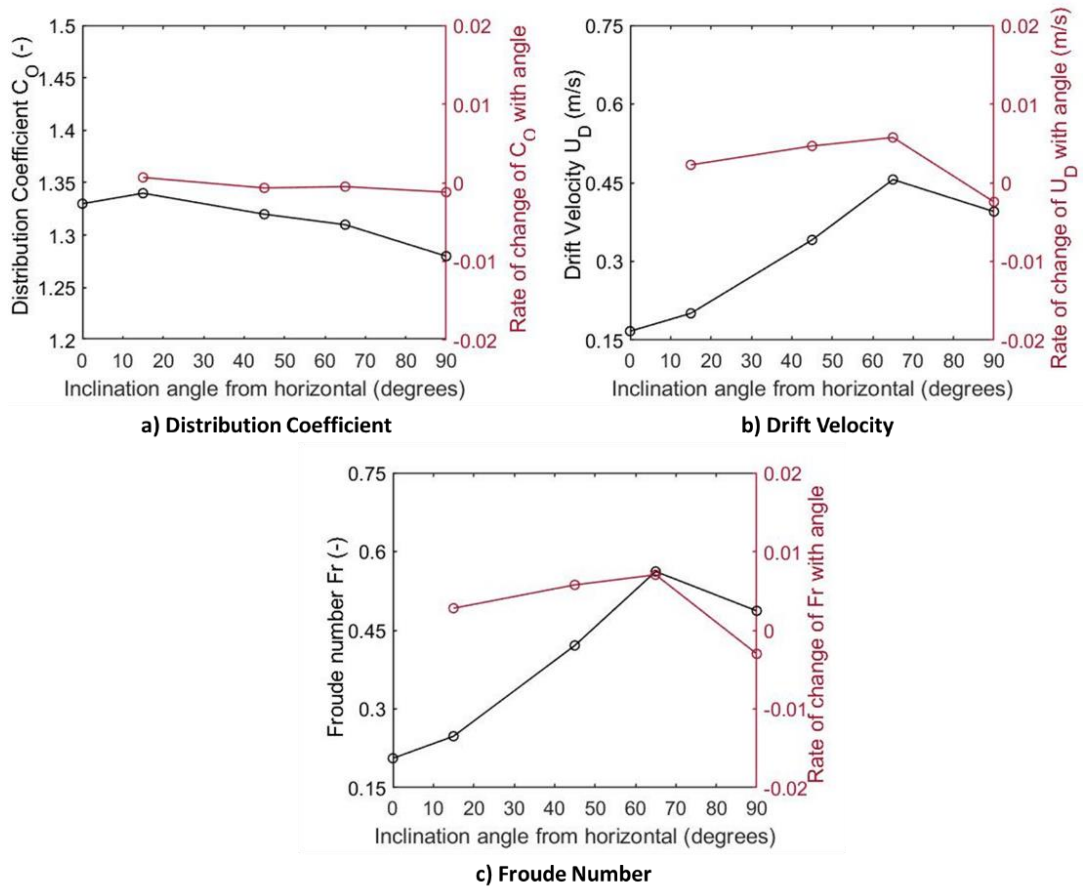


Figure 4.21 – Effect of inclination angle on  $C_O$ ,  $U_D$ ,  $Fr$  and their rate of change with angle for liquid viscosity of 91.5 cP

#### 4.4.3. 236 cP experimental campaign

Figure 4.22 shows the variation of structure velocity against inclination angle for all runs at liquid viscosity of 236 cP. Gas velocities investigated are same as 91.5 cP while only three liquid superficial velocities are investigated for 236 cP. Most individual lines (24 lines out of 33 lines) seem to peak around 65 or 45 degrees, quite close to reported value of 50 degrees by Zukoski (1966).

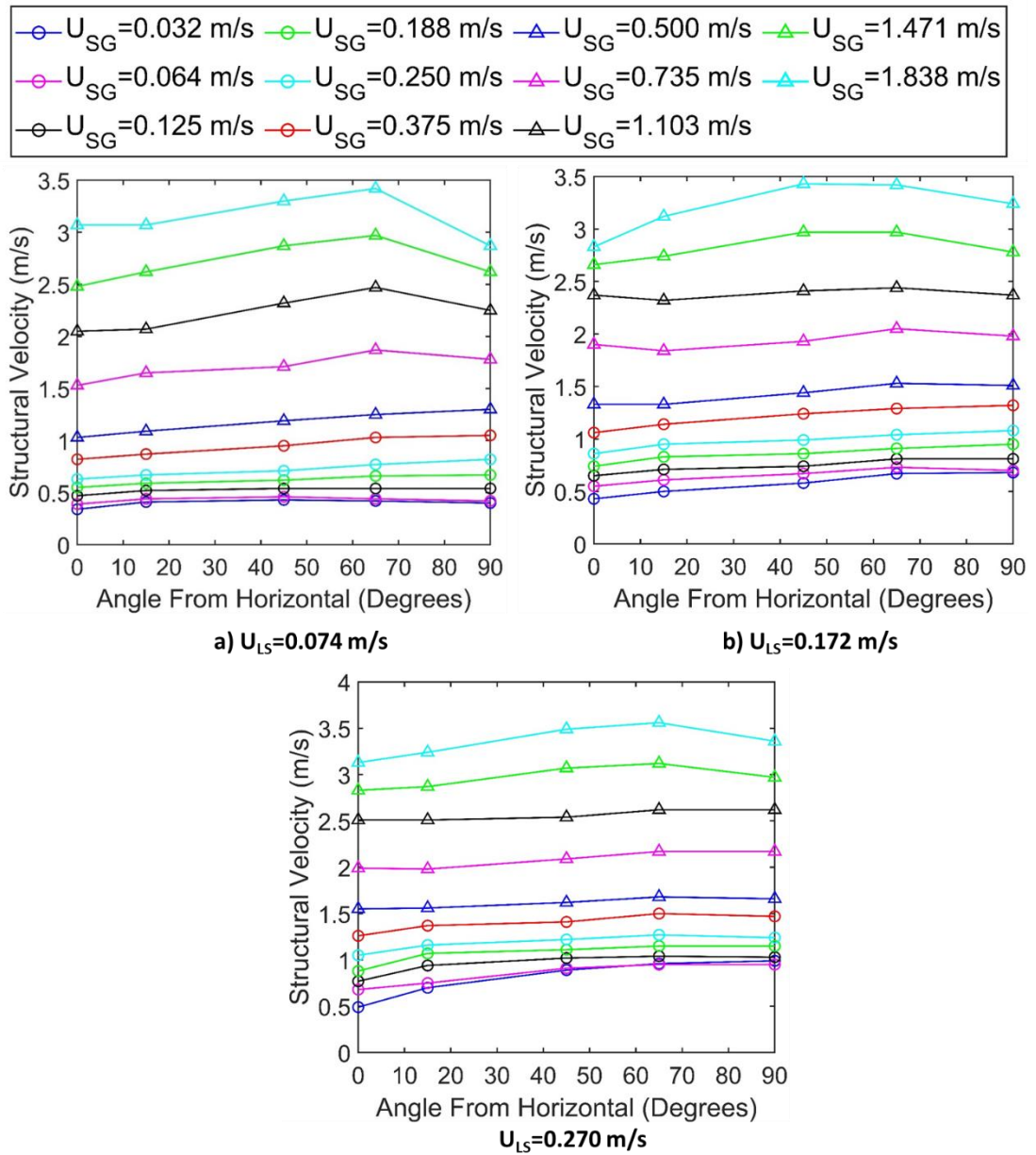


Figure 4.22 – Influence of inclination angle on structure velocity for different liquid and gas velocities at oil viscosity of 236 cP

Figure 4.23 shows how the gas velocity (gas superficial velocity divided by gas void fraction) varies with mixture superficial velocity at each inclination angle for 236 cP data.

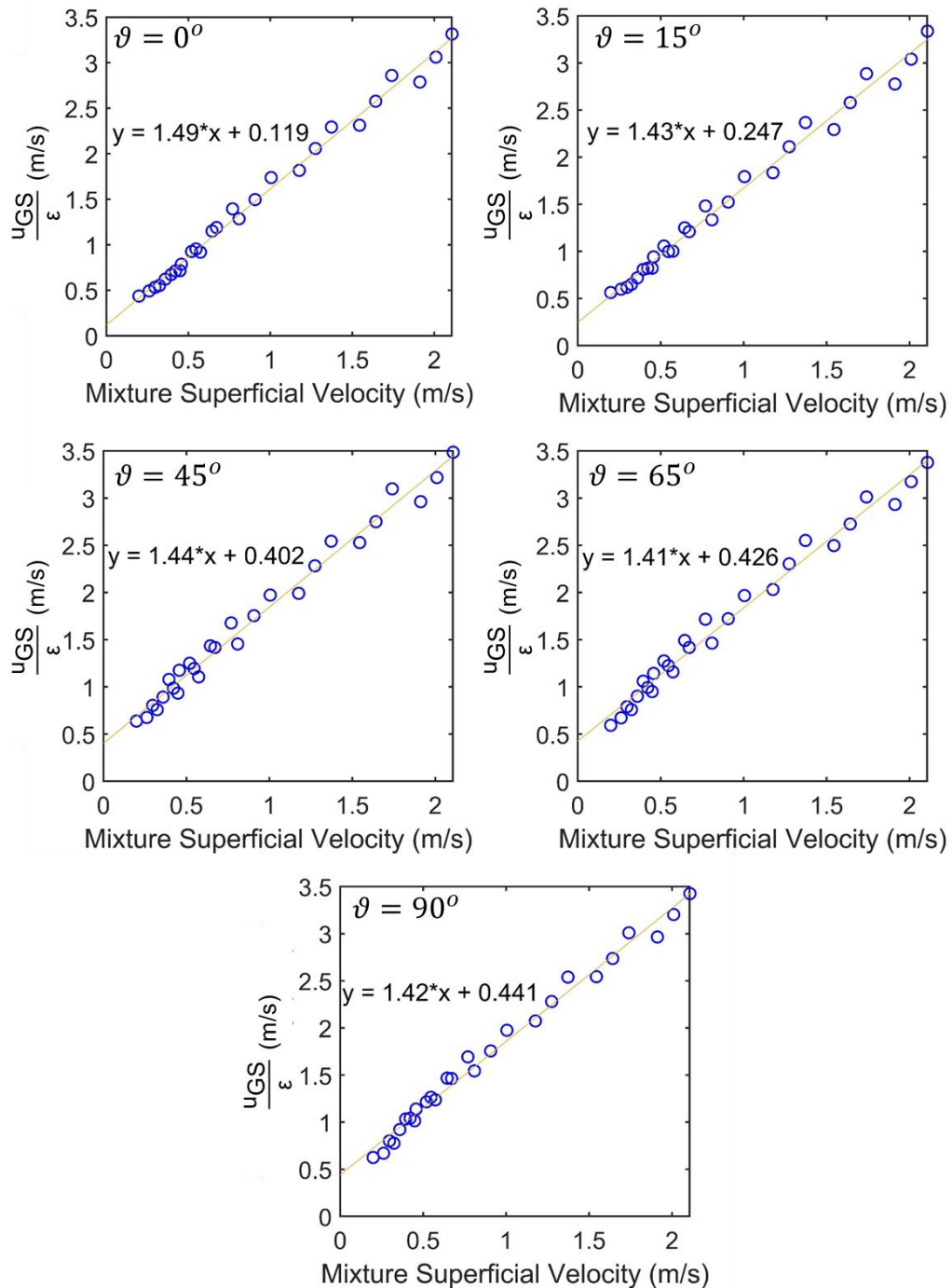


Figure 4.23 –Variation of gas velocity against mixture velocity at each inclination angle for 236 cP data

Table 4.4 summarises the distribution coefficient, drift velocity and Froude Number at each inclination angle for 236 cP data. It is interesting to observe that range of distribution coefficient is shifting to higher values as the liquid viscosity is increased while the range of drift velocity and Froude number is shifting to lower values as the viscosity is increased.

The maximum drift velocity occurs at 90 degrees which is not in agreement with 91.5 cP and 64 cP experiments. The difference in drift velocity for 65 and 90 degrees is 0.015 m/s. For 64 cP and 91.5 cP experiments, the maximum drift velocity occurs at 65 degrees. Similar trends are observed for Froude number.

The possible reason for this discrepancy is due to the limited number of points (particularly lack of liquid superficial velocities) investigated for 236 cP experiments. Moreover, since gas velocity was based on superficial velocity divided by gas void fraction, errors in measurement technique could have also contributed to this deviation.

*Table 4.4 – Summary of distribution coefficient, drift velocity and Froude number at each inclination for 236 cP data*

Angle	$C_o$	$V_d$	Fr	$R^2$
0	1.49	0.119	0.147	0.993
15	1.43	0.247	0.305	0.989
45	1.44	0.402	0.496	0.985
65	1.41	0.426	0.525	0.984
90	1.42	0.441	0.544	0.989

For 236 cP, Figure 4.24 shows how distribution coefficient, drift velocity and Froude number along with their rate of change varies with inclination angle. As with 64 cP and 91.5 cP, rate of change for  $C_D$  is lower than rate of change of drift velocity and Froude number for liquid viscosity of 236 cP.

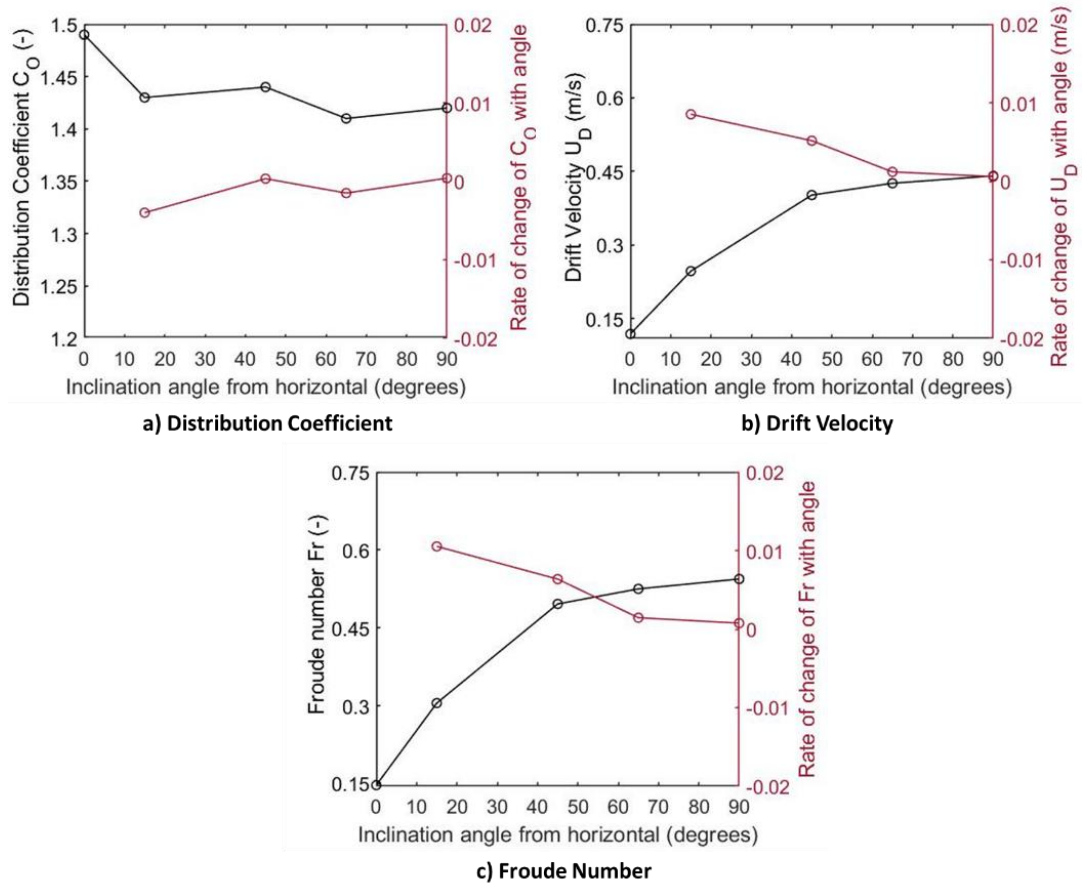


Figure 4.24 – Effect of inclination angle on  $C_D$ ,  $U_D$ ,  $Fr$  and their rate of change with angle for liquid viscosity of 236 cP

## 4.5. Effect of inclination angle on structure frequency

### 4.5.1. 64 cP experimental campaign

Figure 4.25 shows the variation of structure frequency against superficial gas velocity at various liquid velocities for each inclination angle at liquid viscosity of 64 cP. The range of frequency for all data including bubbly flow varied between 0.11 to 2.73 Hz. Hazuku method was utilised for determining structure frequency and is explained in Chapter 3. For each inclination angle plot, the maximum and minimum possible value of frequency is also plotted as a straight horizontal line. This was done by evaluating the standard deviation SDEV at each point. So, for each point, the higher and lower threshold frequency was then evaluated by adding SDEV or subtracting SDEV from the frequency value for that point. This was done for all points from which the maximum and minimum possible frequency for all data was determined.

Starting from horizontal inclination, the gas structures are large in length compared to all other inclinations. As a result, the number of gas structures passing through a fixed cross section for a given period are less comparatively to other inclination angles. The overall trend is that the frequency of the gas structures increases with increasing inclination angle from horizontal. Moreover, it can also be observed from Figure 4.25 that frequency at each inclination angle increases with liquid superficial velocity.

The effect of gas superficial velocity on structure frequency is variable for each inclination angle and liquid superficial velocity. For inclination angles ranging from 0 to 45 degrees, frequency decays to a stable value. There is clear difference in the trend for inclination angles ranging from 45 to 90 degrees where frequency increases to a maximum. For vertical inclination, it reaches a maximum at around  $U_{GS}$  of around 0.75 – 1 m/s and then it starts to decrease in magnitude after  $U_{GS}$  of 1 m/s. For horizontal inclination, the gas frequency is almost constant as the gas superficial velocity is increased at a fixed liquid superficial velocity.

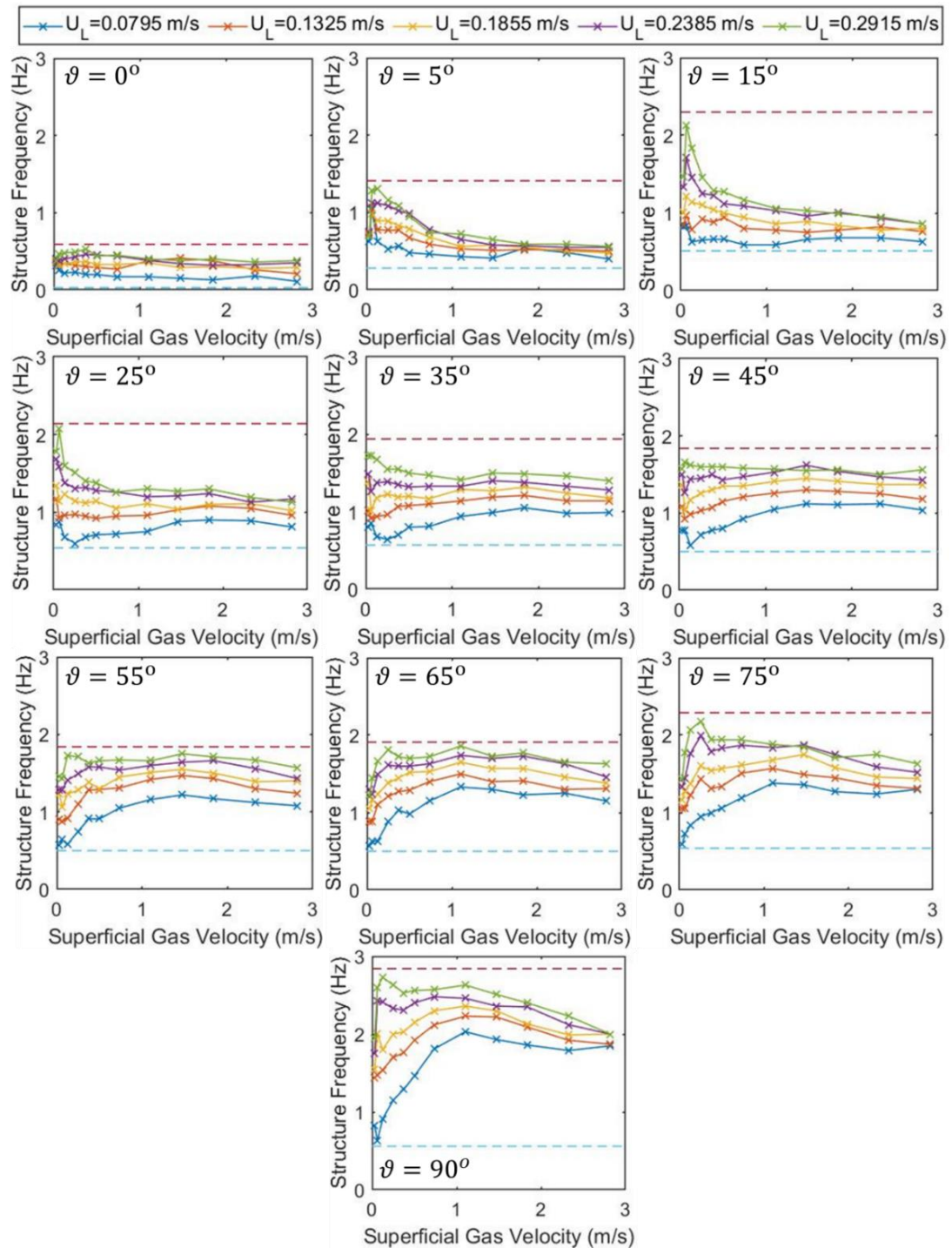


Figure 4.25 – Influence of inclination angle on structure frequency for different liquid and gas velocities at oil viscosity of 64 cP

Strouhal number **St** is a dimensionless number which describes the oscillations in a flow, as represented by Equation 4.2. The parameter **f** presents the structure frequency of the flow conditions in question while **D** represents the diameter of the pipe section.

$$St = \frac{fD}{u} \quad (4.2)$$

The dimensionless number utilises velocity of the flow ( $u$ ) that induces the oscillations in the flow. There are four possibilities for velocity of the flow: gas superficial velocity, liquid superficial velocity, structure velocity and mixture velocity. Escrig (2017) showed that linear plots of  $St$  based on gas superficial velocity against Lockhart – Martinelli Parameter  $X$  had  $R^2$  close to 1 (0.9185) compared to  $St$  based on other flow velocities. Other plots used  $St$  based on liquid superficial velocity, mixture velocity and structure velocity had  $R^2$  of 0.0883, 0.6281, and 0.8127 respectively. Hence, for analysis in this research project, only  $St$  based on gas superficial velocity will be utilised.

Figure 4.26 demonstrates how Strouhal Number based on  $U_{GS}$  varies with Lockhart – Martinelli Parameter  $X$ . Both scales are logarithmic. The relationship between  $St$  and  $X$  is positive for each inclination angle.

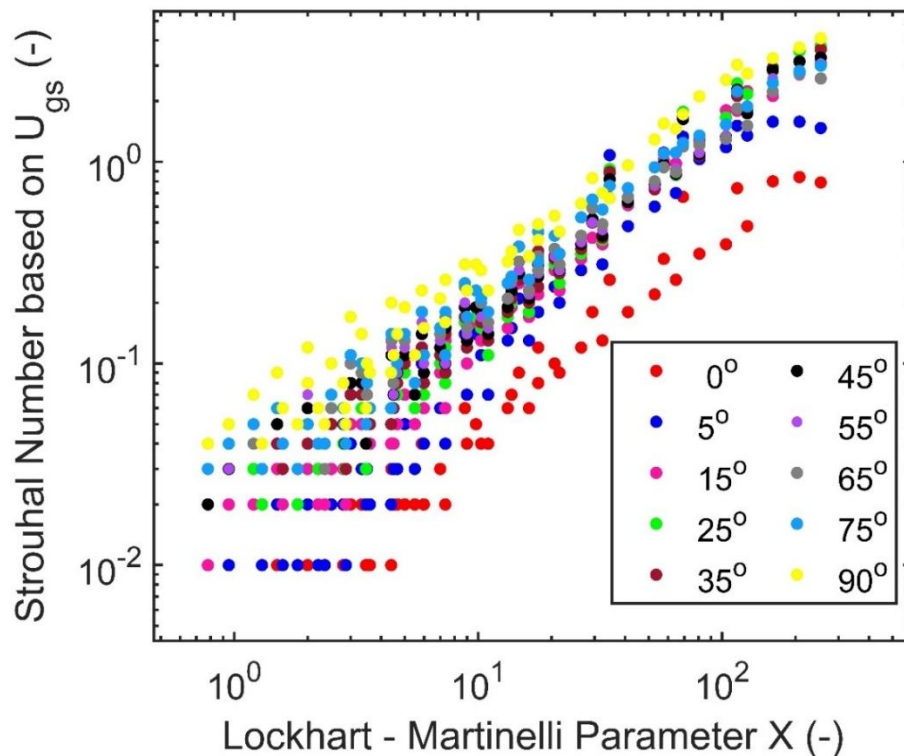


Figure 4.26 – Effect of Strouhal Number (based on gas superficial velocity) on Lockhart – Martinelli Parameter for all runs at silicone viscosity of 64 cP

The relationship between  $St$  and  $X$  can also be represented in linear scales by fitting to a power law as shown in Equation 4.3.

$$St = AX^B \quad (4.3)$$

The coefficients  $A$  and  $B$  were determined for each inclination angle as shown in Table 4.5. The  $R^2$  varies from 0.8 to 0.98 which is a good fit for 64 cP data. Statistical tests (t-test) were also carried out at a significance level of 0.05. Assuming variance were equal or not, t-test yielded that the mean of both datasets was significantly different.

*Table 4.5 – Power law coefficients for frequency data of 64 cP*

<b>Angle (degrees)</b>	<b>A</b>	<b>B</b>	<b>R<sup>2</sup> / Adj. R<sup>2</sup></b>	<b>t-value</b>	<b>p-value (Equal Var.)</b>	<b>p-value (Unequal Var.)</b>
90	0.0374	0.8717	0.98	4.33	3.1x10 <sup>-5</sup>	5.8x10 <sup>-5</sup>
75	0.0271	0.883	0.98	4.36	2.8x10 <sup>-5</sup>	5.3x10 <sup>-5</sup>
65	0.0267	0.854	0.98	4.37	2.7x10 <sup>-5</sup>	5.1x10 <sup>-5</sup>
55	0.0249	0.8685	0.98	4.37	2.7x10 <sup>-5</sup>	5.2x10 <sup>-5</sup>
45	0.0222	0.9049	0.97	4.36	2.8x10 <sup>-5</sup>	5.2x10 <sup>-5</sup>
35	0.0197	0.9314	0.97	4.36	2.8x10 <sup>-5</sup>	5.2x10 <sup>-5</sup>
25	0.0162	0.9869	0.97	4.36	2.8x10 <sup>-5</sup>	5.3x10 <sup>-5</sup>
15	0.0126	1.0324	0.95	4.37	2.7x10 <sup>-5</sup>	5.2x10 <sup>-5</sup>
5	0.0085	1.0645	0.80	4.38	2.5x10 <sup>-5</sup>	4.8x10 <sup>-5</sup>
0	0.0043	1.024	0.88	4.41	2.3x10 <sup>-5</sup>	4.4x10 <sup>-5</sup>

#### 4.5.2. 91.5 cP experimental campaign

Figure 4.27 shows the variation of structure frequency against superficial gas velocity at various liquid velocities for each inclination angle at liquid viscosity of 91.5 cP. The range of frequency for all data varied between 0.14 to 2.99 Hz. On each inclination angle plot, the maximum and minimum possible value of frequency is also plotted as a straight horizontal line.

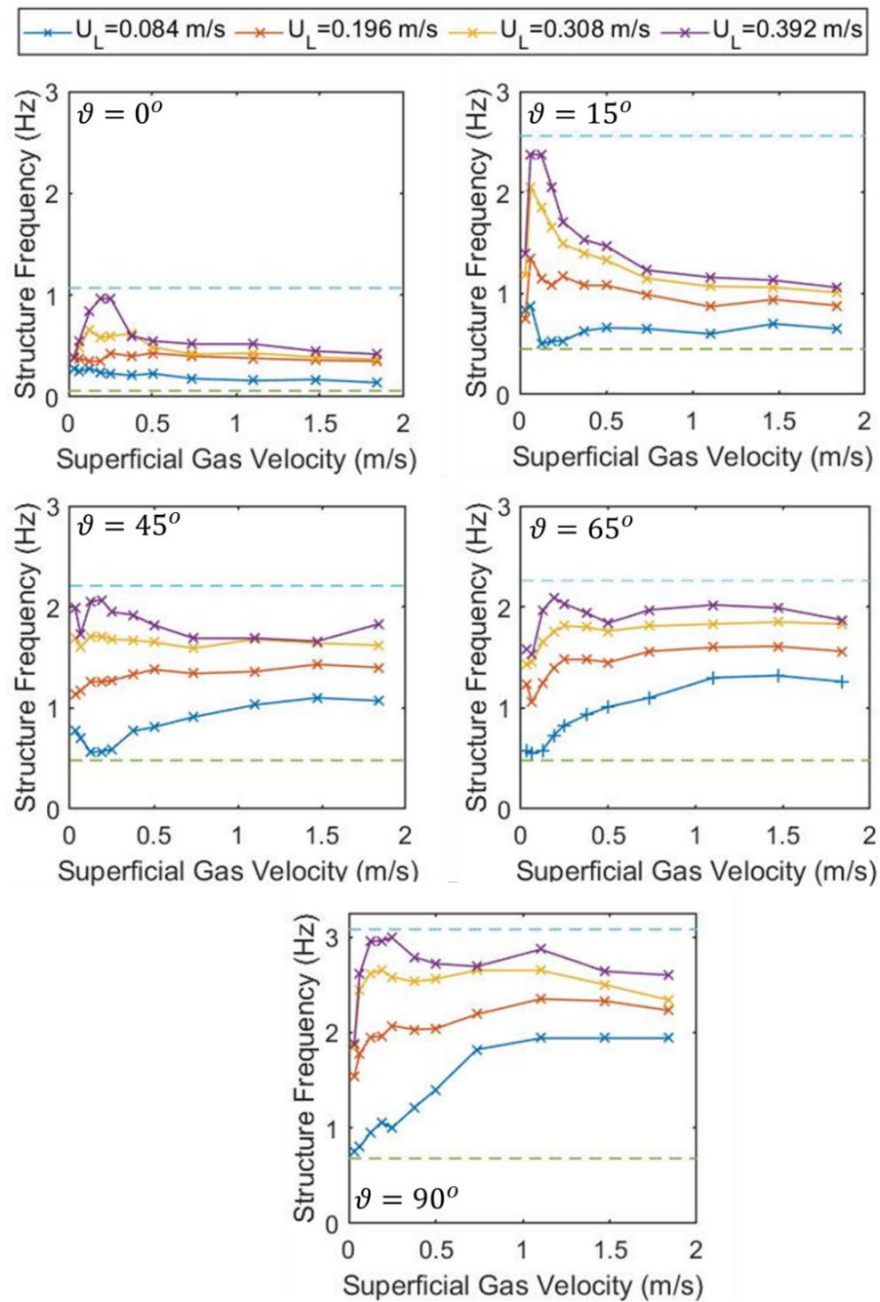


Figure 4.27 – Influence of inclination angle on structure frequency for different liquid and gas velocities at oil viscosity of 91.5 cP

Figure 4.28 demonstrates how Strouhal Number based on  $U_{GS}$  varies with Lockhart – Martinelli Parameter  $X$  for 91.5 cP. Both scales here are logarithmic. Again, the relationship between  $St$  and  $X$  is positive for each inclination angle.

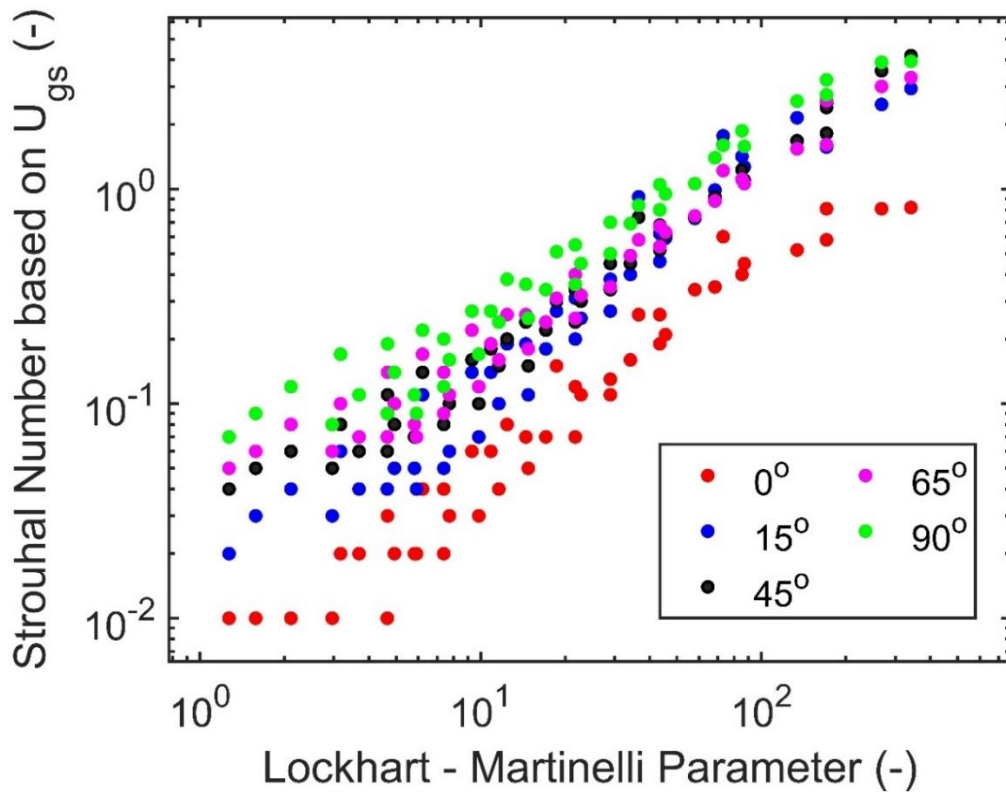


Figure 4.28 – Effect of Strouhal Number (based on gas superficial velocity) on Lockhart – Martinelli Parameter for all runs at silicone viscosity of 91.5 cP

The coefficients A and B were determined for each inclination angle as shown in Table 4.6. The  $R^2$  varies from 0.85 to 0.98 which is a good fit for 91.5 cP data. Similar to 64 cP, statistical tests (t-test) were also carried out at a significance level of 0.05 for 91.5 cP. Assuming variance were equal or not, t-test yielded that the mean of both datasets was significantly different.

Table 4.6 – Power law coefficients for frequency data of 91.5 cP

Angle (degrees)	A	B	$R^2$	t-value	p-value (Equal Var.)	p-value (Unequal Var.)
90	0.0394	0.8172	0.97	4.10	$9.3 \times 10^{-5}$	$1.8 \times 10^{-4}$
65	0.0275	0.8165	0.97	4.12	$8.6 \times 10^{-5}$	$1.7 \times 10^{-4}$
45	0.0209	0.8895	0.98	4.12	$8.7 \times 10^{-5}$	$1.7 \times 10^{-4}$
15	0.0126	0.9932	0.88	4.13	$8.5 \times 10^{-5}$	$1.7 \times 10^{-4}$
0	0.0045	0.9964	0.85	4.16	$7.5 \times 10^{-5}$	$1.5 \times 10^{-4}$

#### 4.5.3. 236 cP experimental campaign

Figure 4.29 shows the variation of structure frequency against superficial gas velocity at various liquid velocities for each inclination angle at liquid viscosity of 236 cP. The range of frequency for all data varied between 0.15 to 2.46 Hz. On each inclination angle plot, the maximum and minimum possible value of frequency is also plotted as a straight horizontal line.

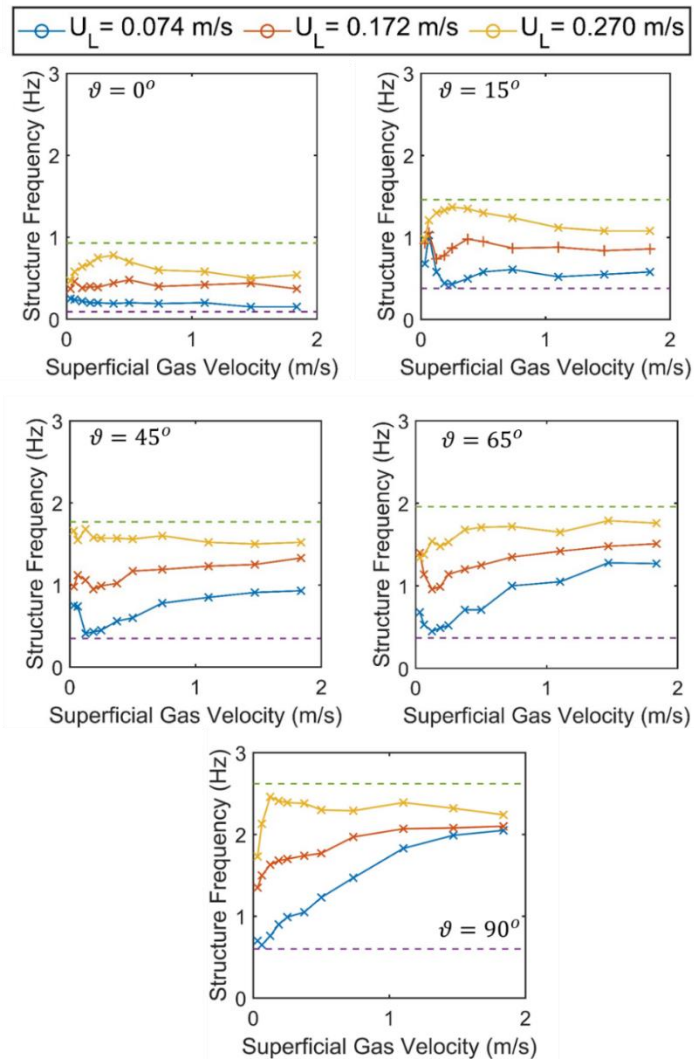


Figure 4.29 – Influence of inclination on structure frequency for different liquid and gas velocities at oil viscosity of 236 cP

Figure 4.30 demonstrates how Strouhal Number based on  $U_{gs}$  varies with Lockhart – Martinelli Parameter  $X$  for 236 cP. Both scales here are logarithmic. Again, the relationship between  $St$  and  $X$  is positive for each inclination angle.

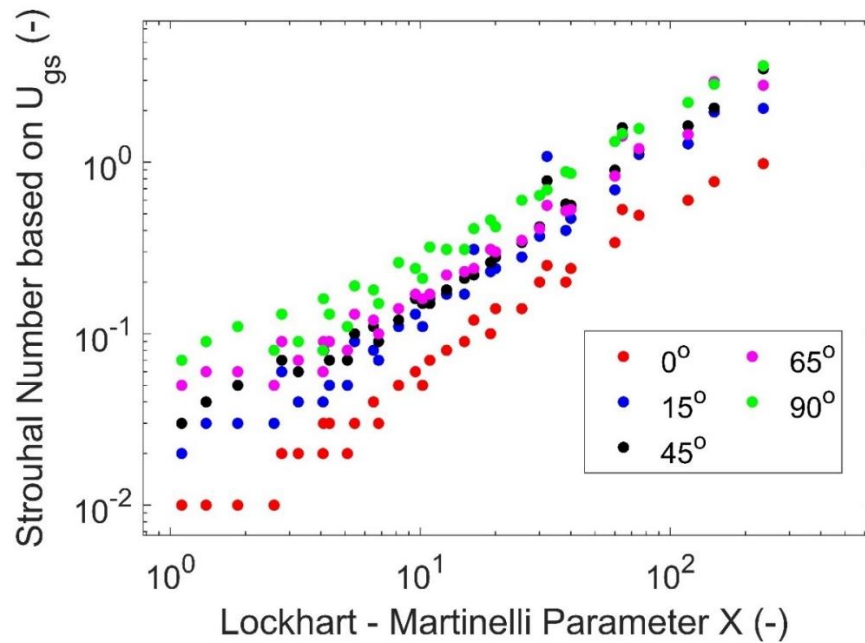


Figure 4.30 – Effect of Strouhal Number (based on gas superficial velocity) on Lockhart – Martinelli Parameter for all runs at silicone viscosity of 236 cP

The coefficients  $A$  and  $B$  from Equation 4.3 were determined for each inclination angle as shown in Table 4.7. The  $R^2$  varies from 0.87 to 0.99 which is a good fit for 236 cP data. Again, statistical checks yielded that the mean of both variable are significantly different.

Table 4.7 – Power law coefficients for frequency data of 236 cP

Angle (degrees)	A	B	$R^2$	t-value	p-value (Equal Var.)	p-value (Unequal Var.)
90	0.0446	0.7964	0.99	3.54	$7.4 \times 10^{-4}$	$12.4 \times 10^{-4}$
65	0.0278	0.8328	0.93	3.56	$7.0 \times 10^{-4}$	$11.8 \times 10^{-4}$
45	0.0211	0.9072	0.97	3.56	$7.0 \times 10^{-4}$	$11.8 \times 10^{-4}$
15	0.0151	0.9579	0.87	3.58	$6.8 \times 10^{-4}$	$11.5 \times 10^{-4}$
0	0.0057	1.0095	0.95	3.60	$6.3 \times 10^{-4}$	$10.7 \times 10^{-4}$

## 4.6. Verification of viscosity effect on two-phase flow parameters

### 4.6.1. Impact of liquid viscosity on liquid holdup

In Figure 4.31, each graph involves a plot of liquid holdup against gas superficial velocity. There are two lines in each graph, one for 64 cP and one for 236 cP, enabling investigation of liquid holdup with liquid viscosity. Each row of subgraphs corresponds to a specific inclination angle (5 in total) while each column of subgraphs corresponds to a specific liquid superficial velocity (3 in total).

As discussed in Section 4.3, liquid holdup decreases with gas superficial velocity while it increases with liquid superficial velocity. In Figure 4.31, for each inclination angle and liquid superficial velocity combination, liquid holdup generally increases with liquid viscosity for gas superficial velocities greater than  $\sim 0.5$  m/s. At lower gas superficial velocities (less than 0.5 m/s), increase in liquid holdup with viscosity is much smaller (or almost negligible/unclear) than that at higher gas superficial velocities. For each inclination angle and liquid superficial velocity combination, the difference in magnitude (or gap) between the 64 cP and 236 cP datapoints increases with gas superficial velocity. At a specific inclination angle, the difference in magnitude between the 64 cP and 236 cP datapoints with gas superficial velocity increases with liquid superficial velocity.

In horizontal pipes, the increase in average liquid holdup with viscosity can be explained by change in height of the liquid film. As viscosity of the liquid phase increases, the height of the liquid film rises as well. As a result of this, forces acting at the gas – liquid interface and the wall play a fundamental role in determining the trend of liquid holdup with viscosity. The viscous nature of high viscosity oils will result in higher shear stresses in the liquid phase. Once these shear forces acting at the wall and interface reach equilibrium, the film thickness will increase as well. These observations or explanations are in line with works carried out by Nadler and Mewes (1995) and Gokcal (2008).

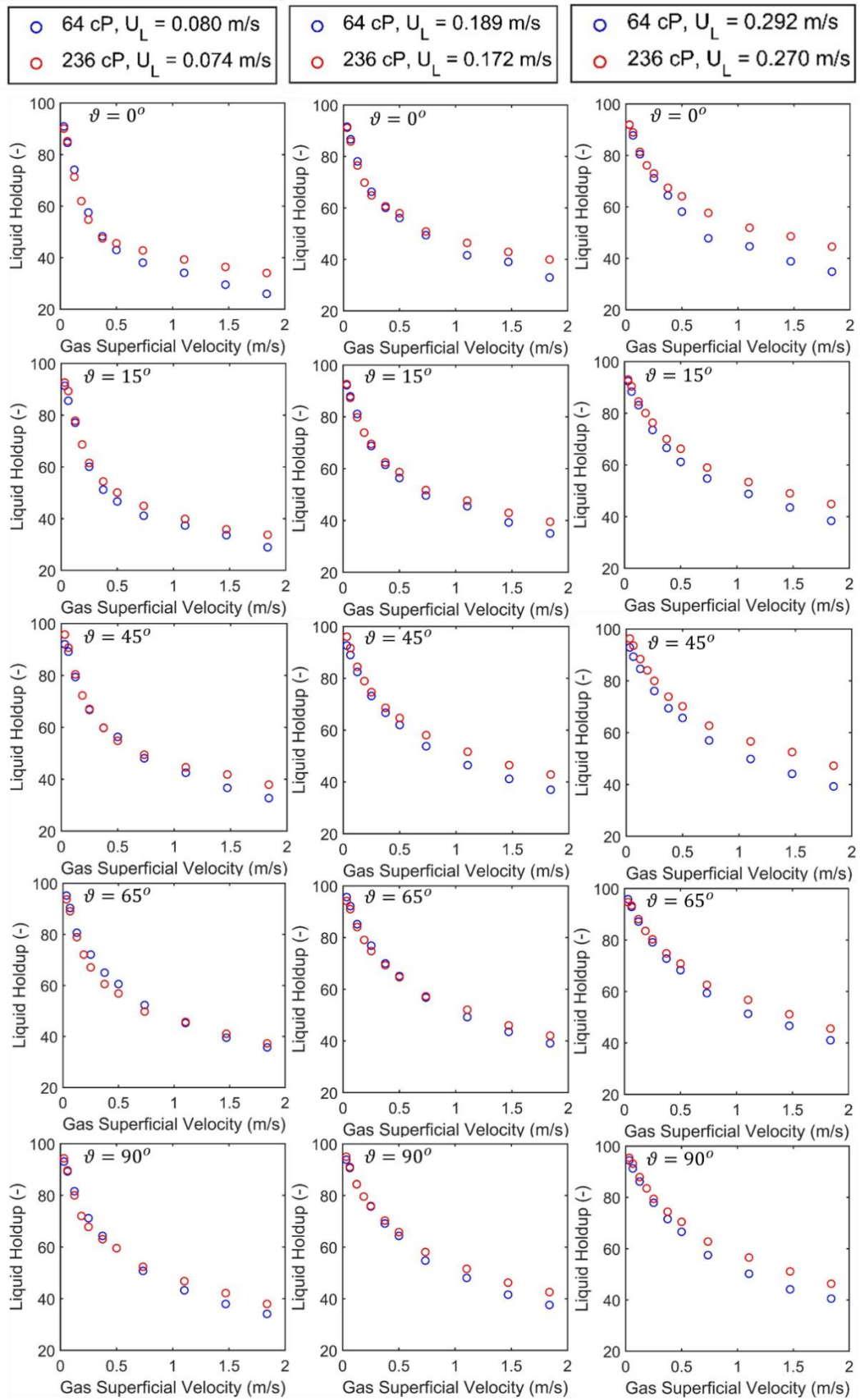


Figure 4.31 – Effect of viscosity on two – phase liquid holdup at different liquid and gas velocities for various inclination angle

Carrying on from Figure 4.31, liquid holdup values for 64 cP and 236 cP (left y axis) were extracted for gas superficial velocity of 1.838 m/s and were plotted against inclination angle for each liquid superficial velocity presented in Figure 4.31. Furthermore, difference between liquid holdup for 64 cP and 236 cP (will be referred as gap onwards) was plotted against inclination angle on the right y axis. For each case of liquid superficial velocity, gap at inclination angles of <45 degrees are generally higher in magnitude in comparison to the gap at inclination angles greater 45 degrees. Highest gap is always recorded at 0 degrees. It can be observed visually in Figure 4.32 that the space between the 64 cP (blue) and 236 cP (red) line is increasing as liquid superficial velocity increases.

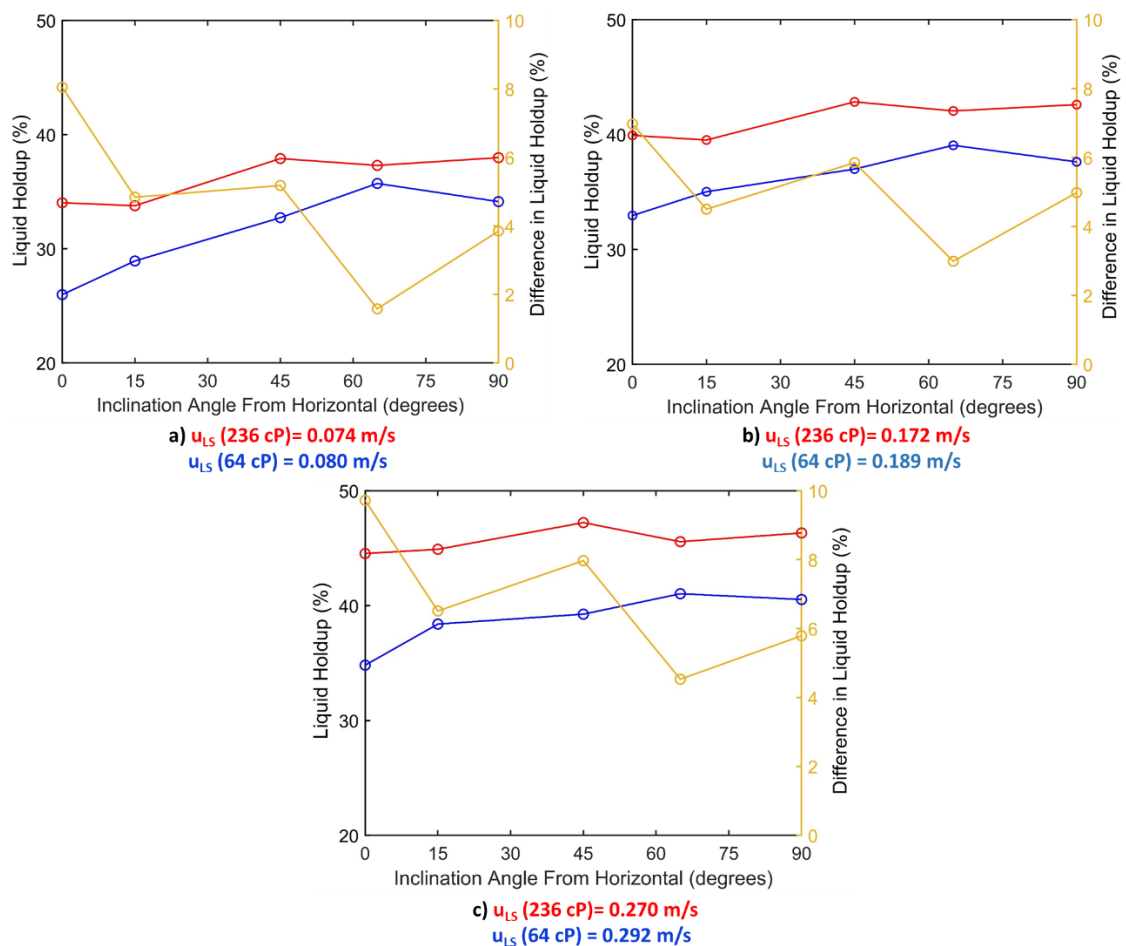


Figure 4.32 – Investigating the difference between liquid holdup at 64 cP and 236 cP with inclination angle for a gas superficial velocity of 1.838 m/s

Figure 4.33 shows how the viscous datasets by other authors compares with high viscosity dataset in this investigation for horizontal pipelines. Table 4.8 shows the properties of the datasets utilised in Figure 4.33.

*Table 4.8 – Dataset from literature to further investigate the effect of viscosity on liquid holdup for horizontal pipelines*

<b>Author</b>	<b><math>\mu_L</math> (cP)</b>	<b><math>\rho_L</math> (kg/m<sup>3</sup>)</b>	<b><math>\sigma</math> (N/m)</b>	<b><math>u_{SL}</math> (m/s)</b>	<b><math>u_{SG}</math> (m/s)</b>	<b>Points</b>
Present Study	64	922.5	0.0202	0.27	0.032, 0.064, 0.125, 0.250, 0.375, 0.500, 0.735, 1.103, 1.471, 1.838	10
Present Study	236	931.7	0.0202	0.29	0.032, 0.064, 0.125, 0.188, 0.250, 0.375, 0.500, 0.735, 1.103, 1.471, 1.838	11
Gokcal (2008)	584 – 601	~ 884	0.034	0.3	0.110, 0.170, 0.310, 0.740, 1.100, 1.500, 2.100	7
Escrig (2017)	5	917	0.0202	0.23	0.170, 0.350, 0.520, 0.700, 0.930, 1.160, 1.390, 1.740, 2.320, 2.900	10

As discussed in Figure 4.31, the increase in liquid holdup with viscosity in Figure 4.33 at lower gas superficial velocities (less than 0.5 m/s) is quite small or almost negligible/unclear. Nevertheless, the trend of liquid holdup with viscosity at higher gas superficial velocities is analogous to that in Figure 4.31. High viscosity dataset of Gokcal (2008) records the highest liquid holdup values for all gas superficial velocities except one compared to other lines. Present study (64 cP and 236 cP) fits in quite well with the trend of liquid holdup variation with viscosity. Escrig (2017) does record the lowest liquid holdup value in comparison to other datasets. However, when comparing liquid holdup value recorded at each gas superficial velocity, liquid holdup for Escrig (2017) is not always the lowest. Nevertheless, dataset of Escrig (2017) records the lowest liquid holdup for gas superficial velocities greater than 1 m/s. One main reason for Escrig (2017) overlapping with the dataset of present study – 64 cP could be due to small difference in their liquid viscosity (only 59 cP).

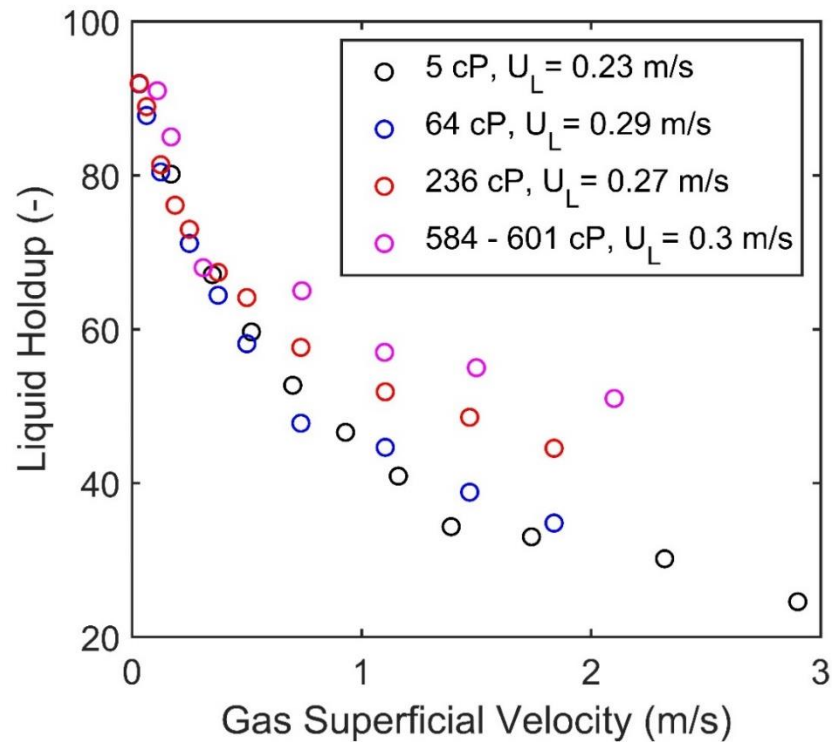


Figure 4.33 – Comparison of high viscosity datasets of Gokcal (2008) and Escrig (2017) with present study’s high viscosity datasets in horizontal pipelines

Figure 4.34 demonstrates how dataset of Escrig (2017) compares with high viscosity dataset in this investigation for vertical pipelines. Table 4.9 shows the properties of the vertical datasets utilised in Figure 4.34.

Table 4.9 – Dataset from literature to further investigate the effect of viscosity on liquid holdup for vertical pipelines

Author	$\mu_L$ (cP)	$\rho_L$ (kg/m <sup>3</sup> )	ST (N/m)	$u_{SL}$ (m/s)	$u_{SG}$ (m/s)	Points
Present Study	64	922.5	0.0202	0.27	0.032, 0.064, 0.125, 0.250, 0.375, 0.500, 0.735, 1.103, 1.471, 1.838	10
Present Study	236	931.7	0.0202	0.29	0.032, 0.064, 0.125, 0.188, 0.250, 0.375, 0.500, 0.735, 1.103, 1.471, 1.838	11
Escrig (2017)	5	917	0.0202	0.23	0.170, 0.350, 0.520, 0.700, 0.930, 1.160, 1.390, 1.740, 2.320, 2.900	10

In Figure 4.34, for vertical pipelines, liquid holdup increases with viscosity. Dataset of Escrig (2017) records the lowest liquid holdup values for all gas superficial velocities in comparison to present study's high viscosity dataset. The lines for each dataset are much smoother and the trend is clearer (especially for Escrig (2017)) compared to that of horizontal pipelines. None of the points at each gas superficial velocity overlap with one another unlike horizontal inclination where the trend was not clear for gas superficial velocities less than 0.5 m/s.

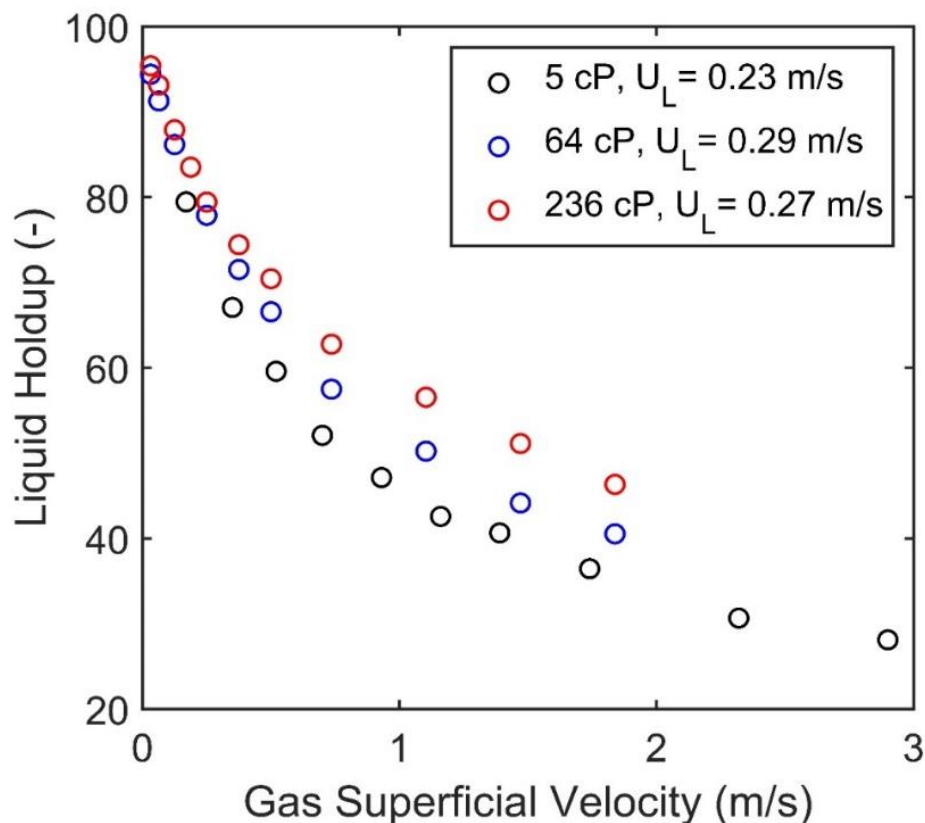


Figure 4.34 – Comparing the effect of viscosity on liquid holdup using datasets from literature (in Table 4.9) and present study for vertical pipelines

#### 4.6.2. Impact of liquid viscosity on structure velocity

In Figure 4.35, each graph involves a plot of structure velocity against gas superficial velocity. There are two lines in each graph, one for 64 cP and one for 236 cP, enabling investigation of structure velocity with liquid viscosity. Each row of subgraphs corresponds to a specific inclination angle (5 in total) while each column of subgraphs

corresponds to a specific liquid superficial velocity (3 in total). Again, each similar liquid superficial velocity pair for 64 cP and 236 cP are within +/- 7.5 % max.

The structure velocity increases with gas and liquid superficial velocity (mixture velocity), an agreement of Nicklin's equation. For each inclination angle and liquid superficial velocity combination, trend of structure velocity with viscosity is not clear for gas superficial velocities of less than 0.5 m/s. For gas superficial velocities greater than 0.5 m/s, the structure velocity generally increases with liquid viscosity. However, it can be established from Figure 4.35 that the effect of viscosity on structure velocity in each sub graph is not significant.

Baba *et al.* (2019) explain the possible mechanism behind the increase in translational velocity with viscosity for horizontal pipes. When the liquid viscosity is increased, the slug length decreases (Al-Safran *et al.*, 2011). As a result, the rate of liquid mass travelling reduces which in turn leads to a higher velocity. Hence, it was shown that the slug translational velocity is proportional to the viscosity of the liquid phase due to reduced slug length and thus increased frequency. Even though the increasing liquid viscosity leads to an increased laminar sublayer, the rise here is dominated by the reduction in the slug body due to reduced slug length. Overall, Baba *et al.* (2019) showed that translational velocity increases with liquid viscosity by comparing their high viscosity datasets (900 cP to 5500 cP) to low and medium viscosity (7 cP to 587 cP) datasets of other authors.

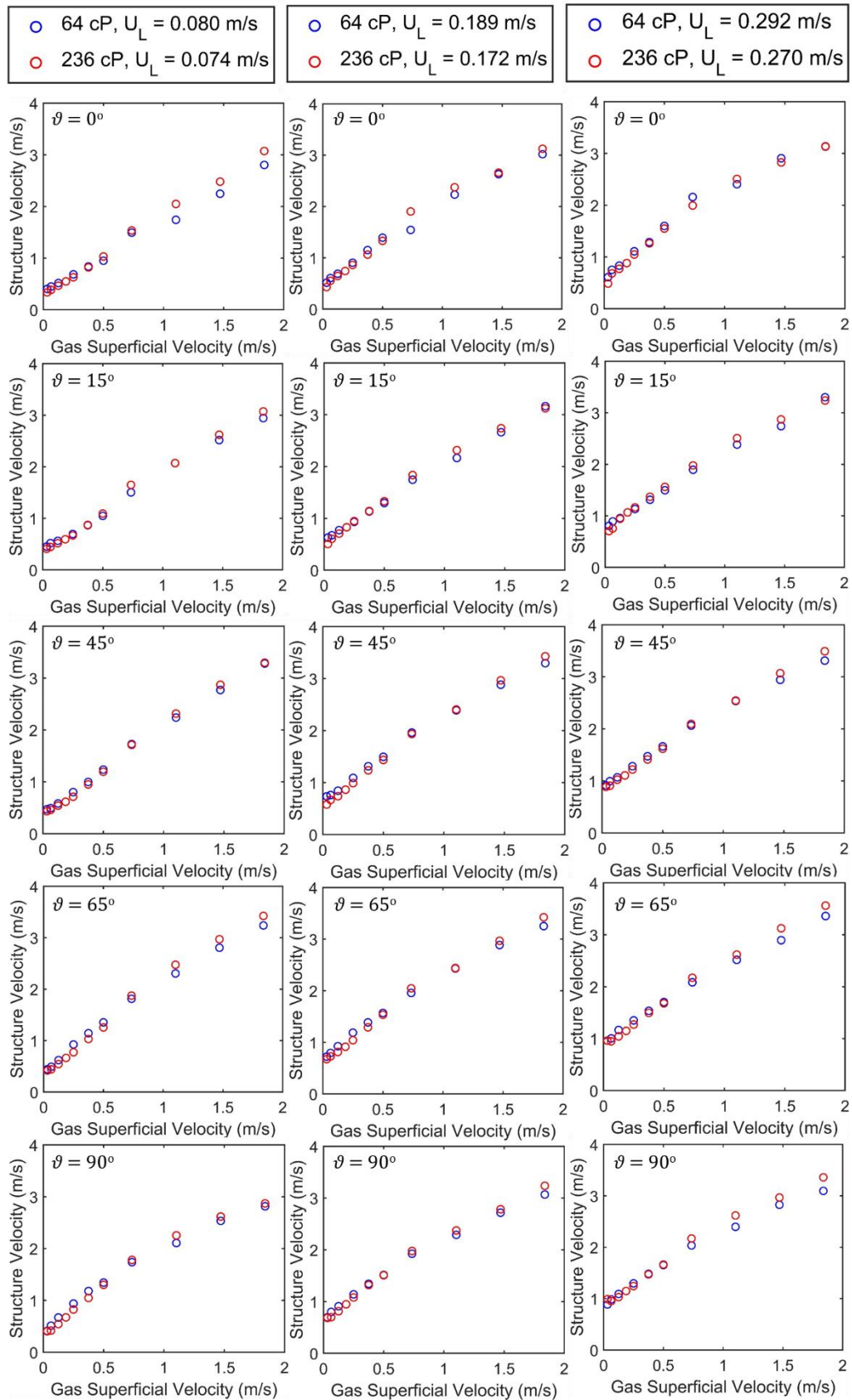


Figure 4.35 – Effect of viscosity on two – phase structure velocity at different liquid and gas velocities for various inclination angle

Figure 4.36 compares how structure velocity varies with gas superficial velocity and viscosity in horizontal pipelines for datasets from literature and datasets of present study. The datasets from literature are the same as the ones in Table 4.8. For lower gas superficial velocities of less than 0.5 m/s, the structure velocity are not that significantly different. However, at gas superficial velocities greater than 0.5 m/s, the overall trend for structure velocity increases with viscosity.

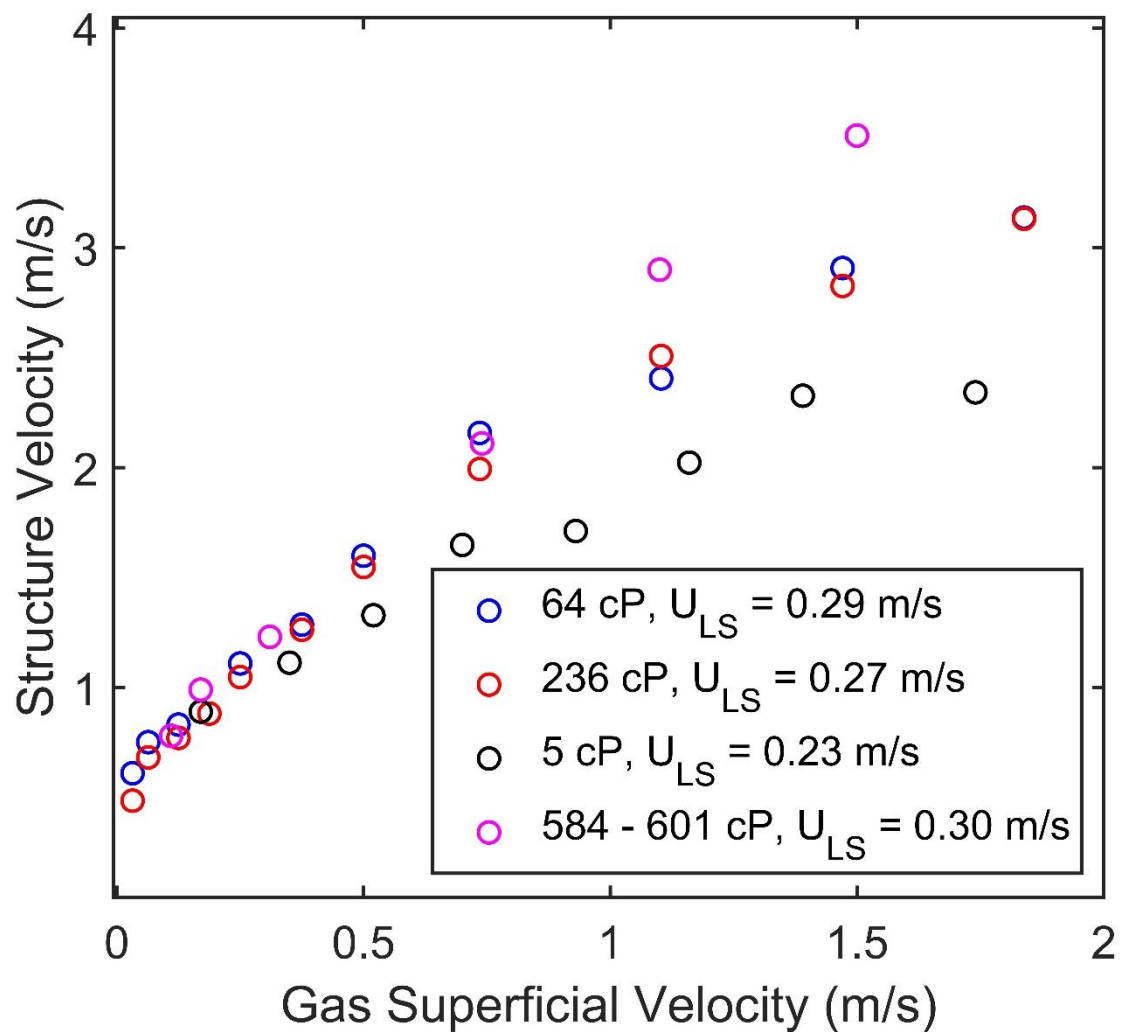


Figure 4.36 – Comparing the effect of viscosity on structure velocity using datasets from literature (in Table 4.8) and present study for horizontal pipelines

Figure 4.37 shows how structure velocity varies with gas superficial velocity and viscosity in vertical pipelines for datasets from literature and datasets of present study. Similar to horizontal inclination, the structure velocity does not vary much with viscosity for gas superficial velocities of less than 0.5 m/s. For gas superficial velocities of more than 0.5 m/s, structure velocity is positively correlated to viscosity.

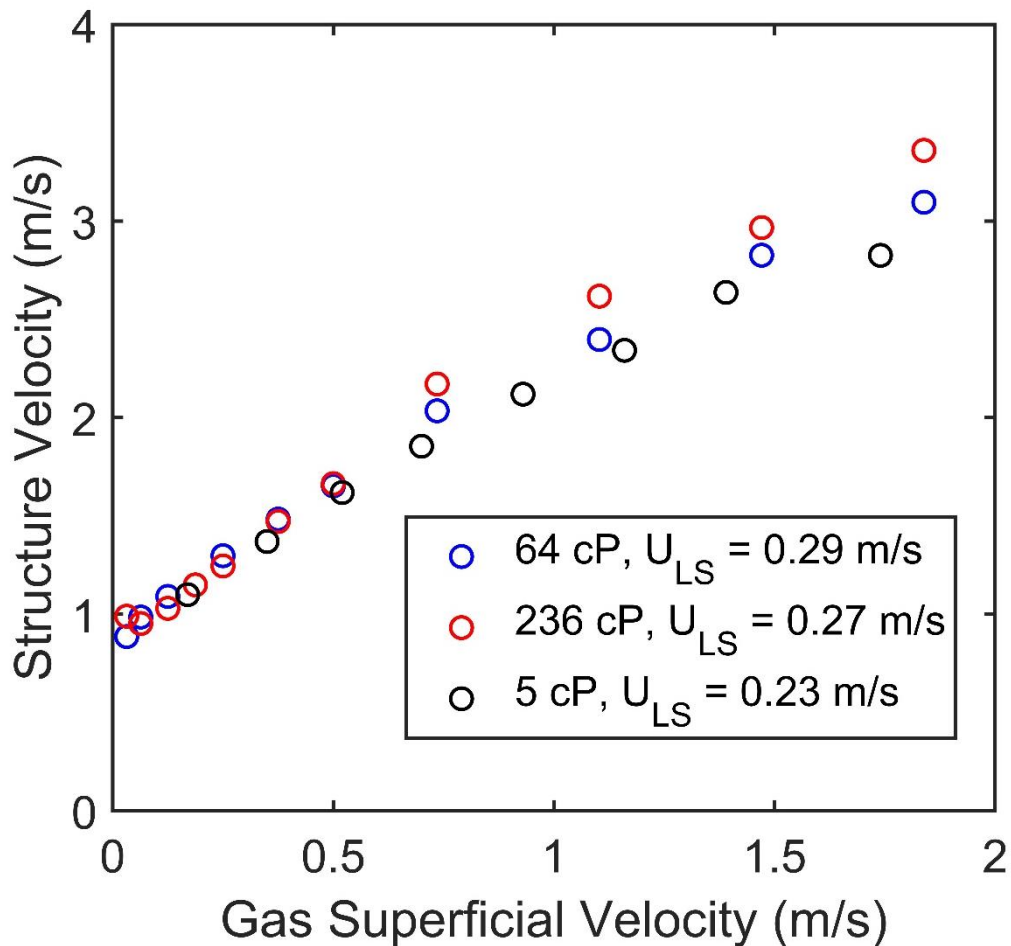


Figure 4.37 – Comparing the effect of viscosity on structure velocity using datasets from literature (in Table 4.9) and present study for vertical pipelines

#### 4.6.3. Impact of viscosity on distribution coefficient and drift velocity

Figure 4.38 illustrates how the range of distribution coefficient (due to experiments carried out at different angles) varies with viscosity. There is a positive correlation between distribution coefficient and liquid phase viscosity. It must be stressed that the data here suggests that the viscosity change must be significant to yield a non – overlapping distribution coefficient range. For example, the distribution coefficient range overlaps for 64 cP and 91.5 cP. However, for 236 cP (which is much larger in magnitude than the other two), the distribution coefficient range does not overlap with the former two. The difference between maximum and minimum distribution coefficient (range) at a particular viscosity is roughly the same when compared to a different viscosity. The range for 64 cP dataset is 0.07 ( $C_o$  varies between 1.23 and 1.30). Moreover, the range for 91.5 cP and 236 cP datasets are 0.06 ( $C_o$  between 1.28 – 1.34) and 0.08 ( $C_o$  between 1.41 – 1.49) respectively. Interestingly, distribution coefficient remains below 2 for all viscosities tested.

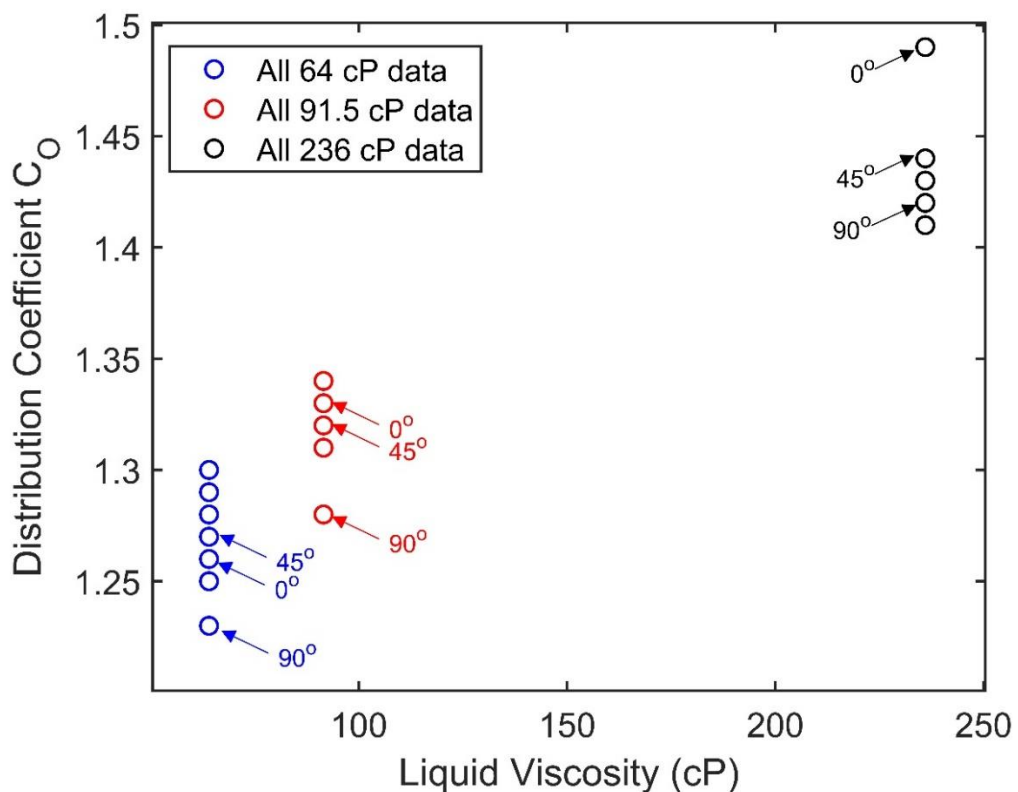


Figure 4.38 – Variation/range of distribution coefficient values at each viscosity tested

Considering the maximum  $C_o$  values for 64 cP and 236 cP, the percentage increase in  $C_o$  is 14.62 %. Similarly, comparing the minimum values for 64 cP and 236 cP, percentage increase in  $C_o$  is 14.63 %. The maximised percentage increase in  $C_o$  for all data of 21.1 % occurs when the minimum  $C_o$  at 64 cP and maximum  $C_o$  at 236 cP are considered. The minimal percentage increase in  $C_o$  of 8.5 % occurs when the maximum  $C_o$  at 64 cP and minimum  $C_o$  at 236 cP are considered.

Besides the percentage change, the change of distribution coefficient with viscosity is also an importance characteristic of interest. Same analysis was carried out for calculating the variation of  $C_o$  with viscosity for each of the four scenarios, as shown in Table 4.10.

*Table 4.10 –Analysing the variation of distribution coefficient with viscosity*

Values considered for the calculation		% change	$\Delta C_o / \text{viscosity (Pas)}^{-1}$
Maximum $C_o$ (64 cP)	Maximum $C_o$ (236 cP)	14.6	1.10
Minimum $C_o$ (64 cP)	Minimum $C_o$ (236 cP)	14.6	1.05
Minimum $C_o$ (64 cP)	Maximum $C_o$ (236 cP)	21.1	1.51
Maximum $C_o$ (64 cP)	Minimum $C_o$ (236 cP)	8.5	0.64

From drift flux model, the drift velocity was also obtained. In Figure 4.39, the range of drift velocity values at each viscosity are presented. There is a negative correlation between drift velocity and liquid phase viscosity. The data points from each viscosity set overlap with the data points from other viscosities, meaning that drift velocity is not significantly different. Nevertheless, the maximum and minimum at each viscosity does alter by some margin.

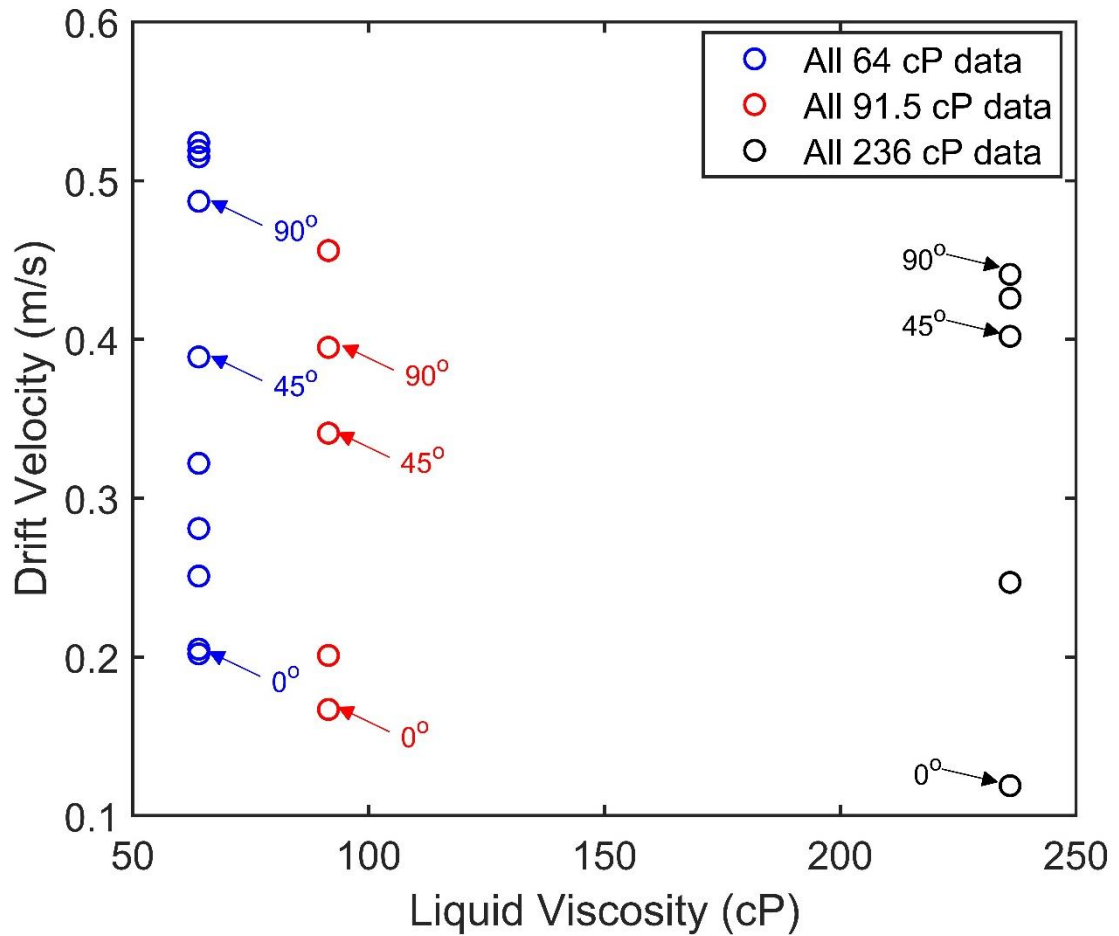


Figure 4.39 – Variation/range of drift velocity values at each viscosity tested

Again, the percentage change and variation of drift velocity with viscosity are evaluated, as shown in Table 4.11. Even though the drift velocity values at each viscosity overlap with one another, the variation and % change is significant for all presented scenarios. This was not the case for distribution coefficient analysis.

Table 4.11 –Analysing the variation of drift velocity (DV) with viscosity

Values considered for the calculation		% change	$\Delta$ DV / viscosity (Pas) <sup>-1</sup>
Maximum DV (64 cP)	Maximum DV (236 cP)	- 15.8	0.48
Minimum DV (64 cP)	Minimum DV (236 cP)	- 41.1	0.48
Minimum DV (64 cP)	Maximum DV (236 cP)	+77.3	2.35
Maximum DV (64 cP)	Minimum DV (236 cP)	- 118.3	1.39

Moreover, the analysis of flow parameter and drift velocity using drift flux model for all points for each viscosity set is also essential. The analysis is illustrated in Figure 4.40. It must be restated that method utilised to carry out drift flux modelling is same as the one discussed in Section 4.4. Gas velocity here is gas superficial velocity divided by void fraction.

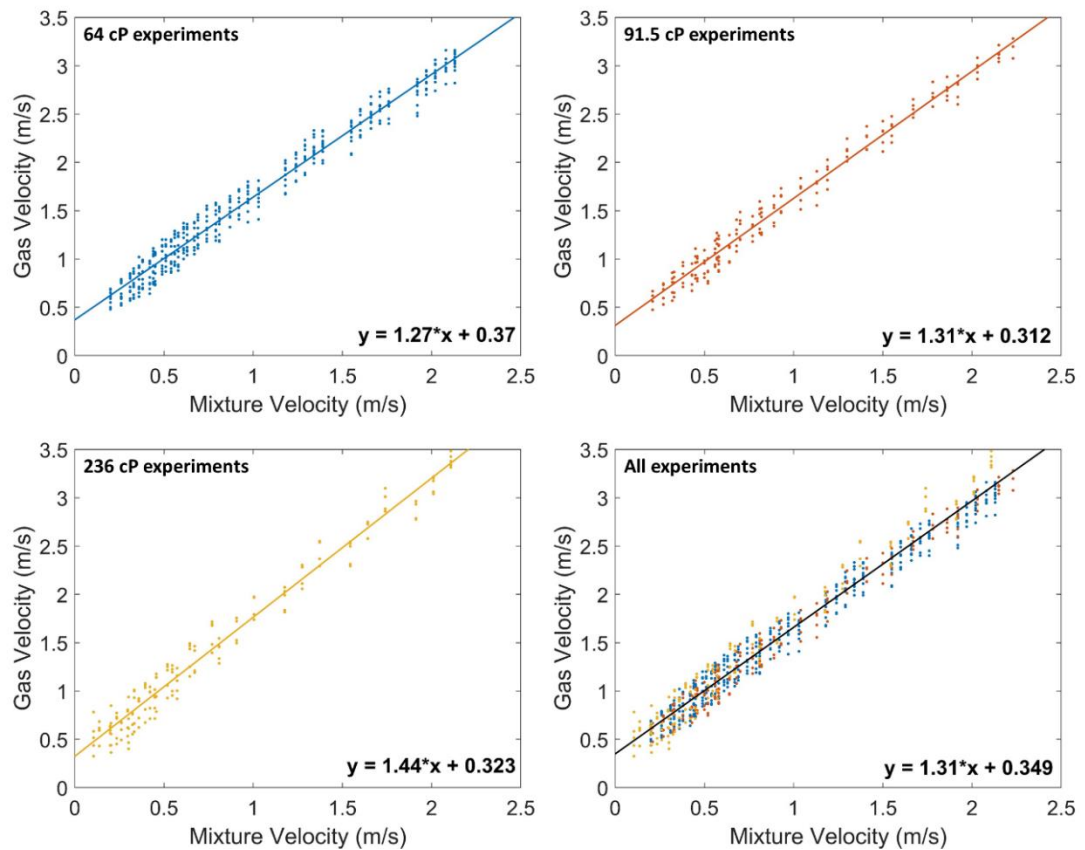


Figure 4.40 – Drift flux model for each individual viscosity and all data points

As determined earlier, it can be established from Table 4.12 that the distribution coefficient or flow parameter increases with viscosity. The overall increase in distribution coefficient is 0.17 (percentage increase of 13.4 %) when 64 cP and 236 cP values are compared. It is envisaged that further larger increases in viscosity will increase the overall distribution coefficient of the system to around 2, as demonstrated by Gokcal who investigated much larger viscosities (586 being the maximum).

Drift velocity decreases with viscosity when comparing 64 and 91.5 cP datasets however it increases slightly when comparing 91.5 cP and 236 cP datasets. The expected trend is that the drift velocity should reduce with viscosity however one possible reason for that slight increase is the number of points are less for 236 cP compared to 64 and 91.5 cP datasets. Overall, drift velocity decreases by 0.05 (percentage decrease of 13.5 %) when comparing 64 cP and 236 cP.

*Table 4.12 – Overall viscosity effect on distribution coefficient and drift velocity*

<b>Viscosity (cP)</b>	<b>Distribution coefficient (-)</b>	<b>Drift velocity (m/s)</b>	<b>Froude Number (-)</b>	<b>R<sup>2</sup></b>
64	1.27	0.37	0.45	0.9731
91.5	1.31	0.31	0.38	0.9795
236	1.44	0.32	0.40	0.9713
64 – 236	1.31	0.35	0.43	0.9690

Finally, drift flux model can be presented for all the data points in this research project, as shown in Equation 4.4.

$$Gas\ Velocity = \frac{u_{GS}}{\varepsilon} = 1.31 u_M + 0.35 = 1.31u_M + 0.43\sqrt{gD} \quad (4.4)$$

#### 4.7. Conclusion

In this chapter, all the experimental data have been presented, focussing on the effect of inclination angle and viscosity on three two – phase characteristics (structure velocity, liquid holdup, and structure frequency).

Liquid holdup follows a non – linear relationship (similar to second order polynomial) as a function of inclination angle. This was true for all three experimental campaigns. For a given gas and liquid superficial velocity, liquid holdup increases with inclination angle until the inclination angle reaches 55 – 75 degrees This was the result of gravitational force acting on the liquid phase, resulting in increased slippage between

phases and thus increased liquid holdup. After that, liquid holdup decreases with inclination angle. The reason for this is that the whole pipe is bridged by the liquid phase, resulting in reduced slippage between phases and thus reduced liquid holdup. The shape of the curve for a given gas and liquid superficial velocity resembles that of Beggs and Brill (1973).

The liquid holdup increases with liquid superficial velocity for a specific gas superficial velocity while it decreases with gas superficial velocity for a specific liquid superficial velocity. The effect of inclination angle on the liquid holdup at higher inclination angle is not significant, an agreement of work carried out by Beggs and Brill (1973). Moreover, liquid holdup was also presented by the quantity holdup ratio as a function of gas superficial velocity. This parameter was utilised by Govier and co-workers (1975). Unlike their work, it was difficult to clearly define the peaks and trough in these plots that they associated with flow pattern transitions. Nevertheless, it is believed that the use of holdup ratio is essential and useful in enabling the comparison of different datasets with different physical properties.

Structure velocity also follows a non – linear relationship (similar to second order polynomial) as a function of inclination angle. This was true for all experimental campaigns. For a specific gas and liquid superficial velocity, structure velocity increases with increasing inclination angle, reaching a maximum. After that, increases in inclination angle decreases the structure velocity. Explanation of the maximum structure velocity can be explained by two forces (friction and buoyancy) acting on the system.

Structure frequency of the gas structures increases with increasing inclination angle from horizontal. Furthermore, increases in liquid velocity also increases the frequency of gas structures at each inclination angle. The impact of gas superficial velocity was variable for each inclination angle and liquid superficial velocity, as discussed in Section 4.5.

At each inclination angle investigated, liquid holdup increases with viscosity for a given gas and liquid superficial velocity. The trend resembles to the works of various authors including Nadler and Mewes (1995) and Gokcal (2008). Furthermore, the present study was also compared to datasets of various authors (Escrig (2017) and Gokcal (2008)) to verify this effect of viscosity on liquid holdup. It can be established that large change in viscosity must be applied for a considerable amount of change in liquid holdup values.

Furthermore, structure velocity also increases with an increase in liquid viscosity however the increase for structure velocity is extremely small when compared to increase experienced by liquid holdup. Baba *et al.* (2019) explains the increase in structure velocity with viscosity is due to reduced slug length and increased frequency. Similar to liquid holdup, the trend was verified by comparing the present study's datasets with Gokcal (2008) and Escrig (2017).

Analysing the ranges of distribution coefficient and drift velocity values at each viscosity set yielded that distribution coefficient increases with viscosity while drift velocity decreases with viscosity. Moreover, a single distribution coefficient and drift velocity were also obtained for each liquid viscosity.

## 5. Investigating the effect of viscosity on flow regime maps

### 5.1. Introduction

Flow patterns in two – phase flow are classified based on spatial distribution of both phases, assisting in characterising the flow. The importance of gas and liquid distribution in circular pipes is essential when evaluating various flow characteristics such as pressure drop. Commonly, flow pattern maps based on superficial velocities are usually used for determining the flow regime for given set of superficial velocities. However, researchers have shown that physical properties such as viscosity, flow direction and channel dimensions are some of the other important factors which are important in determining flow patterns.

One complication of flow pattern maps is that the transition from one regime to another is not instantaneous. Rather, it is developed through intermediate regimes that exhibit mixed characteristics (Wu *et al.*, 2017). In other words, transition boundaries would be a region rather than a single line on a regime map. However, this complication is rather subjective and is heavily dependent on the observer's definition of various flow regimes. Most authors that have proposed flow pattern maps usually propose a single line for each possible transition between flow regimes. Furthermore, various authors have evaluated that slug flow cannot exist in larger pipes and is a characteristic of small pipes. Schlegel *et al.* (2012) has created a criterion based on the dimensionless diameter, as shown in Equation 5.1. They state that a pipe with dimensionless hydraulic diameter of 40 or more will no longer sustain slug flow.

$$D_H^* = \frac{D_H}{\sqrt{\sigma/g\Delta\rho}} \geq 40 \quad (5.1)$$

For each of the three experimental campaigns in this project, hydraulic diameter was calculated, as shown in Table 5.1. The dimensionless hydraulic diameter proposed by

Schlegel *et al.* (2012) is always higher than 40 for the cases considered. However, slug flow was observed in this research venture, as discussed in Chapter 2. The criterion was based on air – water systems which has a low viscosity compared to datasets in question. The effect of viscosity has been neglected in developing the above criterion.

*Table 5.1 – Dimensionless hydraulic diameter proposed by Schlegel et al. (2012) for three experimental campaigns in this project*

<b>Experimental Campaign</b>	<b>Dimensionless hydraulic diameter (<math>D^*_H</math>)</b>
64 cP	44.8
91.5 cP	44.8
236 cP	45.0

Hence, this research opportunity will investigate silicone oil – air system with the main aim of studying the effect of viscosity on flow regimes.

## 5.2. Effect of viscosity on flow regime maps and transitions for present experimental study

### 5.2.1. Methodology

The experimental matrix was explained in detail in Chapters 3 and 4. Overall, the flow regimes observed in this research project were bubbly (ellipsoidal / spherical cap), slug/plug, and churn. The initial two techniques employed for flow pattern identification were PDF (Probability Density Function) and visual observation. For PDF, Costigan and Whalley (1997) method was used in order to identify the flow regime for each experimental data point. However, Probability Density Function could not clearly define the difference between slug and churn flow in vertical flows for medium to high viscosity datasets in this study therefore this technique was not utilised in this work. According to Costigan and Whalley (1997), there should two peaks in PDF plot for slug flow – one peak for Taylor bubble and one peak for liquid slug. However, in this current study, PDF performed yielded single peaks for some

slug data points while it produced two peaks for other slug data points. The possible reason for this could be due to the fact that Costigan and Whalley (1997) focussed on air – water systems while this project venture consists of investigating medium to high viscosity datasets. Therefore, visual observation was the main method utilised for flow regime identification.

The existing flow pattern maps in literature were discussed in Chapter 2. The most commonly used flow pattern maps involve the use of gas and liquid superficial velocities on the x – axis and y – axis respectively. However, such parameters do not take into the account the properties of the fluids as well as the geometry of the pipeline. Since the current study involved investigating the effect of viscosity on flow pattern maps, Reynolds number was used. Furthermore, for investigating datasets from literature accommodating other properties such as surface tension, Weber and Reynolds number was utilised in different forms in order to take such parameters into account, especially viscosity of the liquid phase and surface tension of two – phase systems in question.

#### 5.2.2. Observed flow pattern maps for all three experimental campaigns

Figure 5.1 shows the observed flow patterns and transitions using the typical x and y – axes: liquid superficial velocity against gas superficial velocity plot. Overall, five inclinations were investigated for each experimental campaign. Four main flow patterns were observed in this study. There were three transitions that occurred: Bubbly to Cap Bubble (BtoCB), Cap Bubble to Slug (CBtoS) and Slug to Churn (StoCh). Transition boundaries were also determined visually. Annular flow was not observed in this study due to the limitations of gas flowmeter in achieving high gas superficial velocity required for this flow regime.

The main reason for not observing bubbly flow for other inclination than vertical orientation is due to the limitations of the gas and liquid superficial velocities that can (or cannot) be achieved for inclinable rig. In this study, bubbly flow was only observed at vertical inclination (90 degrees). The shape of the bubbles resembled to

that of an ellipsoid rather than small spherical bubbles. With increasing viscosity, the transition boundary for BtoCB is shifting to the left at high liquid velocities while it shifts to the right at low liquid velocities. In total, only three bubbly points were observed in this study (2 – 64 cP; 1 – 91.5).

The transition CBtoS occurs for all presented inclination angles. At each inclination angle, the transition boundary CBtoS is shifting to the left with increasing viscosity. Similarly, increasing inclination angle shifts the CBtoS boundary to the right, increasing the number of points exhibiting cap bubble. In total, 65 observed data points were cap bubbly while 608 observed data points were slug flow. Churn flow was only observed at vertical inclination. The transition boundary StoCh shifts to the right when liquid viscosity is increased. In total, there were 12 data points (all for 64 cP) for churn flow. The effects of viscosity on a liquid – gas superficial velocity plot can be observed however it is quite minimal. Since this project is focussed on the effect of viscosity, it was proposed that Reynolds Number was experimented so that the viscous effects were captured in the plot. Moreover, Reynolds Number will also capture the slight changes in liquid density as well.

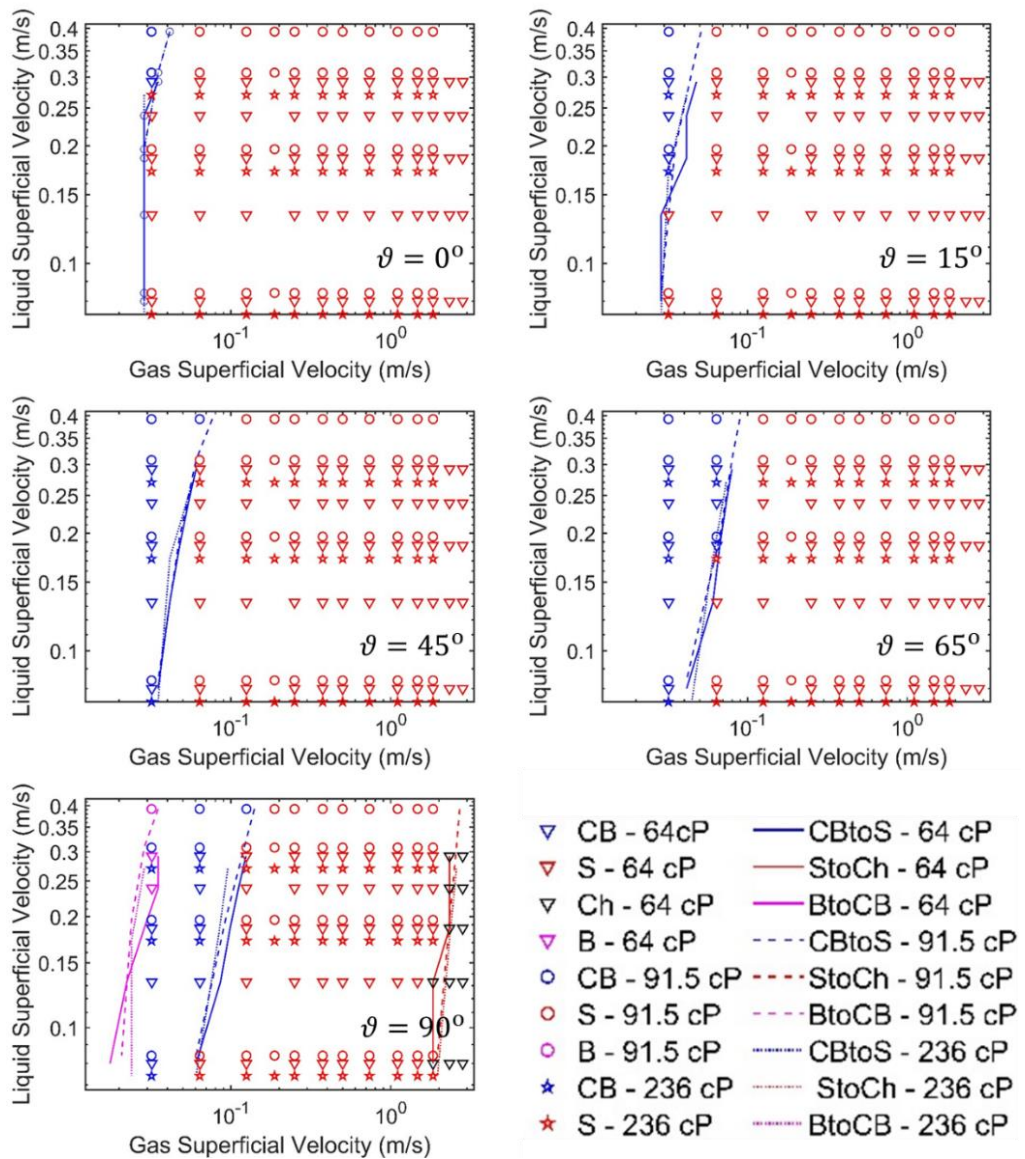


Figure 5.1 – Observed flow patterns and transitions for all three experimental campaigns investigated at five different inclination angles with gas and liquid superficial velocities on x – axis and y – axis respectively

The definition of liquid Reynolds number is given by Equation 5.2. Liquid Reynolds number will capture the effect of viscosity, superficial liquid velocity and slight changes in liquid density. Diameter is constant for all three experimental campaigns. These effects are not captured through the use of superficial velocity coordinate map shown in Figure 5.1. One other reason for using Reynolds number is its dimensionless nature which allows comparison between different experimental datasets.

$$Re_L = \frac{\rho_L u_{SL} D}{\mu_L} \quad (5.2)$$

Equation 5.3 shows the definition of gas Reynolds number. Gas density and viscosity is constant for all three experimental campaigns along with pipe diameter. Nevertheless, using gas Reynolds number captures the effect of gas superficial velocity.

$$Re_G = \frac{\rho_G u_{SG} D}{\mu_G} \quad (5.3)$$

Figure 5.2 shows the observed flow patterns and transitions using gas Reynolds number on the x – axis and liquid Reynolds number on the y – axis. Compared to Figure 5.1, there are notable differences in how the transition lines capture the effect of viscosity. The transition lines are moving down and rightwards for each inclination angle, thus exhibiting the viscosity effect in a much clearer and concise manner.

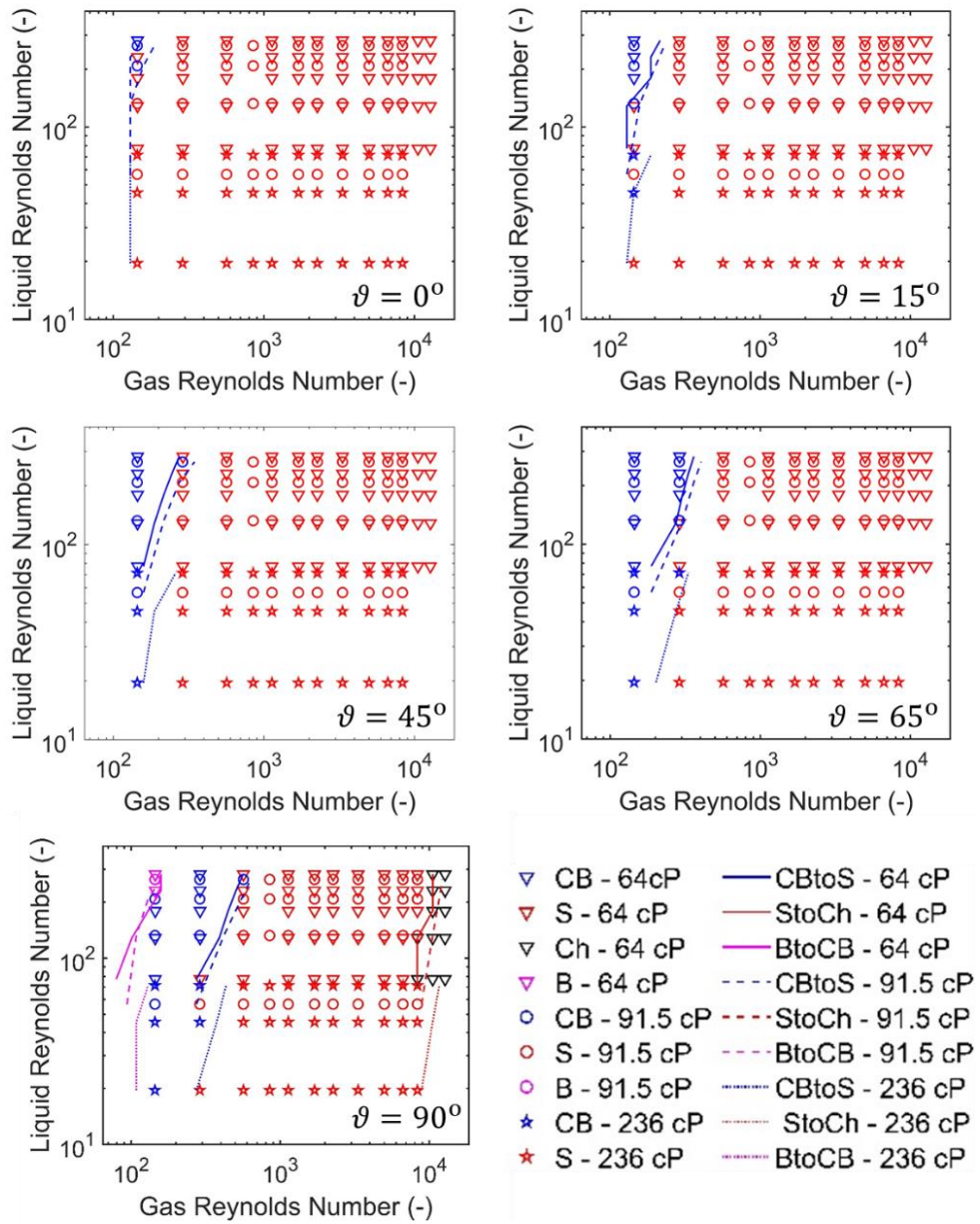


Figure 5.2 – Observed flow patterns and transitions for all three experimental campaigns investigated at five different inclination angles with gas and liquid Reynolds Number on x – axis and y – axis respectively

5.2.3. Comparing the results of present study to commonly used flow regime maps and experimental studies in literature

5.2.3.1. Vertical inclination

The most commonly used flow regime map for vertical pipelines is Taitel *et al.* (1980) map. As shown in Section 5.2.2, Reynolds Number provided much clearer transition boundaries. Therefore, the transition boundaries (default parameters are gas and liquid superficial velocities) in Taitel *et al.* (1980) map were converted to Reynolds Number, as shown in Figure 5.3. Each transition line of default Taitel *et al.* (1980) map can be evaluated by using Equations 2.30, 2.42, 2.44, 2.47 and 2.56 (see Chapter 2), giving us the gas and liquid superficial velocity coordinates. Therefore, the respective gas and liquid Reynolds numbers for the points on these lines can be evaluated using Equations 5.2 and 5.3. Default Taitel *et al.* (1980) map was based on air – water so it enables comparison for each experimental data with a distinct dynamic viscosity. Part of the map is shown in Figure 5.3 to allow comparison between experimental lines and literature.

Table 5.2 – Testing the modified Taitel *et al.* (1980) model for each experimental campaign for vertical dataset

Taitel <i>et al.</i> (1980)	Viscosity dataset (cP)		
	64	91.5	236
Number of points correctly predicted (slug & churn as separate section)	15	11	8
% correctly predicted (slug & churn as separate section)	25	25	24.2
Number of points correctly predicted (slug & churn as intermittent)	60	43	32
% correctly predicted (slug & churn as intermittent)	100	97.7	97.0

In Figure 5.3, observed flow pattern map with transition boundaries is shown on the left while modified Taitel *et al.* (1980) map is shown on the right. Table 5.2 shows the number of points and percentage of points correctly predicted by modified Taitel *et al.* (1980) map for different settings: slug / churn transition treated separately, and slug / churn transition treated as intermittent. For slug / churn transitions treated separately, percentage of points correctly predicted at each viscosity dataset stay constant at around 25 %. In comparison, using a single intermittent regime yields a much higher percentage of data at each viscosity dataset as shown in Table 5.2.

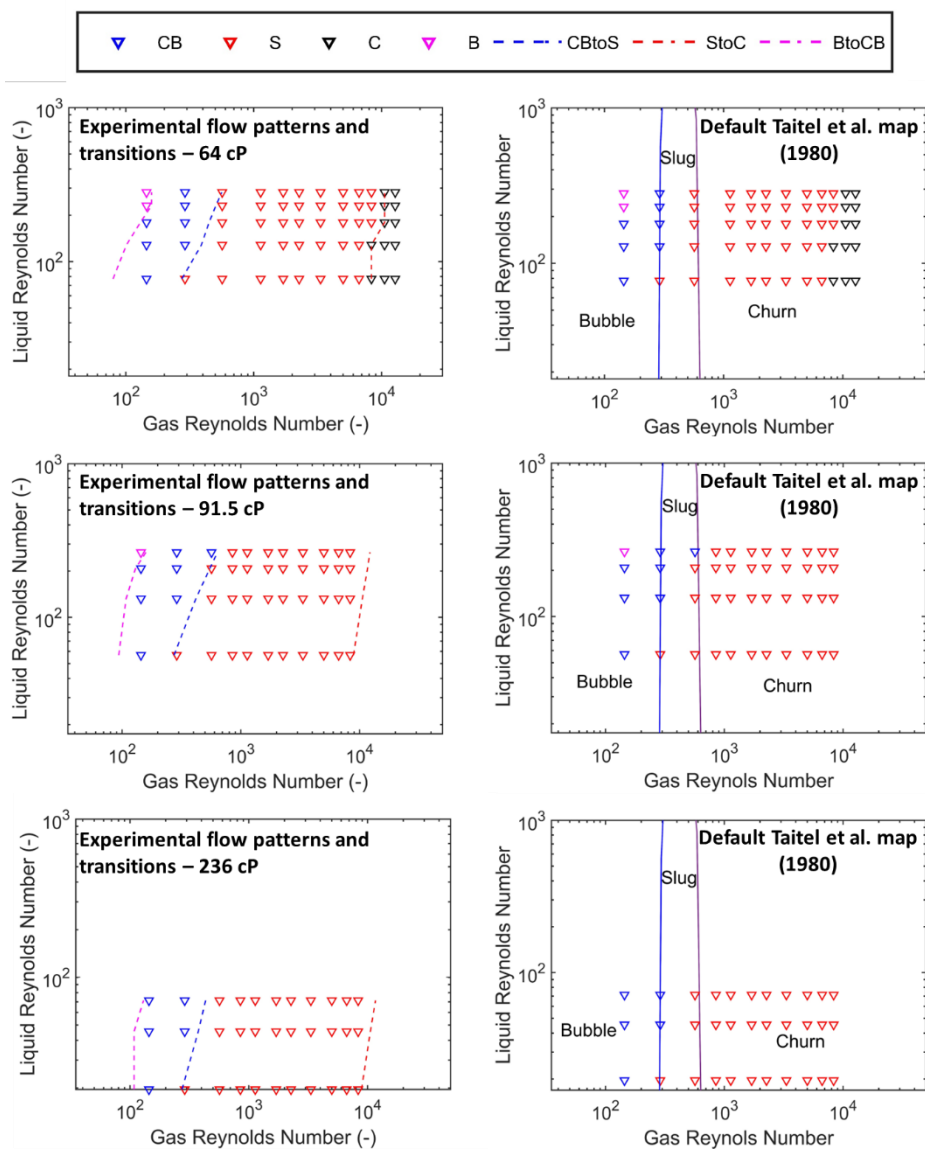


Figure 5.3 – Comparing observed flow patterns and transitions for present study to observed flow patterns plotted on modified Taitel *et al.* (1980) based on Reynolds Number for vertical datasets

5.2.3.2. Horizontal inclination

One of the most common flow regime maps for horizontal inclination is Taitel *et al.* (1976) map. Taitel *et al.* (1976) map for horizontal pipelines uses five dimensionless quantities: F (Froude Number), X (Lockhart – Martinelli Parameter), K, Y and T. Taitel *et al.* (1976) predicts all points for each dataset, as shown in Figure 5.4.

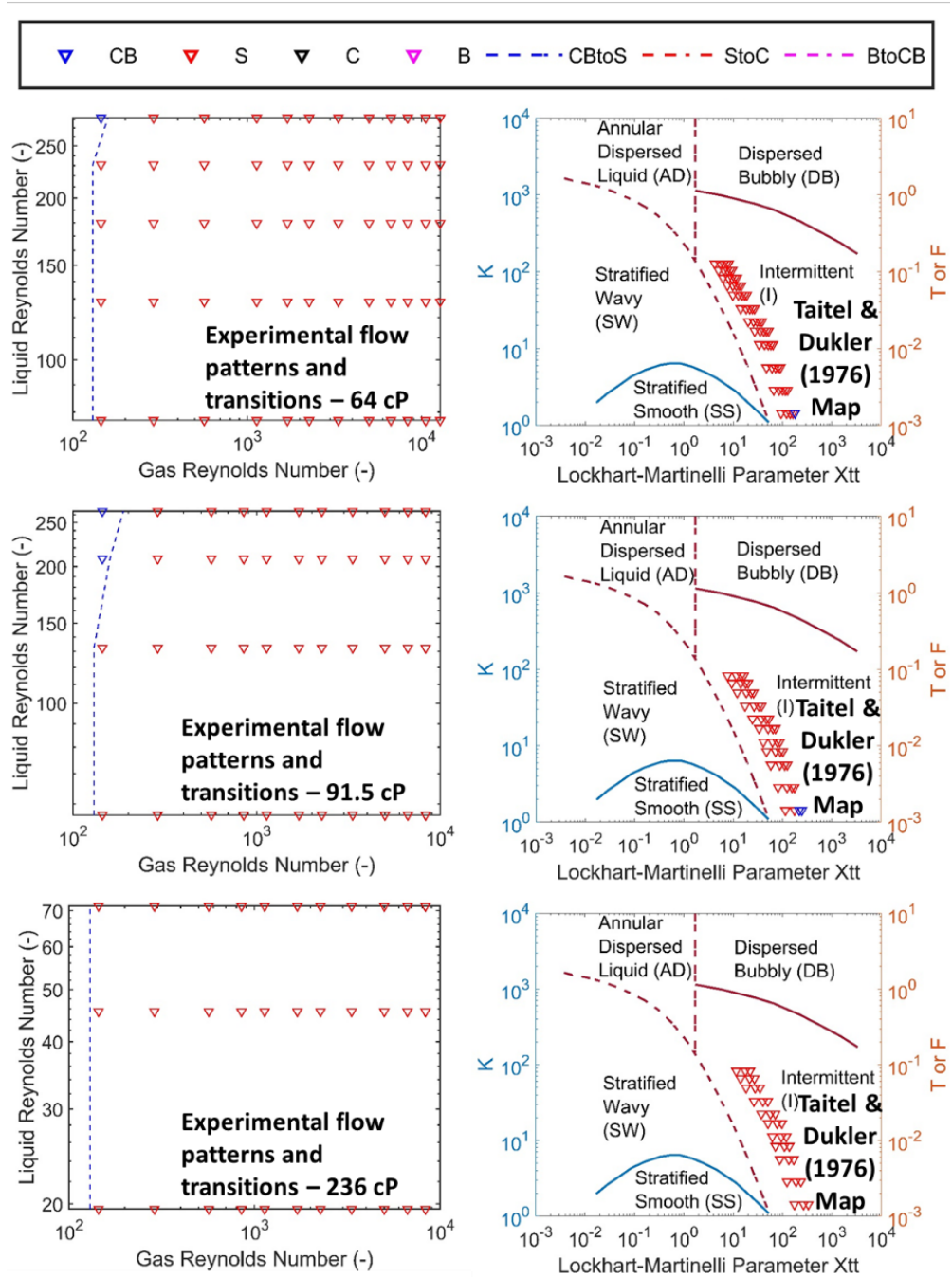


Figure 5.4 – Comparing observed flow patterns and transitions for present study to observed flow patterns plotted on Taitel and Dukler (1976) for horizontal datasets

Another commonly used flow regime map for horizontal flow regime is Mandhane *et al.* (1974). Similar to Taitel *et al.* (1980), the conventional Mandhane *et al.* (1974) was converted into Reynolds Number (based on air – water systems, again allows comparison between different datasets).

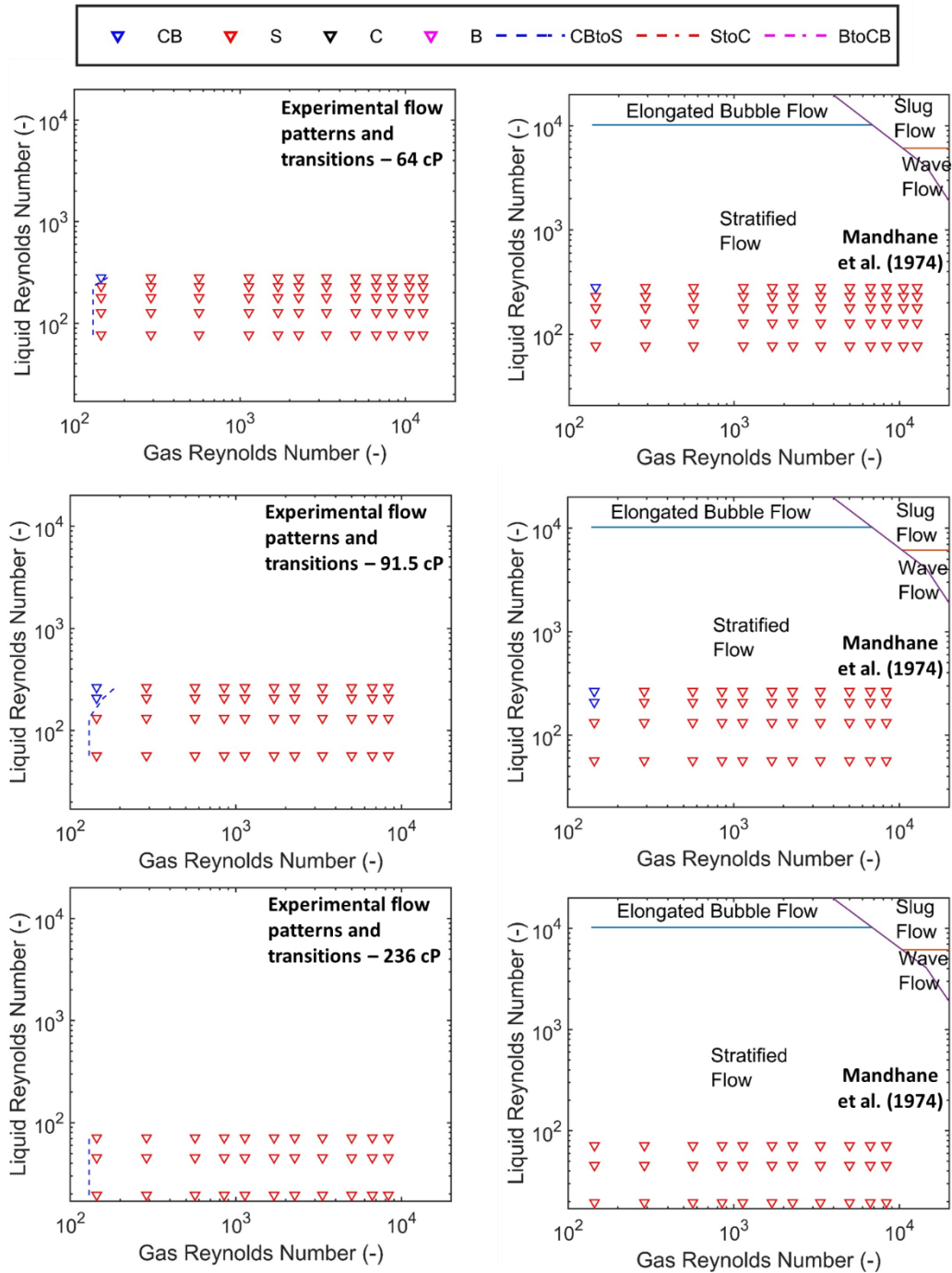


Figure 5.5 – Comparing observed flow patterns and transitions for present study to observed flow patterns plotted on modified Mandhane *et al.* (1974) based on Reynolds Number for horizontal datasets

The transition lines in terms of gas and liquid superficial coordinates are given in Table 2.2. The conversion to Reynolds number was carried out in the same fashion as was done for Taitel *et al.* (1980) in Figure 5.3. In Figure 5.5, observed flow pattern maps with transition boundaries are shown on the left while modified Mandhane *et al.* (1974) are shown on the right. Modified Mandhane *et al.* (1974) map does not predict a single point within the correct flow regime section. Only part of the map is shown, allowing comparison to experimental flow regime.

### 5.2.3.3. *Inclined orientation*

For inclined orientations, one of the most commonly used flow regime maps is Barnea *et al.* (1985). Again, the superficial velocities axes are converted to Reynolds number for Barnea *et al.* (1985) map. Same method used for modified Taitel *et al.* (1980) map was implemented for conversion of gas and liquid superficial velocities into gas and liquid Reynolds number. The conversion was based on air – water properties, allowing comparison to be made between different datasets. Figures 5.6 – 5.8 compares the observed flow pattern map to modified Barnea *et al.* (1985) map for inclination angles of 65, 45 and 15 degrees. For each inclination angle, all slug points are correctly predicted by modified Barnea *et al.* (1985) map however bubble data points are not that well predicted.

*Table 5.3 – Testing the modified Barnea et al. (1985) model for each experimental campaign for inclination angles of 65, 45 and 15 degrees*

<b>Barnea <i>et al.</i> (1985) Map</b>	<b>Inclination angle</b>	<b>Viscosity dataset (cP)</b>		
		<b>64</b>	<b>91.5</b>	<b>236</b>
Number of points correctly predicted	65	57	41	32
% correctly predicted		95.0	93.2	97.0
Number of points correctly predicted	45	60	43	33
% correctly predicted		100.0	97.7	100.0
Number of points correctly predicted	15	57	41	31
% correctly predicted		95.0	93.2	93.9

Table 5.3 shows the number of points and percentage of data points correctly predicted by modified Barnea *et al.* (1985) map for inclination angles of 65, 45 and 15 degrees. As shown in Table 5.3, modified Barnea *et al.* (1985) predicts the dataset quite well for each inclination angle.

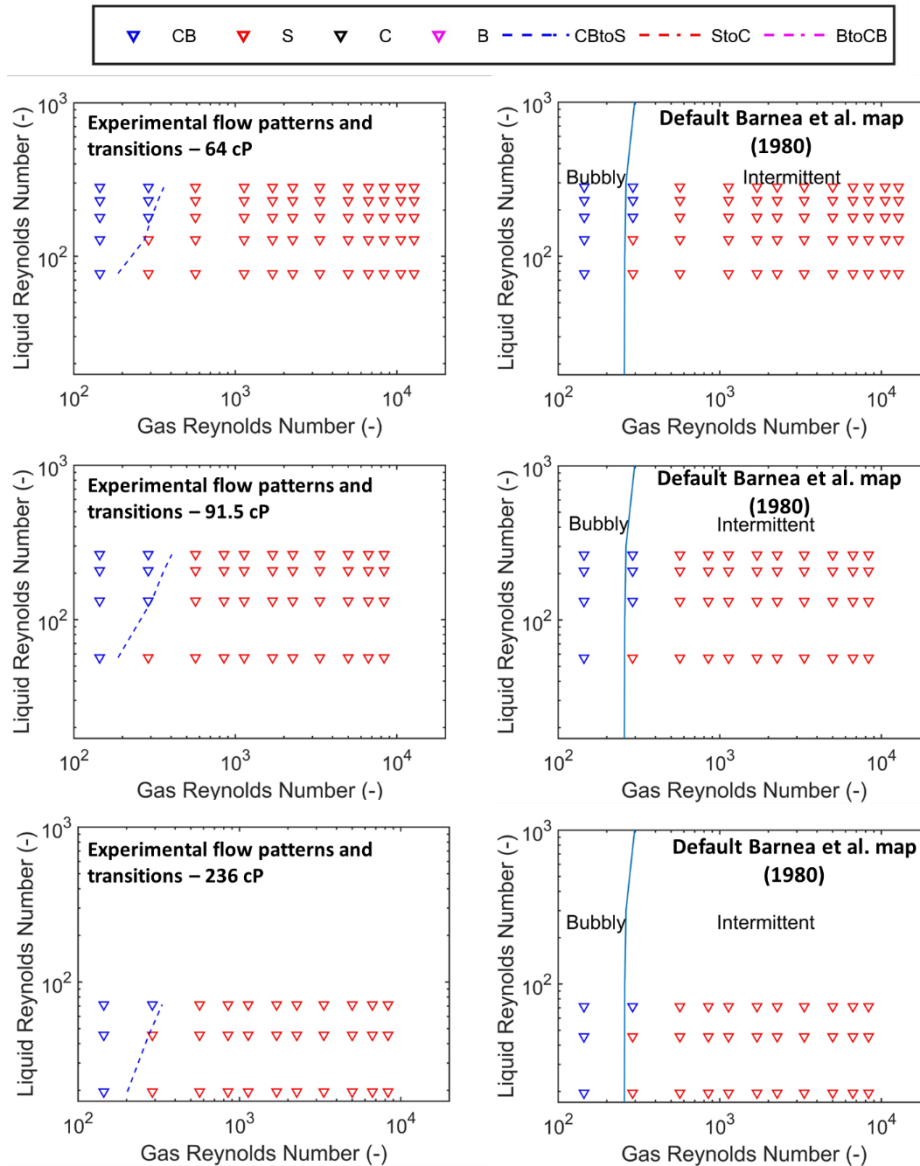


Figure 5.6 – Comparing observed flow patterns and transitions for present study to observed flow patterns plotted on modified Barnea *et al.* (1985) based on Reynolds Number for inclination angle of 65 degrees

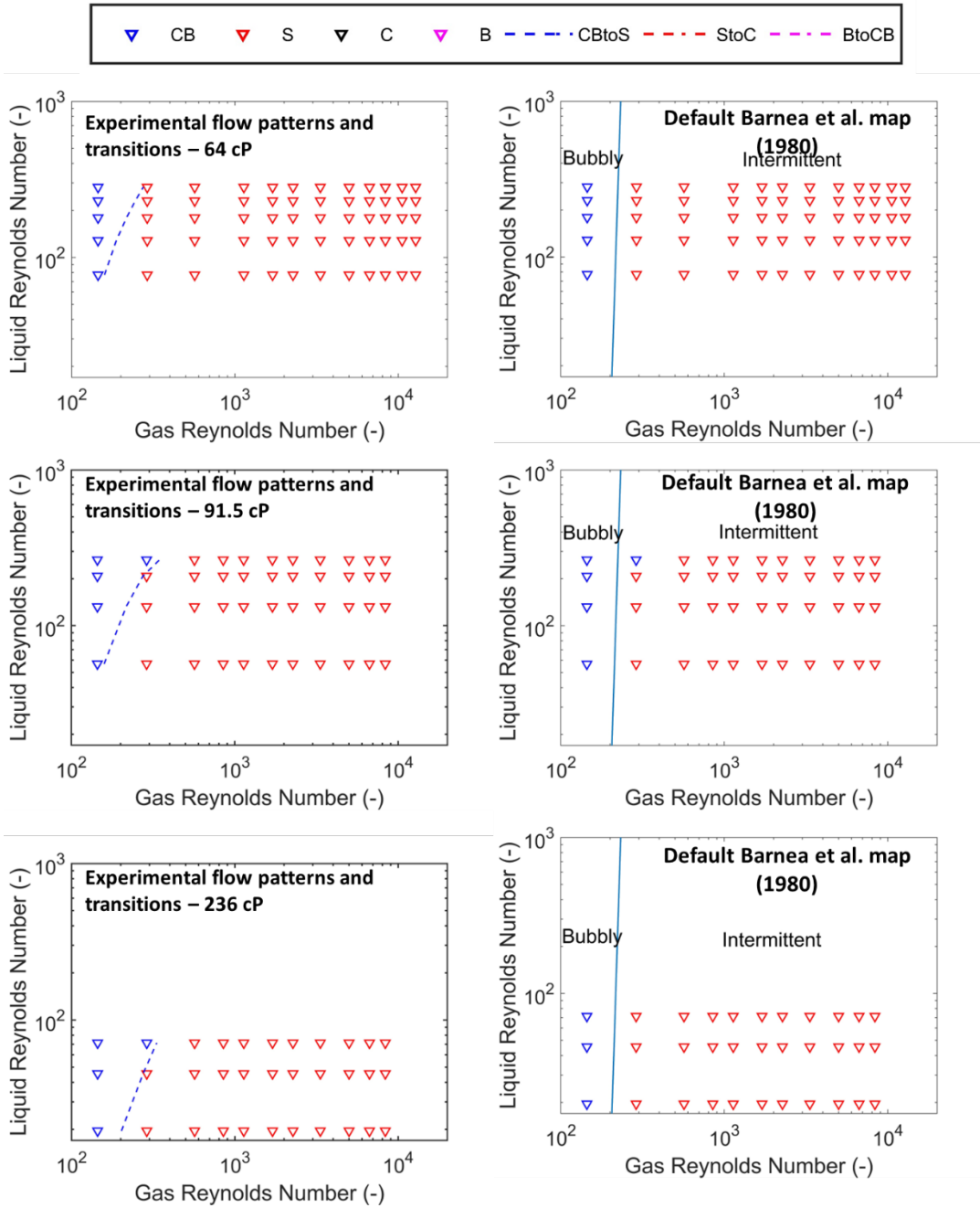


Figure 5.7 – Comparing observed flow patterns and transitions for present study to observed flow patterns plotted on modified Barnea et al. (1985) based on Reynolds Number for inclination angle of 45 degrees

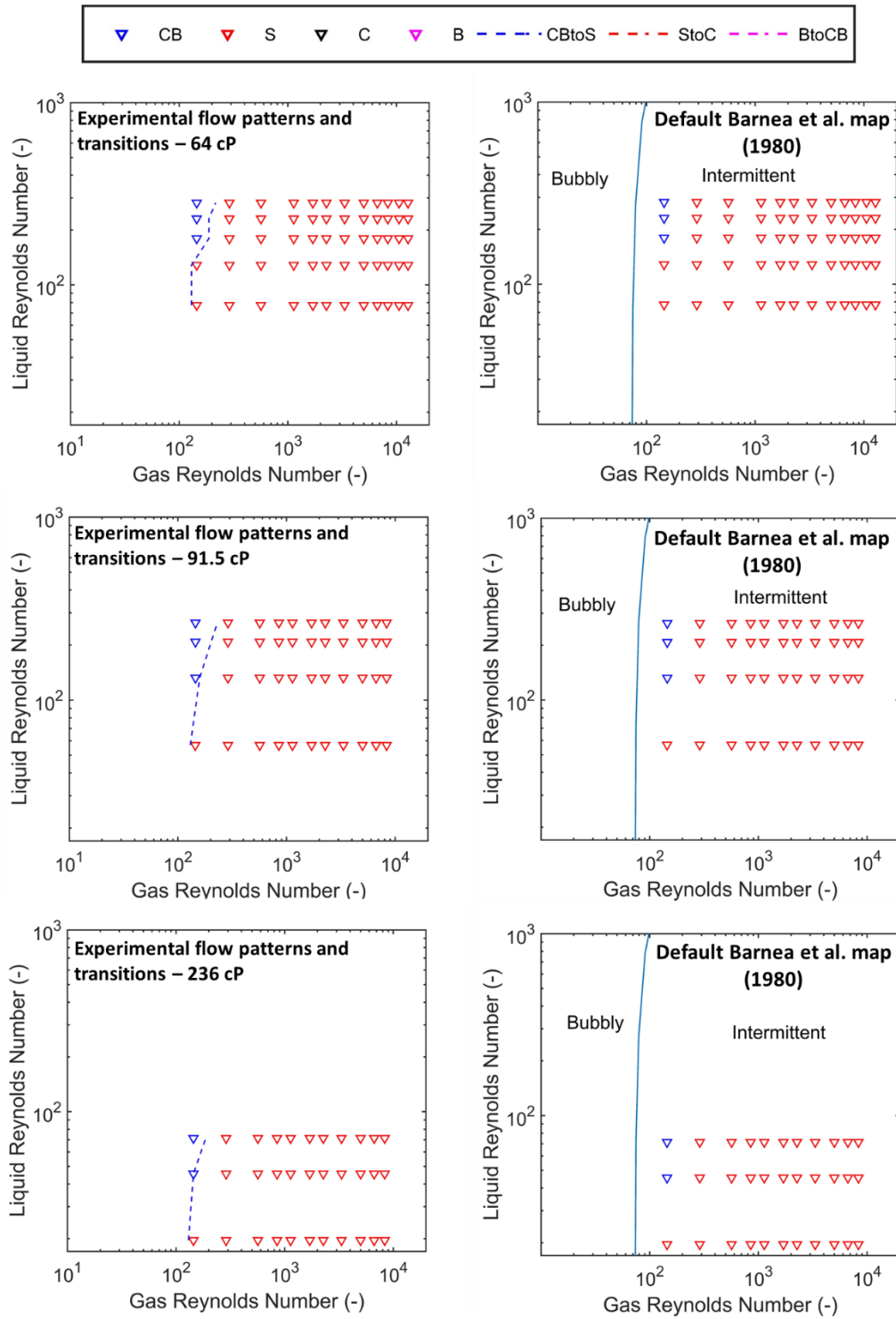


Figure 5.8 – Comparing observed flow patterns and transitions for present study to observed flow patterns plotted on modified Barnea et al. (1985) based on Reynolds Number for inclination angle of 15 degrees

5.2.4. Proposed flow pattern map for present study and comparisons to other experimental studies in literature

Figure 5.9 shows proposed flow regime map for each inclination. The three lines in Figure 5.2 for each transition are combined into a single line. It can be observed that use of Reynolds number beautifully captures the effect of viscosity on flow pattern transitions.

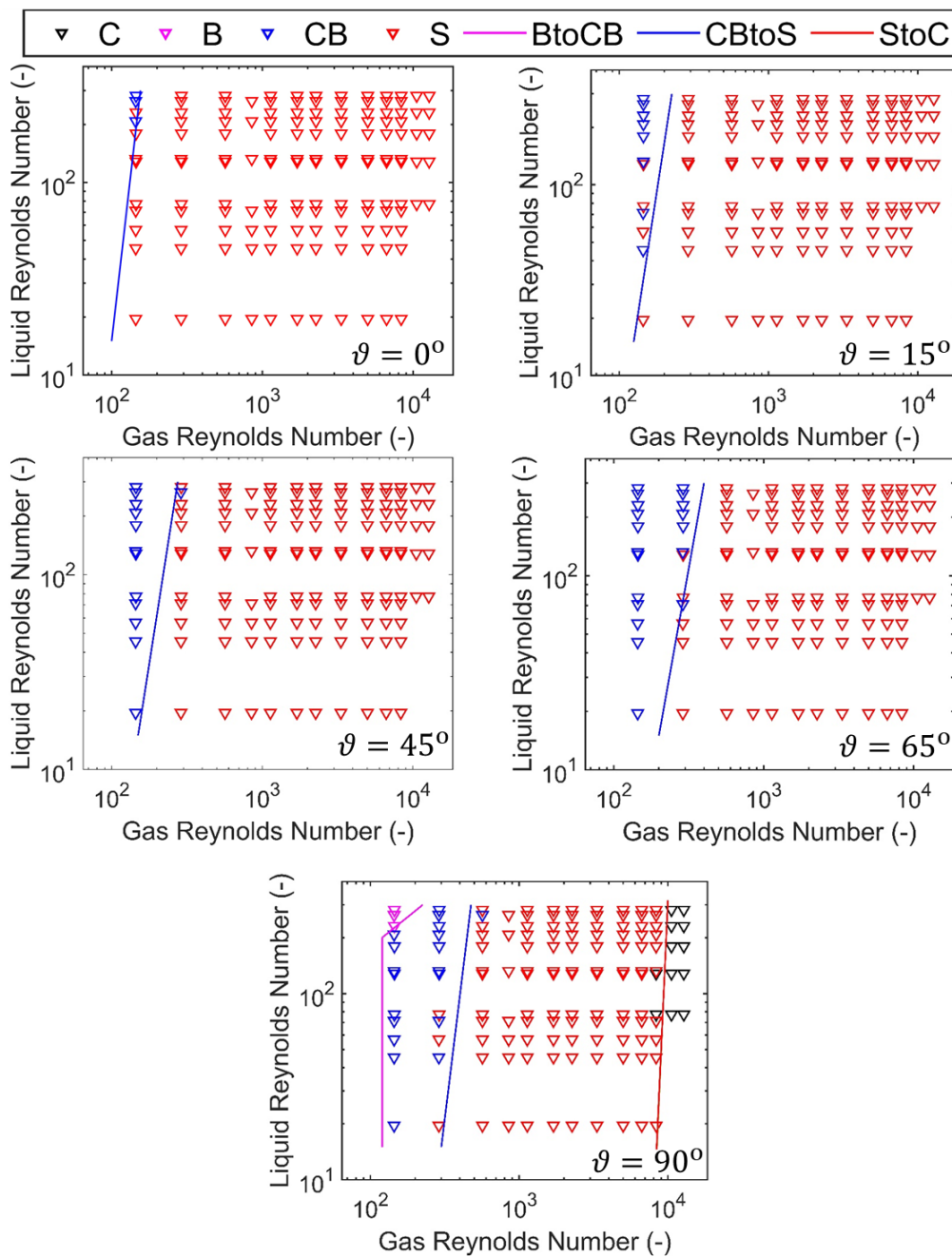


Figure 5.9 –Proposed flow regime map for each inclination angle

Table 5.4 shows the percentage of data points correctly predicted by proposed transition boundaries for each inclination angle. The prediction is good for each inclination (> 97 %).

*Table 5.4 – Performance of proposed model for each inclination angle*

<b>Inclination Angle</b>	<b>% points correctly predicted by proposed model</b>
0	99.3 (136/137)
15	97.8 (134/137)
45	99.3 (136/137)
65	98.5 (135/137)
90	97.1 (133/137)

It is important to compare the proposed flow regime maps for present study to experimental studies in literature. For vertical inclination, datasets of Alruhaimani (2015) – 127 cP and 213 cP were selected – full details of dataset in Section 5.3.1.

For 127 cP dataset of Alruhaimani, 85 % of all points were predicted correctly, as shown in Figure 5.10. The percentage of points correctly predicted by each regime is as follows: bubbly flow (60 %), slug flow (95 %) and churn flow (79 %). For 213 cP dataset of Alruhaimani, 87.5 % of all points were predicted correctly. The percentage of points correctly predicted by each regime is as follows: bubbly flow (60 %), slug flow (100 %) and churn flow (79 %). Note: the annular points were ignored as present study does not study annular flow regime.

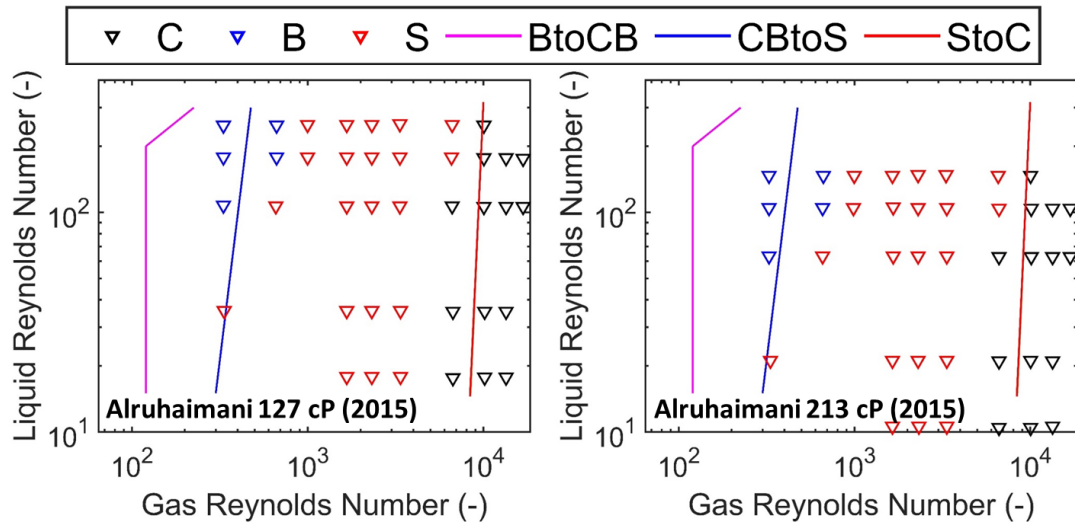


Figure 5.10 – Performance of present study's proposed flow regime map (vertical inclination) for experimental study of Alruhimani (2015)

For horizontal orientation, four different datasets were utilised: Taitel and Dukler (1987) – 90 and 165 cP, Gokcal *et al.* (2006) – 181 cP and Brito *et al.* (2013) – 166 cP. Full details on these datasets are given in Section 5.3.1. For all these datasets, all intermittent data points were selected for comparison as present study's flow regime does not go beyond intermittent flow. Results are presented in Figure 5.11. For each dataset tested, the points lie on the right side of the transition boundary. It must be noted that some intermittent points for each dataset are still beyond the tested conditions of flow regime map.

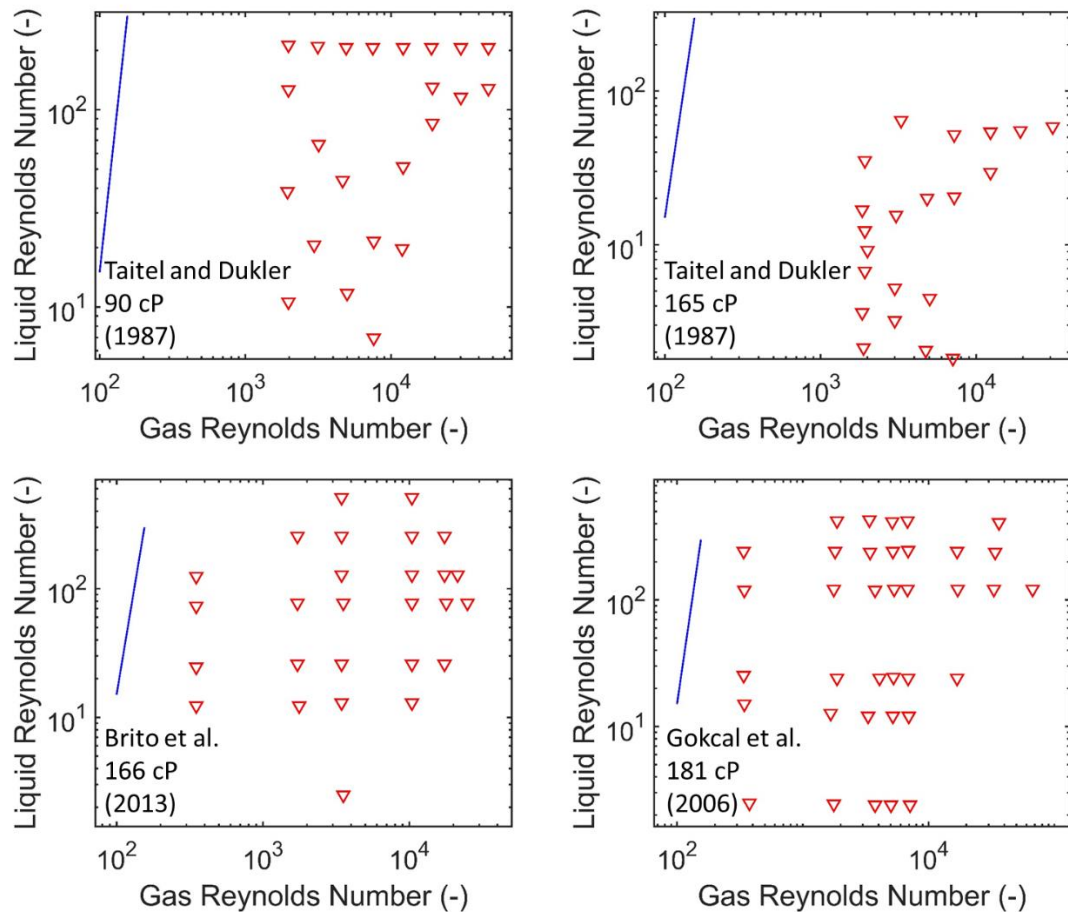


Figure 5.11 – Performance of present study’s proposed flow regime map (horizontal inclination) for various experimental studies in literature.

### 5.3. Literature review of flow pattern experimental studies in vertical and horizontal systems

#### 5.3.1. Methodology including data sources utilised

Various studies have been carried out on flow patterns in vertical and horizontal pipelines. In this section, literature was reviewed to compile experimental studies involving flow patterns with a focus on effect of viscosity and other two – phase properties. Moreover, Weber and Reynolds number in different forms will be utilised on the x and y – axis for these datasets in order to determine the best dimensionless number for each axis.

Table 5.5 – Vertical experimental datasets from literature utilised for investigating the effect of viscosity on flow patterns

Author(s)	Diameter (mm)	Viscosity (cP)	Fluids	Number of points
Alruhaimani (2015)	50.8	127, 213, 401, 586	Air – Oil	39,42,42,42
Akhiyarov <i>et al.</i> (2010)	52.5	385	Air – Oil	16
Furukawa and Fukano (2001)	19.2	6, 17	Air – 53 % / 72 % glycerol – water	73, 72
Szalinski <i>et al.</i> (2010)	67	5	Air – Silicone Oil	30
Furukawa and Fukano (2001)	19.2	1	Air – Water	73
Alruhaimani (2015)	50.8	1	Air – Water	21
Barnea <i>et al.</i> (1983a)	12.3	1	Air – Water	164
Barnea <i>et al.</i> (1985)	25, 51	1	Air – Water	117, 149
Ghanbarzadeh <i>et al.</i> (2012)	50	1	Air – Water	62
Govier and Short (1958)	16, 26, 38.1, 63.5	1	Air – Water	11, 11, 13, 11
Julia <i>et al.</i> (2008)	50.8	1	Air – Water	129
Lucas <i>et al.</i> (2005)	51.2	1	Air – Water	89
Rosa <i>et al.</i> (2010)	26	1	Air – Water	73
Rozenblit <i>et al.</i> (2006)	25	1	Air – Water; Air – Water (Surfactant)	40, 43
Szalinski <i>et al.</i> (2010)	67	1	Air – Water	28
Spedding <i>et al.</i> (1998)	26	1	Air – Water	291
Taitel <i>et al.</i> (1980)	25, 51	1	Air – Water	108, 79
TOTAL	12.3 – 67	1 – 586	Various	1868

Table 5.5 shows the experimental studies for vertical flows from literature that were considered in this study. Since the focus of this project is on effect of viscosity on flow regime maps, a wide range of viscosity (consisting of low and high viscosity datasets) were utilised. Overall range of viscosity considered was 1 cP – 586 cP. Table 5.6 details the experimental studies for horizontal flows from literature. Here, the viscosity range is from low viscosity (~1) to 587 cP.

*Table 5.6 – Horizontal experimental datasets from literature utilised for investigating the effect of viscosity on flow patterns*

<b>Author(s)</b>	<b>Diameter (mm)</b>	<b>Viscosity (cP)</b>	<b>Fluids</b>	<b>Number of points</b>
Gokcal <i>et al.</i> (2006)	50.8	181, 587	Air – Oil	44, 45
Brito <i>et al.</i> (2013)	50.8	166	Air – Oil	38
Taitel and Dukler (1987)	38	90, 165	Air – Glycerine Solutions	46,44
Weisman <i>et al.</i> (1979)	51	1	Air – Water;	303
Barnea <i>et al.</i> (1985)	25, 51	1	Air – Water	209, 193
Govier and Omer (1962)	26	1	Air – Water	15
<b>TOTAL</b>	<b>25 – 51</b>	<b>1 – 587</b>	<b>Various</b>	<b>937</b>

As noted in earlier sections, the scarcity of datasets at high viscosity is one of the factors that is being tackled in this research project. Therefore, three different experimental campaigns (Chapter 4) were carried out in order to increase the breadth of datasets in viscous two-phase systems.

### 5.3.2. Investigating viscosity effect for experimental studies in literature for vertical flow patterns

The datasets represented in Table 5.5 was split into two different sets: low viscosity and medium to high viscosity. Cut – off maximum for low viscosity datasets is 50 cP. The low viscosity datasets consisted of 1687 data points. They were organised into four flow regimes: bubbly, slug, churn and annular. Some data points were labelled mixed because they were deemed transitional in their respective studies. The overall breakdown of points by flow regime is shown below:

- 17.4 % Bubbly (294 points)
- 36.1 % Slug (609 points)
- 25.0 % Churn (422 points)
- 17.0 Annular (287 points)
- 4.4 % Mixed (75 points)

Figures 5.12 (a – d) shows the effect of using different combination of gas/liquid Reynolds and Weber number on flow patterns for low viscosity datasets in vertical pipelines. Gas and liquid Weber numbers are given by Equations 5.4 and 5.5 respectively.

$$We_L = \frac{\rho_L u_{SL}^2 D}{\sigma} \quad (5.4)$$

$$We_G = \frac{\rho_G u_{SG}^2 D}{\sigma} \quad (5.5)$$

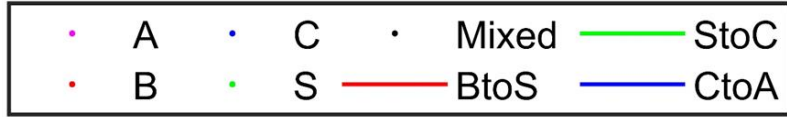
In Figure 5.12 (a), liquid Reynolds number is plotted against gas Reynolds number. As examined in Section 5.2, Reynolds Number exquisitely captures the effect of viscosity on flow patterns. Furthermore, in Figure 5.12 (b), liquid Weber number is plotted against gas Weber number. One noticeable feature of Figure 5.10 (b) is that churn and annular regime sections at high liquid Weber number contain slightly lower

number of data points relevant to other flow regimes, meaning data points separate well according to the flow regime.

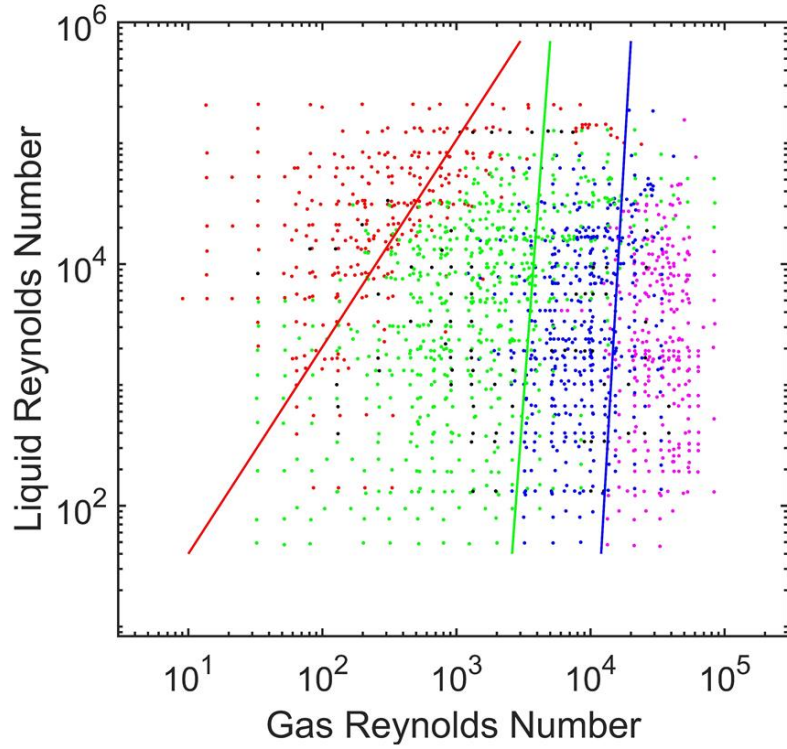
Figure 5.12 (c) shows the effect of liquid Weber number against gas Reynolds number for flow regime map. Figure 5.12 (c) does not capture effect of liquid viscosity on flow regime patterns, same as Figure 5.12 (b). Hence, these two maps will not be considered for further analysis.

In Figure 5.12 (d), liquid  $Re$  is plotted against gas  $We$ . The map in Figure 5.12 (d) enables not only the effect of viscosity to be captured but also the effect of surface tension to be investigated. This map also provides an interesting basis for inclusion for further analysis.

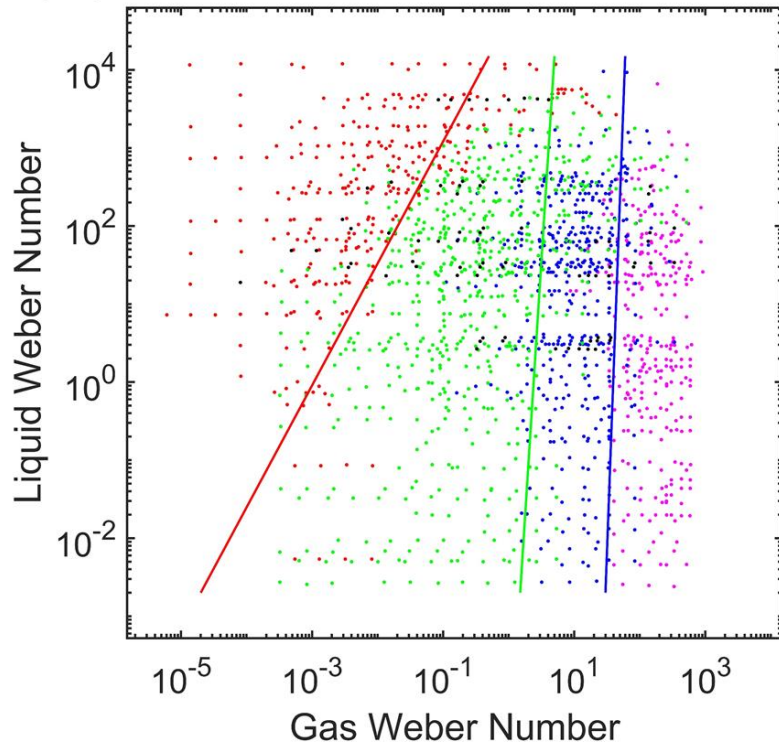
The transition boundary lines were determined by trial and error with an aim of ensuring that best ratio of points lie within the correct flow regime section.



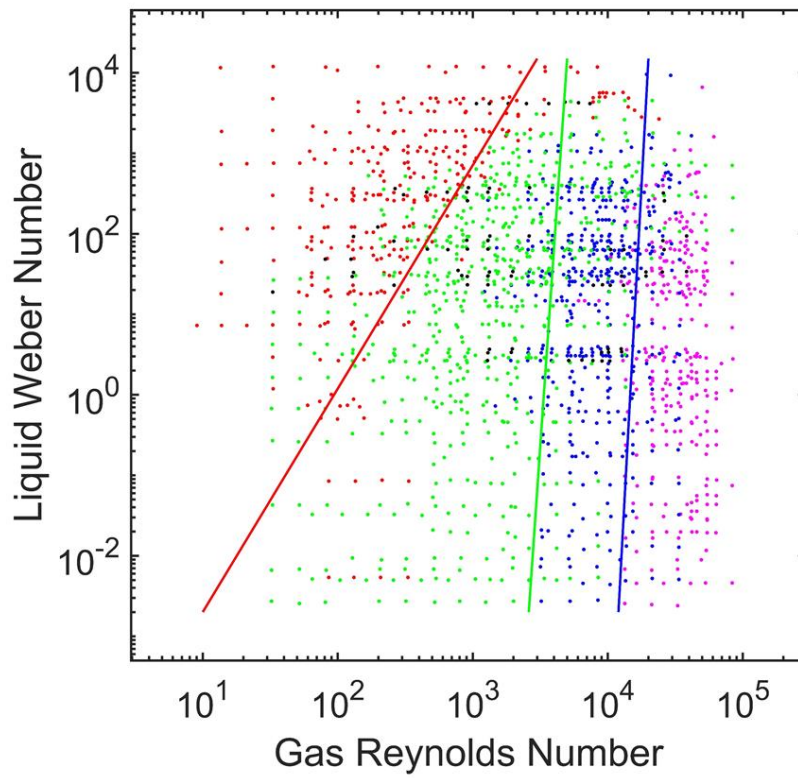
a) Liquid Re vs Gas Re



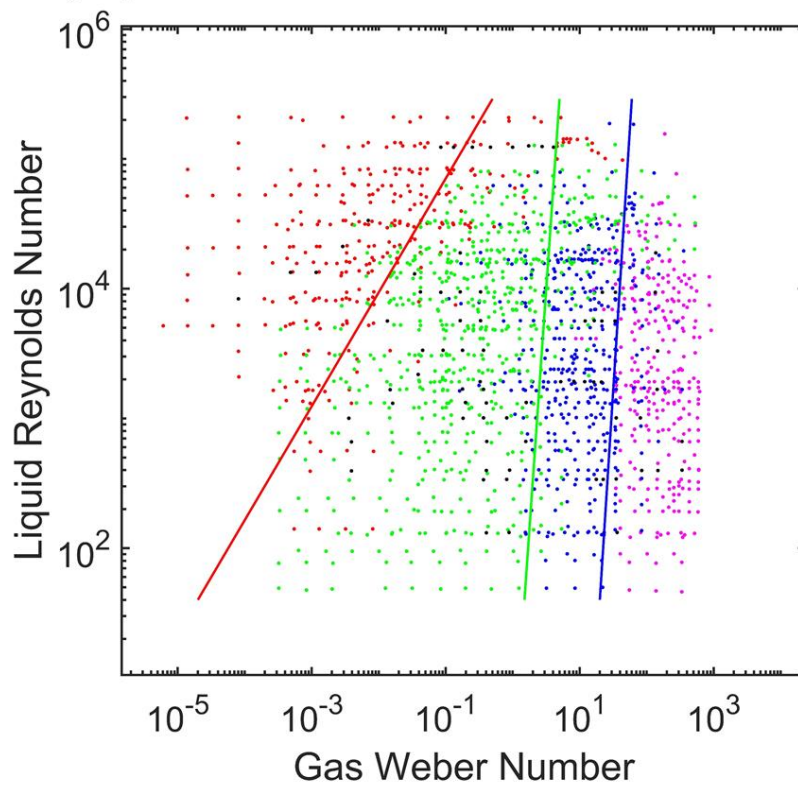
b) Liquid We vs Gas We



c) Liquid We vs Gas Re



d) Liquid Re vs Gas We



Figures 5.12 (a – d) – Effect of Weber and Reynolds number in different forms on flow patterns for low viscosity datasets in vertical pipelines

Table 5.7 – Percentage of each flow pattern in each flow pattern section for all four maps shown in Figures 5.12 (a – d)

Map	Experimental Flow Regime	% of each flow pattern in each flow pattern section			
		Bubbly	Slug	Churn	Annular
Liquid Reynolds Number vs. Gas Reynolds Number	Bubbly	84.4 (178)	15.7 (98)	3.7 (17)	0.3 (1)
	Slug	12.8 (27)	71.5 (446)	24.1 (112)	6.2 (24)
	Churn	0 (0)	6.4 (40)	64.2 (298)	21.6 (84)
	Annular	0 (0)	0 (0)	3.7 (17)	69.6 (270)
	Mixed	2.8 (6)	6.4 (40)	4.3 (20)	2.3 (9)
	Total	100 (211)	100 (624)	100 (464)	100 (388)
Liquid Weber Number vs. Gas Weber Number	Bubbly	82.3 (218)	9.2 (60)	3.6 (16)	0 (0)
	Slug	13.2 (35)	72.7 (472)	19.8 (87)	4.5 (15)
	Churn	0 (0)	12.3 (80)	67.0 (295)	14.1 (47)
	Annular	0 (0)	0 (0)	5.7 (25)	78.7 (262)
	Mixed	4.5 (12)	5.7 (37)	3.9 (17)	2.7 (9)
	Total	100 (265)	100 (649)	100 (440)	100 (333)
Liquid Weber Number vs. Gas Reynolds Number	Bubbly	75.6 (229)	8.5 (47)	3.8 (17)	0.3 (1)
	Slug	19.1 (58)	76.4 (423)	23.7 (107)	5.6 (21)
	Churn	0 (0)	9.7 (54)	63.5 (287)	21.4 (81)
	Annular	0 (0)	0 (0)	4.6 (21)	70.4 (266)
	Mixed	5.3 (16)	5.4 (30)	4.4 (20)	2.4 (9)
	Total	100 (303)	100 (554)	100 (452)	100 (378)
Liquid Reynolds Number vs. Gas Weber Number	Bubbly	85.2 (202)	11.3 (76)	3.9 (16)	0 (0)
	Slug	11.8 (28)	71.8 (481)	20.3 (83)	4.6 (17)
	Churn	0 (0)	10.6 (71)	69.2 (283)	18.3 (68)
	Annular	0 (0)	0 (0)	3.4 (14)	73.6 (273)
	Mixed	3.0 (7)	6.3 (42)	3.2 (13)	3.5 (13)
	Total	100 (237)	100 (670)	100 (409)	100 (371)

Table 5.7 shows the percentage of each flow pattern points in each flow pattern section for all four maps shown in Figures 5.12 (a – d). The two selected maps for further analysis are shown in grey: Liquid Reynolds Number vs. Gas Reynolds Number and Liquid Reynolds Number vs. Gas Weber Number.

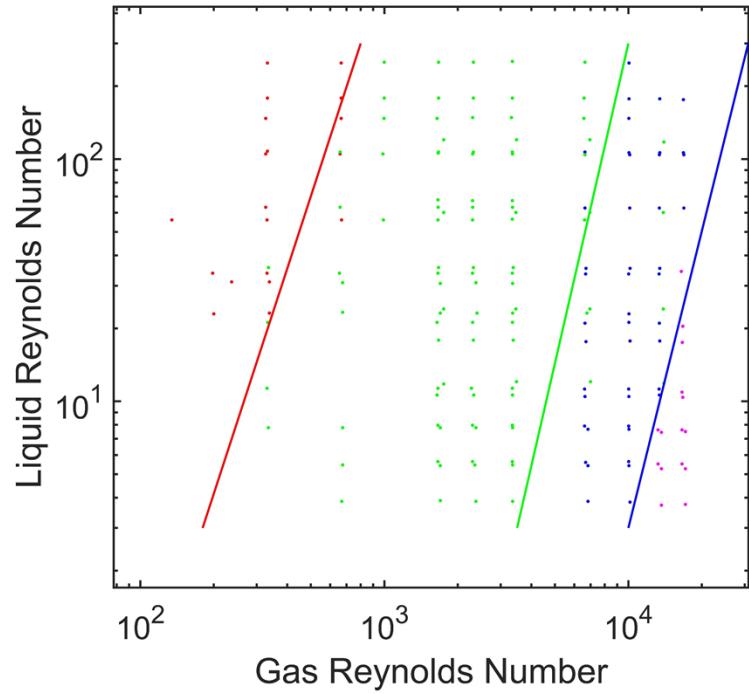
High / medium viscosity datasets consisted of 181 points. Unlike the low viscosity datasets, number of points for annular and bubbly flow patterns are limited for high / medium datasets. The overall breakdown of points by flow regime is shown below:

- 10.5 % Bubbly (19 Points)
- 56.4 % Slug (102 points)
- 24.9 % Churn (45 points)
- 8.3 % Annular (15 points)

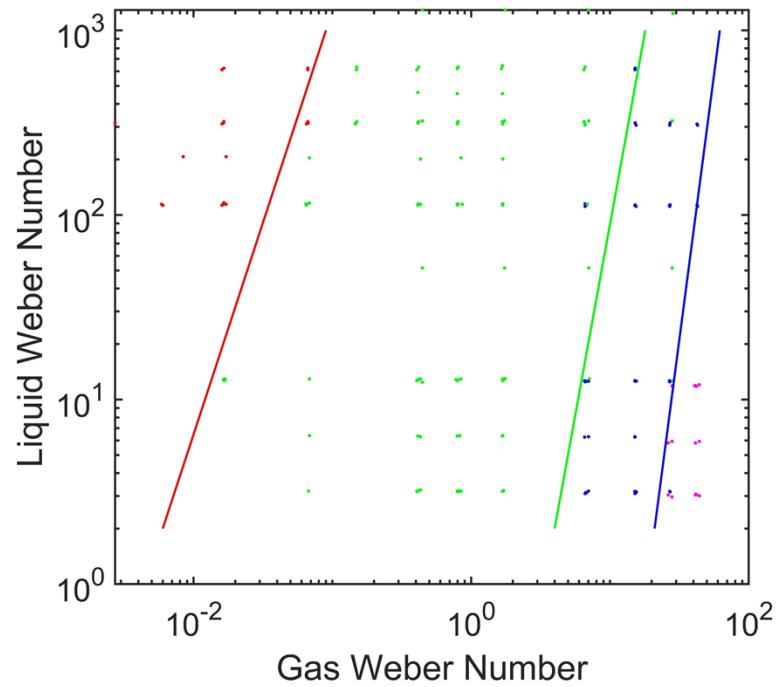
Figures 5.13 (a – d) demonstrates the effect of using different combination of gas/liquid Reynolds and Weber number on flow patterns for high / medium viscosity datasets in vertical pipelines. Although Figure 5.13 (b) presents much segregated section for each flow regime, however, it neglects the use of viscosity. Number of points are limited for viscous datasets compared to low viscosity datasets. Moreover, most of these datasets have a similar surface tension which may be the cause of a segregated section for each flow regime. Figures 5.13 (a, d) provide a slightly compromised flow pattern segregation for each section however they investigate the effect of viscosity on flow regime map. Hence, it is suggested to select Figures 5.13 (a, d) as the proposed flow regime for viscous datasets.

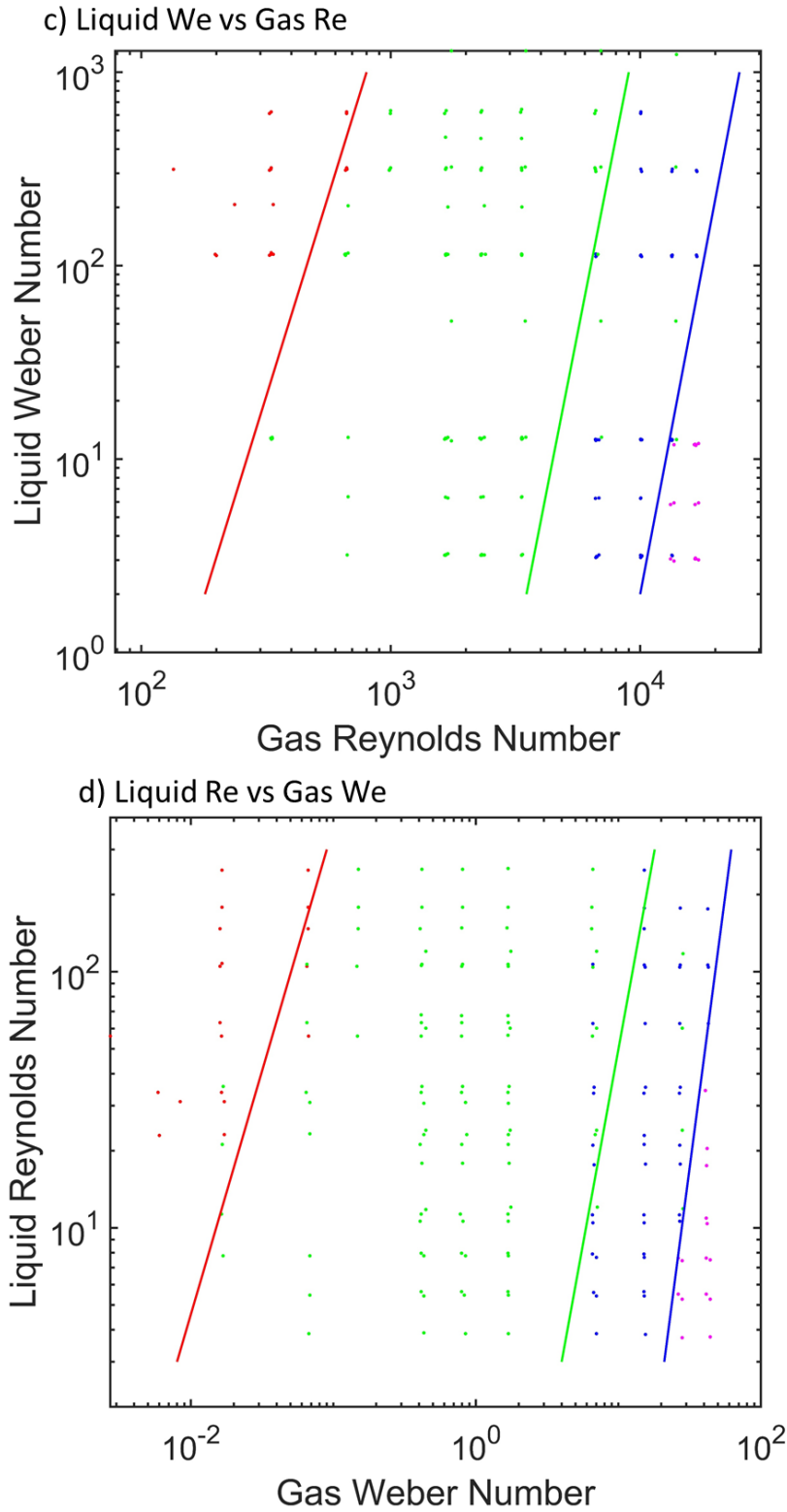


a) Liquid Re vs Gas Re



b) Liquid We vs Gas We





Figures 5.13 (a – d) – Effect of Weber and Reynolds number in different forms on flow patterns for high / medium viscosity datasets in vertical pipelines

Table 5.8 shows the percentage of each flow pattern points in each flow pattern section for all four maps shown in Figures 5.13 (a – d).

*Table 5.8 – Percentage of each flow pattern in each flow pattern section for all four maps shown in Figures 5.13 (a – d)*

Map	Experimental Flow Regime	% of each flow pattern in each flow pattern section			
		Bubbly	Slug	Churn	Annular
Liquid Reynolds Number vs. Gas Reynolds Number	Bubbly	88.9 (16)	3.1 (3)	0 (0)	0 (0)
	Slug	11.1 (2)	94.8 (92)	15.4 (8)	0 (0)
	Churn	0 (0)	2.1 (2)	82.7 (43)	0 (0)
	Annular	0 (0)	0 (0)	1.9 (1)	100 (14)
	Total	100 (18)	100 (97)	100 (52)	100 (14)
Liquid Weber Number vs. Gas Weber Number	Bubbly	100 (16)	2.9 (3)	0 (0)	0 (0)
	Slug	0 (0)	92.4 (97)	11.9 (5)	0 (0)
	Churn	0 (0)	4.8 (5)	85.7 (36)	22.2 (4)
	Annular	0 (0)	0 (0)	2.4 (1)	77.8 (14)
	Total	100 (16)	100 (105)	100 (42)	100 (18)
Liquid Weber Number vs. Gas Reynolds Number	Bubbly	100 (16)	3.1 (3)	0 (0)	0 (0)
	Slug	0 (0)	96.9 (95)	13.0 (6)	4.5 (1)
	Churn	0 (0)	0 (0)	87.0 (40)	23.8 (5)
	Annular	0 (0)	0 (0)	0 (0)	71.4 (15)
	Total	100 (16)	100 (98)	100 (46)	100 (21)
Liquid Reynolds Number vs. Gas Weber Number	Bubbly	88.9 (16)	2.9 (3)	0 (0)	0 (0)
	Slug	11.1 (2)	90.5 (95)	11.6 (5)	0 (0)
	Churn	0 (0)	6.7 (7)	88.4 (38)	0 (0)
	Annular	0 (0)	0 (0)	0 (0)	100 (15)
	Total	100 (18)	100 (105)	100 (43)	100 (15)

The performance of the proposed vertical flow regime maps at low viscosity constructed from literature datasets in Table 5.5 was evaluated. More datasets from literature were used for this analysis purpose, as shown in Table 5.9.

Table 5.9 – Additional literature datasets to test the performance of vertical flow regime maps using literature datasets of low viscosity from Table 5.5

Author(s)	Diameter (mm)	Viscosity (cP)	Fluids	Number of points
Ansari and Azadi (2016)	40	1	Air – Water	175
Mi <i>et al.</i> (2001)	50.8	1	Air – Water	38
Kaji <i>et al.</i> (2009)	51.2	1	Air – Water	52
Shanmugam (1994)	26.1	1	Air – Water	56

Figure 5.14 shows the performance of the proposed vertical flow regime map (Liquid Re vs Gas Re) constructed from datasets at low viscosity. It can be observed that the proposed flow regime map is performing reasonably well for each additional dataset.

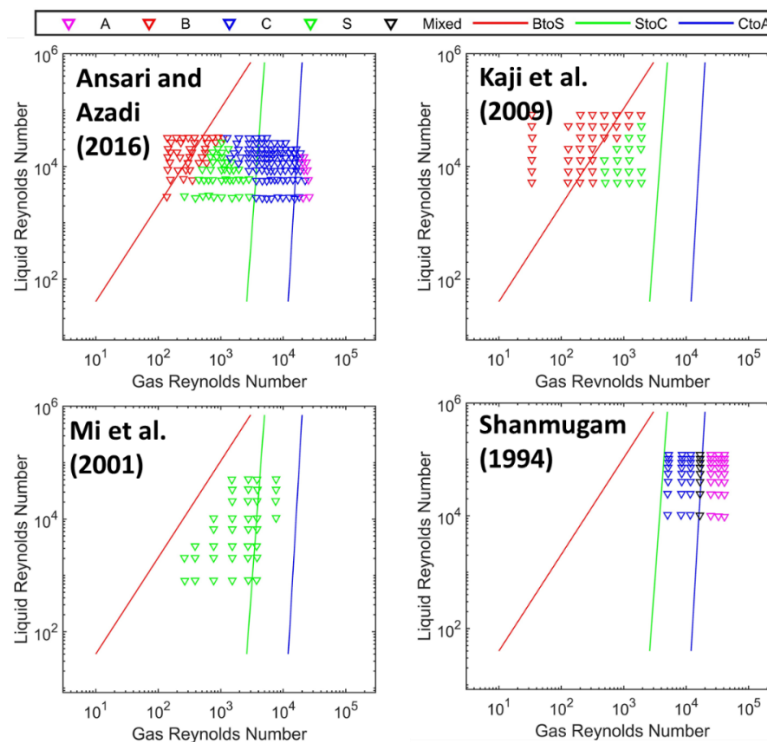


Figure 5.14 – Evaluating the performance of the proposed vertical flow regime map at low viscosity (Liquid Re vs Gas Re)

Figure 5.15 shows the performance of the proposed vertical flow regime map (Liquid  $Re$  vs Gas  $We$ ) constructed from datasets at low viscosity. Again, it can be observed that the proposed flow regime map is performing reasonably well.

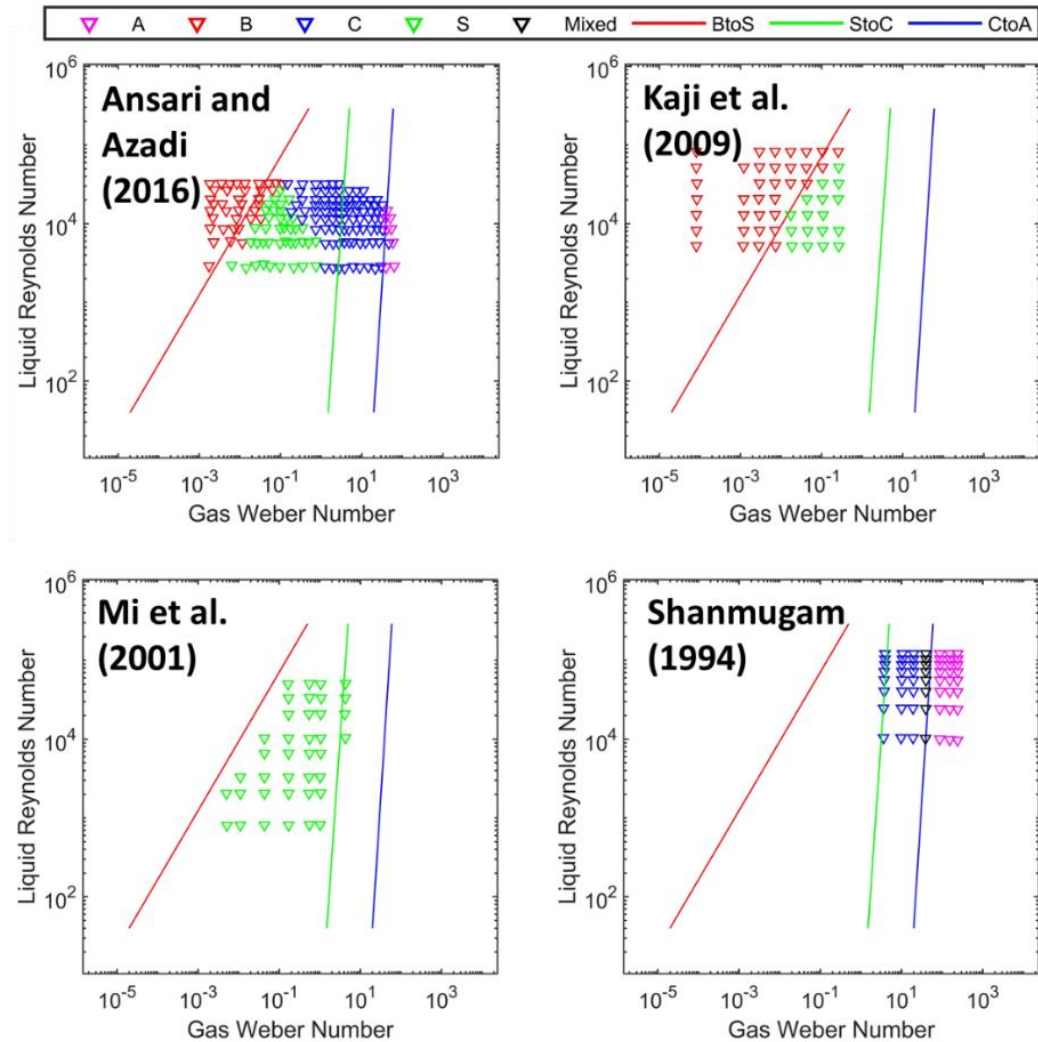


Figure 5.15 – Evaluating the performance of the proposed vertical flow regime map at low viscosity (Liquid  $Re$  vs Gas  $We$ )

Table 5.10 shows the percentage of points correctly predicted by both proposed vertical flow regime maps (Liquid Re vs Gas Re and Liquid Re vs Gas We) constructed from datasets at low viscosity. Liquid Re Vs Gas We map performs best for Mi *et al.* (2001) and Kaji *et al.* (2009) while Liquid Re Vs Gas Re map performs best for Shanmugam (1994) and Ansari and Azadi (2016). Overall, both maps perform reasonably well with an absolute difference of only 0.6 % between them.

*Table 5.10 – Evaluating the performance of both proposed vertical flow regime maps at low viscosity (Liquid Re vs Gas Re and Liquid Re vs Gas We)*

<b>Authors</b>	<b>Liquid Re Vs Gas Re Map</b>		<b>Liquid Re Vs Gas We Map</b>	
	Points correctly predicted	% correctly predicted	Points correctly predicted	% correctly predicted
Ansari and Azadi (2016)	126 / 175	72.0	120 / 175	68.6
Mi <i>et al.</i> (2001)	29 / 38	76.3	34 / 38	89.5
Kaji <i>et al.</i> (2009)	43 / 52	83.0	48 / 52	92.3
Shanmugam (1994)	All (ignoring transition points)	100 % (ignoring transition points)	42 / 48 (ignoring transition points)	87.5
Overall	246/313	78.6 %	244/313	78.0

The same analysis was carried out on proposed vertical flow regime maps at high viscosity constructed from literature datasets in Table 5.5. Due to the lack of high viscosity datasets in literature, datasets of the present study were utilised for evaluating the performance of the flow regime maps. In Figure 5.16, the datasets of all viscosities in present study were plotted on both proposed flow regime maps at high viscosity (Liquid Re vs Gas Re on left and Liquid Re vs Gas We on right). The performance for each flow regime map is further discussed in Table 5.11.

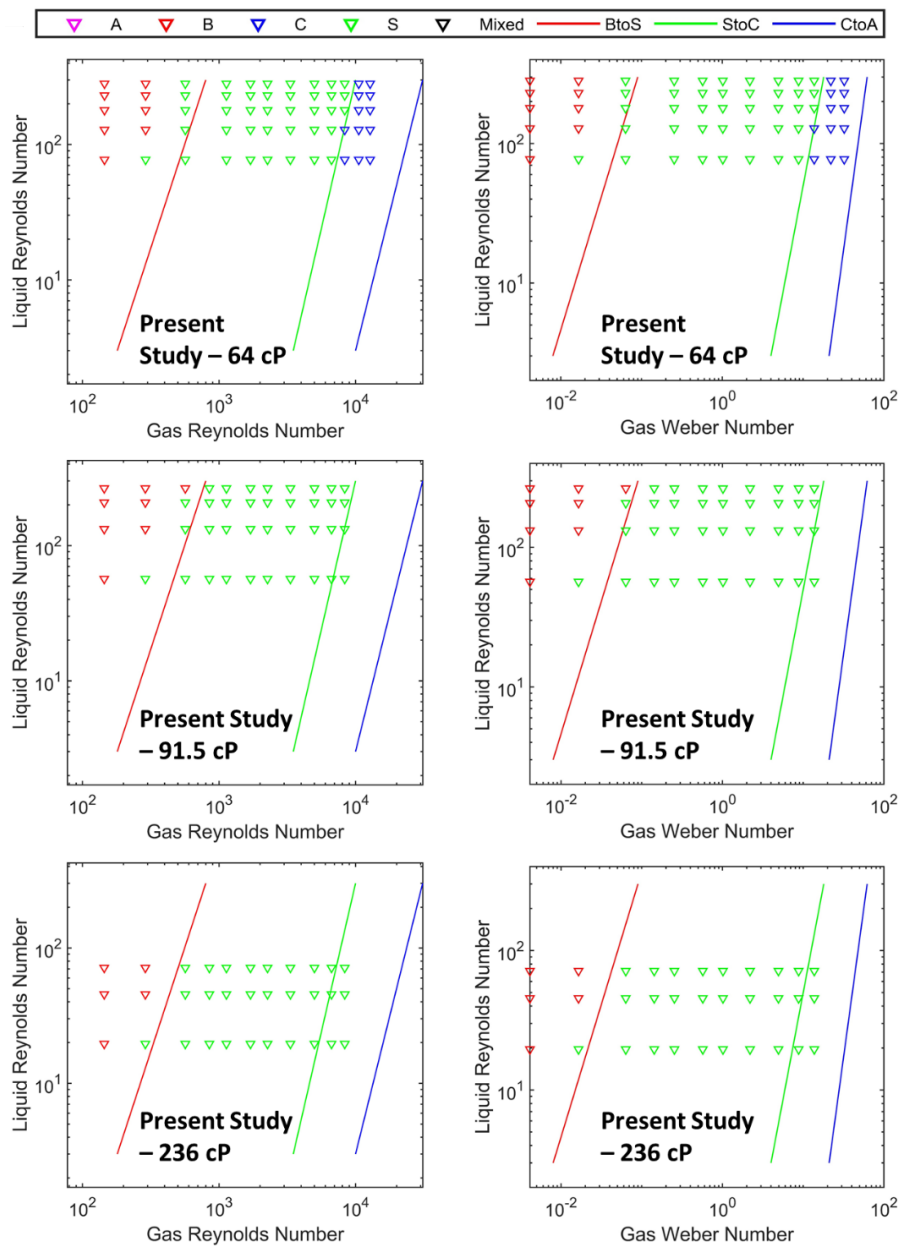


Figure 5.16 – Evaluating the performance of the proposed vertical flow regime maps at high viscosity (Liquid Re vs Gas Re and Liquid Re vs Gas We)

Table 5.11 demonstrates that both proposed vertical flow regime maps at high viscosity are performing well. The Liquid Re Vs Gas We map performs marginally better, with overall correct prediction of 91.2 % compared to 88.3 %.

*Table 5.11 – Evaluating the performance of both proposed vertical flow regime maps at high viscosity (Liquid Re vs Gas Re and Liquid Re vs Gas We)*

<b>Viscosity</b>	<b>Liquid Re Vs Gas Re Map</b>		<b>Liquid Re Vs Gas We Map</b>	
	Points correctly predicted	% correctly predicted	Points correctly predicted	% correctly predicted
64 cP	55/60	91.7	56/60	93.3
91.5 cP	39/44	88.6	41/44	93.2
236 cP	27/33	81.2	28/33	84.9
<b>Overall</b>	<b>121/137</b>	<b>88.3</b>	<b>125/137</b>	<b>91.2</b>

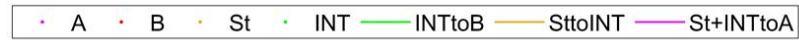
### 5.3.3. Investigating viscosity effect for experimental studies in literature for horizontal flow patterns

Table 5.6 represents the horizontal datasets from literature and were split into two different sets: low viscosity and medium plus high viscosity. Again, cut – off maximum for low viscosity is 50 cP. The total number of points for low viscosity datasets was 720. They were organised into four flow regimes: bubbly, intermittent, stratified and annular. The overall breakdown of points by flow regime is shown below:

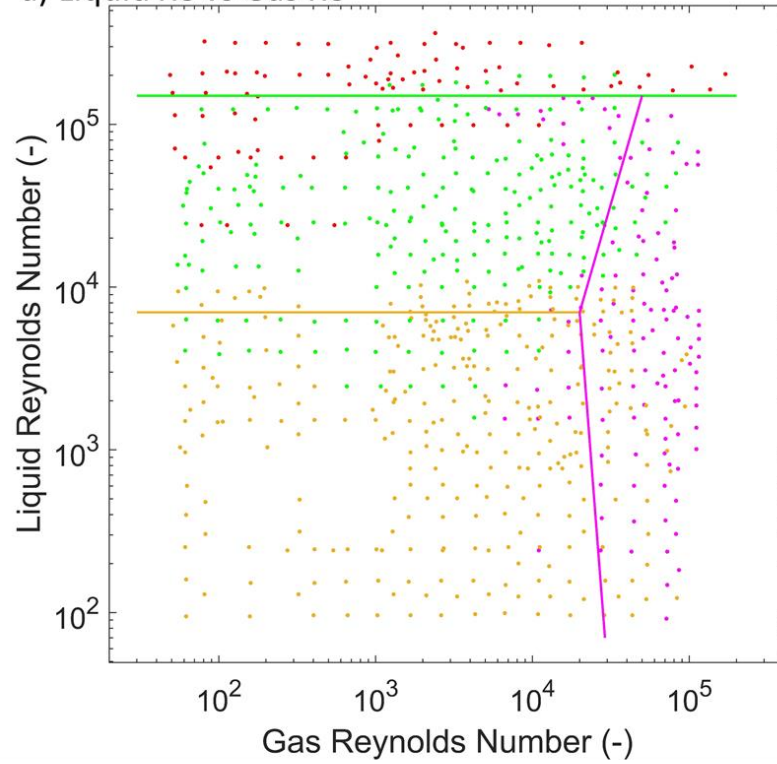
- 11.8 % Bubbly (85 points)
- 32.1 % Intermittent (231 points)
- 40.1 % Stratified (289 points)
- 16.0 Annular (115 points)

Figures 5.17 (a – d) shows the effect of different combinations of gas/liquid Reynolds and Weber number for horizontal pipelines at low viscosity. The difference in the performance of each flow regime map varies slightly. However, the interest lies

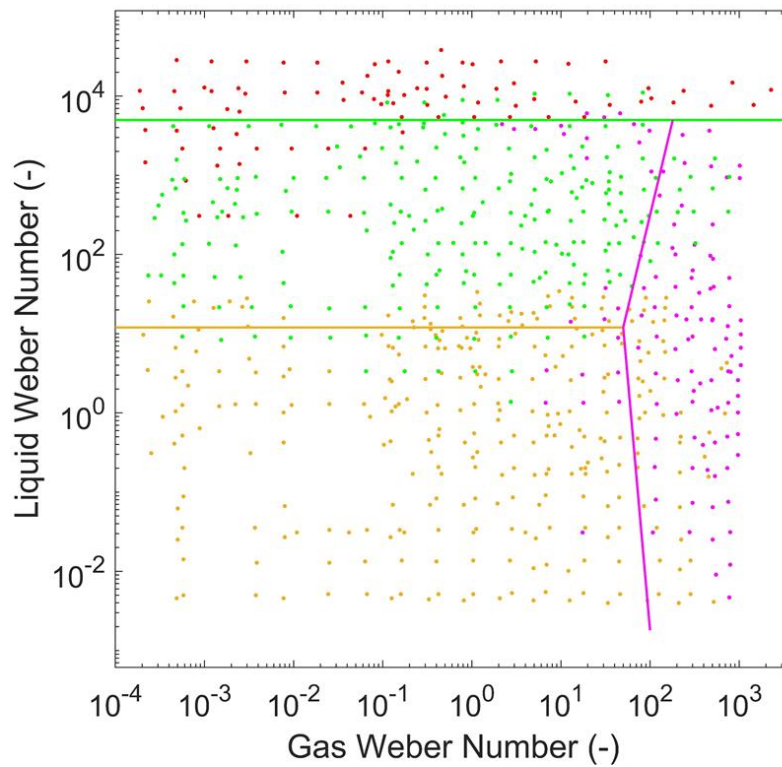
within the effect of viscosity. Therefore, Figures 5.17 (a and d) were utilised for the analysis as done with vertical inclination flow regime maps.



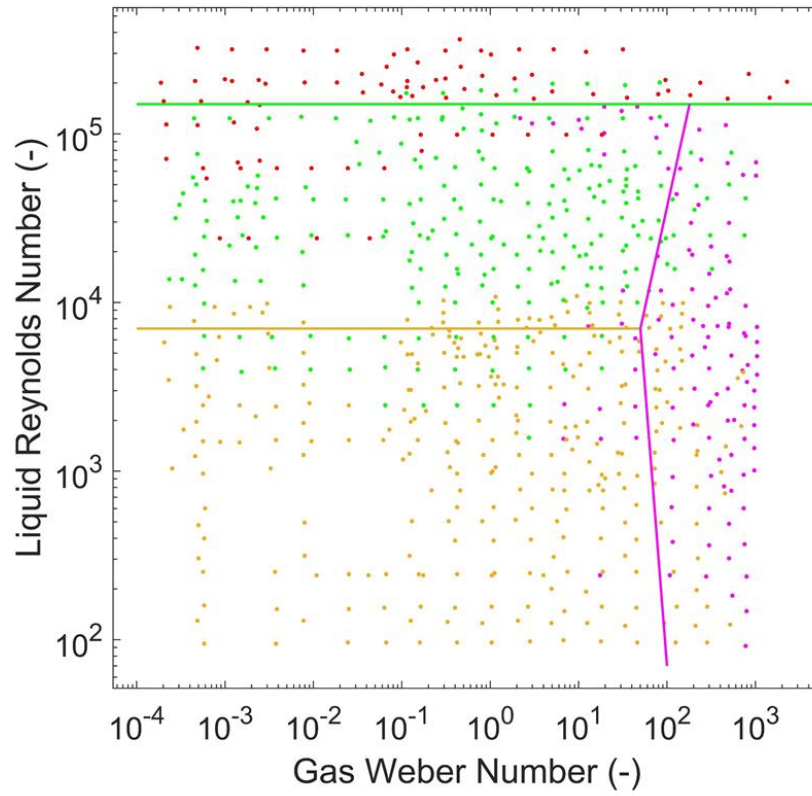
a) Liquid Re vs Gas Re



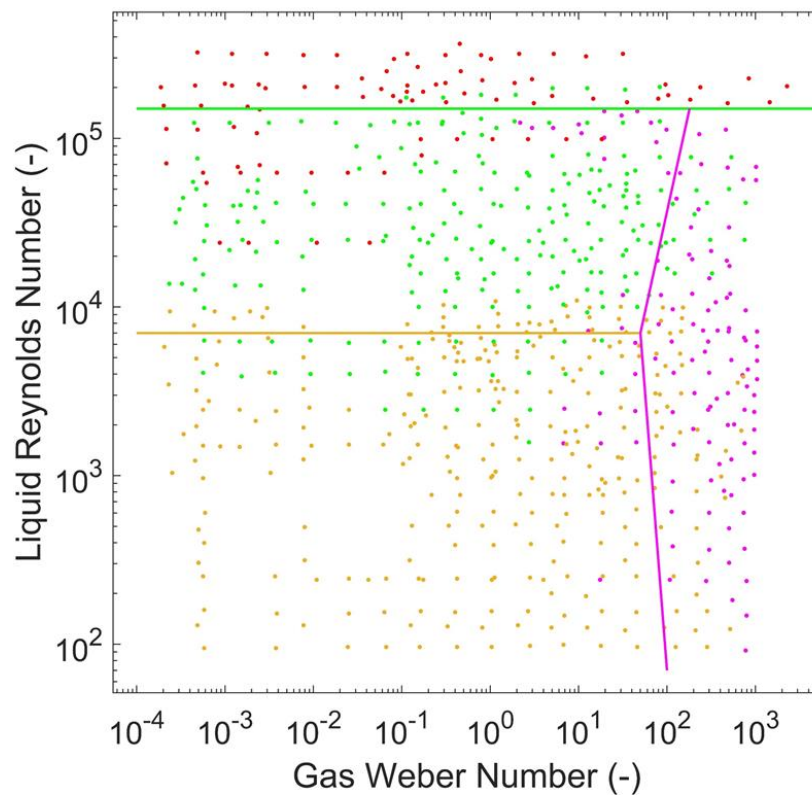
b) Liquid We vs Gas We



c) Liquid We vs Gas Re



d) Liquid Re vs Gas We



Figures 5.17 (a – d) – Effect of Weber and Reynolds number in different forms on flow patterns for low viscosity datasets in horizontal pipelines

Table 5.12 shows the percentage of each flow pattern points in each flow pattern section for all four maps shown in Figures 5.17 (a – d).

*Table 5.12 – Percentage of each flow pattern in each flow pattern section for all four maps shown in Figures 5.17 (a – d)*

Map	Experimental Flow Regime	% of each flow pattern in each flow pattern section			
		Annular	Bubbly	Intermittent	Stratified
Liquid Reynolds Number vs. Gas Reynolds Number	Annular	58.2 (89)	0 (0)	6.8 (17)	3.6 (9)
	Bubbly	0 (0)	88.1 (59)	10.3 (26)	0 (0)
	Intermittent	9.8 (15)	11.9 (8)	70.6 (178)	12.1 (30)
	Stratified	32.0 (49)	0 (0)	12.3 (31)	84.3 (209)
	Total	100 (153)	100 (67)	100 (252)	100 (248)
Liquid Weber Number vs. Gas Weber Number	Annular	60.1 (89)	3.9 (3)	5.8 (15)	3.4 (8)
	Bubbly	0 (0)	84.6 (66)	7.3 (19)	0 (0)
	Intermittent	9.5 (14)	11.5 (9)	73.1 (190)	7.7 (18)
	Stratified	30.4 (45)	0 (0)	13.9 (36)	88.9 (208)
	Total	100 (148)	100 (78)	100 (260)	100 (234)
Liquid Weber Number vs. Gas Reynolds Number	Annular	58.6 (89)	3.9 (3)	5.8 (15)	3.5 (8)
	Bubbly	0 (0)	84.6 (66)	7.3 (19)	0 (0)
	Intermittent	9.2 (14)	11.5 (9)	73.4 (190)	7.8 (18)
	Stratified	32.2 (49)	0 (0)	13.5 (35)	88.7 (205)
	Total	100 (152)	100 (78)	100 (259)	100 (231)
Liquid Reynolds Number vs. Gas Weber Number	Annular	58.6 (89)	0 (0)	6.8 (17)	3.6 (9)
	Bubbly	0 (0)	88.1 (59)	10.4 (26)	0 (0)
	Intermittent	11.2 (17)	11.9 (8)	70.1 (176)	12.0 (30)
	Stratified	30.3 (46)	0 (0)	12.8 (32)	84.4 (211)
	Total	100 (152)	100 (67)	100 (251)	100 (250)

In total, there are 212 points for high viscosity datasets in horizontal pipelines that were taken from literature. The overall breakdown of points by flow regime is shown below:

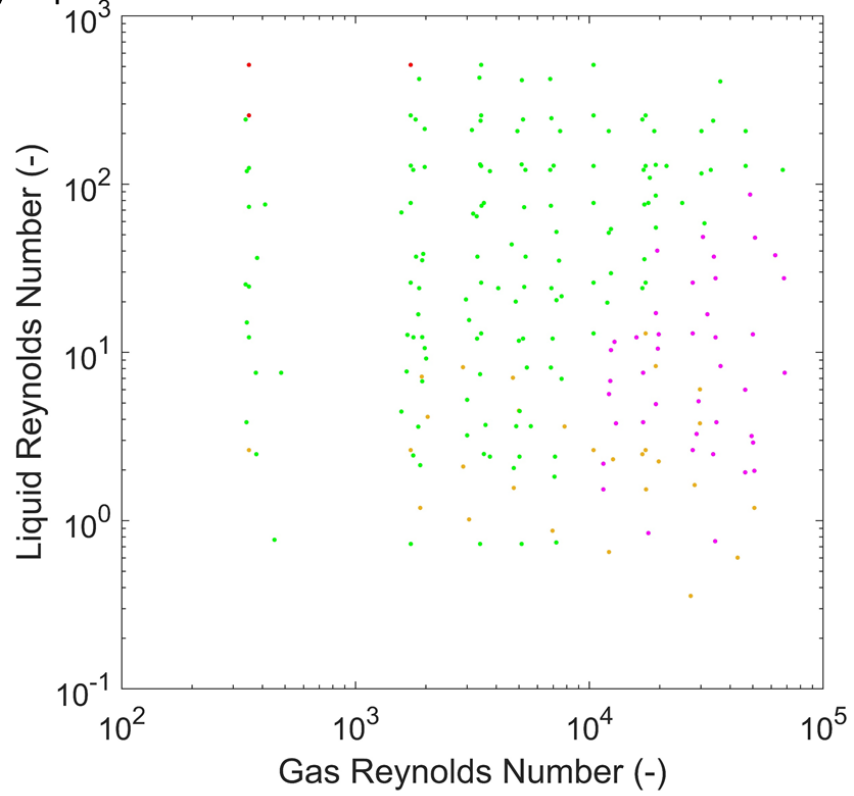
- 1.4 % Bubbly (3 Points)
- 66.0 % Intermittent (140 points)
- 13.2 % Stratified (28 points)
- 19.3 % Annular (41 points)

Scarcity of points in high viscosity datasets for horizontal pipelines must be taken into consideration because, for selected datasets, there are a limited number of points for other flow regimes than intermittent flow. It is envisaged that this will affect the accuracy of the proposed flow regimes.

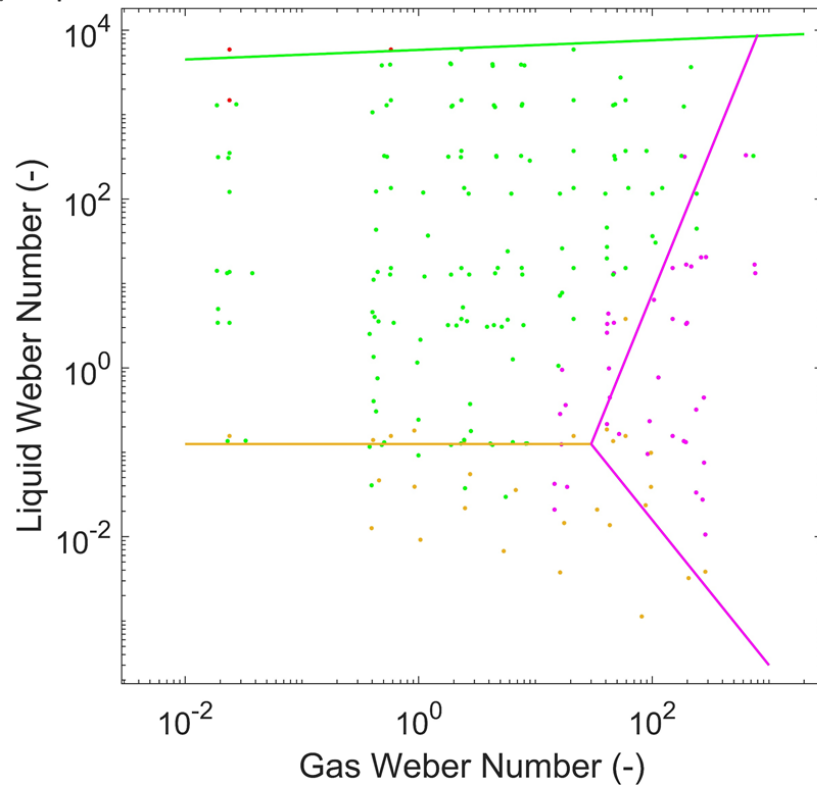
Figures 5.18 (a – e) shows the effect of different combinations of gas/liquid Reynolds and Weber number for horizontal pipelines at high viscosity. As can be observed, use of liquid and gas Reynolds number in Figure 5.18 a does not work as the intermittent and stratified points completely overlap. Same is observed for liquid Reynolds number and gas Weber number coordinates (Figure 5.18 d). Figures b and c differentiates between intermittent and stratified datasets. However, these figures ignore the effect of liquid viscosity. Therefore, ratio of Weber number to Reynolds number to a power for each axis was tested. Upon trial and error, it was found that ratio of Weber number to the Reynolds number raised to the power of 0.2 provided a slightly better flow regime map, as shown in Figure 5.18 e. However, the differences between 5.18 c, d and e were insignificant.



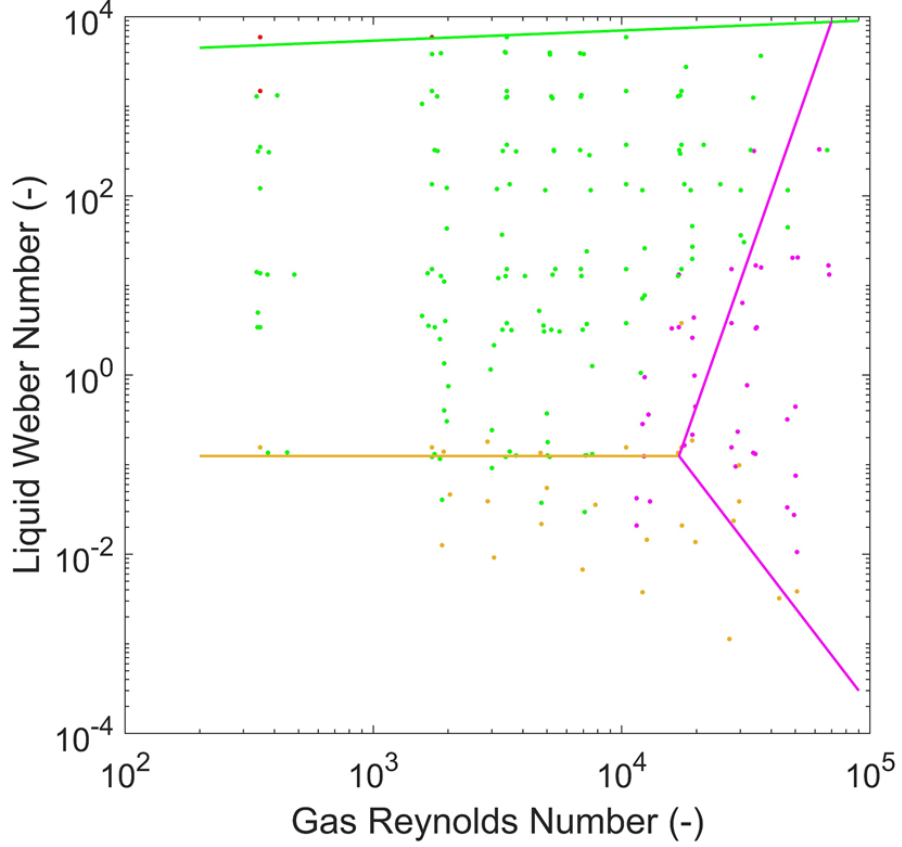
a) Liquid Re vs Gas Re



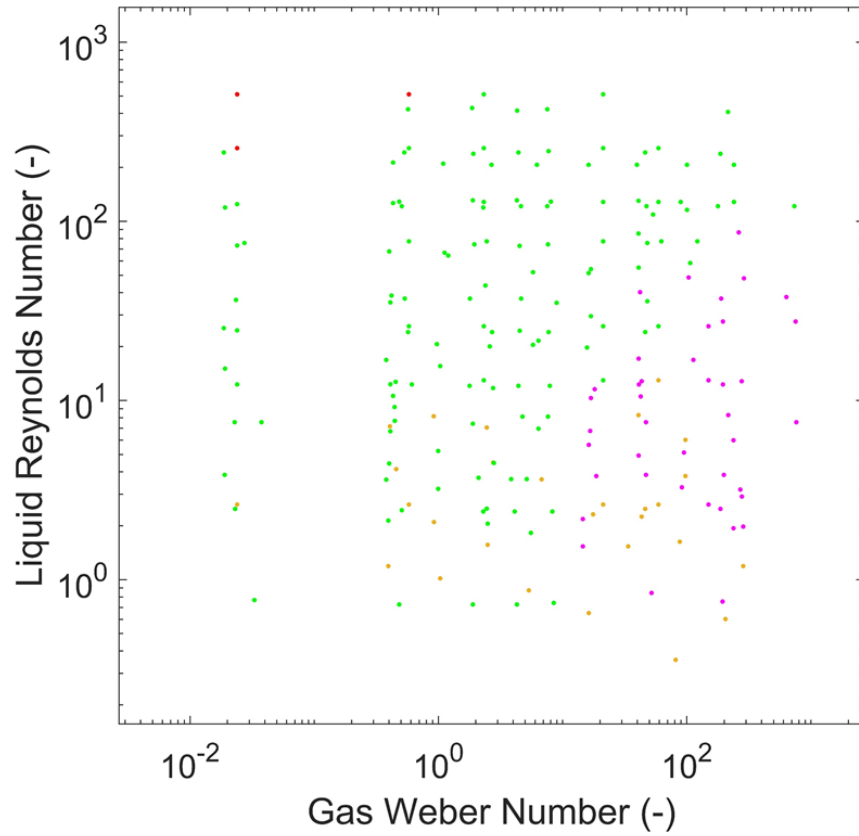
b) Liquid We vs Gas We



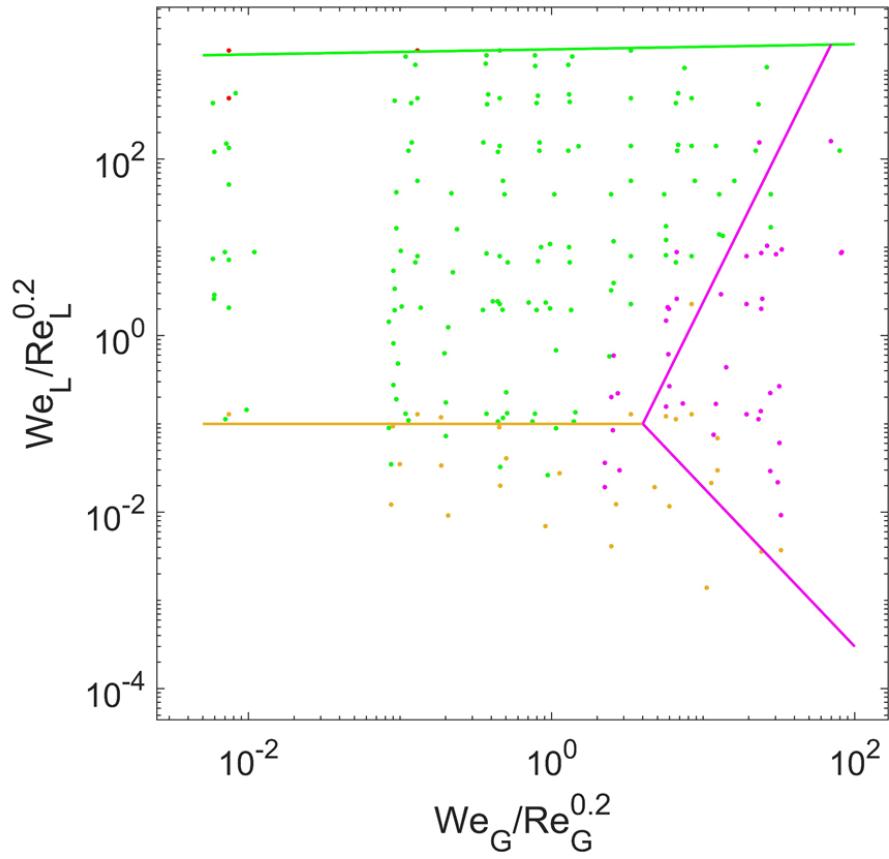
c) Liquid We vs Gas Re



d) Liquid Re vs Gas We



e) Reynolds Number – Weber Number Ratio



Figures 5.18 (a – e) – Effect of Weber and Reynolds number in different forms on flow patterns for high viscosity datasets in horizontal pipelines

Table 5.13 shows the percentage of each flow pattern points in each flow pattern section for all three maps shown in Figures 5.18 (b, c and e).

*Table 5.13 – Percentage of each flow pattern in each flow pattern section for all three maps shown in Figures 5.18 (b, c and e)*

Map	Experimental Flow Regime	% of each flow pattern in each flow pattern section			
		Annular	Bubbly	Intermittent	Stratified
Liquid Weber Number vs. Gas Weber Number	Annular	72.2 (26)	0 (0)	7.4 (11)	15.4 (4)
	Bubbly	0 (0)	100 (2)	0.7 (1)	0 (0)
	Intermittent	8.3 (3)	0 (0)	87.2 (129)	30.8 (8)
	Stratified	19.4 (7)	0 (0)	4.7 (7)	53.9 (14)
	Total	100 (36)	100 (2)	100 (148)	100 (26)
Liquid Weber Number vs. Gas Reynolds Number	Annular	75.8 (25)	0 (0)	8.0 (12)	15.4 (4)
	Bubbly	0 (0)	100 (2)	0.7 (1)	0 (0)
	Intermittent	9.1 (3)	0 (0)	85.4 (129)	30.8 (8)
	Stratified	15.2 (5)	0 (0)	6.0 (9)	53.9 (14)
	Total	100 (33)	100 (2)	100 (151)	100 (26)
$We_L Re_L^{-0.2}$ vs $We_G Re_G^{-0.2}$	Annular	73.0 (27)	0 (0)	6.8 (10)	15.4 (4)
	Bubbly	0 (0)	100 (2)	0.7 (1)	0 (0)
	Intermittent	8.1 (3)	0 (0)	89.1 (131)	23.1 (6)
	Stratified	18.9 (7)	0 (0)	3.4 (5)	61.5 (16)
	Total	100 (37)	100 (2)	100 (147)	100 (26)

The performance of both proposed horizontal flow regime maps at low viscosity constructed for datasets in Table 5.6 is evaluated. The additional datasets that were used to analyse the performance are shown in Table 5.14.

*Table 5.14 – Additional datasets to test the performance of horizontal flow regime maps using literature datasets of low viscosity*

<b>Author(s)</b>	<b>Diameter (mm)</b>	<b>Viscosity (cP)</b>	<b>Fluids</b>	<b>Number of points</b>
Morshed <i>et al.</i> (2020)	73.66	1	Air – Water	90
Lamari (2001)	25.4	1	Air – Water	90
Xia and Chai (2012)	59	1	Air – Water	131

Table 5.15 evaluates the performance of both proposed horizontal flow regime maps at low viscosity (Liquid Re vs Gas Re and Liquid Re vs Gas We).

*Table 5.15 – Evaluating the performance of both proposed horizontal flow regime maps at low viscosity (Liquid Re vs Gas Re and Liquid Re vs Gas We)*

<b>Authors</b>	<b>Liquid Re Vs Gas Re Map</b>		<b>Liquid Re Vs Gas We Map</b>	
	Points correctly predicted	% correctly predicted	Points correctly predicted	% correctly predicted
Morshed <i>et al.</i> (2020)	71/90	78.9	71/90	78.9
Lamari (2001)	74/90	82.2	72/90	80.0
Xia and Chai (2012)	117/131	89.3	120/131	91.6

Figure 5.19 shows the performance of both proposed horizontal flow regime maps at low viscosity (left – Liquid Re vs Gas Re and right – Liquid Re vs Gas We).

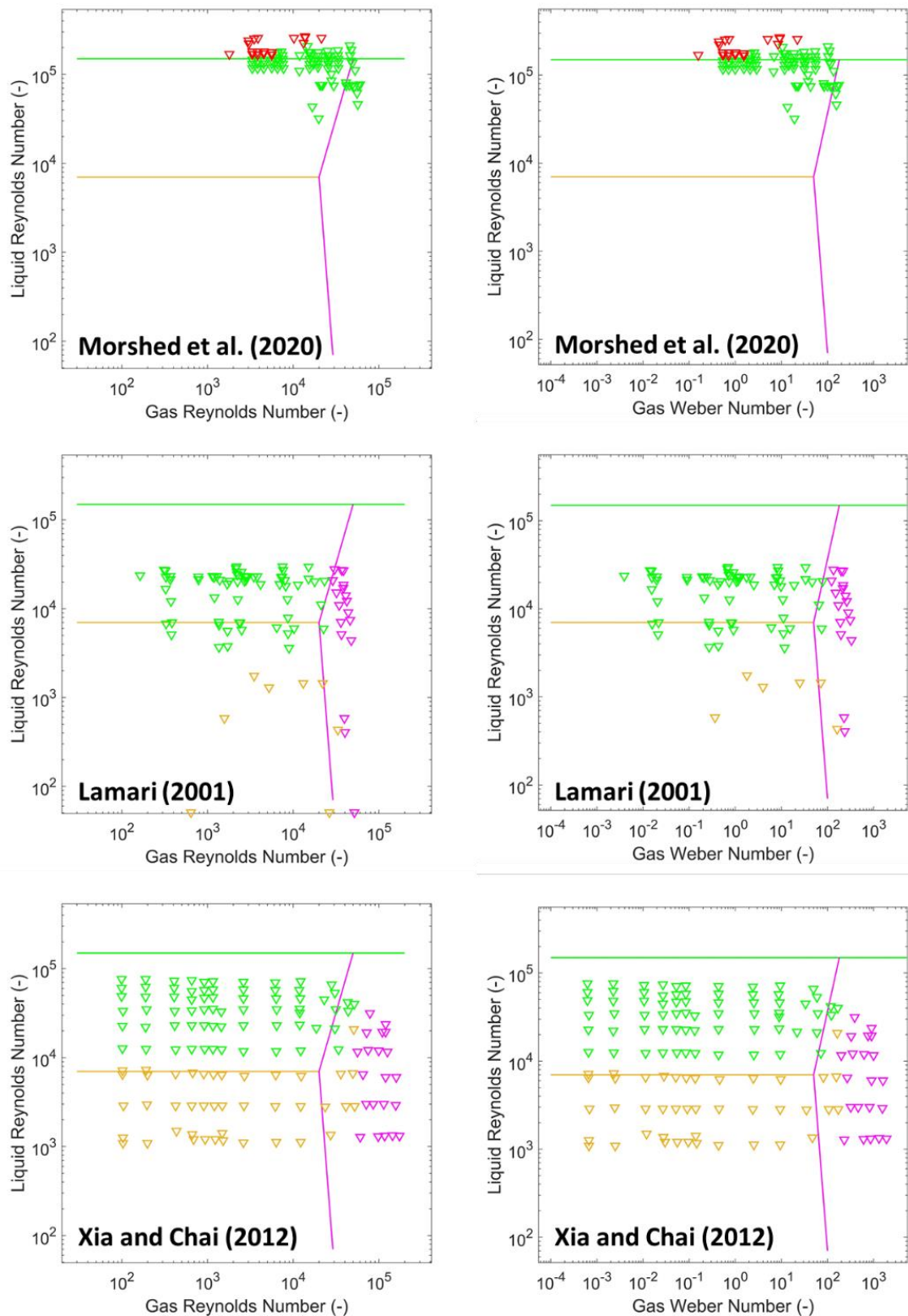


Figure 5.19 – Evaluating the performance of the proposed horizontal flow regime maps at low viscosity (Liquid Re vs Gas Re and Liquid Re vs Gas We)

It was evaluated that, for high viscosity, three flow regime maps for horizontal pipelines were proposed:  $We_L$  vs  $We_G$ ,  $We_L$  vs  $Re_G$  and  $We_L/Re_L^{0.2}$  vs  $We_G/Re_G^{0.2}$ . For performance purposes, only the work from present study were utilised due to lack of high viscosity datasets in literature. Figure 5.20 shows the performance of one of three proposed horizontal flow regime maps at high viscosity ( $We_L/Re_L^{0.2}$  vs  $We_G/Re_G^{0.2}$ ). The points in red are bubbly while green points are slug flow.

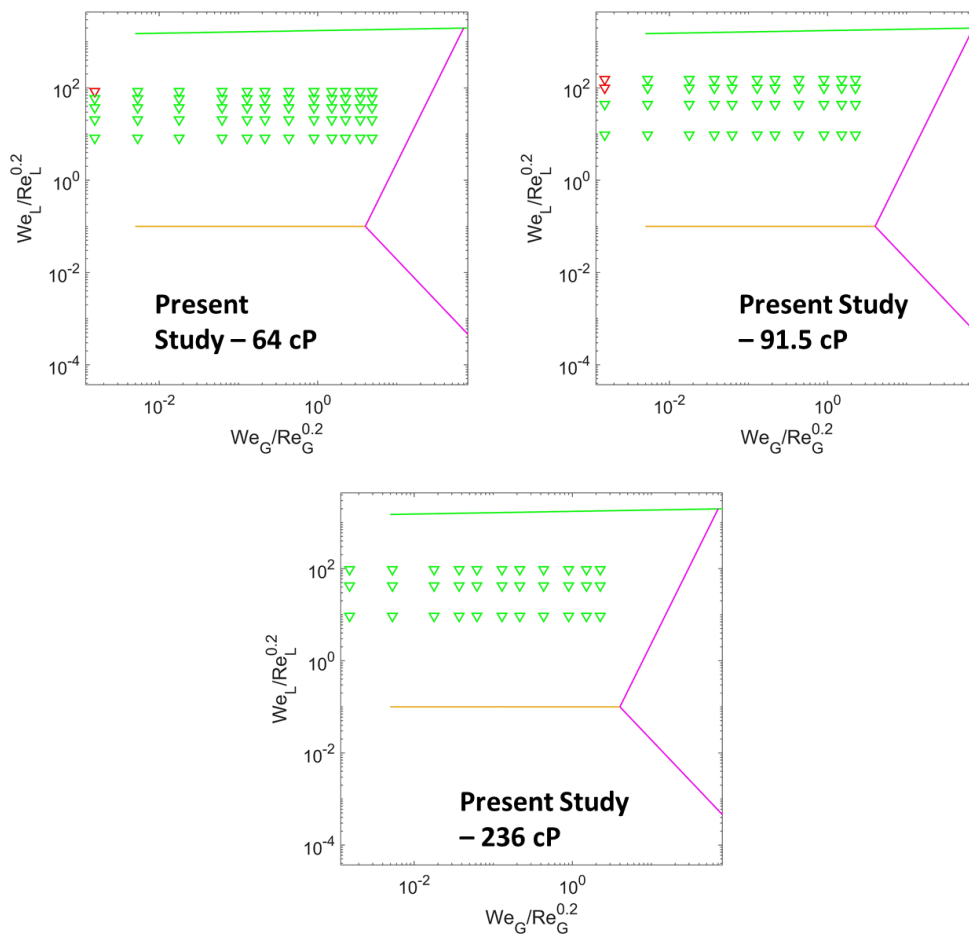


Figure 5.20 – Evaluating the performance of one of the proposed horizontal flow regime map at high viscosity ( $We/Re^{0.2}$  vs  $We/Re^{0.2}$ )

#### 5.4. Evaluating the performance of proposed coordinates for vertical inclination

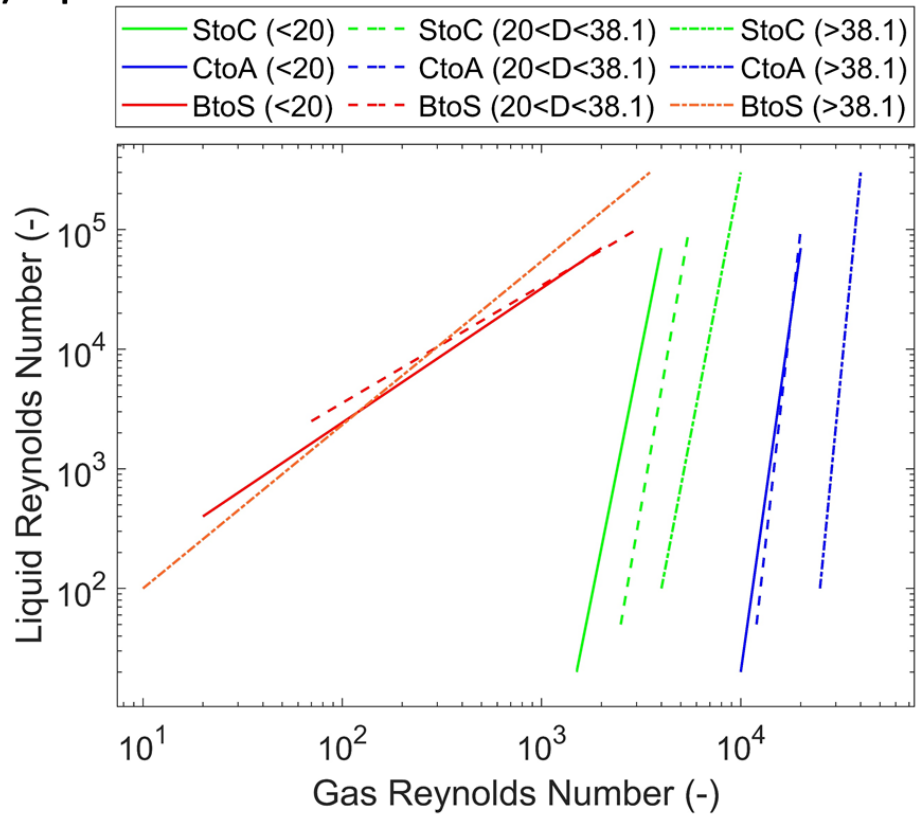
In Section 5.3, low viscosity and high viscosity flow regime maps were constructed using datasets from literature. This was carried out for horizontal and vertical inclination. However, for horizontal inclination, number of points were limited for both low viscosity and high viscosity. Moreover, for horizontal inclination, individual datasets don't usually test all the flow regimes possible (especially for high viscosity datasets). Therefore, the performance of proposed coordinates is critically evaluated for vertical inclination only.

Firstly, the two proposed low viscosity flow regime maps for vertical inclination were discussed. The range of viscosity investigated for low viscosity flow regime maps was 1 – 17 cP. Due to the tight range of viscosity, low viscosity datasets in Table 5.5 were sorted by diameters into three different groups: less than 20 mm, between 20 mm and 38.1 mm and more than 38.1 mm. The division described here not only allows the effect of diameter to be investigated but it also evaluates the performance of different model coordinates as well.

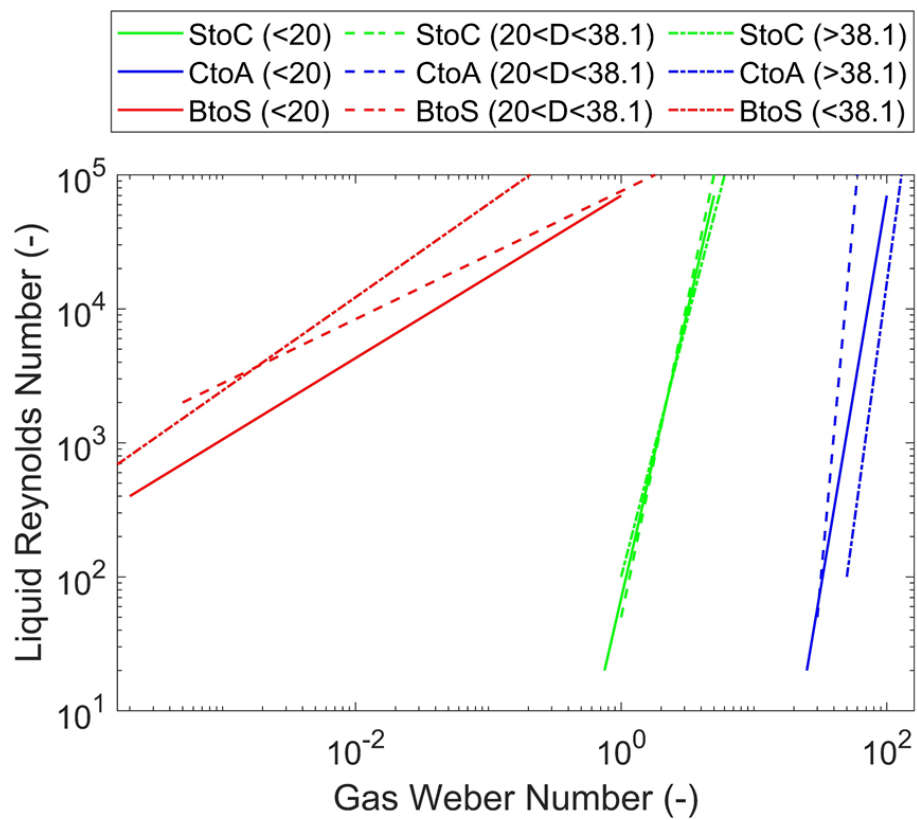
Figure 5.21 a shows the low viscosity flow regime map using the liquid Reynolds number and gas Reynolds number coordinates while Figure 5.21 b shows the low viscosity flow regime map using the liquid Reynolds number and gas Weber number coordinates. The key observation is that the use of liquid Reynolds number and gas Reynolds number coordinates predicts transition lines occupying tighter region for bubble to slug transition. However, transition lines for slug to churn and churn to annular occupy wider regions for the liquid Reynolds number and gas Reynolds number coordinates.

In comparison, the opposite is observed for the map using the liquid Reynolds Number and gas Weber number coordinates. Transition lines for bubble to slug transition occupy a much wider region while transition lines for slug to churn and churn to annular transitions occupy much tighter regions.

**a) Liquid Re vs Gas Re**

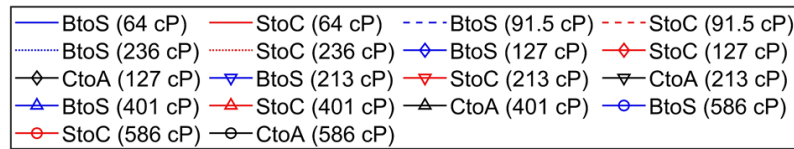


**b) Liquid Re vs Gas We**

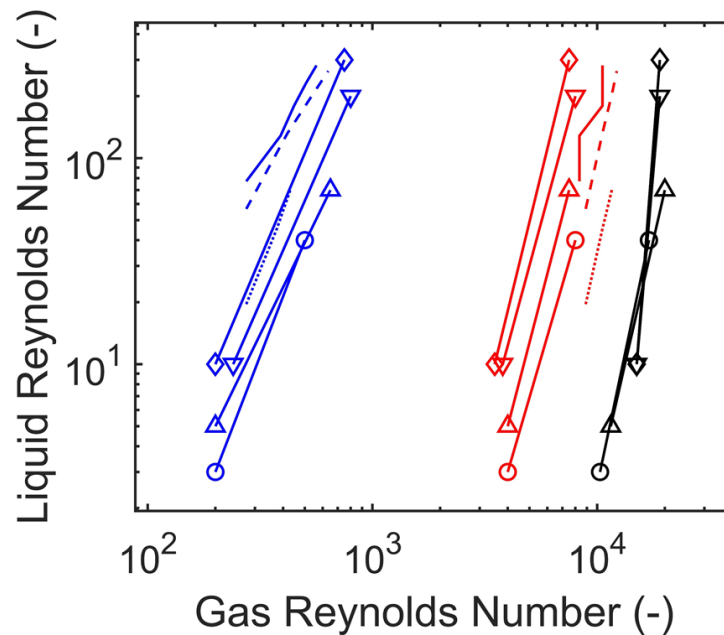


Figures 5.21 (a – b) – Evaluating the effect of using different coordinates on the flow regime transitions for different groups of datasets (low viscosity flow regime maps)

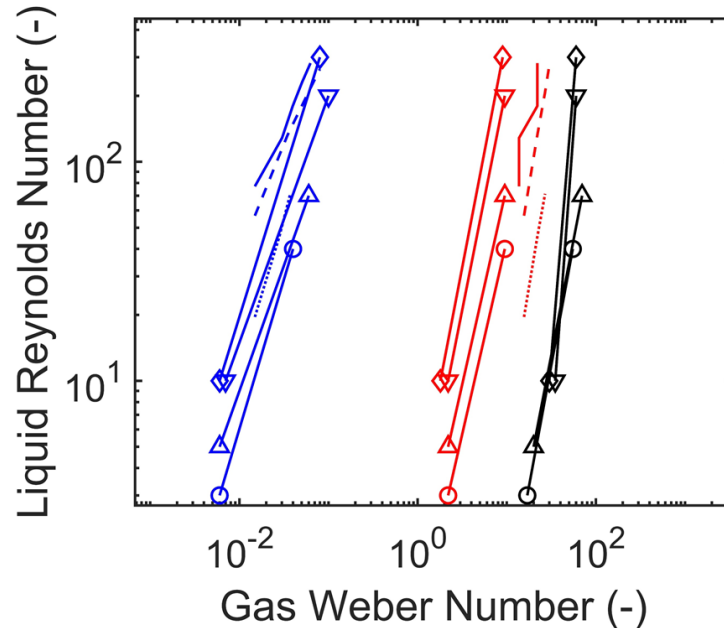
Similarly, the two proposed maps for high viscosity datasets were similarly analysed. The transition boundaries for three experimental campaigns in this study along with four different viscosity datasets from Alruhaimani (2015) were plotted in Figure 5.22.



a) Liquid Re vs Gas Re



b) Liquid Re vs Gas We



Figures 5.22 (a – b) – Evaluating the effect of using different coordinates on the flow regime transitions for different datasets (high viscosity flow regime maps)

Unlike the low viscosity datasets, the difference between Figures 5.22 a and b are insignificant. Even though the transition lines occupy wider region for a given transition, there is some overlap in the transition boundaries between the datasets of the present study and that of Alruhaimani (2015).

## 5.5. Conclusion

In this chapter, the effect of physical properties and inclination angle from horizontal (focus on viscosity) on flow regime transitions were investigated. Firstly, the three experimental campaigns of the present study were investigated to establish the effect of viscosity on flow regime transitions for five different inclination angles. For this part, only Reynolds number was used. After that, literature was reviewed in order to investigate the effect of physical parameters on flow regime transitions for vertical and horizontal pipes. For each pipe orientation, two maps were produced, one for low viscosity and one for high viscosity. Different forms of Weber and Reynolds number combinations were tested for this part.

The key findings are listed below:

- The use of conventional coordinates such as superficial velocities do not capture the effect of physical properties on the flow regime transition as shown in Section 5.2.
- Reynolds number for the present study yield promising results in terms of capturing the effect of viscosity on the flow regime transitions compared to the use of conventional coordinates. Flow regime maps for each inclination were produced, as shown in Figure 5.9.
- It must be emphasised that use of Weber numbers on both axes (liquid  $We$  vs gas  $We$ ) would simplify down to  $\rho_L U_{SL}^2$  vs  $\rho_G U_{SG}^2$  as the diameter and surface tension component will cancel out. This is similar to Hewitt and Roberts map (1969)
- Modified Taitel *et al.* (1980) provide promising results if the slug and churn regimes are combined to consider as intermittent flow.

- The low and high viscosity maps constructed utilising literature datasets for vertical inclination as well as the low viscosity maps constructed utilising literature datasets for horizontal inclination also produced promising results. The two proposed flow regime maps included: liquid Re vs gas Re and liquid Re vs gas We.
- However, high viscosity maps constructed utilising literature datasets for horizontal inclination require further datasets as several issues must be tackled. There is a lack of data generally for high viscosity. Furthermore, lack of coverage of each flow regime in a given experimental study also makes it difficult when it comes to analysing flow regime maps. Proposed flow regime map for high viscosity horizontal maps included: liquid We vs gas We, liquid We vs gas Re and  $We_L/Re_L^{0.2}$  vs  $We_L/Re_L^{0.2}$ .
- The project study has shown the use of Weber and Reynolds definitely provides more differentiation than the conventional superficial velocity maps. Nevertheless, with more datasets, it is believed that future work may need to investigate more complex dimensionless numbers or their combinations in order to establish tighter transition line boundaries.

## 6. Development of a general liquid holdup model

### 6.1. Introduction

Prediction of liquid holdup for two – phase flow within petroleum, nuclear and process industry is pivotal for practical applications within these industries which include equipment sizing, gathering, pumping, transporting and storage. In addition to lack of understanding of the basic underlying physics, determining liquid holdup from input conditions is still challenging as a result of following phenomena: slippage between both phases, flow pattern dependency and mass transfer between phases (Beggs and Brill, 1973). As a result, various authors have developed numerous empirical correlations in order to allow the prediction of liquid holdup. However, most of these correlations are limited to a narrow range of conditions. For a design engineer, the task is to choose a suitable liquid holdup correlation which will accurately predict the liquid holdup for the application in question. Once the liquid holdup (and its complement void fraction) is known, two – phase flow problem is further simplified so that it can be approached and tackled in a similar fashion to single – phase flow. Hence, the use of this phase distribution parameter is essential for determination of pressure drop and heat transfer coefficients in two – phase applications (Woldesemayat and Ghajar, 2007).

Moreover, the method of recording liquid holdup varies from dataset to dataset therefore the accuracy or the error of that method will be variable. In this present study, the datasets utilised for comparison are either collected by quick – closing valves or capacitance probes. Quick – closing valves measures a true average over a restricted length of pipe at one instant of time while capacitance probes or instrumentations measures a complex spatial average over a short length of pipe (Hewitt, 1978). For example, datasets from Mukherjee (1979) and four University of Nottingham datasets – Escrig (2017) and Fayyaz (2022) were collected using capacitance probes while other datasets in this study were collected by using the quick – closing valves methods. ECT (Electrical Capacitance Tomography) is the data

acquisition instrumentation that was used in studies of Fayyaz (2022) and Escrig (2017).

Understanding the effect of various physical parameters on liquid holdup correlation is essential for approaching two – phase problems. When the angle of inclination from horizontal is increased, the gravity forces acting on the liquid cause a decrease in liquid velocity. As a result, the slippage between the phases increases, leading to an increase in liquid holdup. Further increases in inclination angle leads to bridging of liquid phase across the entire pipe that decreases the slippage between phases which in turn decreases the liquid holdup (Beggs and Brill, 1973). For a horizontal pipe, increases in viscosity induces an increase in liquid holdup due to higher shear stresses in the liquid phase. The main reason for this is the increase in the height of the liquid film which is the result of the forces acting at the gas – liquid interface and pipe wall. Moreover, lower surface tension and density differences also cause higher void fraction values and thus lower liquid holdup values. (Nädler and Mewes, 1995).

In this study, a general two – phase liquid holdup correlation will be developed which will be applicable for a wide range of physical parameters without having dependency on flow regime changes. Various datasets from literature and Nottingham University were utilised for the development and evaluation of this model. Moreover, various void fraction correlations were searched from open literature in order to compare the performance of each model. The focus of this study is to develop a model which is applicable to a wide range of physical parameters such as density, viscosity, and surface tension. The need for development of such models is essential because various models fail when used to predict liquid holdup for high viscosity liquid. The reason for this is due to the lack of experimental data for viscous fluids in literature. Moreover, another particular area of focus in this research is the prediction of lower liquid holdup values which are often predicted with a higher error margin by most correlations.

## 6.2. Methodology

### 6.2.1. Summary of experimental database utilised for model development

Various experimental datasets covering a wide range of physical parameters were utilised for development of a new (general) liquid holdup correlation, as shown in Table 6.1. The gas phase for these experiments was air. Of these datasets, five of them involved an extensive investigation of inclination angle on liquid holdup:

- Beggs (1972) investigated the variation in liquid holdup for an air – water system at two different pipe diameters (25.4 mm and 38.1 mm). Using his data, Beggs (1972) developed a liquid holdup correlation which allowed evaluation of liquid holdup for air – water system with pipe diameters of 25.4 mm and 38.1 mm.
- Mukherjee (1979) investigated how liquid holdup varies with viscosity for kerosene – air (less viscous) and lube oil – air (more viscous) system. The experimental investigation was carried for a pipe diameter of 38.1 mm. Compared to Beggs (1972), Mukherjee used a different data capturing technique (capacitance probes) compared to quick closing valves in most research at that time.
- Escrig (2017) investigated liquid holdup for air – 5 cP silicone oil system. Fayyaz (2022) investigated liquid holdup for air – (64, 91.5 and 236 cP) silicone oil system. Both research ventures were carried out at University of Nottingham for a pipe diameter of 67 mm. Both research works used ECT (Electrical Capacitance Tomography) for data capturing. Rig operated for these experiments is shown in Chapter 3.

Moreover, four datasets in Table 6.1 involved experimental investigation of liquid holdup in horizontal pipes only while one dataset involved experimental investigation of liquid holdup in vertical pipe only.

Table 6.1 – Experimental datasets utilised for the development of a new liquid holdup correlation

Dataset	Liquid Phase	Angle investigated	Diameter	Density	Viscosity	Surface Tension	Liquid Holdup
-	-	degrees	mm	kg m <sup>-3</sup>	cP	N/m	-
Beggs (1972)	Water	0, 5, 10, 15, 20, 35, 55, 75, 85, 90	38.1, 25.4	~1000	0.7 – 1.4	0.070 – 0.076	2 – 88
Mukherjee (1979)	Kerosene AK	0, 5, 20, 30, 45, 50, 60, 70, 80, 90	38.1	771 – 829	0.6 – 2.7	0.021 – 0.027	1 – 94
Mukherjee (1979)	Lube oil AL	0, 30, 90	38.1	832 – 867	11 – 74	0.033 – 0.037	3 – 97
Minami and Brill (1987)	Kerosene	0	77.93	791 – 805	1.3 – 2.0	0.026 – 0.028	1 – 44
Minami and Brill (1987)	Water	0	77.93	~1000	0.6 – 0.9	0.068 – 0.072	1 – 45
Abdulmajeed (1996)	Kerosene	0	50.8	790 – 805	1.3 – 2.0	0.024 – 0.026	1 – 61
Sujumnong (1997)	Water	90	12.7	997 – 1000	0.8 – 1.0	0.071 – 0.073	1 – 98
Gokcal (2008)	Citgo Sentry	0	50.8	834 – 885	178 – 601	0.032 – 0.034	50 – 92
Escrig (2017)	Silicone oil	0, 15, 30, 45, 60, 75, 90	67	917	5	0.0202	20 – 88
Fayyaz (2022a)	Silicone oil	0, 10, 20, 30, 40, 50, 60, 70, 80, 90	67	922.5	64	0.0202	23 – 96
Overall	Various	0 – 90	12.7 – 77.9	771 – 1000	0.6 – 601	0.0202 – 0.078	1 – 98

A methodical approach was taken in ensuring that the data points considered for model development must be unbiased and realistic with an acceptable quality. In order to accomplish that, two main tests were utilised to filter all the points in each dataset: homogenous gas void fraction test and drift – flux test. The homogeneous void fraction test comprises of comparing the homogeneous gas void fraction to the experimental void fraction. If the data point had a value greater than the homogeneous void fraction, then this point is eradicated from the analysis and thus from model development (Woldesemayat & Ghajar, 2007). Figure 6.1 shows the homogeneous gas void fraction test carried out on the dataset of Mukherjee AK (1979). Sixty-one (61) data points were eradicated because they were greater than the homogeneous gas void fraction (points above the red line). The process is then repeated for all other datasets as well.

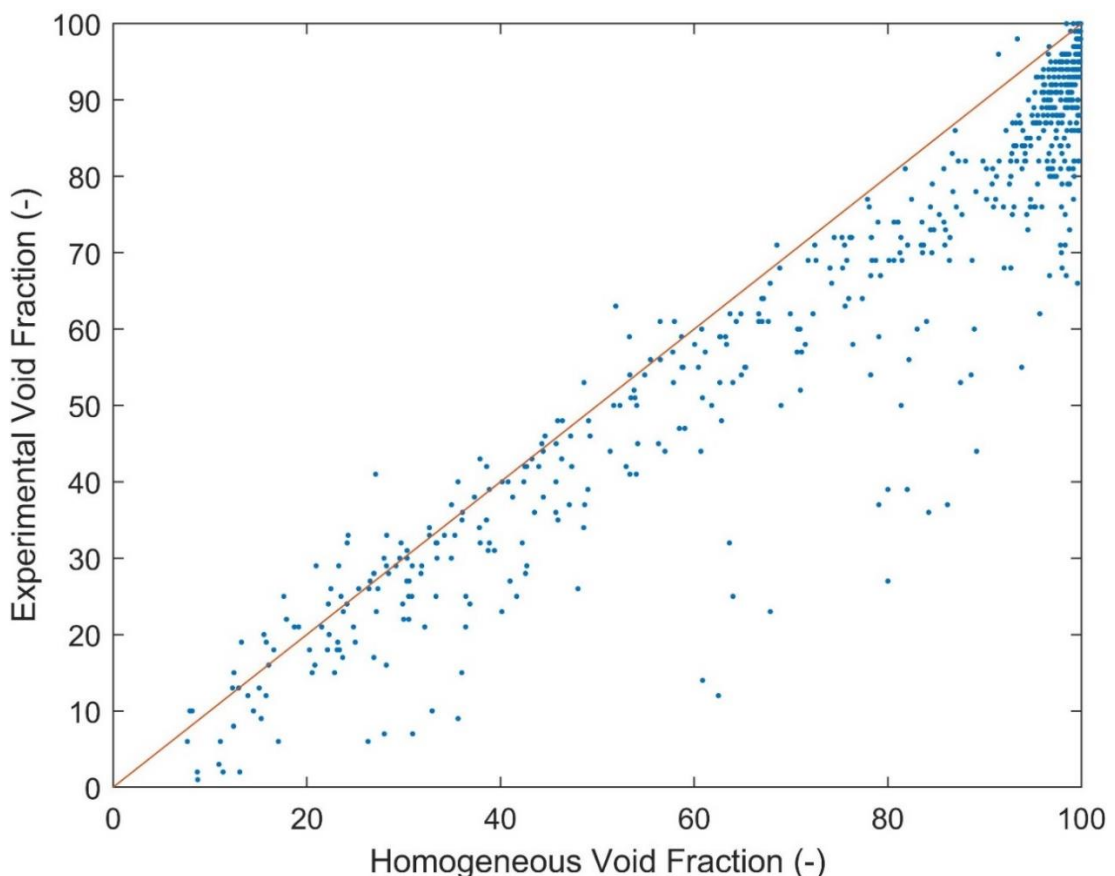


Figure 6.1 – Homogeneous gas void fraction test for Mukherjee AK (1979) dataset

The main reason to use this test can be explained through the use of Equation 6.1 which represents the void fraction in two – phase flow. For homogeneous flow, slip ratio  $S$  is equal to one. For vertical, inclined, and horizontal co-current upward flow, slip ratio  $S$  will be greater than or equal to one because  $u_G$  is nearly always greater than  $u_L$ . In addition, the buoyancy force acting on the gas flow maintains the slip ratio at greater than one. Therefore, homogeneous gas void fraction is set as the upper limit for possible values of measured void fraction.

$$\varepsilon = \frac{1}{1 + \left(\frac{1-x}{x}\right) \frac{\rho_G}{\rho_L} S} \quad (6.1)$$

In drift flux test, all the data points for each dataset were then plotted in a  $u_G$  ( $u_{GS}/\varepsilon$ ) versus  $U_M$  linear plot. Then, the software package ORIGIN 2020b (Origin 2020b, OriginLab Corporation, USA) was used in order to evaluate the 99 % prediction and confidence bands.

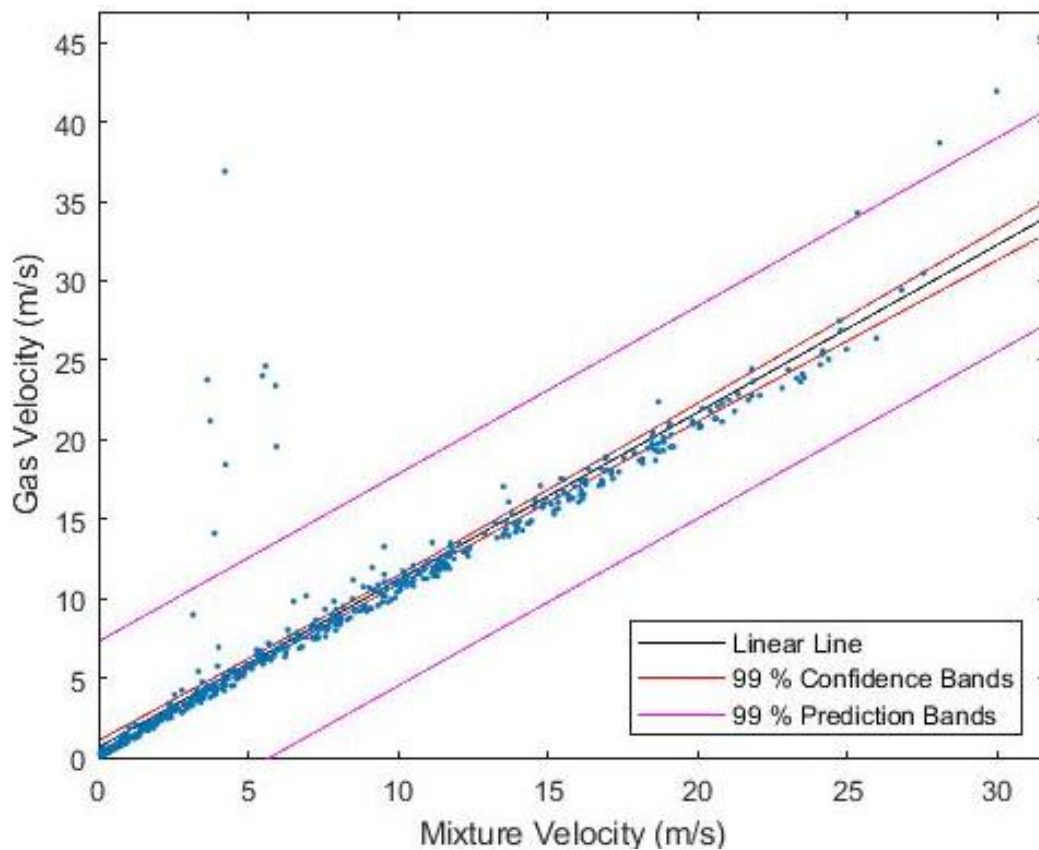


Figure 6.2 – Drift flux test for Mukherjee AK (1979) dataset

A typical example of this test is shown in Figure 6.2 for Mukherjee AK (1979) dataset. Any data point outside the lower and upper threshold of prediction bands are eradicated from analysis and thus from model development. In the case of Mukherjee AK (1979) dataset in Figure 6.2, there are a total of 13 points which were excluded because they do not meet these criteria.

*Table 6.2 – Treatment of liquid holdup data for each individual dataset utilised in this study*

<b>Dataset</b>	<b>Points before treatment</b>	<b>Points after homogeneous test</b>	<b>Points after drift flux test</b>	<b>Percentage of data eliminated</b>
Beggs (1972)	321	305	304	5.3
Mukherjee AK (1979)	606	545	532	12.2
Mukherjee AL (1979)	161	161	157	2.5
Minami and Brill AK (1987)	57	57	57	0.0
Minami and Brill AW (1987)	54	54	54	0.0
Abdulmajeed (1996)	88	83	83	5.7
Sujumnong (1997)	104	101	99	4.8
Gokcal (2008)	167	166	164	1.8
Escrig (2017)	441	441	432	2.0
Fayyaz (2022a)	600	600	596	0.7
All datasets	2599	2513	2478	4.7

Table 6.2 shows the total number of points before and after treatment (2599 and 2478 respectively), eliminating a total of 121 points. Mukherjee AK (1979) actually had 35 data points which were duplicated for inclination angle of 80 degrees and were not included in 606 data points utilised at the start of its data treatment.

### 6.2.2. Development of the liquid holdup model

In this research study, a new form of empirical model is presented for prediction of liquid holdup in two – phase flow. The present correlation was developed through data fitting of extensive experimental studies shown in Table 6.1, covering a wide range of parameters. Initially, a cubic polynomial (see Equation 6.2) was fitted to the datasets in Table 6.1. Even though the approach yielded good results for individual datasets, however it was difficult to fit constants A – D to physical parameters and superficial velocities (in other words to all datasets collectively). Hence, the approach was not selected for the development of the present correlation.

$$H_L(\vartheta, \mu_L, \sigma, D, u_{SL}, u_{SG}, \rho_L, \varepsilon_H, \rho_G) = A\vartheta^3 + B\vartheta^2 + C\vartheta + D \quad (6.2)$$

Since the Taylor series of  $\sin x$  also results in a polynomial expression, different powers of  $\sin x$  were then trialled as the next suitable model type, see Equation 6.3. In the end,  $\sin^2(x)$  was the chosen power. Powers greater than two did not improve the accuracy and efficiency of the correlation significantly. Therefore, starting equation chosen took the form of Equation 6.3.

$$H_L(\vartheta, \mu_L, \sigma, D, u_{SL}, u_{SG}, \rho_L, \varepsilon_H, \rho_G) = E\sin^2(F\vartheta) + G \quad (6.3)$$

Equation 6.3 was then fitted to all datasets in Table 6.1 individually and it was found that parameters E and G changed significantly with physical parameters of the liquid and gas. Constant F did not change by much. In order to improve the performance of the correlation, various model expressions were tested for variable G from which it was found that G can be swapped with a harmonic decline function which can be represented by Equation 6.4. As expected, variable G (and hence liquid holdup) will

decrease with an increase in gas superficial velocity at constant liquid superficial velocity.

$$G = \frac{H}{1 + \frac{u_{GS}}{Iu_{LS}^J}} \quad (6.4)$$

Therefore, the final form of the equation for the present correlation is shown in Equation 6.5. Each dataset in Table 6.1 is fitted again to Equation 6.5 from which it was determined that F and I do not change significantly with datasets however E, H and J altered with different datasets.

$$H_L(\vartheta, \mu_L, \sigma, D, u_{SL}, u_{SG}, \rho_L, \varepsilon_H, \rho_G) = E \sin^2(F\vartheta) + \frac{H}{1 + \frac{u_{GS}}{Iu_{LS}^J}} \quad (6.5)$$

Finally, variables E, F, H, I and J were then determined through data fitting using combined datasets (all 2478 points). The final resultant equation is shown in Equation 6.6.

$$H_L(\vartheta, \mu_L, \sigma, D, u_{SL}, u_{SG}, \rho_L, \varepsilon_H, \rho_G) = E \sin^2(1.25\vartheta) + \frac{H}{1 + \frac{u_{GS}}{2.87u_{LS}^J}} \quad (6.6)$$

Variable constants E, H and J are dependent upon physical properties as listed: viscosity, diameter, liquid density, gas density and surface tension. Moreover, variable constants (E, H and J) are also dependent upon homogeneous void fraction or liquid holdup. For given set of physical parameters of liquid and gas phases, variable constants E, H and J can be determined by using Equations 6.7 – 6.9.

$$E = \frac{D^{0.015}}{\rho_G^{1.32} \rho_L^{0.0019} \sigma^{0.39}} \quad (6.7)$$

$$H = \frac{\rho_L^{0.658} D^{0.031} \mu_L^{0.019} \rho_G^{0.07}}{(1 - \varepsilon_H)^{0.01} \varepsilon_H^{0.072} \sigma^{0.0034}} \quad (6.8)$$

$$J = \frac{(1 - \varepsilon_H)^{0.026} \rho_G^{0.15} \sigma^{0.13}}{D^{0.025} \rho_L^{0.077} \mu_L^{0.011} \varepsilon_H^{0.44}} \quad (6.9)$$

Otherwise, for extremely low gas flows and high liquid flows, a single simple equation for liquid holdup must be used, as shown in Equation 6.10. Equation 6.10 has no variable constant and only consist of fixed constants (1.51, 97.6, 2.69, and 0.5).

$$H_L(\vartheta, u_{LS}, u_{GS}) = 1.51 \sin(\vartheta) + \frac{97.6}{1 + \frac{u_{GS}}{2.69u_{LS}^{0.5}}} \quad (6.10)$$

Eight models were chosen for comparison based on research from literature to the new liquid holdup correlation, as listed in Table 6.3. Based on classification explained in “Literature Review”, there are:

- Four drift flux correlations – Zuber and Findlay (1965), Choi *et al.* (2012), Jowitt *et al.* (1984) and Toshiba from Coddington and Macian (2002)
- One slip ratio correlation – Premoli *et al.* (1970)
- Two general correlations – Mukherjee and Brill (1983) and Woldesemayat and Ghajar (2007)
- One  $K\varepsilon_H$  correlation – Armand – Massina from Leung (2005)

Table 6.3 – List of correlations utilised for comparison to new liquid holdup correlation

Model	Set of equations
Zuber and Findlay (1965)	$C_O = 1.2; u_D = 1.53 \left( \frac{g\sigma\Delta\rho}{\rho_L^2} \right)^{0.25}; H_L = 1 - \frac{u_{SG}}{C_O(u_{SL}+u_{SG})+u_D}$
Jowitt <i>et al.</i> (1984)	$C_O = 1 + 0.796 \exp\left(-0.061 \sqrt{\frac{\rho_G}{\rho_L}}\right); u_D = 0.034 \left( \sqrt{\frac{\rho_G}{\rho_L}} - 1 \right)$ $H_L = 1 - \frac{u_{SG}}{C_O(u_{SL} + u_{SG}) + u_D}$
Choi <i>et al.</i> (2012)	$C_O = \frac{2}{1 + \left(\frac{Re}{1000}\right)^2} + \frac{1.2 - 0.2 \sqrt{\frac{\rho_G}{\rho_L}} (1 - \exp(-18\varepsilon))}{1 + \left(\frac{1000}{Re}\right)^2}$ $u_D = A_C \cos\vartheta + B_C \left( \frac{g\sigma\Delta\rho}{\rho_L^2} \right)^{0.25} \sin\vartheta; H_L = 1 - \frac{u_{SG}}{C_O(u_{SL} + u_{SG}) + u_D}$
Woldesemayat & Ghajar (2007)	$H_L = 1 - \frac{u_{SG}}{u_{SG} \left( 1 + \left( \frac{u_{SL}}{u_{SG}} \right) \left( \frac{\rho_G}{\rho_L} \right)^{0.1} \right) + 2.9 \left[ \frac{gD\sigma(1+\cos\vartheta)(\rho_L-\rho_G)}{\rho_L^2} \right]^{0.25} (1.22+1.22 \sin\vartheta)^{\frac{P_a}{P_s}}}$
Armand – Massina (2005)	$H_L = 1 - [0.833 + 0.167x_G]\varepsilon_H$
Toshiba (2002)	$C_O = 1.08; u_D = 0.45; H_L = 1 - \frac{u_{SG}}{C_O(u_{SL}+u_{SG})+u_D}$
Premoli <i>et al.</i> (1970)	$u_R = 1 + E_1 \left( \frac{j}{1 + E_2 j} - jE_2 \right)^{0.5}$ if $\frac{1}{1 + jE_2} > E_2$ Otherwise, $u_R = 1$ $j = \frac{\varepsilon_H}{1 - \varepsilon_H}; E_1 = 1.578 Re_P^{-0.19} \left( \frac{\rho_L}{\rho_G} \right)^{0.22}$ $E_2 = 0.0273 We Re_P^{-0.51} \left( \frac{\rho_L}{\rho_G} \right)^{-0.08}; H_L = 1 - \frac{1}{1 + u_R \left( \frac{1 - x_G}{x_G} \right) \left( \frac{\rho_G}{\rho_L} \right)}$
Mukherjee and Brill (1983)	$H_L = \exp(C_1 + C_2 \sin\vartheta + C_3 \sin^2\vartheta + C_4 N_L^2) \frac{N_{GV}^{C_5}}{N_{LV}^{C_6}}$ $N_L = \mu_L \left( \frac{1}{\rho_L \sigma^3} \right)^{0.25}; N_{GV} = u_{SG} \left( \frac{\rho_L}{g\sigma} \right)^{0.25}; N_{LV} = u_{SL} \left( \frac{\rho_L}{g\sigma} \right)^{0.25}$

### 6.3. Analysis of proposed correlation

#### 6.3.1. Model results for current three experimental campaigns

An experimental study (same as one analysed in Chapter 4) was carried out at University of Nottingham, evaluating the effect of inclination on liquid holdup using various air – silicon oil system. Viscosities investigated were 64, 91.5 and 236 cP.

For 64 cP, ten inclination angles, five liquid velocities, and twelve gas superficial velocities formed the matrix of this study. For each liquid superficial velocity, the liquid holdup was plotted against angle for each gas superficial velocity. Figure 6.3 shows a plot of liquid holdup against angle for twelve different gas superficial velocities at a liquid superficial velocity of 0.292 m/s.

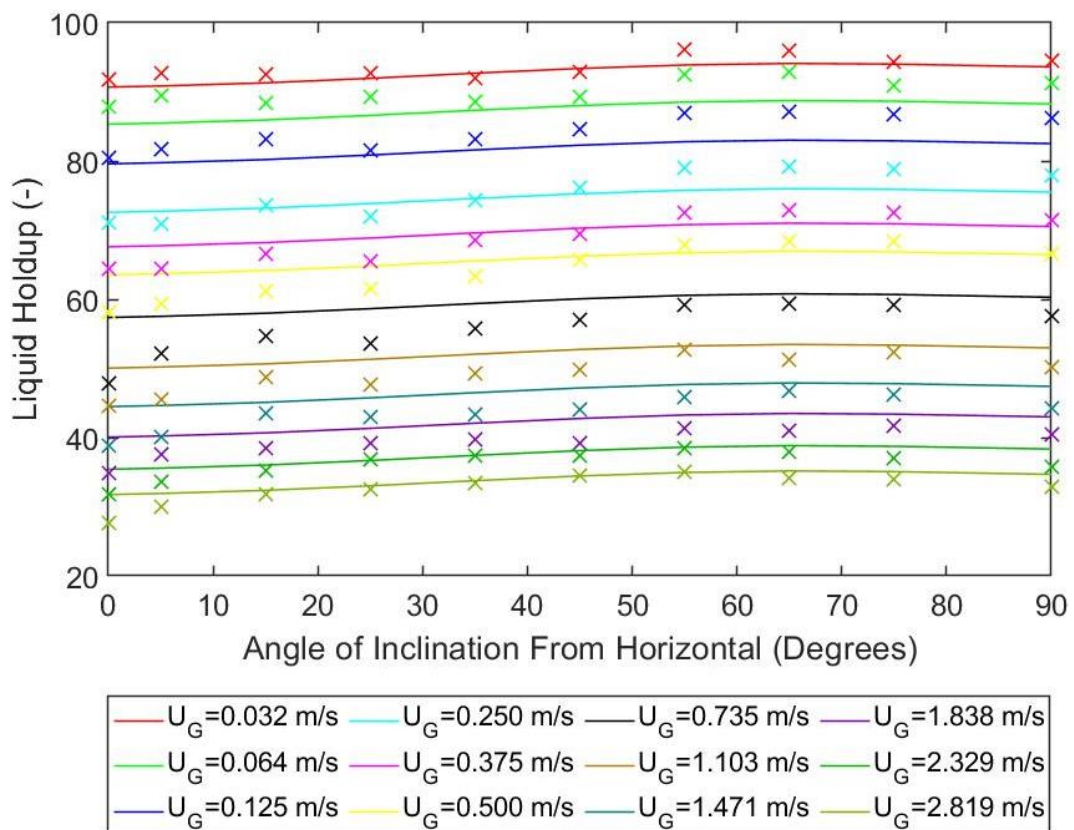


Figure 6.3 – How liquid holdup varies with angle for different gas superficial velocities for a given liquid superficial velocity of 0.292 m/s at 64 cP silicone oil  
(Points – Experimental; Lines – Model)

The model was also evaluated against the 91.5 cP dataset as well, as shown in Figure 6.4. Five inclination angles, four liquid velocities, and eleven gas superficial velocities formed the matrix of this study. For each liquid superficial velocity, the liquid holdup was plotted against angle for each gas superficial velocity. Figure 6.4 shows a plot of liquid holdup against angle for eleven different gas superficial velocities at a liquid superficial velocity of 0.308 m/s.

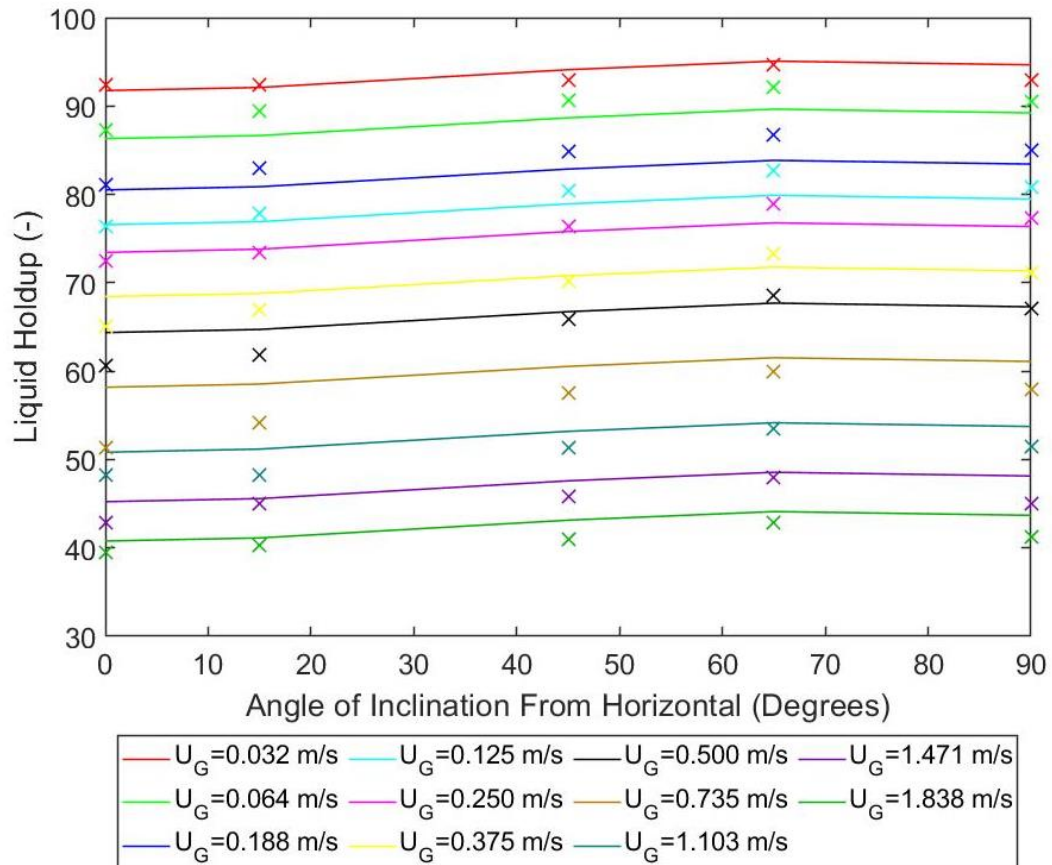


Figure 6.4 – How liquid holdup varies with angle for different gas superficial velocities for a given liquid superficial velocity of 0.308 m/s at 91.5 cP silicone oil  
(Points – Experimental; Lines – Model)

The model was also evaluated against the 236 cP dataset as well, as shown in Figure 6.5. Five inclination angles, three liquid velocities, and eleven gas superficial velocities formed the matrix of this study. For each liquid superficial velocity, the liquid holdup was plotted against angle for each gas superficial velocity. Figure 6.5 shows a plot of liquid holdup against angle for eleven different gas superficial velocities at a liquid superficial velocity of 0.27 m/s.

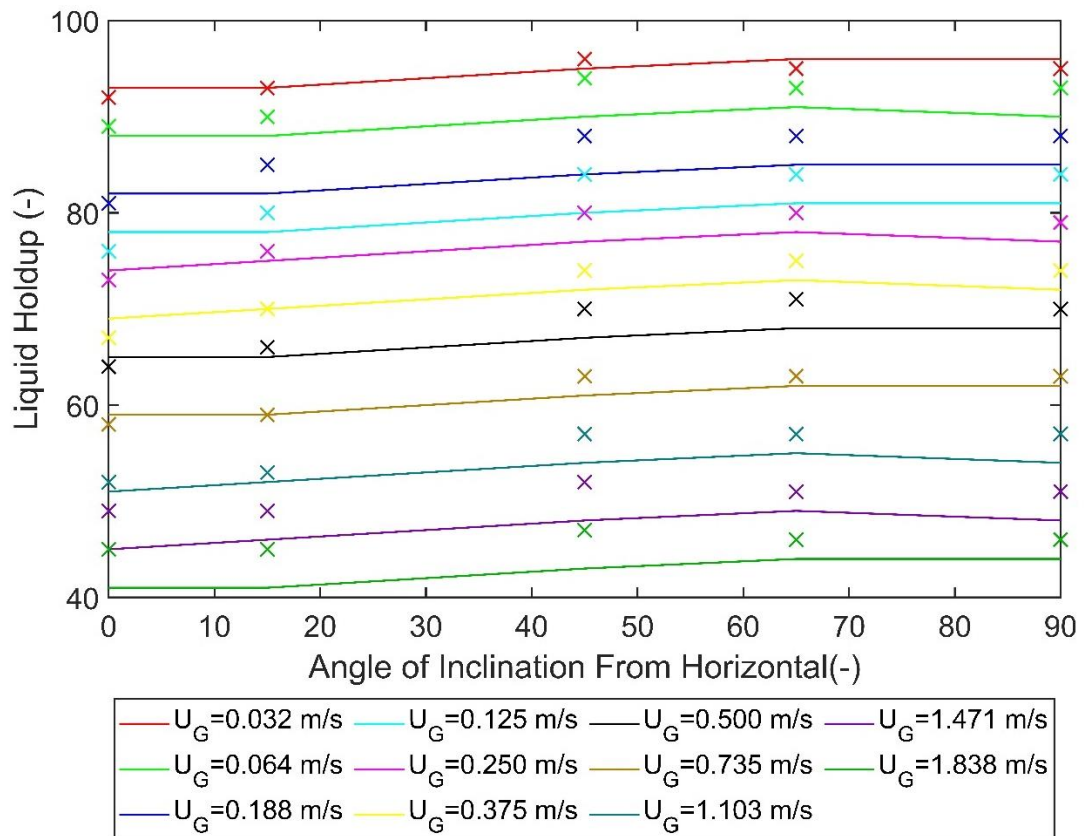


Figure 6.5 – How liquid holdup varies with angle for different gas superficial velocities for a given liquid superficial velocity of 0.27 m/s at 236 cP silicone oil  
(Points – Experimental; Lines – Model)

### 6.3.2. Comparing current study with other models for experimental dataset utilised for model development

In order to compare current model to other models, three different metrics were used in order to robustly evaluate their performance and are as follows:

1. Firstly, the average absolute error (AAE), average error (AE) and standard deviation (STD using short - cut method) will be calculated. These statistical measures (SM) are listed in Table 6.4 for each model – dataset combination.

2. The percentage of data within thirty percent (see Equation 6.14) predicted by each model for each dataset mentioned in Table 6.1 was also a useful metric.

3. For each dataset, the percentage of data predicted within thirty percent by each model for selected holdup ranges was the third metric. Each dataset was divided into two sets with following holdup ranges: 0 – 25 % and >25 %.

The absolute average error, average error and standard deviation were calculated using Equations 6.11 – 6.13 respectively.

$$AAE = \frac{\sum |Model Value - Experimental Value|}{N} \quad (6.11)$$

$$AE = \frac{\sum (Model Value - Experimental Value)}{N} \quad (6.12)$$

$$STD = \left[ \frac{\sum (Model Value - Experimental Value)^2}{N} - AE^2 \right]^{0.5} \quad (6.13)$$

$$\% \text{ Difference} = \frac{Model Value - Experimental Value}{Experimental Value} \times 100 \quad (6.14)$$

Table 6.4 shows AAE, AE and STD for each model – individual dataset combination. AK, AL and AW are shortforms for air – kerosene, air – lube oil and air – water. Current study (2022) has the lowest AAE for Abdulmajeed (1996), Minami and Brill AK (1987), Minami and Brill AW (1987), Sujumnong (1997) and Mukherjee AK (1979) while it has similar AAE to other models (within +/- 0.8 max) for Escrig (2017) and Fayyaz (2022a). Datasets of Mukherjee AL (1979), Beggs (1972) and Gokcal (2008) are predicted within a reasonable error by current study (2022) in terms of AAE. However, in terms of absolute average error, Mukherjee AL (1979) is best predicted by Zuber and Findlay (1965) with an AAE of 3.9 while Gokcal (2008) is best predicted by Choi *et al.* (2012) with an AAE of 3.3. Beggs (1972) is best predicted by Woldesemayat and Ghajar (2007) with an AAE of 2.6. It must be noted that Mukherjee and Brill (1983) correlation was not able to predict the high viscosity dataset of Gokcal (2008) therefore it is labelled as N/A for this part of the analysis.

The model – dataset combination with minimum AAE occurs for current study model (2022) - Minima and Brill AK dataset (1987) where the AAE is 1.7. In comparison, the model – dataset combination with maximum AAE of 38.8 occurs for Mukherjee and Brill (1983) model – Fayyaz (2022a) dataset combination. Moreover, model – dataset combinations with minimum STD of 2.1 are current study model (2022) – Minima and Brill AK dataset (1987) and Woldesemayat and Ghajar (2007) model – Fayyaz (2022a) dataset. In comparison, the model – dataset combination with maximum STD of 20.0 occurs for Mukherjee and Brill (1983) model – Fayyaz dataset (2022a).

The model with narrowest range in terms of AAE was current study (2022). The range of AAE for current study (2022) varied from 1.7 to 9.5. The model with widest range in terms of AAE was Mukherjee and Brill (1983) which varied between 3.4 and 38.8. The model with narrowest range in terms of STD was current study (2022). The range of STD for current study (2022) varied from 2.1 to 8.6. The model with widest range in terms of STD was Mukherjee and Brill (1983) which varied between 2.9 and 20.0.

Table 6.4 – Absolute average error (AAE), average error (AE) and standard deviation (STD) for each model – dataset combination  
(AK is air –kerosene, AW is air – water and AL is air – lube oil)

Model	SM	Dataset									
		Fayyaz (2022a)	Escrig (2017)	Gokcal (2008)	Sujumnong (1997)	Abdul majeed (1996)	Minami and Brill (1987)		Mukherjee (1979)		Beggs (1972)
							AK	AW	AK	AL	
<b>Current Study (2022)</b>	AAE	2.8	4.1	9.5	2.9	2.5	1.7	2.4	4.3	5.2	4.5
	AE	0.0	-2.6	-7.7	-1.7	-0.6	-0.3	-1.0	-0.7	-3.6	3.3
	STD	3.6	4.7	8.6	3.5	3.9	2.1	2.8	6.2	5.1	4.9
<b>Jowitt <i>et al.</i> (1984)</b>	AAE	8.1	10.6	4.9	22.1	30.5	30.8	29.3	26.4	17.2	24.8
	AE	2.6	4.2	-4.0	22.1	30.1	30.8	29.3	25.4	15.6	24.8
	STD	9.6	12.2	4.4	12.6	14.3	9.8	10.7	13.9	14.1	10.0
<b>Choi <i>et al.</i> (2012)</b>	AAE	2.0	9.8	3.3	5.2	11.1	8.0	7.9	7.4	4.0	4.8
	AE	0.8	-9.8	0.9	4.9	4.5	4.0	2.8	6.5	1.7	4.2
	STD	2.5	5.9	4.1	4.8	11.4	8.4	9.0	5.8	5.3	5.1
<b>Woldesemayat and Ghajar (2007)</b>	AAE	2.4	3.3	13.6	4.4	3.9	2.9	3.0	4.7	6.8	2.6
	AE	-1.9	-2.7	-11.8	-1.9	1.1	1.8	2.7	1.4	-5.7	-0.5
	STD	2.1	3.1	10.2	5.7	5.0	3.1	3.0	6.3	5.3	3.2

<b>Premoli <i>et al.</i> (1970)</b>	AAE	3.3	6.8	12.9	2.9	3.8	3.5	4.6	4.6	6.8	2.8
	AE	-1.1	-6.1	-7.1	2.5	-2.4	-3.0	-4.0	0.7	-5.3	1.4
	STD	3.9	7.4	15.4	3.4	6.4	4.2	5.4	6.4	6.8	3.2
<b>Toshiba (2002)</b>	AAE	4.6	3.8	12.1	3.0	6.2	7.6	7.1	6.3	4.6	4.0
	AE	-2.5	-3.4	-7.6	0.9	5.9	7.5	7.0	5.2	-1.2	3.1
	STD	4.7	2.9	12.2	4.0	6.0	5.8	5.4	6.9	5.7	3.9
<b>Zuber and Findlay (1965)</b>	AAE	6.7	7.9	13.1	5.4	11.1	9.9	9.7	8.6	3.9	6.8
	AE	-6.6	-7.8	-11.5	5.1	9.2	9.7	9.7	8.1	0.8	6.7
	STD	4.3	5.0	10.0	4.9	7.5	5.6	5.0	5.8	5.3	4.8
<b>Armand – Massina (2005)</b>	AAE	15.4	17.5	22.1	3.5	8.2	5.3	5.8	5.9	7.0	3.1
	AE	-15.4	-17.5	-22.1	1.3	-0.3	-2.0	-2.7	1.5	-5.6	0.2
	STD	7.0	10.7	9.0	4.4	10.8	6.8	7.4	8.0	8.3	3.9
<b>Mukherjee and Brill (1983)</b>	AAE	38.8	9.6	N/A	6.4	3.6	3.4	4.0	5.2	7.0	3.4
	AE	38.8	-9.5		-5.5	2.4	-2.7	-3.1	-0.2	-4.4	1.2
	STD	20.0	7.4		5.2	5.0	2.9	3.5	7.0	7.0	4.1

As AAE, AE, and STD of each model are variable for each dataset, more information can be obtained by analysing the errors and standard deviation (Table 6.5) for the complete dataset. To remove bias from the analysis, two combined datasets were formed: all data and all data excluding Nottingham University. All data contains the entire database utilised for model development while all data excluding Nottingham University contains all the database except Escrig (2017) and Fayyaz (2022a).

*Table 6.5 – Absolute average error (AAE), average error (AE) and standard deviation (STD) for both combined dataset scenarios*

Model	SM	Combined Datasets	
		All data	All data excluding Nottingham University
<b>Current Study (2022)</b>	AAE	4.1	4.7
	AE	-1.0	-1.0
	STD	5.7	6.5
<b>Jowitt <i>et al.</i> (1984)</b>	AAE	17.2	22.9
	AE	13.8	21.3
	STD	16.4	15.5
<b>Choi <i>et al.</i> (2012)</b>	AAE	5.8	6.1
	AE	1.1	4.4
	STD	7.7	6.4
<b>Woldesemayat and Ghajar (2007)</b>	AAE	4.3	5.3
	AE	-1.8	-1.4
	STD	5.9	7.4
<b>Premoli <i>et al.</i> (1970)</b>	AAE	5.0	5.2
	AE	-2.0	-1.1
	STD	7.4	8.0
<b>Toshiba (2002)</b>	AAE	5.3	6.1
	AE	0.3	2.5
	STD	7.2	8.1
<b>Zuber and Findlay (1965)</b>	AAE	7.8	8.2
	AE	-0.2	4.8
	STD	9.4	8.8
<b>Armand – Massina (2005)</b>	AAE	11.0	7.2
	AE	-8.3	-2.6
	STD	11.9	10.4
<b>Mukherjee and Brill (1983)</b>	AAE	14.5	4.9
	AE	7.6	-1.1
	STD	22.0	6.3

Overall, as shown in Table 6.5, current study (2022) has the lowest standard deviation (STD) and absolute average error (AAE) for all data. Similarly, current study (2022) has the lowest STD and AAE for all data excluding Nottingham University. The worst model for both sets (in terms of AAE, AE and STD) is Jowitt *et al.* (1984).

Table 6.6 shows percentage of data within 30 % for each model – individual dataset combination. Current study (2022) predicts the highest percentage of data within 30 % for each dataset except Gokcal (2008), Sujumnong (1997) and Mukherjee AL (1979). Nevertheless, current study (2022) predicts the second highest percentage of data within 30 % for Gokcal (2008) – high viscosity dataset while it predicts approximately 71 % of the data within 30 % for Mukherjee AL (1979) which is quite reasonable even though it is not the highest percentage in the analysis. Both these datasets are best predicted by Choi *et al.* (2012). For Sujumnong (1997) dataset, current study (2022) is the third best model in terms of percentage of data (79.8 %) within 30 %. Premoli *et al.* (1970) is the best model for Sujumnong (1997) with prediction of 87.9 % of the data within 30 %.

The datasets that were poorly predicted (<50 %) by most models were found to be Abdul majeed (1996), Minami and Brill (1987) AK and Minami and Brill (1987) AW. Seven out of nine models could not predict more than 50 % of the datasets within 30 % for datasets of Abdul majeed (1996) and Minami and Brill (1987) AW. Nevertheless, current study (2022) predicts these datasets with good accuracy.

On the other hand, datasets that were best predicted (100 % prediction) by most models were found to be Fayyaz (2022a), Escrig (2017) and Gokcal (2008). Three out of nine models (with current study being one of them) were able to predict (100 %) datasets of Fayyaz (2022a) and Escrig (2017) within 30 %. Whereas, for Gokcal (2008), two out of nine models (with current study not being one of them) were able to predict 100 % of the data within 30 %.

Table 6.6 – Percentage of data within 30 % for each model – dataset combination

Model	Dataset									
	Fayyaz (2022a)	Escrig (2017)	Gokcal (2008)	Sujumnong (1997)	Abdul majeed (1996)	Minami and Brill (1987)		Mukherjee (1979)		Beggs (1972)
						AK	AW	AK	AL	
<b>Current Study (2022)</b>	100.0	100.0	84.8	79.8	86.7	75.4	83.3	74.2	70.7	91.8
<b>Jowitt <i>et al.</i> (1984)</b>	76.0	68.3	100.0	35.4	14.5	3.5	5.6	22.4	39.0	16.4
<b>Choi <i>et al.</i> (2012)</b>	100.0	84.0	100.0	69.7	18.1	35.1	42.6	52.3	84.1	72.4
<b>Woldesemayat and Ghajar (2007)</b>	100.0	100.0	74.4	83.8	49.4	59.6	63.0	68.0	74.5	81.3
<b>Premoli <i>et al.</i> (1970)</b>	98.8	85.4	78.7	87.9	75.9	66.7	46.3	70.7	64.3	80.9
<b>Toshiba (2002)</b>	100.0	100.0	75.0	76.8	42.2	38.6	46.3	62.6	81.5	72.4
<b>Zuber and Findlay (1965)</b>	99.7	95.1	70.1	69.7	27.7	33.3	33.3	47.2	83.4	63.8
<b>Armand – Massina (2005)</b>	47.3	45.8	38.4	71.7	20.5	36.8	33.3	56.6	70.7	76.6
<b>Mukherjee and Brill (1983)</b>	27.2	72.2	0.0	64.6	44.6	47.4	44.4	60.3	70.1	77.6

Again, even though current study (2022) is performing well for most datasets compared to other models, a clearer view can be provided by comparing this metric for the whole dataset, as shown in Table 6.7. Overall, for both combined dataset scenarios, current study (2022) is the best model for highest percentage of data (88.4 % and 80.2 % respectively) within 30 %. For all data scenario, Woldesemayat and Ghajar (2007) is the second-best model predicting 83.5 % of the data while Premoli *et al.* (1970) is the second-best model for all data excluding Nottingham University predicting 73.4 % of the data.

*Table 6.7 – Percentage of data within 30 % for combined dataset scenarios*

Model	Combined datasets	
	All data	All data excluding Nottingham University
<b>Current Study (2022)</b>	88.4	80.2
<b>Jowitt <i>et al.</i> (1984)</b>	48.3	30.9
<b>Choi <i>et al.</i> (2012)</b>	75.9	63.5
<b>Woldesemayat and Ghajar (2007)</b>	83.5	71.7
<b>Premoli <i>et al.</i> (1970)</b>	81.6	73.4
<b>Toshiba (2002)</b>	80.3	66.3
<b>Zuber and Findlay (1965)</b>	73.6	56.6
<b>Armand – Massina (2005)</b>	53.1	57.6
<b>Mukherjee and Brill (1983)</b>	52.2	56.5

Each dataset listed in Table 6.1 was divided into two different sets: one containing data with liquid holdup values  $> 25\%$  and other with liquid holdup values  $\leq 25\%$ . The main focus of this metric is to analyse how accurately a model can predict lower liquid holdups. Table 6.8 shows the percentage of data within 30% of these two sets for each model – dataset combination. For liquid holdups  $\leq 25\%$ , current study seems to be the best for all datasets except Minami and Brill AK (1987), Mukherjee AL (1979) and Sujumngong (1997). For Mukherjee AL (1979) dataset, the best model is Toshiba (2002) while the best model for Sujumngong (1997) and Minami and Brill AK (1987) for liquid holdups  $\leq 25\%$  is Premoli *et al.* (1970).

Table 6.8 – Percentage of data within 30 % for each individual set (each model – dataset combination)

Model	Dataset									
	Fayyaz (2022a)	Escrig (2017)	Gokcal (2008)	Sujumnong (1997)	Abdul majeed (1996)	Minami and Brill (1987)		Mukherjee (1979)		Beggs (1972)
						AK	AW	AK	AL	
<b>Current Study (2022)</b>	100.0	100.0	ND	54.5	81.0	70.2	79.1	60.1	34.5	87.2
	100.0	100.0	84.8	100.0	100.0	100.0	100.0	93.0	91.9	95.7
<b>Jowitt <i>et al.</i> (1984)</b>	0.0	0.0	ND	0.0	0.0	0.0	0.0	0.0	0.0	0.0
	76.4	71.4	100.0	63.6	48.0	20.0	27.3	52.0	63.6	30.7
<b>Choi <i>et al.</i> (2012)</b>	100.0	100.0	ND	31.8	5.2	34.0	44.2	21.8	62.1	40.4
	100.0	83.3	100.0	100.0	48.0	40.0	36.4	92.6	97.0	100.0
<b>Woldesemayat and Ghajar (2007)</b>	100.0	100.0	ND	65.9	32.8	53.2	58.1	49.5	46.6	61.0
	100.0	100.0	74.4	98.2	88.0	90.0	81.8	92.6	90.9	98.8
<b>Premoli <i>et al.</i> (1970)</b>	100.0	84.2	ND	75.0	81.0	74.5	51.2	57.4	29.3	61.0
	98.8	85.5	78.7	98.2	64.0	30.0	27.3	88.2	84.8	98.2
<b>Toshiba (2002)</b>	100.0	100.0	ND	50.0	22.4	31.9	41.9	45.9	67.2	45.4
	100.0	100.0	75.0	98.2	88.0	70.0	63.6	84.7	89.9	95.7
<b>Zuber and Findlay (1965)</b>	100.0	100.0	ND	31.8	3.4	21.3	20.9	16.2	55.2	25.5
	99.7	94.9	70.1	100.0	84.0	90.0	81.8	88.2	100.0	96.9
<b>Armand – Massina (2005)</b>	100.0	63.2	ND	43.2	12.1	40.4	37.2	32.7	60.3	51.8
	47.0	45.0	38.4	94.5	40.0	20.0	18.2	88.2	76.8	98.2
<b>Mukherjee and Brill (1983)</b>	0.0	15.8	ND	20.5	25.9	36.2	32.6	38.0	32.8	58.2
	27.3	74.8	0.0	100.0	88.0	100.0	90.9	90.0	91.9	94.5

For liquid holdup > 25 %, current study (2022) performs the best for the following datasets: Fayyaz (2022a), Escrig (2017), Sujumnong (1997), Abdulmajeed (1996), Minima and Brill AK (1987), Minima and Brill AW (1987) and Mukherjee AK (1979). For Gokcal (2008) dataset, the best models are Choi *et al.* (2012) and Jowitt *et al.* (1984) followed by current study (2022). For Mukherjee AL (1979) dataset, the best model is Choi *et al.* (2012) followed by current study (2022) and Mukherjee and Brill (1983). The best model for Beggs (1972) is Choi *et al.* (2012).

Overall, as shown in Table 6.9, current study (2022) outperforms all the other models for both combined datasets for liquid holdups of less than or equal to 25. Furthermore, the best model for liquid holdup > 25 % is current study (2022) for all data while the best models for all data excluding Nottingham University for liquid holdup > 25 % is Choi *et al.* (2012) followed by current study (2022) but this ranking is quite marginal (difference of ten points or 1.3 %).

*Table 6.9 – Percentage of data within 30 % for each individual set (combined dataset scenarios)*

Model	Combined dataset	
	All data	All data excluding Nottingham University
<b>Current Study (2022)</b>	67.7	66.7
	96.8	92.6
<b>Jowitt <i>et al.</i> (1984)</b>	0.0	0.0
	67.9	59.3
<b>Choi <i>et al.</i> (2012)</b>	32.5	30.4
	93.5	93.9
<b>Woldesemayat and Ghajar (2007)</b>	53.5	52.0
	95.6	89.8
<b>Premoli <i>et al.</i> (1970)</b>	60.5	59.7
	90.2	86.1
<b>Toshiba (2002)</b>	46.4	44.7
	94.1	86.2
<b>Zuber and Findlay (1965)</b>	24.3	21.9
	93.7	88.4
<b>Armand – Massina (2005)</b>	39.5	38.6
	58.6	75.0
<b>Mukherjee and Brill (1983)</b>	38.3	39.0
	57.8	72.5

Figure 6.6 shows how the model liquid holdup varies with the experimental liquid holdup for all data. It only shows the best six models in terms of AAE. Overall, current study (2022) performs much better at all liquid holdups compared to all models. Current study also predicts the highest percentage of data within 30 % as well. Woldesemayat and Ghajar (2007) also has a good performance but prediction of lower holdup values is much better by current study (2022). Even though drift flux models such as Choi *et al.* (2012) and Toshiba (2002) also perform good on average, the major issue with these models is that they have poor agreement for liquid holdups < 25 % or just low liquid holdups.

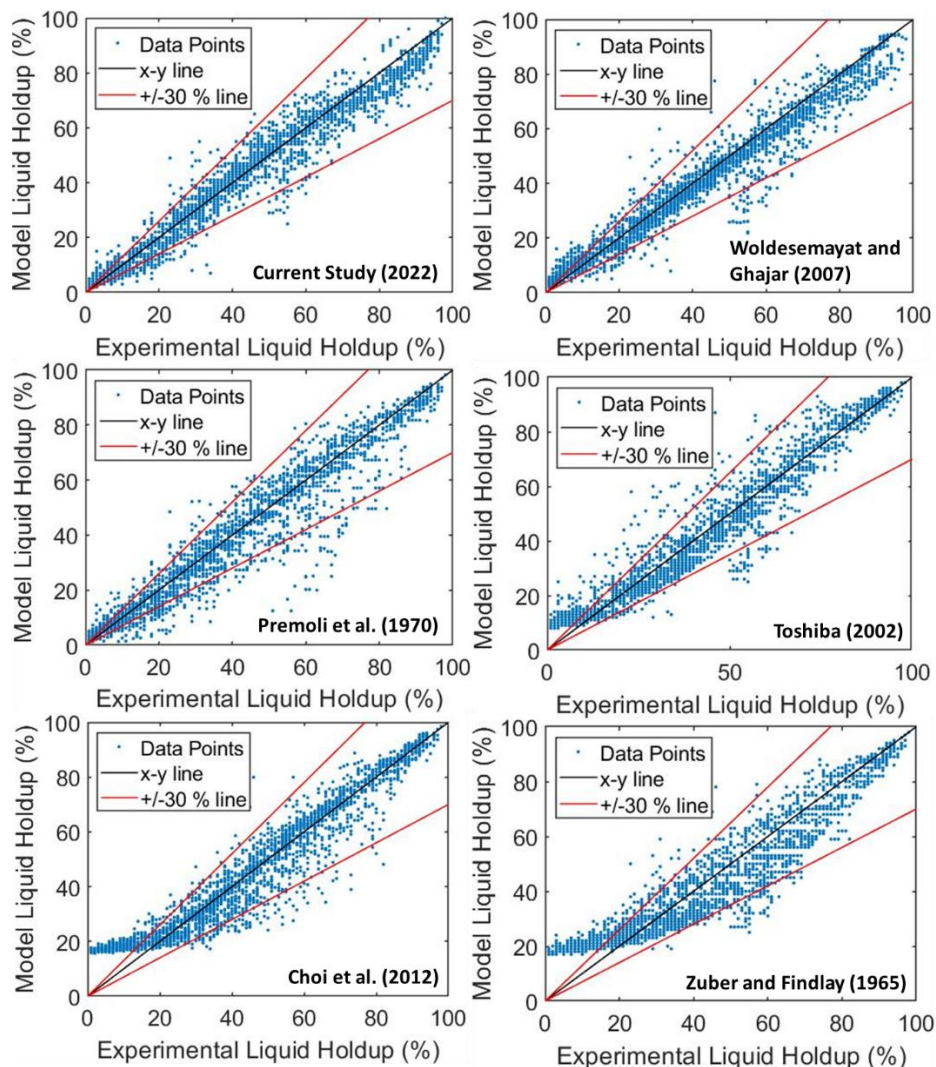


Figure 6.6 – Overall performance of the best six models for combined dataset (all data)

Figure 6.7 shows how the model liquid holdup varies the experimental liquid holdup for combined dataset with all data except Nottingham University datasets. It only shows the best six models in terms of AAE. Overall, current study (2022) performs much better at all liquid holdups compared to other models. Moreover, low liquid holdup values are predicted well by current study (2022) followed by Woldesemayat and Ghajar (2007).

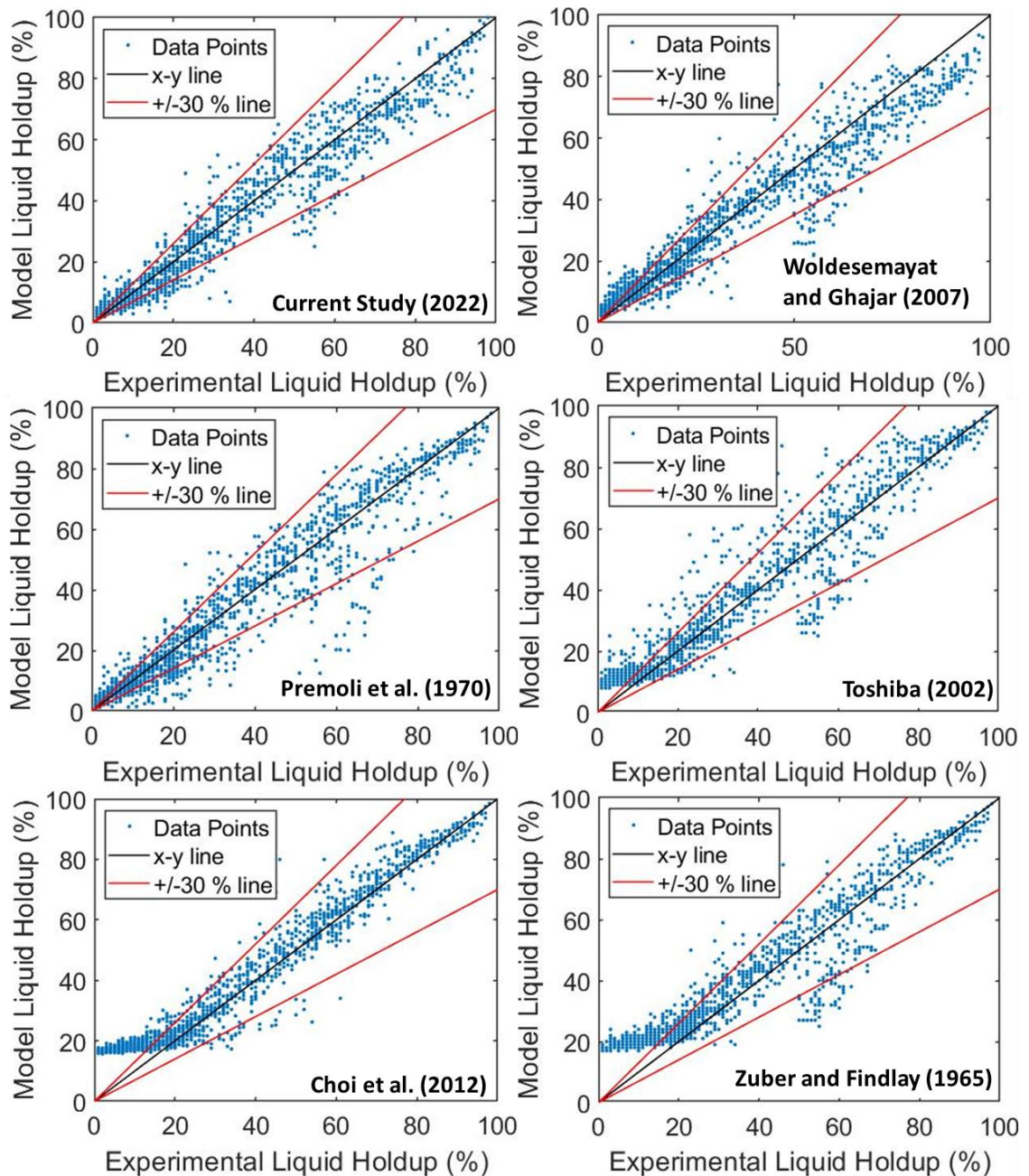


Figure 6.7 – Overall performance of the best six models for combined dataset (all data except Nottingham University)

#### 6.4. Further performance evaluation of present study model (2022) using data not utilised in model development

The main aim of the analysis in this section is to test the performance of the current study (2022) to datasets not utilised for its development. The analysis in this section will focus on two types of data: one for low liquid loading (i.e. low liquid holdup) and one for mixed liquid loading. The division of datasets in this manner will not only allow further overall evaluation of the general correlation proposed in the present study but it also allows to predict the performance of the present correlation for low liquid holdup values. As discussed earlier, quantification of low liquid holdup by existing models is quite poor, as shown in Section 6.3.2.

Table 6.10 summarises 16 additional datasets utilised for evaluating the performance of the models. These datasets were not utilised in the development of the model – current study. The gas phase is air for all datasets except Schmidt *et al.* (2008) where the gas phase is nitrogen. Additional datasets also include two further datasets from University of Nottingham carried out in this present study – 91.5 cP and 236 cP. The treatment of these datasets was carried out in the same method as mentioned in Methodology. The selected datasets again cover a wide range of viscosities, densities, surface tension and diameters. The first eight datasets in Table 6.10 include studies that only investigated low liquid holdup while rest of the datasets in Table 6.10 includes studies that investigate mixed liquid loading.

Table 6.10 – Experimental dataset not utilised for the development of a new liquid holdup correlation

Dataset	Liquid Phase	Angle investigated	Diameter	Density	Viscosity	Surface Tension	Liquid Holdup
-	-		mm	kg m <sup>-3</sup>	cP	N/m	-
<b>Paras <i>et al.</i> (1994)</b>	Water	0	50.8	1000	1	0.072	1 – 11
<b>Meng (1999)</b>	Mineral Oil	0, 1, 2	50.1	883 – 889	4.8 – 6.3	0.030 – 0.031	0 – 15
<b>Badie <i>et al.</i> AW (2000)</b>	Water	0	79	1000	1	0.037	1 – 6
<b>Badie <i>et al.</i> AO (2000)</b>	Oil	0	79	865	40	0.032	1 – 11
<b>Ottens <i>et al.</i> AW (2001)</b>	Water	0, 1, 2	52	998 – 999	0.96 – 1.01	0.072	1 – 9
<b>Ottens <i>et al.</i> AG (2001)</b>	Water + Glycerol	0, 1, 2	52	1087 – 1088	2.0 – 3.2	0.061	2 – 10
<b>Fan Small Pipe (2005)</b>	Water	0, 1, 2	50.8	1000	1	0.072	0 – 6
<b>Fan Large Pipe (2005)</b>	Water	0, 2	149.6	947 – 973	1	0.072	0 – 14

<b>Schmidt <i>et al.</i> (2008)</b>	Water (N <sub>2</sub> )	90	54.5	997 – 998	1	0.066, 0.036	4 – 94
<b>Waltrich <i>et al.</i> (2013)</b>	Water	90	40.8	997.4	1	0.072	1 – 60
<b>Escrig Large Pipe (2017)</b>	Silicon oil	90	127	917	5	0.0202	25 – 84
<b>Kokal (1987)</b>	Light Oil	0, 1, 5, 9	25.8, 51.2, 76.3	854 – 866	5.6 – 9.6	0.039	1 – 99
<b>Mattar (1973)</b>	Oil	0, 3, 6, 10	25.8	875	9.6	0.030	24 – 81
<b>Kim (2019)</b>	Synthetic Oil	0	50.8	839 – 854	242 – 995	0.033	56 – 94
<b>Fayyaz (2022b)</b>	Silicone oil	0, 15, 45, 65, 90	67	922.5	91.5	0.0202	29 – 95
<b>Fayyaz (2022c)</b>	Silicone oil	0, 15, 45, 65, 90	67	9	236	0.0202	34 – 96
<b>All datasets</b>	Various	0 – 90	25.8 – 149.6	865 – 1000	0.96 – 995	0.0202– 0.072	0 – 95

Table 6.11 shows the total number of points before and after treatment (2280 and 2237 respectively) for datasets not utilised in the model development of current study (2022), eliminating a total of 43 points.

*Table 6.11 – Treatment of each dataset not utilised in development of model*

<b>Dataset</b>	<b>Data points before treatment</b>	<b>Total data points after homogeneous points test</b>	<b>Number of points after drift flux test</b>	<b>Percentage of data eliminated</b>
<b>Paras <i>et al.</i> (1994)</b>	19	19	19	0.0
<b>Meng (1999)</b>	108	108	107	0.9
<b>Badie <i>et al.</i> AW (2000)</b>	36	36	36	0.0
<b>Badie <i>et al.</i> AO (2000)</b>	30	30	30	0.0
<b>Ottens <i>et al.</i> AW (2001)</b>	95	95	93	2.1
<b>Ottens <i>et al.</i> AG (2001)</b>	51	51	49	3.9
<b>Fan Small Pipe (2005)</b>	107	107	103	3.7
<b>Fan Large Pipe (2005)</b>	120	120	116	3.3
<b>Schmidt <i>et al.</i> (2008)</b>	20	18	18	10.0
<b>Waltrich <i>et al.</i> (2013)</b>	90	89	89	1.1
<b>Escrig Large Pipe (2017)</b>	36	36	36	0.0
<b>Kokal (1987)</b>	1036	1027	1018	1.7
<b>Mattar (1973)</b>	40	40	39	2.5
<b>Kim (2019)</b>	107	104	103	3.7
<b>Fayyaz (2022b)</b>	220	218	216	1.8
<b>Fayyaz (2022c)</b>	165	165	165	0.0
<b>All datasets</b>	2280	2263	2237	1.9

Table 6.12 shows AAE, AE and STD for model – dataset combination (for first eight datasets in Table 6.10 which are for low liquid loading datasets). Individually, for current study (2022), AAE is lowest or similar for all datasets except Badie *et al.* AO

(2000) and Meng (1999). For Badie *et al.* AO (2000), Armand - Massina (2005) has the lowest AAE of 0.6. The best model for Meng (1999) is Premoli *et al.* (1970) followed by Woldesemayat and Ghajar (2007) and current study (2022). The worst model for all individual datasets is Jowitt *et al.* (1984).

Table 6.12 – Absolute average error (AAE), average error (AE) and standard deviation (STD) for each model – dataset combination (for low liquid loading)

Model	SM	Dataset							
		Fan Small Pipe (2005)	Fan Large Pipe (2005)	Ottens <i>et al.</i> AW (2001)	Ottens <i>et al.</i> AG (2001)	Badie <i>et al.</i> AW (2000)	Badie <i>et al.</i> AO (2000)	Meng (1999)	Paras <i>al.</i> (1994)
<b>Current Study (2022)</b>	AAE	0.5	1.2	0.6	0.7	0.4	3.2	1.6	1.4
	AE	0.4	-0.6	-0.1	-0.4	0.0	-3.2	-0.8	-1.3
	STD	0.4	1.6	0.9	1.1	0.5	1.9	2.6	1.1
<b>Jowitt <i>et al.</i> (1984)</b>	AAE	42.7	40.3	40.9	40.2	41.6	38.6	40.4	38.9
	AE	42.7	40.3	40.9	40.2	41.6	38.6	40.4	38.9
	STD	1.0	2.6	1.7	1.9	1.4	2.7	4.0	2.5
<b>Choi <i>et al.</i> (2012)</b>	AAE	14.7	12.5	13.1	12.5	13.7	10.7	12.5	11.1
	AE	14.7	12.5	13.1	12.5	13.7	10.7	12.5	11.1
	STD	0.9	2.6	1.6	1.8	1.3	2.6	3.8	2.4
<b>Woldesemayat and Ghajar (2007)</b>	AAE	2.5	2.5	2.5	1.8	1.6	2.0	2.3	1.6
	AE	2.5	2.4	2.5	1.6	1.6	-1.9	1.6	1.6
	STD	1.0	1.3	0.9	1.1	0.2	1.7	2.1	0.5
<b>Premoli <i>et al.</i> (1970)</b>	AAE	0.9	1.1	1.6	1.1	0.5	3.3	1.1	1.7
	AE	0.9	0.2	1.4	0.9	0.4	-3.3	-0.2	1.7
	STD	0.7	1.4	1.0	1.0	0.3	1.3	2.1	0.4
<b>Toshiba (2002)</b>	AAE	8.8	6.4	8.1	7.6	6.8	3.9	6.7	4.8
	AE	8.8	6.3	8.1	7.6	6.8	3.8	6.5	4.8
	STD	1.4	2.2	1.1	1.3	1.2	2.5	3.1	2.0
<b>Zuber and Findlay (1965)</b>	AAE	16.5	14.1	15.2	14.5	14.8	11.9	14.0	12.6
	AE	16.5	14.1	15.2	14.5	14.8	11.9	14.0	12.6
	STD	1.0	2.4	1.2	1.5	1.3	2.6	3.6	2.2
<b>Armand – Massina (2005)</b>	AAE	1.9	4.7	3.5	2.5	4.5	0.6	2.4	6.2
	AE	1.9	4.7	3.3	2.3	4.5	-0.3	1.6	6.2
	STD	1.5	2.0	1.5	1.3	2.4	0.7	3.0	0.8
<b>Mukherjee and Brill (1983)</b>	AAE	1.4	3.5	3.0	3.8	2.5	5.3	3.4	4.1
	AE	-1.4	-3.5	-3.0	-3.8	-2.5	-5.3	-3.4	-4.1
	STD	0.8	2.2	1.4	1.7	1.2	2.4	3.5	1.4

Table 6.13 shows AAE, AE and STD for model – dataset combination (for last eight datasets in Table 6.10 which are for mixed liquid loading). Individually, for current study (2022), AAE is lowest or similar for all datasets except Escrig LP (2017), Kokal (1987), Mattar (1973) and Kim (2019). The best model for Escrig LP (2017) is Toshiba (2002) with an AAE of 1.7. The best model for Kokal (1987) and Mattar (1973) with an AAE of 3.9 and 4.2 respectively is Zuber and Findlay (1965). Kim (2019) is best predicted by Choi *et al.* (2012) with an AAE of 3.8.

Table 6.13 – Absolute average error (AAE), average error (AE) and standard deviation (STD) for each model – dataset combination (for mixed liquid loading)

Model	SM	Dataset							
		Escrig LP (2017)	Waltrich <i>et al.</i> (2013)	Schmidt <i>et al.</i> (2008)	Kokal (1987)	Mattar (1973)	Kim (2019)	Fayyaz (2022b)	Fayyaz (2022c)
Current Study (2022)	AAE	4.0	2.7	1.8	5.6	6.1	10.4	2.4	2.8
	AE	3.0	1.2	0.5	-4.4	-5.9	-10.1	0.4	-0.5
	STD	3.5	3.2	2.4	5.3	3.7	9.1	3.1	3.6
Jowitt <i>et al.</i> (1984)	AAE	8.9	34.9	23.0	14.9	9.5	5.9	5.8	6.3
	AE	7.0	34.8	22.9	12.4	8.6	-4.4	0.4	-3.4
	STD	8.4	9.9	13.2	14.2	6.7	5.6	7.4	7.1
Choi <i>et al.</i> (2012)	AAE	4.8	11.5	5.6	6.1	5.7	3.8	3.5	4.6
	AE	-4.8	10.9	5.3	-3.6	-5.4	-0.21	3.1	3.7
	STD	3.1	5.5	3.9	6.9	3.7	4.6	2.6	4.7
Woldesemayat and Ghajar (2007)	AAE	2.8	4.4	4.8	6.0	5.6	14.7	2.8	4.8
	AE	2.6	3.7	4.0	-4.7	-5.3	-14.2	-2.4	-4.2
	STD	2.2	3.3	3.6	5.6	3.5	10.2	2.1	3.9
Premoli <i>et al.</i> (1970)	AAE	3.2	4.1	2.8	4.5	4.6	19.7	4.6	7.5
	AE	-3.1	1.7	-0.2	-2.6	3.7	-18.2	-2.7	-5.4
	STD	3.1	4.9	3.8	5.3	3.8	17.5	7.0	10.7
Toshiba (2002)	AAE	1.7	6.1	5.7	4.1	5.0	12.6	4.0	5.7
	AE	-1.4	5.8	1.7	-0.1	-2.4	-10.2	-1.4	-3.4
	STD	1.4	3.2	2.5	5.6	5.9	12.9	4.6	6.4
Zuber and Findlay (1965)	AAE	4.9	12.0	5.8	3.9	4.2	13.2	6.4	9.3
	AE	-4.9	11.4	5.5	0.4	-3.8	-12.3	-6.1	-9.2
	STD	3.3	5.7	4.1	5.4	3.2	11.3	4.4	5.1
Armand – Massina (2005)	AAE	12.3	6.9	6.0	6.3	11.0	19.5	17.7	22.3
	AE	-12.3	3.3	2.2	-5.0	11.0	-19.5	-17.7	-22.3
	STD	6.2	7.8	7.0	2.8	6.2	11.2	10.4	12.0
Mukherjee and Brill (1983)	AAE	4.6	3.1	6.1	7.1	5.0	N/A	N/A	N/A
	AE	-4.3	-1.2	0.2	-6.1	-4.9			
	STD	3.8	4.1	11.9	5.9	4.4			

As carried out in Sections 6.2 and 6.3, it is essential to analyse which percentage of data is predicted within 30 %. Table 6.14 shows percentage of data within 30 % for each model – individual dataset combination (for first eight datasets in Table 6.10 which are for low liquid loading datasets). Current study (2022) predicts the highest percentage of data within 30 % for all datasets except Meng (1999), Badie *et al.* AO (2000) and Badie *et al.* AW (2000). For Badie *et al.* AW (2000), the best model is Premoli *et al.* (1970) however current study is able to predict 75 % of the data within 30 % compared to 83.3 predicted by Premoli *et al.* (1970). The difference in terms of points is just two points which is quite marginal. For Badie *et al.* AO (2000), Armand – Massina (2005) is the best model and predicts 83.3 % of the data within 30 %. Current study (2022) is the fourth best model for this dataset. However, Armand – Massina (2005) has poor performance for all other datasets.

*Table 6.14 – Percentage of data within 30 % for each model – dataset combination (for low liquid loading)*

Model	Dataset							
	Fan Small Pipe (2005)	Fan Large Pipe (2005)	Ottens <i>et al.</i> AW (2001)	Ottens <i>et al.</i> AG (2001)	Badie <i>et al.</i> AW (2000)	Badie <i>et al.</i> AO (2000)	Meng (1999)	Paras <i>et al.</i> (1994)
<b>Current Study (2022)</b>	42.7	56.0	75.3	89.8	75.0	13.3	41.1	78.9
<b>Jowitt <i>et al.</i> (1984)</b>	0.0	0.0	0.0	0.0	0.0	0.0	0.0	0.0
<b>Choi <i>et al.</i> (2012)</b>	0.0	1.7	0.0	0.0	0.0	0.0	5.6	0.0
<b>Woldesemayat and Ghajar (2007)</b>	0.0	19.8	8.6	22.4	8.3	36.7	23.4	47.4
<b>Premoli <i>et al.</i> (1970)</b>	23.3	50.0	18.3	40.8	83.3	0.0	56.1	47.4
<b>Toshiba (2002)</b>	0.0	6.9	0.0	0.0	0.0	26.7	15.0	21.1
<b>Zuber and Findlay (1965)</b>	0.0	0.0	0.0	0.0	0.0	0.0	2.8	0.0
<b>Armand – Massina (2005)</b>	16.5	7.8	4.3	8.2	8.3	83.3	26.2	0.0
<b>Mukherjee and Brill (1983)</b>	0.0	0.0	0.0	0.0	0.0	0.0	0.0	0.0

Table 6.15 shows percentage of data within 30 % for each model – individual dataset combination (for last eight datasets in Table 6.10 which are for mixed liquid loading datasets). Current study (2022) predicts the highest percentage of data within 30 % for all datasets except Kokal (1987), Mattar (1973) and Kim (2019). For Kokal (1987), the best model is Toshiba (2002). For Mattar (1973), Zuber and Findlay (1965) and Premoli *et al.* (1970) predicts the highest percentage of data within 30 %. Kim (2019) is best predicted by Jowitt *et al.* (1984) and Choi *et al.* (2012). However, the third best model for Kim (2019) is current study (2022).

*Table 6.15 – Percentage of data within 30 % for each model – dataset combination (for mixed liquid loading)*

Model	Dataset							
	Escrig Large Pipe (2017)	Waltrich <i>et al.</i> (2013)	Schmidt <i>et al.</i> (2008)	Kokal (1987)	Mattar (1973)	Kim (2019)	Fayyaz (2022b)	Fayyaz (2022c)
<b>Current Study (2022)</b>	100.0	46.1	94.4	79.9	87.2	82.5	100.0	100.0
<b>Jowitt <i>et al.</i> (1984)</b>	72.2	3.4	27.8	52.5	64.1	100.0	94.9	98.9
<b>Choi <i>et al.</i> (2012)</b>	100.0	13.5	55.6	82.1	89.7	100.0	100.0	94.5
<b>Woldesemayat and Ghajar (2007)</b>	100.0	28.1	61.1	81.9	92.3	72.8	100.0	100.0
<b>Premoli <i>et al.</i> (1970)</b>	100.0	29.2	88.9	85.4	100.0	58.3	90.7	88.5
<b>Toshiba (2002)</b>	100.0	23.6	88.9	86.6	84.6	75.7	100.0	99.4
<b>Zuber and Findlay (1965)</b>	100.0	13.5	55.6	86.1	100.0	72.8	99.5	86.1
<b>Armand – Massina (2005)</b>	72.2	20.2	55.6	71.8	69.2	56.3	61.1	35.2
<b>Mukherjee and Brill (1983)</b>	100.0	39.3	77.8	76.3	89.7	N/A	N/A	N/A

Table 6.16 shows overall summary of error analysis (statistical measures) and percentage of data within 30 % for all data not utilised in model development. For all data, the best model in terms of AAE and STD is current study (2022). The next best model in terms of AAE and STD for all data is Premoli *et al.* (1970) followed by Woldesemayat and Ghajar (2007). Overall, the worst model in terms of AAE and STD is Jowitt *et al.* (1984). Overall, the best model in terms of percentage of data within 30 % is current study (2022) which predicts 76.9 % of the data within 30 %, as shown in Table 6.16. The second-best model for all data is Premoli *et al.* (1970) which predicts 71.8 % of the data.

*Table 6.16 – Overall summary of error analysis and percentage of data within 30 % for all data not utilised in model development*

<b>Model</b>	<b>SM</b>		<b>% of percentage of data within 30 %</b>
<b>Current Study (2022)</b>	AAE	4.0	76.9
	AE	-2.6	
	STD	5.3	
<b>Jowitt <i>et al.</i> (1984)</b>	AAE	20.1	47.6
	AE	17.1	
	STD	18.8	
<b>Choi <i>et al.</i> (2012)</b>	AAE	7.5	63.1
	AE	2.5	
	STD	8.8	
<b>Woldesemayat and Ghajar (2007)</b>	AAE	4.9	66.5
	AE	-2.7	
	STD	6.1	
<b>Premoli <i>et al.</i> (1970)</b>	AAE	4.6	71.8
	AE	-2.5	
	STD	7.6	
<b>Toshiba (2002)</b>	AAE	5.4	66.2
	AE	1.0	
	STD	6.9	
<b>Zuber and Findlay (1965)</b>	AAE	8.0	62.9
	AE	2.3	
	STD	9.8	
<b>Armand – Massina (2005)</b>	AAE	9.1	51.4
	AE	-6.6	
	STD	10.6	
<b>Mukherjee and Brill (1983) – Excludes Kim (2019) &amp; Fayyaz (2022)</b>	AAE	5.5	52.0
	AE	-4.8	
	STD	5.1	

Figure 6.8 shows how the model liquid holdup varies with the experimental liquid holdup for all data not utilised for model development. It only shows the best six models. Overall, current study (2022) is performing well at all liquid holdup values. However, closeness of points to 30 % for Premoli *et al.* (1970) at low liquid holdup values is quite commendable. Nevertheless, its performance at higher liquid holdup values is more dispersive compared to current study (2022) and Woldesemayat and Ghajar (2007).

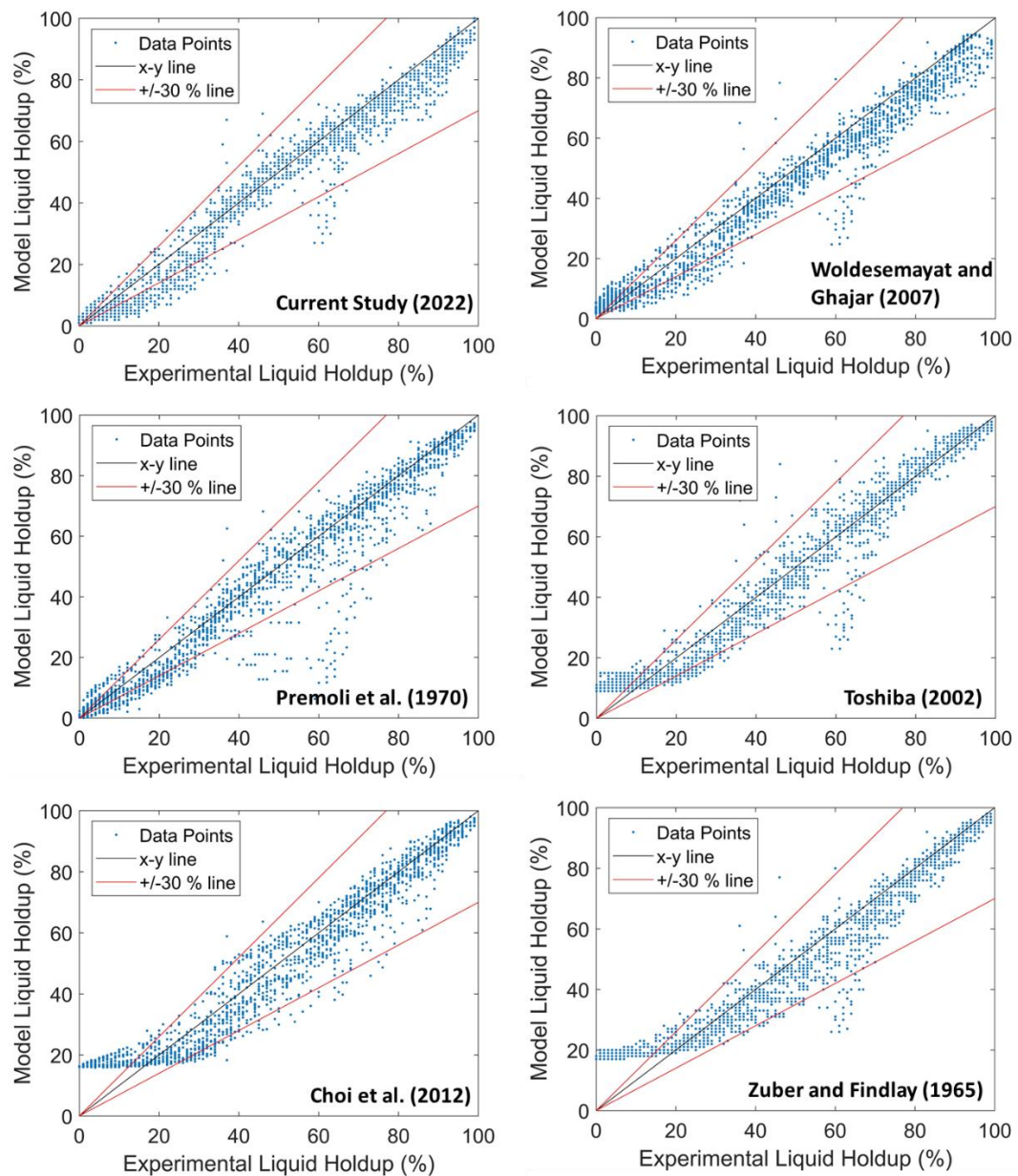


Figure 6.8 – Overall performance of the best six models for all data listed in Table

## 6.5. Conclusion

In this present study, a new liquid holdup relationship has been developed using a wide range of data points (2478 points) which constituted of 10 different datasets as listed in Table 6.1. Current study (2022) was compared to eight other comparative models as well. The current study model was able to predict most percentage of all data utilised for model development within 30 %. After model development, more datasets were obtained in order to assess the performance of current study (2022) on datasets not utilised in model development. Sixteen further datasets (2237 points) were assessed by each model and current study yielded the best results again in terms of absolute average error and percentage of data predicted within 30 %.

Therefore, key findings of this research analysis are as follows:

- Overall performance of current study model (2022) is the best in terms of AAE and percentage of data within 30 % for data utilised in model development and data not utilised in model development.
- As shown in Section 6.4, current study (2022) followed by Premoli *et al.* (1970) can predict lower holdup values with an excellent margin than all models. Models such as Toshiba (2002), Choi *et al.* (2012), and Zuber and Findlay (1965) fail to predict lower liquid holdup with an acceptable error as they plateau out at low liquid holdup.
- Mukherjee and Brill (1983) model fail to predict most of the high viscosity datasets. Moreover, this model also gives poor results for low liquid holdup.

## 7. Conclusions and future Work

### 7.1. General conclusions

In this chapter, general conclusions and recommendations for future works are presented for each analysis chapter of the thesis. In this section, key conclusions from each chapter (Chapters 4 – 6) are discussed.

#### Effect of inclination angle and viscosity on two phase parameters

Chapter 4 focussed on the effect of inclination angle and viscosity on flow characteristics carried out in this study. Three main flow characteristics were investigated: structure velocity, structure frequency and liquid holdup. The main instrumentation technique utilised for the experiments was ECT. A total of 985 points were tested – 600 for 64 cP, 220 for 91.5 cP and 165 for 236 cP.

The main conclusions are presented below:

- From literature review, it was apparent that there were limited number of data points for liquid viscosities of between 16 cP and 121 cP. This study has now covered this gap by adding a total of 985 datapoints for that limitation and beyond.
- As shown in Chapter 4, liquid holdup increases with liquid viscosity at a given gas and liquid superficial velocity. However, it was shown that change in viscosity must be considerable in order to initiate a considerable change in liquid holdup values. This finding became more apparent by comparing medium to high viscosity dataset of this study to lower and higher viscosities from historical datasets. By doing this, it also allowed reverification of trends stated by various studies such as Nadler and Mewes (1995) and Gokcal (2008). Both these studies observed that liquid holdup increases with viscosity which is in sync with the findings of the present study.

- Structure velocity also increases with liquid viscosity (as predicted by Nicklin (1962) model). The trend is more prominent at higher gas superficial velocities. At low gas superficial velocities, there is no real correlation between structure velocity and liquid viscosity (meaning that no real trend between them). The trend observed in the present study was compared to historical datasets of Escrig (2017) and Gokcal (2008) in order to reverify the trend of structure velocity with viscosity.
- Distribution coefficient increased with liquid viscosity. The range of distribution coefficient was 1.27 for 64 cP to 1.44 for 236 cP. In comparison, drift velocity and Froude number decreased with liquid viscosity. The range of drift velocity decreases from 0.37 m/s for 64 cP to 0.32 m/s for 236 cP while the range of Froude number ranged from 0.45 for 64 cP to 0.40 for 236 cP.
- For all dataset combined, drift flux modelling yielded a single equation given by Equation 7.1.

$$\frac{u_{GS}}{\varepsilon} = 1.31u_M + 0.43\sqrt{gD} \quad (7.1)$$

#### Investigating the effect of viscosity on flow regime maps

The effect of inclination angle and viscosity on flow regime transitions were investigated in Chapter 5 for the experimental datasets, achieving a single dimensionless map for each inclination angle showing the effect of viscosity. The dimensionless number utilised for experimental analysis was Reynolds number. Moreover, flow regime studies in literature were also collated and analysed for vertical and horizontal orientations. The literature datasets were divided into two sets: low viscosity and high viscosity. The objective was the same as experimental analysis which was to create a dimensionless map for each viscosity set and orientation combination. However, for literature analysis, dimensionless numbers utilised added Weber number as well along with Reynolds number into the analysis. Different combinations of these dimensionless numbers were tried and tested in

order to attain the best possible map for each viscosity set and orientation combination.

Following conclusions were drawn out:

- Using superficial velocity coordinates do not capture the effect of viscosity on flow regime transitions. This was shown in Section 5.2 for present study.
- For experimental study, Reynolds number produced promising results in capturing the effect of viscosity on flow regime transitions. Figure 5.9 illustrates the dimensionless map for each inclination angle tested, demonstrating this effect of viscosity.
- Modified Taitel *et al.* (1980) yielded excellent results when slug and churn regimes are combined as intermittent flow.
- For proposed experimental vertical flow regime map, historical dataset of Alruhaimani (2015) were predicted correctly with an accuracy of 85 % and 87.5 % for liquid viscosities of 127 cP and 213 cP respectively.
- For proposed experimental horizontal flow regime map, historical datasets of Taitel and Dukler (1987), Brito *et al.* (2013) and Gokcal *et al.* (2006) were predicted with an 100 % accuracy. It must be stated that the present study did not go beyond intermittent region so datapoints selected from literature for comparison were only intermittent.

#### Development of a general liquid holdup model

Chapter 6 presents the general model for evaluating liquid holdup from a set of given physical parameters and pipe geometry. The general development utilised 2478 points from present study and literature. Further datasets were utilised to critically evaluate the performance of the general model.

Following conclusions can be drawn out:

- General liquid holdup model is presented in Equation 7.2. Parameters E, H and J can be evaluated using Equations 6.7 – 6.9 from Chapter 6.

$$H_L = E \sin^2(1.25\theta) + \frac{H}{1 + \frac{u_{GS}}{2.87u_{LS}}} \quad (7.2)$$

- For datasets utilised for model development, current study (2022) had an AAE of 4.1 which was the lowest in comparison to eight other correlations that were evaluated for the same datasets. Moreover, percentage of data predicted within 30 % was 88.4 % with Woldesemayat and Ghajar (2007) predicting 83.5 % of the data.
- Sixteen further datasets were utilised for evaluating the performance of the current study model (2022). Current study (2022) yielded an AAE of 4.0, predicting 76.9 % of these datasets within 30 %.
- Mukherjee and Brill (1983) model fail to predict most of the high viscosity datasets. Moreover, this model also gives poor results for low liquid holdup.

## 7.2. Future works

There are number of different aspects which have been noted and require further work. These aspects are discussed in this section.

### Physical parameters

The focus of the present study was investigating the effect of viscosity on various flow parameter. The maximum viscosity investigated was 236 cP using ECT. Future works may include looking at even higher viscosity grades of silicone oil (even greater than the ones Gokcal (2008) dealt). For higher viscosity grades, a range (1000 cP to 5500 cP) similar to that carried out by Baba et al. (2019) is recommended with application focus on oil exploration of heavy oils. Future of these studies will depend on interest from energy sector as there is prominent focus on green energy. Escrig

(2017) used 5 cP and lowest viscosity present study utilises is 64 cP. Therefore, future work may also investigate lower viscosity grades (between 5 and 64 cP) of silicone oil. This will be pivotal in further developing the general liquid holdup model as well as further upgrading the flow regime map presented in this study. A greater care must be taken on the measurement techniques in the proposed work as it can play a part in comparison.

Other areas of interest from liquid properties are investigating different liquid densities or surface tension. Most of the datasets used in this study focussed on air as the gas phase. Different gas phases can be explored in order to investigate the effect of gas density and viscosity on flow parameters and regime identifications.

#### Pipe orientation and diameter

The study focussed on a single pipe diameter – 67 mm. Similar inclination angles and viscosities can be investigated for a series of different diameters (larger and smaller).

#### Limitations on gas and liquid superficial velocities

The maximum liquid and gas superficial velocity tested were 0.392 m/s and 2.819 m/s respectively. The maximum superficial velocities limit the flow regimes observed in the pipeline to a certain degree as all the possible flow regimes cannot be observed for a given orientation. For example, annular flow and bubbly/stratified flow (in horizontal orientation) are not observed due to these limitations. Future works may include utilising a modified rig system (maintenance) which will allow to explore all flow regimes (including annular flow).

#### Probability Density Function

Conventional PDF from Costigan and Whalley (1997) fails when it was utilised for slug flow identification. For some slug flow datapoints, there was only one peak. This is in

disagreement to the characteristic two peaks presented in Costigan and Whalley (1997). The reason for this is due to the present study utilising high viscosity datasets whereas Costigan and Whalley (1997) focussed on air – water systems. In this study, visual observations with some high-speed video images were utilised for flow regime identifications. Future work may include investigating whether PDF can be modified in some way in order to accomplish accurate flow regime identification especially for slug flow regime.

#### Flow regime analysis

In Chapter 5, two different dimensionless numbers were utilised – Weber number and Reynolds number. Even though some promising results were obtained, future work may involve looking at complex dimensionless numbers (see Introduction of Chapter 2) which may combine various different numbers.

## References

- Abdelsalam, A., Cem, S. and Eduardo, P., 2016. "New dimensionless number for gas–liquid flow in pipes," *International Journal of Multiphase Flow*, 81, pp. 15–19.
- Abdul-Majeed, G., 1996. Liquid holdup in horizontal two-phase gas—liquid flow. *Journal of Petroleum Science and Engineering*, 15(2-4), pp.271-280.
- Abdulkadir, M., 2011. Experimental and Computational Fluid Dynamics (CFD) Studies of Gas-Liquid Flow in Bends. PhD thesis, University of Nottingham.
- Akhiyarov, D.T., Zhang, H.Q. and Sarica, C., 2010, May. High-viscosity oil-gas flow in vertical pipe. In *Offshore Technology Conference*. OnePetro.
- Al-Ruhaimani, F.A., 2015. Experimental analysis and theoretical modeling of high liquid viscosity two-phase upward vertical pipe flow. The University of Tulsa, Tulsa, OK.
- Al-Ruhaimani, F., Pereyra, E., Sarica, C., Al-Safran, E.M. and Torres, C.F., 2017. Experimental analysis and model evaluation of high-liquid-viscosity two-phase upward vertical pipe flow. *SPE Journal*, 22(03), pp.712-735.
- Al-Safran, E., Gokcal, B. and Sarica, C., 2011. High viscosity liquid effect on two-phase slug length in horizontal pipes. In *15th International Conference on Multiphase Production Technology*. OnePetro.
- Al-Safran, E., Kora, C. and Sarica, C., 2015. Prediction of slug liquid holdup in high viscosity liquid and gas two-phase flow in horizontal pipes. *Journal of Petroleum Science and Engineering*, 133, pp.566-575.
- Amani, P., Hurter, S., Rudolph, V. and Firouzi, M., 2020. "Comparison of flow dynamics of air-water flows with foam flows in vertical pipes," *Experimental Thermal and Fluid Science*, 119, p. 110216.
- Amaya-Gómez, R., López, J., Pineda, H., Urbano-Caguasango, D., Pinilla, J., Ratkovich, N. and Muñoz, F., 2019. "Probabilistic approach of a flow pattern map for horizontal, vertical, and inclined pipes," *Oil & Gas Science and Technology – Revue d'IFP Energies nouvelles*, 74, p. 67.
- Andreussi, P., Paglianti, A. and Silva, F.S., 1999. "Dispersed bubble flow in horizontal pipes," *Chemical Engineering Science*, 54(8), pp. 1101–1107.

- Ansari, M. and Azadi, R., 2016. Effect of diameter and axial location on upward gas–liquid two-phase flow patterns in intermediate-scale vertical tubes. *Annals of Nuclear Energy*, 94, pp.530-540.
- Armand, A.A., 1946. The Resistance During The Movement of a Two-Phase System in Horizontal Pipes. *Izvestia Vses. Teplotekh. Inst.*, 1, 16-23.
- Azzopardi, B.J., 2006. Gas-liquid flows. New York: Begell house.
- Azzopardi, B., Abdulkareem, L., Zhao, D., Thiele, S., da Silva, M., Beyer, M. and Hunt, A., 2010. Comparison between Electrical Capacitance Tomography and Wire Mesh Sensor Output for Air/Silicone Oil Flow in a Vertical Pipe. *Industrial & Engineering Chemistry Research*, 49(18), pp.8805-8811.
- Azzopardi, B.J., Do, H.K., Azzi, A. and Perez, V.H., 2015. Characteristics of air/water slug flow in an intermediate diameter pipe. *Experimental Thermal and Fluid Science*, 60, pp.1-8.
- Baba, Y.D., Archibong-Eso, A., Aliyu, A.M., Fajemidupe, O.T., Ribeiro, J.X., Lao, L. and Yeung, H., 2019. Slug translational velocity for highly viscous oil and gas flows in horizontal pipes. *Fluids*, 4(3), p.170.
- Badie, S., 2000. Horizontal stratifying/annular gas-liquid flow. PhD Thesis, Imperial College London.
- Badie, S., Hale, C.P., Lawrence, C.J. and Hewitt, G.F., 2000. Pressure gradient and holdup in horizontal two-phase gas–liquid flows with low liquid loading. *International Journal of Multiphase Flow*, 26(9), pp.1525-1543.
- Baker, G., Azzopardi, B.J., Clark, W. W., and Dyakowski, T., 2003. Transients in stratified/slug flow – observations using electrical capacitance tomography. *Proceedings of the 11th International Conference on Multiphase flow*, San Remo, Italy, pp 457 – 472.
- Bankoff, S., 1960. A Variable Density Single-Fluid Model for Two-Phase Flow With Particular Reference to Steam-Water Flow. *Journal of Heat Transfer*, 82(4), pp.265-272.
- Barnea, D., Luninski, Y. and Taitel, Y., 1983. Flow pattern in horizontal and vertical two phase flow in small diameter pipes. *The Canadian Journal of Chemical Engineering*, 61(5), pp.617-620.
- Barnea, D., Shoham, O., Taitel, Y. and Dukler, A., 1985. Gas-liquid flow in inclined tubes: Flow pattern transitions for upward flow. *Chemical Engineering Science*, 40(1), pp.131-136.

- Beggs, D.H. and Brill, J.P., 1973. A study of two-phase flow in inclined pipes. *Journal of Petroleum technology*, 25(05), pp.607-617.
- Beggs, H.D., 1972. An experimental study of two-phase flow in inclined pipes, PhD thesis, University of Tulsa, Tulsa, OK.
- Bendat, J.S. and Piersol, A.G., 2010. *Random data: analysis and measurement procedures*. John Wiley & Sons.
- Bendiksen, K., 1984. An experimental investigation of the motion of long bubbles in inclined tubes. *International Journal of Multiphase Flow*, 10(4), pp.467-483.
- Benjamin, T., 1959. Shearing flow over a wavy boundary. *Journal of Fluid Mechanics*, 6(2), pp.161-205.
- Bhaga, D. and Weber, M.E. (1981) Bubbles in Viscous Liquids: Shapes, Wakes and Velocities. *Journal of Fluid Mechanics*, 105, 61-85.
- Bonnecaze, R., Erskine, W. and Greskovich, E., 1971. Holdup and pressure drop for two-phase slug flow in inclined pipelines. *AIChE Journal*, 17(5), pp.1109-1113.
- Bottin, M., Berlandis, J.P., Hervieu, E., Lance, M., Marchand, M., Öztürk, O.C. and Serre, G., 2014. "Experimental investigation of a developing two-phase bubbly flow in horizontal pipe," *International Journal of Multiphase Flow*, 60, pp. 161–179.
- Bouyahiaoui, H., Azzi, A., Zegloul, A., Hasan, A.H., Al-Sarkhi, A. and Parsi, M., 2020. Vertical upward and downward churn flow: Similarities and differences. *Journal of Natural Gas Science and Engineering*, 73, p.103080.
- Brito, R., Sarica, C., and Pereyra, E.J., 2013. Effect of medium oil viscosity on two phase oil gas flow behavior in horizontal pipes. *In Offshore Technology Conference*. OnePetro.
- Brodkey, R. S., 1967. *The phenomena of fluid motions*. Reading, Mass, Addison-Wesley.
- Butterworth, D., 1967. A visual study of mechanisms in horizontal air water flow. UKAEA Report, AERE M 2556.
- Butterworth, D. and Pulling, D.J., 1973. A visual study of mechanisms in horizontal annular, air water flow. UKAEA Report, AERE M 2556.
- Chaves, G.S., Karami, H., Filho, V.J.M.F. and Vieira, B.F., 2022. "A comparative study on the performance of multiphase flow models against offshore field production data," *Journal of Petroleum Science and Engineering*, 208, p. 109762.

- Cheng, H., Hills, J. and Azzopardi, B., 1998. A study of the bubble-to-slug transition in vertical gas-liquid flow in columns of different diameter. *International Journal of Multiphase Flow*, 24(3), pp.431-452.
- Chen, X. T., Cal, X. D., and Brill, J. P., 1997. "Gas-Liquid Stratified-Wavy Flow in Horizontal Pipelines." *ASME. J. Energy Resources Technology*, 119(4): 209–216.
- Chisholm, D., 1973. Void Fraction during Two-Phase Flow. *Journal of Mechanical Engineering Science*, 15(3), pp.235-236.
- Choi, J., Pereyra, E., Sarica, C., Park, C. and Kang, J.M., 2012. An efficient drift-flux closure relationship to estimate liquid holdups of gas-liquid two-phase flow in pipes. *Energies*, 5(12), pp.5294-5306.
- Coddington, P. and Macian, R., 2002. A study of the performance of void fraction correlations used in the context of drift-flux two-phase flow models. *Nuclear Engineering and Design*, 215(3), pp.199-216.
- Coney, M., 1974. The analysis of a mechanism of liquid replenishment and draining in horizontal two-phase flow. *International Journal of Multiphase Flow*, 1(5), pp.647-669.
- Costigan, G. and Whalley, P., 1997. Slug flow regime identification from dynamic void fraction measurements in vertical air-water flows. *International Journal of Multiphase Flow*, 23(2), pp.263-282.
- Davies, R.M. and Taylor, G.I., 1950. The mechanics of large bubbles rising through extended liquids and through liquids in tubes. *Proceedings of the Royal Society of London. Series A. Mathematical and Physical Sciences*, 200(1062), pp.375-390.
- Da Hlaing, N., Sirivat, A., Siemanond, K., and Wilkes, J.O., 2007. "Vertical two-phase flow regimes and pressure gradients: Effect of viscosity," *Experimental Thermal and Fluid Science*, 31(6), pp. 567–577.
- Eaton, B. A. (1966), "The predication of flow patterns, liquid holdup and pressure losses occurring during continuous two-phase flow in horizontal pipelines," PhD dissertation, U. of Texas, Austin.
- Elshawaf, M., 2018, September. Investigation of graphene oxide nanoparticles effect on heavy oil viscosity. In *SPE Annual Technical Conference and Exhibition*. OnePetro.
- Escrig, J., 2017. *Influence of geometrical parameters on gas-liquid intermittent flows*. PhD thesis, University of Nottingham.

- Fabre, J. and Liné, A., 1992. Modeling of two-phase slug flow. *Annual review of fluid mechanics*, 24(1), pp.21-46.
- Fan, Y., 2005. An investigation of low liquid loading gas-liquid stratified flow in near-horizontal pipes, Ph. D. Dissertation. *U. of Tulsa, Tulsa, OK*.
- Fukano, T., Ousaka, A., Morimoto, T. and Sekoguchi, K., 1983. Air-water annular two-phase flow in a horizontal tube: 2nd report, circumferential variations of film thickness parameters. *Bulletin of JSME*, 26(218), pp.1387-1395.
- Furukawa, T. and Fukano, T., 2001. Effects of liquid viscosity on flow patterns in vertical upward gas-liquid two-phase flow. *International Journal of Multiphase Flow*, 27(6), pp.1109-1126.
- Ghanbarzadeh, S., Hanafizadeh, P. and Hassan Saidi, M., 2012. Intelligent Image-Based Gas-Liquid Two-Phase Flow Regime Recognition. *Journal of Fluids Engineering*, 134(6).
- Gokcal, B., 2008. An experimental and theoretical investigation of slug flow for high oil viscosity in horizontal pipes, PhD thesis, University of Tulsa, Tulsa, OK.
- Gokcal, B., Wang, Q., Zhang, H.Q. and Sarica, C., 2006, September. Effects of high oil viscosity on oil/gas flow behavior in horizontal pipes. In *SPE Annual Technical Conference and Exhibition*. OnePetro.
- Govier, G. and Omer, M., 1962. The horizontal pipeline flow of air-water mixtures. *The Canadian Journal of Chemical Engineering*, 40(3), pp.93-104.
- Govier, G. and Short, W., 1958. The upward vertical flow of air-water mixtures: II. Effect of tubing diameter on flow-pattern, holdup and pressure drop. *The Canadian Journal of Chemical Engineering*, 36(5), pp.195-202.
- Griffith, P. and Snyder, G.A., 1964. The bubbly-slug transition in a high velocity two phase flow. Cambridge, Mass.: MIT Division of Sponsored Research.
- Griffith, P. and Wallis, G.B., 1961. Two-phase slug flow. *Journal of Heat Transfer*, 83(3).
- Guo, K., Li, H. and Yu, Z., 2016. In-situ heavy and extra-heavy oil recovery: A review. *Fuel*, 185, pp.886-902.
- Harmathy, T., 1960. Velocity of large drops and bubbles in media of infinite or restricted extent. *AIChE Journal*, 6(2), pp.281-288.
- Hasan, A. and Kabir, C., 1988. A Study of Multiphase Flow Behavior in Vertical Wells. *SPE Production Engineering*, 3(02), pp.263-272.

- Hazuku, T., Takamasa, T. and Matsumoto, Y., 2008. Experimental study on axial development of liquid film in vertical upward annular two-phase flow. *International Journal of Multiphase Flow*, 34(2), pp.111-127.
- Hernandez-Perez, V., 2017. Gas-liquid two-phase flow in inclined pipes. PhD thesis, University of Nottingham.
- Hewitt, G., and Hall-Taylor, N. 1970. *Annular Two – Phase Flow*, Pergamon, Oxford.
- Hewitt, G.F. and Roberts, D.N., 1969. Studies of two-phase flow patterns by simultaneous x-ray and fast photography (No. AERE-M-2159). *Atomic Energy Research Establishment*, Harwell, England (United Kingdom).
- Hewitt, G.F., 1978. Measurement of two phase flow parameters. *Nasa Sti/recon Technical Report A*, 79, p.47262.
- Heywood, N.I. and Richardson, J.F., 1979. Slug flow of air—water mixtures in a horizontal pipe: Determination of liquid holdup by  $\gamma$ -ray absorption. *Chemical engineering science*, 34(1), pp.17-30.
- Hinze, J., 1955. Fundamentals of the hydrodynamic mechanism of splitting in dispersion processes. *AIChE Journal*, 1(3), pp.289-295.
- Hoogendoorn, C., 1959. Gas-liquid flow in horizontal pipes. *Chemical Engineering Science*, 9(4), pp.205-217.
- Huang, S., Plaskowski, A., Xie, C. and Beck, M., 1989. Tomographic imaging of two-component flow using capacitance sensors. *Journal of Physics E: Scientific Instruments*, 22(3), pp.173-177.
- Hudaya, A.Z., Widyatama, A., Dinaryanto, O., Juwana, W.E., Indarto and Deendarlianto, 2019. The liquid wave characteristics during the transportation of air-water stratified co-current two-phase flow in a horizontal pipe. *Experimental Thermal and Fluid Science*, 103, pp.304-317.
- Isaksen, Ø., 1996. A review of reconstruction techniques for capacitance tomography. *Measurement Science and Technology*, 7(3), pp.325-337.
- Iskandrani, A. and Kojasoy, G. (2001) "Local void fraction and velocity field description in horizontal bubbly flow," *Nuclear Engineering and Design*, 204(1-3), pp. 117–128.
- Jeffreys, H., 1925. On the formation of water waves by wind. *Proceedings of the Royal Society (London) vol. A107*, pp 189-206.

- Jeffreys, H., 1926. On the formation of waves by wind. *Proceedings of the Royal Society (London)* vol. A110, pp 241-247.
- Jepson, D.M., Azzopardi, B.J. and Whalley, P.B., 1990. The effect of physical properties on drop size in annular flow. In International Heat Transfer Conference Digital Library.
- Juliá, J., Liu, Y., Paranjape, S. and Ishii, M., 2008. Upward vertical two-phase flow local flow regime identification using neural network techniques. *Nuclear Engineering and Design*, 238(1), pp.156-169.
- Kaji, R., Azzopardi, B. and Lucas, D., 2009. Investigation of flow development of co-current gas–liquid vertical slug flow. *International Journal of Multiphase Flow*, 35(4), pp.335-348.
- Kim, T., 2019. *Detailed flow field analysis of air and highly viscous liquid slug flow in horizontal pipes*. The University of Tulsa.
- Kocamustafaogullari, G. and Wang, Z. (1991) “An experimental study on local interfacial parameters in a horizontal bubbly two-phase flow,” *International Journal of Multiphase Flow*, 17(5), pp. 553–572.
- Kocamustafaogullari, G., Huang, W.D. and Razi, J. (1994) “Measurement and modeling of average void fraction, bubble size and interfacial area,” *Nuclear Engineering and Design*, 148(2-3), pp. 437–453.
- Kocamustafaogullari, G. and Huang, W.D. (1994) “Internal structure and interfacial velocity development for bubbly two-phase flow,” *Nuclear Engineering and Design*, 151(1), pp. 79–101.
- Kokal, S.L., 1987. An experimental study of two phase flow in inclined pipes. University of Calgary.
- Kong, R. and Kim, S. (2017) “Characterization of horizontal air–water two-phase flow,” *Nuclear Engineering and Design*, 312, pp. 266–276.
- Kora, C., Sarica, C., Zhang, H.Q., Al-Sarkhi, A. and Alsafran, E.M., 2011, November. Effects of high oil viscosity on slug liquid holdup in horizontal pipes. In Canadian Unconventional Resources Conference. OnePetro.
- Lamari, M.L., 2001. *An Experimental Investigation of Two-Phase (Air-Water) Flow Regimes in Horizontal Tube at Near Atmospheric Conditions*. Ottawa, Ontario, Canada: Carleton University.

- Leung, L.K.H., 2005. Two phase flow, Thermal hydraulics branch, Chalk River Laboratories, AECL, UNENE Thermal hydraulics course.
- Levich, V., 1962. Physicochemical hydrodynamics. (*No Title*), pp.689-700.
- Lockhart, R.W. and Martinelli, R.C. (1949) Proposed Correlation of Data for Isothermal Two-Phase, Two-Component Flow in Pipes. *Chemical Engineering Progress*, 45, 38-48.
- Lucas, D., Krepper, E. and Prasser, H., 2005. Development of co-current air–water flow in a vertical pipe. *International Journal of Multiphase Flow*, 31(12), pp.1304-1328.
- Liu, T.T., 1989. Experimental investigation of turbulence structure in two-phase bubbly flow, PhD thesis, Northwestern University.
- Liu, T.J. and Bankoff, S.G., 1993. Structure of air-water bubbly flow in a vertical pipe—II. Void fraction, bubble velocity and bubble size distribution. *International Journal of Heat and Mass Transfer*, 36(4), pp.1061-1072.
- Liu, T.J. and Bankoff, S.G., 1993. Structure of air-water bubbly flow in a vertical pipe—I. Liquid mean velocity and turbulence measurements. *International Journal of Heat and Mass Transfer*, 36(4), pp.1049-1060.
- Liu, L., Yan, H. and Zhao, G., 2015. Experimental studies on the shape and motion of air bubbles in viscous liquids. *Experimental Thermal and Fluid Science*, 62, pp.109-121.
- Lin, P.Y. and Hanratty, T.J., 1986. Prediction of the initiation of slugs with linear stability theory. *International journal of multiphase flow*, 12(1), pp.79-98.
- Lin, P.Y. and Hanratty, T.J., 1987. Effect of pipe diameter on flow patterns for air-water flow in horizontal pipes. *International journal of multiphase flow*, 13(4), pp.549-563.
- Mandhane, J., Gregory, G. and Aziz, K., 1974. A flow pattern map for gas—liquid flow in horizontal pipes. *International Journal of Multiphase Flow*, 1(4), pp.537-553.
- Mattar, L., 1973. Slug flow uphill in an inclined pipe (Unpublished master's thesis). University of Calgary, Calgary, AB.
- Matsui G., 1984. Identification of flow regimes in vertical gas-liquid two-phase flow using differential pressure fluctuations. *Int. J. of Multiphase flow*, Vol. 10, No. 6, pp 711-720
- McNulty, J.G., 1987. Fluid property effects of Freon two-phase flow in a horizontal pipeline. *Proceedings of the 2nd International Conference on Multiphase Flow* (BHRA Pub.), 149–160.

- McQuillan, K. and Whalley, P., 1985. Flow patterns in vertical two-phase flow. *International Journal of Multiphase Flow*, 11(2), pp.161-175.
- Mendez-Diaz, S., Zenit, R., Chiva, S., Muñoz-Cobo, J.L. and Martinez-Martinez, S., 2012. A criterion for the transition from wall to core peak gas volume fraction distributions in bubbly flows. *International journal of multiphase flow*, 43, pp.56-61.
- Meng, W., Chen, X.T., Kouba, G.E., Sarica, C. and Brill, J.P., 2001. Experimental study of low-liquid-loading gas-liquid flow in near-horizontal pipes. *SPE Production & Facilities*, 16(04), pp.240-249.
- Meng, W., 1999. Low liquid loading gas-liquid two-phase flow in near-horizontal pipes. The University of Tulsa.
- Michiyoshi, I. and Serizawa, A., 1986. "Turbulence in two-phase bubbly flow," *Nuclear Engineering and Design*, 95, pp. 253–267.
- Mi, Y., Ishii, M. and Tsoukalas, L., 2001. Flow regime identification methodology with neural networks and two-phase flow models. *Nuclear Engineering and Design*, 204(1-3), pp.87-100.
- Milne-Thomson, L.M., 1960. *Theoretical hydrodynamics*. Courier Corporation.
- Minami, K. and Brill, J., 1987. Liquid Holdup in Wet-Gas Pipelines. *SPE Production Engineering*, 2(01), pp.36-44.
- Mishima, K. and Ishii, M., 1984. Flow regime transition criteria for upward two-phase flow in vertical tubes. *International Journal of Heat and Mass Transfer*, 27(5), pp.723-737.
- Mohammed, A.O., Al-Kayiem, H.H., Nasif, M.S., and Time, R.W., 2019. "Effect of slug flow frequency on the mechanical stress behavior of pipelines," *International Journal of Pressure Vessels and Piping*, 172, pp. 1–9.
- Mori, K., Kaji, M., Miwa, M., and Sakaguchi, K., 1999. Interfacial structure and void fraction of liquid slug for upward gas-liquid two-phase slug flow. *Two Phase Flow Modelling and Experimentation*, Edizioni ETS, Pisa
- Morshed, M., Khan, M., Rahman, M. and Imtiaz, S., 2020. Flow Regime, Slug Frequency and Wavelet Analysis of Air/Newtonian and Air/non-Newtonian Two-Phase Flow. *Applied Sciences*, 10(9), p.3272.
- Mukherjee, H. and Brill, J., 1983. Liquid Holdup Correlations for Inclined Two-Phase Flow. *Journal of Petroleum Technology*, 35(05), pp.1003-1008.

- Mukherjee, H., 1979. An experimental study of inclined two-phase flow, PhD thesis, University of Tulsa, Tulsa, OK.
- Nädler, M. and Mewes, D., 1995. Effects of the liquid viscosity on the phase distributions in horizontal gas-liquid slug flow. *International Journal of Multiphase Flow*, 21(2), pp.253-266.
- Nicklin, D., 1962. Two-phase bubble flow. *Chemical Engineering Science*, 17(9), pp.693-702.
- Nuland, S., 1999. Bubble fraction in slugs in two-phase flow with high viscosity liquid. In International Symposium on Two-phase Flow Modeling and Experimentation, Pisa, Italy.
- Osundare, O., Elliott, A., Falcone, G. and Lao, L., 2022. "Gas-liquid flow regime maps for horizontal pipelines: Predicting flow regimes using dimensionless parameter groups," *Multiphase Science and Technology*, 34(4), pp. 75–99.
- Ottens, M., Hoefsloot, H. and Hamersma, P., 2001. Correlations Predicting Liquid Hold-up and Pressure Gradient in Steady-State (Nearly) Horizontal Co-Current Gas-Liquid Pipe Flow. *Chemical Engineering Research and Design*, 79(5), pp.581-592.
- Origin Version 2020b. OriginLab Corporation, Northampton, MA, USA.
- Paras, S.V., Vlachos, N.A. and Karabelas, A.J., 1994. Liquid layer characteristics in stratified—Atomization flow. *International journal of multiphase flow*, 20(5), pp.939-956.
- Pereyra, E., Torres, C., Mohan, R., Gomez, L., Kouba, G. and Shoham, O., 2012. "A methodology and database to quantify the confidence level of methods for gas–liquid two-phase flow pattern prediction," *Chemical Engineering Research and Design*, 90(4), pp. 507–513.
- Pioli, L., Bonadonna, C., Azzopardi, B.J., Phillips, J.C. and Ripepe, A.M., 2012. Experimental constraints on the outgassing dynamics of basaltic magmas. *Journal of Geophysical Research: Solid Earth*, 117(B3).
- Premoli, A., D. Francesco and A. Prima, 1970. An Empirical Correlation for Evaluating Two-Phase Mixture Density under Adiabatic Conditions. *European Two-Phase Flow Group Meeting*, Milan, Italy
- Radovcich, N.A. and Moissis, R., 1962. THE TRANSITION FROM TWO PHASE BUBBLE FLOW TO SLUG FLOW. Report No. 7-7673-22. Technical Report No. 22 (No. NP-11845). Massachusetts Inst. of Tech., Cambridge. Dept. of Mechanical Engineering.

- Razzaque, M.M., Afacan, A., Liu, S., Nandakumar, K., Masliyah, J.H., and Sanders, R.S., 2003. "Bubble size in coalescence dominant regime of turbulent air–water flow through horizontal pipes," *International Journal of Multiphase Flow*, 29(9), pp. 1451–1471.
- Rea, S., 1998. Stratified flow at T-junctions. PhD Thesis. University of Nottingham.
- Ribeiro, J., Liao, R., Aliyu, A., Luo, W. and Liu, Z., 2019. Experimental study of horizontal two- and three-phase flow characteristics at low to medium liquid loading conditions. *Heat and Mass Transfer*, 55(10), pp.2809-2830.
- Rosa, E., Salgado, R., Ohishi, T. and Mastelari, N., 2010. Performance comparison of artificial neural networks and expert systems applied to flow pattern identification in vertical ascendant gas–liquid flows. *International Journal of Multiphase Flow*, 36(9), pp.738-754.
- Rozenblit, R., Gurevich, M., Lengel, Y. and Hetsroni, G., 2006. Flow patterns and heat transfer in vertical upward air–water flow with surfactant. *International Journal of Multiphase Flow*, 32(8), pp.889-901.
- Sakaguchi, T., Akagawa, K., Hamaguchi, H., Imoto, M. and Ishida, S., 1979. Flow regime maps for developing steady air-water two-phase flow in horizontal tubes. *Memoirs of the Faculty of Engineering, Kobe University*, pp.191-202.
- Sandberg, O. and Sundqvist, B., 1982. Thermal properties of two low viscosity silicon oils as functions of temperature and pressure. *Journal of Applied Physics*, 53(12), pp.8751-8755.
- Sanders, R.S., Razzaque, M.M., Schaan, J., Nandakumar, K., Masliyah, J.H., Afacan, A. and Liu, S., 2008. "Bubble Size Distributions for Dispersed Air - Water Flows in a 100 mm Horizontal Pipeline," *The Canadian Journal of Chemical Engineering*, 82(4), pp. 858–864.
- Sawai, T., Kaji, M., Kasugai, T., Nakashima, H. and Mori, T., 2004. Gas–liquid interfacial structure and pressure drop characteristics of churn flow. *Experimental thermal and fluid science*, 28(6), pp.597-606.
- Schlegel, J., Miwa, S., Chen, S., Hibiki, T. and Ishii, M., 2012. Experimental study of two-phase flow structure in large diameter pipes. *Experimental Thermal and Fluid Science*, 41, pp.12-22.

- Schmidt, J., Giesbrecht, H. and Van der Geld, C.W.M., 2008. Phase and velocity distributions in vertically upward high-viscosity two-phase flow. *International Journal of Multiphase Flow*, 34(4), pp.363-374.
- Sekoguchi, K. and Mori, K., 1997. New development of experimental study on interfacial structure in gas-liquid two-phase flow. In *Proc. 4th World Conference on Experimental Heat Transfer, Fluid Mechanics and Thermodynamics, Brussels* (pp. 1177-1188).
- Serizawa, A., Michiyoshi, I., Kataoka, I. and Zun, I., 1988. Bubble size effect on phase distribution. In *Dynamics of Two-Phase Flows*. Begell House.
- Shanmugam, N., 1994. Upward cocurrent gas-liquid two-phase flow in vertical tubes (Doctoral dissertation, Oklahoma State University).
- Shawkat, M.E., Ching, C.Y. and Shoukri, M., 2008. Bubble and liquid turbulence characteristics of bubbly flow in a large diameter vertical pipe. *International Journal of Multiphase Flow*, 34(8), pp.767-785.
- Shippen, M. and Bailey, W., 2012. Steady-State Multiphase Flow—Past, Present, and Future, with a Perspective on Flow Assurance. *Energy & Fuels*, 26(7), pp.4145-4157.
- Shoham, O., 2006. Mechanistic modeling of gas-liquid two-phase flow in pipes. Richardson, TX: Society of Petroleum Engineers.
- Simmons, M.J. and Hanratty, T.J., 2001. Droplet size measurements in horizontal annular gas-liquid flow. *International journal of multiphase flow*, 27(5), pp.861-883.
- Syikilili, A.M., Nydal, O.J., Kimambo, C.Z. and Kihedu, J.H., 2022. Effect of pipeline inclination on multiphase flow. *Experimental and Computational Multiphase Flow*, pp.1-12.
- Spedding, P.L., Woods, G.S., Raghunathan, R.S. and Watterson, J.K., 1998. Vertical Two-Phase Flow: Part I: Flow Regimes. *Chemical Engineering Research and Design*, 76(5), pp.612-619.
- Stanislav, J., Kokal, S. and Nicholson, M., 1986. Intermittent gas-liquid flow in upward inclined pipes. *International Journal of Multiphase Flow*, 12(3), pp.325-335.
- Sujumnong, M., 1997. *HEAT TRANSFER, PRESSURE DROP AND VOID FRACTION IN TWO-PHASE, TWO-COMPONENT FLOW IN A VERTICAL TUBE* (Doctoral dissertation, The University of Manitoba).
- Szalinski, L., Abdulkareem, L., Da Silva, M., Thiele, S., Beyer, M., Lucas, D., Hernandez Perez, V., Hampel, U. and Azzopardi, B., 2010. Comparative study of gas-oil and gas-water

- two-phase flow in a vertical pipe. *Chemical Engineering Science*, 65(12), pp.3836-3848.
- Taitel, Y. and Dukler, A., 1976. A model for predicting flow regime transitions in horizontal and near horizontal gas-liquid flow. *AIChE Journal*, 22(1), pp.47-55.
- Taitel, Y. and Dukler, A., 1987. Effect of pipe length on the transition boundaries for high-viscosity liquids. *International Journal of Multiphase Flow*, 13(4), pp.577-581.
- Taitel, Y., Barnea, D. and Dukler, A., 1980. Modelling flow pattern transitions for steady upward gas-liquid flow in vertical tubes. *AIChE Journal*, 26(3), pp.345-354.
- Taitel, Y., Lee, N. and Dukler, A., 1978. Transient gas-liquid flow in horizontal pipes: Modeling the flow pattern transitions. *AIChE Journal*, 24(5), pp.920-934.
- UEDA, T., 1979. Entrainment rate and size of entrained droplets in annular two-phase flow. *Bulletin of JSME*, 22(171), pp.1258-1265.
- Van Hout, R., Gulitski, A., Barnea, D. and Shemer, L., 2002. Experimental investigation of the velocity field induced by a Taylor bubble rising in stagnant water. *International Journal of Multiphase Flow*, 28(4), pp.579-596.
- Vieira, C., Kallager, M., Vassmyr, M., La Forgia, N. and Yang, Z., 2018, June. Experimental investigation of two-phase flow regime in an inclined pipe. In 11th North American Conference on Multiphase Production Technology. OnePetro.
- Wallis, G. B., 1961. Flooding velocities for air and water in vertical tubes. Winfrith, Dorchester, Dorset, Reactor Development Division, Atomic Energy Establishment.
- Wallis, G., 1969. *One dimensional two phase flow*. New York: McGraw-Hill.
- Wang, S., Zhang, H.Q.Q., Sarica, C. and Pereyra, E., 2014. A mechanistic slug-liquid-holdup model for different oil viscosities and pipe-inclination angles. *SPE Production & Operations*, 29(04), pp.329-336.
- Wang, G., Sawant, P. and Ishii, M., 2020. A new entrainment rate model for annular two-phase flow. *International Journal of Multiphase Flow*, 124, p.103185.
- Wang, Z., Liu, H., Zhang, Z., Sun, B., Zhang, J. and Lou, W., 2020. Research on the effects of liquid viscosity on droplet size in vertical gas-liquid annular flows. *Chemical Engineering Science*, 220, p.115621.
- Waltrich, P.J., Falcone, G. and Barbosa Jr, J.R., 2013. Axial development of annular, churn and slug flows in a long vertical tube. *International journal of multiphase flow*, 57, pp.38-48.

- Weisman, J. and Kang, S., 1981. Flow pattern transitions in vertical and upwardly inclined lines. *International Journal of Multiphase Flow*, 7(3), pp.271-291.
- Weisman, J., Duncan, D., Gibson, J. and Crawford, T., 1979. Effects of fluid properties and pipe diameter on two-phase flow patterns in horizontal lines. *International Journal of Multiphase Flow*, 5(6), pp.437-462.
- Whalley, P. B., Hewitt, G. F. and Hutchinson, P. 1974 Experimental wave and entrainment measurements in vertical annular two-phase flow. *Symp. on Multi-phase Flow Systems*, Univ. of Strathclyde, Strathclyde, Scotland, Paper A1.
- Wijayanta, S., Indarto, Deendarlianto, Catrawedarma, I.G.N.B. and Hudaya, A.Z., 2022. Statistical characterization of the interfacial behavior of the sub-regimes in gas-liquid stratified two-phase flow in a horizontal pipe. *Flow Measurement and Instrumentation*, 83, p.102107.
- Woldesemayat, M.A. and Ghajar, A.J., 2007. Comparison of void fraction correlations for different flow patterns in horizontal and upward inclined pipes. *International journal of multiphase flow*, 33(4), pp.347-370.
- Wu, B., Firouzi, M., Mitchell, T., Rufford, T., Leonardi, C. and Towler, B., 2017. A critical review of flow maps for gas-liquid flows in vertical pipes and annuli. *Chemical Engineering Journal*, 326, pp.350-377.
- Xia, G.D. and Lei, C., 2012. Influence of surfactant on two-phase flow regime and pressure drop in upward inclined pipes. *Journal of Hydrodynamics, Ser. B*, 24(1), pp.39-49.
- Xie, C., Huang, S., Beck, M., Hoyle, B., Thorn, R., Lenn, C. and Snowden, D., 1992. Electrical capacitance tomography for flow imaging: system model for development of image reconstruction algorithms and design of primary sensors. *IEE Proceedings G Circuits, Devices and Systems*, 139(1), p.89.
- Yang, W.Q. and Byars, M., 1999, April. An improved normalisation approach for electrical capacitance tomography. In *1st World Congress on Industrial Process Tomography* (pp. 215-218).
- Zhang, J., Grace, J., Epstein, N. and Lim, K., 1997. Flow regime identification in gas-liquid flow and three-phase fluidized beds. *Chemical Engineering Science*, 52(21-22), pp.3979-3992.

- Zhen T., Cheng Y, Li X, Wang L. Bubble shape and rising velocity in viscous liquids at high temperature and pressure. *Experimental Thermal and Fluid Science*. 2019 Apr 1;102:528-38.
- Zhu, Q., 2019. Intermittent Flow Analysis in Inclined Large Diameter Pipes, Master's thesis, University of Tulsa, Tulsa, OK.
- Zuber, N. and Findlay, J., 1965. Average Volumetric Concentration in Two-Phase Flow Systems. *Journal of Heat Transfer*, 87(4), pp.453-468.
- Zukoski, E., 1966. Influence of viscosity, surface tension, and inclination angle on motion of long bubbles in closed tubes. *Journal of Fluid Mechanics*, 25(4), pp.821-837.